













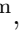




# Target mass corrections in lepton–nucleus DIS: theory and applications to nuclear PDFs

R. Ruiz <sup>a,\*</sup>, K.F. Muzakka <sup>b,c</sup>, C. Léger <sup>d</sup>, P. Risse <sup>b</sup>, A. Accardi <sup>e,f</sup>, P. Duwentäster <sup>b,g,h</sup>,  
T.J. Hobbs <sup>i</sup>, T. Ježo <sup>b</sup>, C. Keppel <sup>e</sup>, M. Klasen <sup>b,j</sup>, K. Kovařík <sup>b</sup>, A. Kusina <sup>a</sup>, J.G. Morfin <sup>k</sup>,  
F.I. Olness <sup>l,\*</sup>, J.F. Owens, <sup>m</sup>, I. Schienbein <sup>d,\*</sup>, J.Y. Yu. <sup>d</sup>

<sup>a</sup>*Institute of Nuclear Physics Polish Academy of Sciences, PL-31342 Krakow, Poland*

<sup>b</sup>*Institut für Theoretische Physik, Westfälische Wilhelms-Universität Münster,  
Wilhelm-Klemm-Straße 9, D-48149 Münster, Germany*

<sup>c</sup>*Institut für Energie- und Klimaforschung, Forschungszentrum Jülich GmbH, 52425 Jülich, Germany*

<sup>d</sup>*Laboratoire de Physique Subatomique et de Cosmologie, Université Grenoble-Alpes,  
CNRS/IN2P3, 53 avenue des Martyrs, 38026 Grenoble, France*

<sup>e</sup>*Jefferson Lab, Newport News, VA 23606, U.S.A.*

<sup>f</sup>*Hampton University, Hampton, VA 23668, USA*

<sup>g</sup>*University of Jyväskylä, Department of Physics, P.O. Box 35, FI-40014, Finland*

<sup>h</sup>*Helsinki Institute of Physics, P.O. Box 64, FI-00014 University of Helsinki, Finland*

<sup>i</sup>*High Energy Physics Division, Argonne National Laboratory, Argonne, Illinois 60439, USA*

<sup>j</sup>*School of Physics, The University of New South Wales, Sydney NSW 2052, Australia*

<sup>k</sup>*Fermi National Accelerator Laboratory, Batavia, Illinois 60510, USA*

<sup>l</sup>*Department of Physics, Southern Methodist University, Dallas, TX 75275-0175, U.S.A.*

<sup>m</sup>*Department of Physics, Florida State University, Tallahassee, Florida 32306-4350, USA*

## Abstract


















Motivated by the wide range of kinematics covered by current and planned deep-inelastic scattering (DIS) facilities, we revisit the formalism, practical implementation, and numerical impact of target mass corrections (TMCs) for DIS on unpolarized nuclear targets. An important aspect is that we only use nuclear and later partonic degrees of freedom, carefully avoiding a picture of the nucleus in terms of nucleons. After establishing that formulae used for individual nucleon targets ( $p, n$ ), derived in the Operator Product Expansion (OPE) formalism, are indeed applicable to nuclear targets, we rewrite expressions for nuclear TMCs in terms of re-scaled (or averaged) kinematic variables. As a consequence, we find a representation for nuclear TMCs that is approximately independent of the nuclear target. We go on to construct a single-parameter fit for all nuclear targets that is in good numerical agreement with full computations of TMCs. We discuss in detail qualitative and quantitative differences between nuclear TMCs built in the OPE and the parton model formalisms, as well as give numerical predictions for current and future facilities.

*Keywords:* DIS, Structure Functions, Target Mass Corrections, OPE, nuclear PDFs

Journal: *Prog. Part. Nucl. Phys.* **136** (2024) 104096

ArXiv: [2301.07715](https://arxiv.org/abs/2301.07715)

\*Corresponding authors

rruiz@ifj.edu.pl (R. Ruiz ) , k.muzakka@fz-juelich.de (K.F. Muzakka ) , leger@lpsc.in2p3.fr (C. Léger ) ,  
risse.p@uni-muenster.de (P. Risse ) , accardi@jlab.org (A. Accardi ) , pitduwen@jyu.fi (P. Duwentäster ) , tim@anl.gov  
(T.J. Hobbs ) , tomas.jezo@uni-muenster.de (T. Ježo ) , keppel@jlab.org (C. Keppel ) , michael.klasen@uni-muenster.de  
(M. Klasen ) , karol.kovarik@uni-muenster.de (K. Kovařík ) , Aleksander.Kusina@ifj.edu.pl (A. Kusina ) ,  
morfin@fnal.gov (J.G. Morfin ) , olness@smu.edu (F.I. Olness ) , owens@hep.fsu.edu (J.F. Owens, ) ,  
schien@lpsc.in2p3.fr (I. Schienbein ) , yu@physics.smu.edu (J.Y. Yu. )

# Contents

<b>1</b>	<b>Introduction</b>	<b>3</b>
<b>2</b>	<b>Kinematics of lepton-nucleus DIS</b>	<b>7</b>
2.1	Definitions of kinematic variables	7
2.2	Leptonic and hadronic tensors in DIS from experimentally observable kinematics	9
<b>3</b>	<b>Nuclear structure functions in the OPE</b>	<b>11</b>
3.1	Light-cone dominance of nuclear DIS	11
3.2	Structure functions in the OPE	13
3.3	Master formula for structure functions with TMCs in $\ell A$ DIS	17
<b>4</b>	<b>Rescaling</b>	<b>19</b>
4.1	Nuclear and nucleon kinematics	19
4.2	Rescaled structure functions	21
4.3	Impact of quark masses	22
<b>5</b>	<b>Parton model</b>	<b>23</b>
5.1	Nuclear DGLAP evolution	24
5.2	Relation to the OPE	25
5.3	Rescaling	25
5.4	Kinematic $W$ cut	28
5.5	nPDFs for $x_N \geq 1$	30
5.6	Threshold problem and higher twist contributions	33
<b>6</b>	<b>The parton model with quark and hadron masses</b>	<b>34</b>
6.1	Helicity formulation of the parton model	34
6.2	Helicity decomposition	35
6.3	Boost-invariant polarizations	37
6.4	Relationship between TMCs on the light-front and in the OPE	38
6.5	Relation of the parton model to the OPE	38
<b>7</b>	<b>Numerical results</b>	<b>40</b>
7.1	Proton structure functions with TMCs	41
7.2	Nuclear structure functions with TMCs	42
7.3	Parameterizing $F_i^{\text{TMC}}/F_i^{\text{Leading-TMC}}$	49
7.4	Reduced cross sections with TMCs for nuclei	53
<b>8</b>	<b>Conclusions</b>	<b>55</b>
<b>A</b>	<b>Nuclear structure functions with TMCs in the OPE</b>	<b>58</b>
A.1	Preliminaries and the inclusive DIS cross section formula	58
A.2	The DIS matrix element and inclusive hadronic tensor	59
A.3	Nuclear structure functions from the OPE I: organization	62
A.4	Nuclear structure functions from the OPE II: structure-function mixing	75
A.5	Nuclear structure fns. from the OPE III: massless and massive targets	77
<b>B</b>	<b>Derivation of the Full/Leading TMC Parameterization</b>	<b>86</b>

# 1. Introduction

Deep-inelastic scattering (DIS) of high-energy leptons off nucleons and nuclei is a key process for studying the structure of hadrons in terms of their quark and gluon degrees of freedom [1–4]. For both nucleons [5–10] and nuclei [11–28], present data from electron and neutrino DIS experiments form the backbone of modern determinations of parton distribution functions (PDFs), which describe and encode the internal structure of hadrons. This process will again be at the forefront of the future Electron-Ion Collider (EIC) [29, 30], where DIS off nucleons and various nuclear targets will be studied with high precision over a wide kinematic range. Similar endeavors are also in discussion for the proposed Forward Physics Facility at CERN [31]. Furthermore, high-precision fixed-target measurements from JLab provide complementary information [32]. In addition to these facilities, DIS also plays an important role at current and future accelerator-based neutrino oscillation facilities such as DUNE and the Short-Baseline Neutrino Program at Fermilab [33–35], where experiments operate at somewhat lower energies compared to the EIC, and where the (quasi)elastic and resonant processes must also be taken into account. Here, precise control over the contributions from each of these processes is essential, and duality-based arguments for the scaling of DIS cross sections at higher energies into the resonance region can play an important role [36, 37]. However, due to the relative weakness of the effective neutrino-nucleon interaction, neutrino experiments typically use massive nuclear targets to enhance event rates.

In order to reach the ambitious physics goals of future experiments, charged lepton-nucleus and neutrino-nucleus interactions need to be precisely understood, both experimentally and theoretically. On the theory side, there are broad efforts to improve the description of DIS in Monte Carlo simulation tools [38–44], increase the perturbative accuracy of matrix elements, particularly for more exclusive DIS channels, and of course improve determinations of parton distribution functions of nuclei [15, 17, 22, 28, 45, 46]. Still, it is a fact that the different properties of charged lepton-nucleus and neutrino-nucleus DIS are not well understood, particularly for extreme kinematics, and is a topic of ongoing study [23]. The specific case in DIS when, simultaneously, momentum transfers are small while the scaling variable approaches unity is the focus of this work.

**Operator Product Expansion (OPE):** Along these lines, there are two major theoretical approaches to lepton-*nucleon* DIS that are standard material in textbooks and review articles; both have been employed to include the effects of target nucleons having nonzero masses. One approach is based on the operator product expansion (OPE) [47–49]. The other is the QCD-improved parton model rigorously derived from first principles of QCD in the context of the collinear factorization theorems [50–57]. The OPE was first employed to derive target mass corrections (TMCs) to structure functions in DIS at leading order (LO) in QCD in the seminal paper by Georgi & Politzer in 1976 [58, 59]. While the application of the OPE to DIS is widely accepted, proofs of the OPE have only been presented for simple scalar models [60, 61]. The question as to whether this result can be extended to QCD in general remains open to the best of our knowledge.

**Target Mass Corrections (TMCs):** Qualitatively, TMCs in DIS accounts for the mass of the target nucleon (or target nucleus) in kinematical variables and structure functions, which are typically derived in the limit of a massless target. In the work of Georgi & Politzer it was argued that for each power, or “twist”<sup>1</sup>, of the OPE expansion of hadronic matrix elements in DIS there is a tower of (kinematical [62, 63]) corrections of the form  $x_A^j (M_A^2/Q^2)^{j'}$ , and specifically  $(x_A M_A^2/Q^2)^j$  at leading power, where  $x_A$  is the Bjorken scaling variable,  $M_A$  is the mass of the target hadron,  $Q^2 > 0$  is the (squared) virtuality of the intermediate exchange boson, and  $j, j'$  are some positive powers. Remarkably, the entire tower of  $(x_A M_A^2/Q^2)^k$  corrections at leading power can be summed, leading to a closed-form solution for TMCs at this power [58, 59]. In the same year, Barbieri, et al., derived TMCs at LO including effects arising from non-zero quark masses [64, 65]. Later, the original work of Georgi & Politzer was extended to next-to-leading order (NLO) in QCD for the structure functions  $W_{1,2}$  in the context of local duality in electro-production and using off-shell regularization [66]. More recently, Kretzer & Reno presented TMCs for charged current (CC) and weak neutral current (NC) neutrino-nucleon

---

<sup>1</sup>In the context of the OPE we define the twist  $\tau = d - s$  of a field operator  $\hat{O}$  in the canonical fashion, i.e., the dimension  $d$  of  $\hat{O}$  (in the usual power-counting sense) minus its spin  $s$  (the number of un-contracted Lorentz indices). For structure functions in DIS, “higher twist” terms are generally power-suppressed by some positive power of a hard scale of the process, i.e.,  $Q$ .

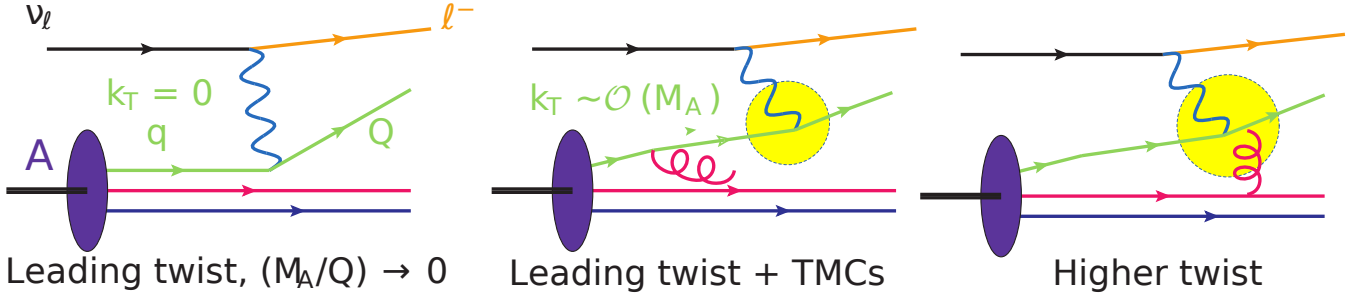


Figure 1.1: Schematic of  $\nu_\ell A \rightarrow \ell X$  for a lowest-order heavy quark production,  $qW^* \rightarrow Q$ . a) [left] Leading twist  $\{M_A = 0, k_T = 0\}$ . b) [center] Leading twist with TMCs  $\{\text{finite } M_A, k_T \sim \mathcal{O}(M_A)\}$ . The “hard scattering” is indicated by the yellow circle. The hadron dynamics gives the parton (green) a finite  $k_T$ , illustrated by the (red) gluon radiation; this is not a next-to-leading order (NLO) correction as the soft (low energy) gluon radiation is outside (before) the hard scattering process (yellow circle). c) [right] Higher twist. A second parton (gluon) is exchanged between the hadron and the hard scattering (yellow circle).

DIS, including NLO QCD corrections and heavy quark mass effects using modern conventions [67].

**Parton Model:** In the context of the parton model, Ellis, Furmanski, & Petronzio derived TMCs at LO in QCD in the framework of a non-collinear version of the parton model that includes the effects of partonic transverse momentum ( $k_T$ ) [62, 63]. Agreement with the OPE-based results [58, 59, 64, 65] was found at leading power, thereby demonstrating the equivalence of the OPE at LO in QCD to a non-collinear parton approach, where the incident parton is on-shell but not collinear with its parent nucleon. In these works, the terminology “kinematical” operators was introduced to describe TMCs in the OPE in order to distinguish them from “dynamical” higher twist operators that remain in the OPE when  $(x_A M_A^2/Q^2) \rightarrow 0$  [62, 63].

**Higher Twist (HT):** At this point, we stress the distinction between TMCs and (genuine) higher-twist corrections. TMCs arise from the modification of kinematics due to the presence of a hadron’s mass  $M_A$ . The behavior of amplitudes in the massless limit implies that mass terms are relatively suppressed by the hard scale of the process, leading to corrections that scale as powers of  $(M_A^2/Q^2)$ . In contrast, higher-twist corrections can arise from exchanges of extra bosons (gluons and pions) between the hard process and the hadronic remnant. Hence, they are *dynamical*. Examples include double parton scattering and color (re)connection between active and spectator quarks. The presence of an “extra” boson exchange in higher-twist processes implies additional propagators, and therefore amplitudes that are also suppressed by the hard scale of the process.<sup>2</sup> This leads to corrections in powers of  $(\Lambda_{\text{NP}}^2/Q^2)$ , where  $\Lambda_{\text{NP}}$  is the characteristic non-perturbative scale of a hadron. Since, in practice,  $\Lambda_{\text{NP}}$  is often set to  $M_A$ , the two corrections can be confused despite their distinct origins; in some sense, TMCs in DIS “accidentally” have the same characteristic power-suppression as in higher-twist corrections.

We illustrate the differences between leading twist, TMCs, and higher twist in Fig. 1.1 for leading-order heavy quark  $Q$  production in the charged current process  $\nu_\ell A \rightarrow \ell X$ . In the left panel (a) is a depiction of the leading-twist process in the limit of vanishing TMCs, i.e.,  $k_T = 0$  and  $(M_A/Q) \rightarrow 0$ . In the center panel (b) is the leading-twist process with finite  $(M_A/Q)$  which yields TMCs and generates  $k_T \sim \mathcal{O}(M_A)$  via a gluon emission that occurs at a time  $\tau_{\text{TMC}} \sim 1/k_T$  **before** the hard process (indicated with a yellow circle). In the right panel (c) is the same process but with a typical higher-twist correction, i.e., an additional parton (gluon) exchange between the hadron and the hard scattering. The characteristic time of the interactions is inversely proportional to the energy scale, (time)  $\sim 1/(\text{Energy})$ . For large  $Q$ , the hard scattering time scale ( $1/Q$ ) is short, while the characteristic time scale of the hadron dynamics ( $1/\Lambda_{\text{NP}}$ ) is long. The probability of a second parton (gluon) participating in the hard interaction is proportional to the ratio of the time scales; thus, we

<sup>2</sup>For sufficiently inclusive observables, the contributions from soft gluons are subject to cancellations [56, 68].

expect higher twist contributions to be suppressed by powers of  $(\Lambda_{NP}/Q)$ .

**ACOT Formalism:** Returning to the literature, we also note that TMC prescriptions based on the OPE and the factorization approach of Ellis, Furmanski, and Petronzio were similarly compared for semi-inclusive processes in Ref. [69]. In the collinear parton model ( $k_T = 0$ ), TMCs have been accounted for in the Aivazis-Collins-Olness-Tung (ACOT) formalism [70, 71], which is rigorously based on the factorization theorem including heavy quark masses [55]. Furthermore, the full QCD framework for the evaluation of tau-neutrino deep-inelastic CC cross sections, including NLO corrections, charm production, tau-mass threshold, and target mass effects in the collinear approximation, was also presented in Ref. [72].

**Proton TMCs:** An earlier review [73] of TMCs for nucleons in unpolarized DIS culminated in a set of so-called master formulae [67], which we extend and present below in Eq. (3.23) for *nuclei*. This set of equations is quite remarkable, organizing the rather complicated expressions in the aforementioned OPE-based papers into a simple, easy-to-use, and modular form, valid at all orders in perturbative QCD while still taking into account quark masses. In principle, TMCs derived for DIS off nucleons [58, 59, 67, 73, 74] apply also to DIS off nuclear targets since the OPE is (in theory) independent of target states. However, previous discussions [73] do not address the subtle distinctions between a nucleon and nuclear target. Furthermore, the fact that established notation does not consistently distinguish between nucleons and nuclei in their respective kinematics, the fact that the spin of a generic nucleus can be different from 1/2, and the fact that the master equations in Eq. (3.23) can be expressed conveniently in terms of “averaged nucleon kinematics” (as they are in Eq. (4.14)) have led to the question, why nucleon-like expressions could possibly be valid for nuclear targets?

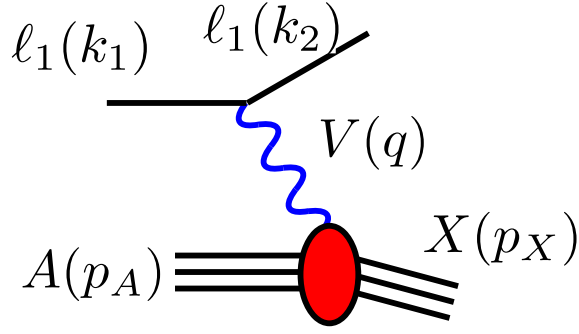
**Nuclear TMCs:** With an abundance of recent nuclear data from both electron and neutrino beams, and with the EIC and 3rd-generation long-baseline oscillations experiments on the horizon, there is a compelling need to rigorously revisit the derivation of TMCs to structure functions in charged-lepton and neutrino DIS with a particular focus on the *nuclear* case. One of the main goals for this article is to demonstrate the validity of the TMC master equations, as given in Eq. (3.23), for the case of massive nuclear targets within the framework of the OPE. Compared to past works on the subject [67, 73], here we present the derivation of TMCs from the OPE in much greater detail. We hope that this material will be useful for students and researchers looking for a modern, in-depth discussion of the many technicalities that are frequently omitted in the literature and textbooks.

**Comparing OPE and Parton Model:** In this work, we discuss and contrast the results for TMCs obtained in both the OPE and the collinear parton model; throughout this review, we consider them on equal footing. As discussed above, the collinear parton model is rigorously based on factorization theorems. These provide field-theoretic definitions of PDFs and make statements about the error of the factorization approximation, which is generally inversely proportional to a positive power of a hard scale of the process. It is generally believed that collinear factorization remains valid in lepton-nucleus and proton-nucleus collisions, possibly with nuclear-enhanced higher twist terms [75]. However, the literature on factorization in the nuclear case is sparse and we consider this a working assumption. Moreover, the non-collinear parton model (where the TMCs were shown to be equivalent to the OPE results at leading power) is not covered by the factorization proofs cited above. Exploring these more theoretical questions is interesting and relevant but beyond the scope of this article. Here, we take the collinear parton model and the OPE for granted, and explore extensively what happens when we transition from nucleons to nuclei in DIS.

**Overview:** The starting point of our analysis is to consider the full nucleus as our target and apply only general symmetry principles, e.g., Lorentz invariance, in deriving nuclear structure functions and their TMCs. This means that until Sec. 4 there is no reference to (or dependence on) nucleon degrees of freedom. Furthermore, until Sec. 5 there is no reference to (or dependence on) the individual partonic degrees of freedom.<sup>3</sup> To do this, we first outline in Sec. 2 key kinematic relations and definitions in DIS of a lepton off a nucleus,  $\ell_1(k_1) + A(p_A) \rightarrow \ell_2(k_2) + X(p_X)$ . As depicted in Fig. 1.2,  $A$  is a nuclear target with mass number  $A$ ,  $\ell$  denotes either a charged lepton ( $\ell^\pm$ ) or neutrino ( $\nu$ ), and  $X$  represents all final-state hadrons. In Sec. 3, we discuss

---

<sup>3</sup>Explicitly, until Sec. 5 we consider operators and matrix elements derived from quark, antiquark, and gluon fields but do not identify these as partons, nor identify structure functions as combinations of PDFs, i.e., the parton model.



Kinematic variable	Description
$\nu_A = \frac{q \cdot p_A}{M_A} \stackrel{lab}{=} E_{\ell_1} - E_{\ell_2}$	Lepton energy loss in the nucleon rest frame (laboratory frame)
$y_A = \frac{q \cdot p_A}{k_1 \cdot p_A} \stackrel{lab}{=} \frac{\nu_A}{E_{\ell_1}}$	Inelasticity $y_A \in [0, 1]$
$Q^2 = -q^2 > 0$	Squared boson momentum transfer
$x_A = \frac{Q^2}{2p_A \cdot q} = \frac{Q^2}{2M_A \nu_A}$	Bjorken $x_A$ with $x_A \in [0, 1]$
$W_A^2 = (p_A + q)^2 = M_A^2 + Q^2 \frac{1 - x_A}{x_A}$	Squared mass of the recoil system
$s = (k_1 + p_A)^2 = \frac{Q^2}{x_A y_A} + M_A^2 + m_\ell^2$	Squared center-of-mass System (CMS) energy

Figure 1.2: We consider the basic charged current ( $V=W^\pm$ ) or neutral current ( $V=\{\gamma, Z\}$ ) lepton-nucleus DIS process  $\ell_1(k_1) + A(p_A) \rightarrow \ell_2(k_2) + X(p_X)$  where the incoming lepton can be a charged lepton ( $e, \mu$ ) or a neutrino ( $\nu_e, \nu_\mu, \nu_\tau$ ). Note, the energy loss symbol  $\nu_A$  should not be confused with the neutrino symbols. The 4-momentum of the exchange boson is denoted  $q = k_1 - k_2$ , and  $p_A^2 = M_A^2$ . Here, the “lab frame” denotes the rest frame of  $A$ , meaning that  $p_A = (M_A, 0, 0, 0)$ .

precisely the criteria for light-cone dominance in nuclear DIS, and then present in Sec. 3.3 a formula for nuclear TMCs. The result is analogous to the nucleon case [73], but expressed in terms of the nuclear scaling variable  $x_A$  and the mass of the nucleus  $M_A$ .

In Sec. 4, we go on to perform a rescaling in order to express our formula for nuclear TMCs to the more familiar averaged nucleon quantities  $x_N = Ax_A$  and  $M_N = M_A/A$ . This is the key step that allows us to compare structure functions across different nuclei, including the proton, in a meaningful way. As an important consequence of rescaling, we obtain an alternative formula for nuclear TMCs that is universally applicable to all nuclei. In Sec. 5 we introduce the QCD-improved parton model, both before and after rescaling. We show that rescaling at the hadronic level and in the parton model are consistent, and we comprehensively discuss the relationship between nuclear structure functions and nuclear PDFs (nPDFs). We believe that the discussions in Secs. 4 and 5, while relatively straight forward, are original and have never been presented in full detail. Our motivation for these later discussions is the importance of establishing proper theoretical definitions of nuclear structure functions and nPDFs as they are intuitively used in the literature.



In Sec. 6, we derive nuclear TMCs in the ACOT light cone formalism, which has been used in past nCTEQ analyses [16, 17, 19–21, 76, 77], and compare them to the OPE results. Having provided rigorous theoretical definitions for the physical observables, we perform numerical studies in Sec. 7. This includes a comparison to a selection of data, as well as cross section predictions for current and future DIS experiments. We provide a parameterization of the TMCs that is accurate at the sub-percent level and can be used with any underlying set of nuclear structure functions available in the massless parton model to obtain the full TMCs for any nucleus in a simple way. We hope that this parameterization will be useful for the community investigating hadron structure. Finally, in Sec. 8 we highlight the key observations of this analysis and conclude.

A detailed derivation of TMCs at twist  $\tau = 2$  for nuclear structure functions using the OPE is provided in Appendix A. Finally, technical details on our parameterization of the TMCs have been relegated to Appendix B.

## 2. Kinematics of lepton-nucleus DIS

Before proceeding with an in-depth treatment of nuclear structure functions, we layout the definitions, notation, and baseline assumptions used throughout this work. (However, assumptions related to light-cone dominance are discussed in Sec. 3.1.) While much of the following is standard material for modern textbooks, many conventions are used in the literature. Therefore, this section serves (a) to fix the notation and conventions that we use, and (b) to make the work both self-consistent and self-contained. We start with definitions of kinematic variables in Sec. 2.1 and move onto the definitions of the leptonic and hadronic tensors for DIS in Sec. 2.2.

### 2.1. Definitions of kinematic variables

Throughout this work we consider the basic charged-current (CC) or neutral-current (NC) lepton-nucleus DIS process involving a high-energy lepton  $\ell_1$  of four-momentum  $k_1$  scattering off an unpolarized nuclear target  $A$ , with an outgoing lepton  $\ell_2$  of momentum  $k_2$  in association with the inclusive hadronic remnant  $X$  of momentum  $p_X$  and mass  $W_A = \sqrt{p_X^2}$ . We assume that  $A$  has momentum  $p_A$ , mass  $M_A = \sqrt{p_A^2}$ , atomic number  $Z$ , mass number  $A$ , and neutron number  $(A - Z)$ . As sketched in Fig. 1.2, this is given by the hadron-level expression

$$\ell_1(k_1) + A(p_A) \rightarrow \ell_2(k_2) + X(p_X). \quad (2.1)$$

We consider that the incoming lepton can be a light charged lepton  $\{e^\pm, \mu^\pm\}$ , a neutrino  $\{\nu_e, \nu_\mu, \nu_\tau\}$ , or an antineutrino  $\{\bar{\nu}_e, \bar{\nu}_\mu, \bar{\nu}_\tau\}$  in the Standard Model. We work in the limit that all incoming leptons are massless but allow for possibility that the outgoing lepton is a (massive)  $\tau^\pm$  lepton.  $X(p_X)$ , sometimes denoted with a subscript as  $X_n(p_X)$ , represents the fragmentation of  $A$ . This fragmentation is an  $n$ -body final state with net quantum numbers corresponding to a colorless state carrying the same spin statistic, QED charge, and weak isospin charge as nucleus  $A$ , modulo differences between  $\ell_1$  and  $\ell_2$ . The momentum of  $X$  can be parameterized by its  $n$  constituents, with  $p_X = \sum_{i=1}^n p_{Xi}$ .

We work at lowest order in the electroweak theory, in the so-called “one-boson-exchange” approximation. Under this assumption, the leptonic system  $(\ell_2 \ell_1)$  probes the hadronic system via the exchange of a single (off-mass-shell) electroweak boson  $V$  ( $V \in \{\gamma, Z\}$  for NC DIS or  $V = W^\pm$  for CC DIS) with time-like momentum  $q = k_1 - k_2 = p_X - p_A$ . The kinematic invariants and scaling variables of DIS are given and defined by

$$k_1^2 = m_{\ell_1}^2, \quad k_2^2 = m_{\ell_2}^2, \quad p_A^2 = M_A^2 > 0, \quad Q^2 = -q^2 > 0, \quad s = (k_1 + p_A)^2 = m_{\ell_1}^2 + M_A^2 + 2p_A \cdot k_1, \quad (2.2a)$$

$$x_A = \frac{Q^2}{2p_A \cdot q}, \quad \nu_A = \frac{p_A \cdot q}{M_A}, \quad y_A = \frac{p_A \cdot q}{p_A \cdot k_1}, \quad Q^2 = (s - m_{\ell_1}^2 - M_A^2)x_A y_A, \quad (2.2b)$$

$$W_A^2 = p_X^2 = (p_A + q)^2 = M_A^2 - Q^2 + 2\nu_A M_A = M_A^2 + Q^2 \frac{1 - x_A}{x_A} \geq M_A^2. \quad (2.2c)$$

Importantly, the above are defined at the level of hadrons (or nuclei). While some are related to the kinematics of a hadron’s constituents, the quantities in Eq. (2.2) are defined without referencing this internal structure.

Throughout this work we generally neglect the lepton masses  $\{m_{\ell_1}, m_{\ell_2}\}$ , except for the case of  $\tau$  leptons.  $\sqrt{s}$  is the hadron-level center-of-mass (cm) energy and the total energy available in the DIS process. The (dimensionless) Bjorken scaling variable  $x_A \in [0, 1]$  is defined<sup>4</sup> such that in the elastic scattering limit, i.e., where  $X$  remains as an intact and on-shell  $A$ , the condition  $W_A^2 = M_A^2$  leads to  $2(p_A \cdot q) = Q^2$ , or that  $x_A = 1$ . In the inelastic scattering limit, i.e., where  $A$  disassociates, the condition  $W_A^2 > M_A^2$  leads to  $2(p_A \cdot q) > Q^2$ , or that  $x_A < 1$ . And in the no-scattering limit, the lepton momenta obey the condition  $k_2 = k_1$ , which implies  $Q^2 = 0$ , or the  $x_A = 0$ . The quantity  $\nu_A$ , which has mass dimension 1, is a measure of the energy carried by the virtual state  $V$ . In the rest frame of  $A$ , it simplifies precisely to this:  $\nu_A|_{lab} = k_1^0 - k_2^0$ . Here and below, the “lab frame” denotes the rest frame of  $A$ , meaning that  $p_A = (M_A, 0, 0, 0)$ . The (dimensionless) inelasticity variable spans  $y_A \in [0, 1]$ , and in the “lab frame” we have  $y_A = \nu_A/E$ . In the rest frame of  $A$ , it is a measure of  $\ell_2$ ’s energy; in other frames,  $y_A$  is a measure of  $\ell_2$ ’s outgoing angle. (Note the inelasticity variable  $y_A \in [0, 1]$  should not be confused with the rapidity or pseudorapidity variables  $y, \eta \in [-\infty, \infty]$  which measure of a particle’s direction.)

For later use with TMCs to structure functions (Secs. 3.3 and 4), we also define the quantity

$$r_A = \sqrt{1 + 4x_A^2 M_A^2 / Q^2} = 1 + \frac{2x_A^2 M_A^2}{Q^2} + \mathcal{O}\left(\frac{4x_A^4 M_A^4}{Q^4}\right), \quad (2.3)$$

as well as the so-called Nachtmann scaling variable [78]

$$\xi_A = \frac{2}{1 + r_A} x_A \equiv R_M x_A, \quad \text{where} \quad R_M = \frac{2}{1 + r_A}. \quad (2.4)$$

$R_M$  is the target-mass-dependent factor relating the Bjorken scaling variable  $x_A$  to the Nachtmann scaling variable  $\xi_A$ . In other words,  $\xi_A$  is the true scaling variable in DIS when one accounts for the mass of the hadronic target [58, 59]. The “ $M$ ” subscript of  $R_M$  indicates this quantity depends on the hadron mass  $M_A$ . In the limit that  $(M_A/Q) \rightarrow 0$  or that  $x_A \rightarrow 0$ , we have  $r_A \rightarrow 1$ ,  $R_M \rightarrow 1$ , and  $\xi_A \rightarrow x_A$  since:

$$\xi_A = x_A \left[ 1 - \frac{x_A^2 M_A^2}{Q^2} + \mathcal{O}\left(\frac{x_A^4 M_A^4}{Q^4}\right) \right]. \quad (2.5)$$

We see in Eq. (2.5) that the Nachtmann variable  $\xi_A$  is essentially the Bjorken scaling  $x_A$  modified by the target mass  $M_A$ . The  $r_A$  and  $R_M$  factors are ultimately kinematical in origin [this is shown below Eq. (A.122) in App. A.5] and take into account that  $M_A$  is non-zero. For example: in the rest frame of  $A$ , the energy of the time-like exchange boson  $V$  is  $q^0|_{lab} = Q^2/(2x_A M_A)$  and its speed is  $\beta_q = |\vec{q}|/q^0|_{lab} = r_A$ .

Qualitatively, the  $R_M$  factor indicates that (slightly) less  $\beta$ -momentum is available than suggested by  $x_A$  and simplified arguments based purely on energy conservation. In other words, the leading kinematics in DIS are modified by  $\mathcal{O}(x_A M_A^2 / Q^2)$  terms that can be neglected at high momentum-transfers. As discussed and demonstrated in later chapters of this work, this is often remedied in practice by the appropriate substitution of  $x_A$  with  $\xi_A$ . Quantitatively, the difference between  $\xi_A$  and  $x_A$  is illustrated in Fig. 2.1, where  $\xi_A$  is plotted as a function of  $x_A$  for a selection of exchange-boson virtualities  $Q$  with  $M_A = M_{\text{proton}}$ . Fig. 2.1(a) displays the full  $\{\xi_A, x_A\}$  plane. Fig. 2.1(b) highlights the large  $x$  region, where the difference between  $\xi_A$  and  $x_A$  is more pronounced. Overall,  $x_A$  and  $\xi_A$  are mostly indistinguishable for  $x_A \lesssim 0.4 - 0.5$  over a large range of  $Q$  and  $M_A$ . At around  $x_A = 0.8$ , one has approximately  $\xi_A \approx 0.63$  (0.71) [0.76] for  $Q = 1.3$  (2) [3] GeV. For the same  $Q$  values, one has approximately  $\xi_A \approx 0.76$  (0.78) [0.84] at around  $x_A = 0.9$ .

<sup>4</sup>Eventually in Sec. 5 we note that the quantity  $p_i = x_A p_A$  can be identified in the parton model as the momentum of a massless parton of  $A$ . One can see this correspondence by evaluating  $W_A^2 = (p_i + (1 - x_A)p_A + q)^2$ , setting all  $p_i^2 = 0$ , and yet still recover Eq. (2.2c). Similarly, other hadronic-level variables in Eqs. (2.2)-(2.4) have correspondence with partonic-level kinematics.



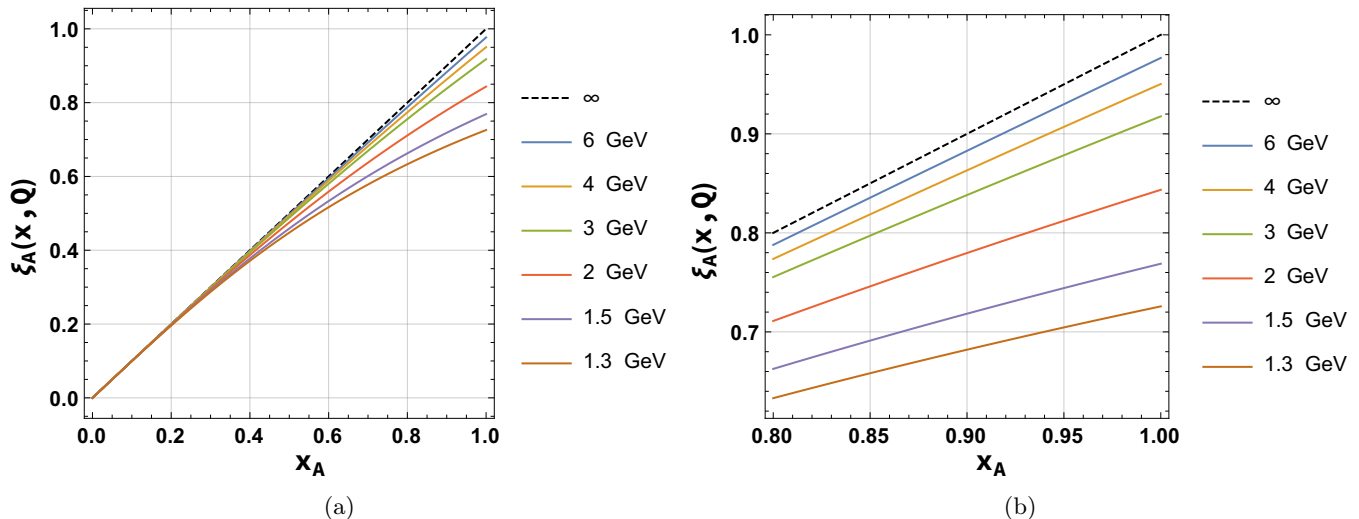


Figure 2.1: (a) The Nachtmann scaling variable  $\xi_A(x_A, Q)$  as a function of the Bjorken scaling variable  $x_A$  for a selection of  $Q$  values [GeV], as indicated in the legend, with  $M_A = M_{\text{proton}}$ . (b) Same as (a) but for large  $x_A$ . We observe that for large  $x_A$  and small  $Q$  values, the target mass  $M_A$  modifies the true (Nachtmann) scaling variable  $\xi_A$  relative to the usual Bjorken scaling variable  $x_A$ , *c.f.*, Ref. [73].

## 2.2. Leptonic and hadronic tensors in DIS from experimentally observable kinematics

Deep-inelastic scattering is a powerful, elucidating probe of the internal structure of nucleons and nuclei, *i.e.*, hadrons. This ability stems from the fact that under strong but general assumptions one can write the cross section for any sufficiently inclusive DIS process  $\ell_1 + A \xrightarrow{V} \ell_2 + X$  as a combination of: (a) leptonic and hadronic kinematics, which can be measured, and (b) hadronic structure functions, which parameterize the internal dynamics of  $A$ . This discussion is based solely on kinematics and symmetries, including Lorentz symmetry. The only approximation of consequence that is made when constructing structure functions *from experimentally observable kinematics* is the one where DIS is mediated by the exchange of only one electroweak boson. (Relaxing this has been explored elsewhere [79–82].) Apart from this assumption, expressions derived from kinematics are completely general: they take into account all twist contributions, at all orders in the strong coupling constant, and all hadron- and quark-mass effects. And in particular, the parton model does not need to be invoked.

Schematically, the differential DIS cross section  $d\sigma$  is proportional to the product of a leptonic tensor  $L^{\mu\nu}(k_1, k_2)$ , which is the square of the  $\ell_1 \rightarrow \ell_2 V$  splitting matrix element (the matrix element of the leptonic current), and a hadronic tensor  $\tilde{W}_{\mu\nu}^A(p_A, q)$ , which is proportional to the square of the  $AV \rightarrow X$  matrix element (the matrix element of the hadronic current). Subsequently,  $d\sigma$  can be written as

$$d\sigma \propto \tilde{W}_{\mu\nu}^A L^{\mu\nu} \quad , \quad (2.6)$$

and is given more completely by Eq. (A.6) in App. A.1. Often in the literature there are ambiguities as to whether a quantity in lepton-nucleus scattering is defined at the *nucleus* level or the *nucleon* level. Indeed, a key takeaway of this work is how the two levels are related in the DIS limit. Therefore, to maximize clarity, we denote hadronic quantities, *e.g.*, **structure functions, at the nucleus level using the tilde notation** ( $\tilde{\cdot}$ ). Hadronic quantities at the **nucleon** level do not use the tilde notation. We introduce this second notation in Sec. 4, where we perform a rescaling of nuclear momentum to average nucleon momentum.

The leptonic tensor can be constructed from Feynman diagrams for  $\ell_1 \rightarrow \ell_2 V$  splitting with standard methods, *e.g.*, trace technology or helicity amplitudes. For the case of massless charged leptons exchanging a

photon with the nucleus  $A$ , the spin-summed leptonic tensor for massless leptons is

$$\sum_{\{\lambda\}} L^{\mu\nu} \Big|_{\text{QED}} = 4e^2 \left\{ k_1^\mu k_2^\nu + k_1^\nu k_2^\mu - (k_1 \cdot k_2) g^{\mu\nu} \right\} . \quad (2.7)$$

Here,  $\{\lambda\}$  represents the sum over spins of external particles; spin-averaging is not yet performed. Analogous expressions for the exchange of the  $W$  and  $Z$  bosons can be found in App. A.2.

In practice, the tensor  $\tilde{W}_{\mu\nu}^A(p_A, q)$ , which can only be a function of external momenta  $p_A$  and  $q$  for unpolarized targets, is decomposed into a sum over tensor-valued coefficient functions multiplied by dimensionless, scalar-valued functions  $\tilde{W}_i$ . These  $\tilde{W}_i$  are known in the literature as ‘‘structure functions’’ since they parameterize the structure of nucleons and nuclei. Formally there are six<sup>5</sup> linearly independent  $\tilde{W}_i$  into which  $\tilde{W}_{\mu\nu}^A(p_A, q)$  can be decomposed. Lorentz symmetry and Hermiticity dictate that only certain combinations of  $p_A$  and  $q$  are allowed in the coefficient functions. For the case of an unpolarized (spin-averaged) nuclear target, the ‘‘hadronic’’ tensor  $\tilde{W}_{\mu\nu}^A(p_A, q)$ , in terms of the square of the  $AV \rightarrow X$  current  $J(z)$  in coordinate space, is given by

$$\tilde{W}_{\mu\nu}^A(p_A, q) \equiv \frac{1}{4\pi} \oint d^4z e^{iq \cdot z} \langle A(p_A) | J_\mu(z) | X(p_X) \rangle \langle X(p_X) | J_\nu(0) | A(p_A) \rangle \quad (2.8)$$

$$\begin{aligned} &= -g_{\mu\nu} \tilde{W}_1 + \frac{p_{A\mu} p_{A\nu}}{M_A^2} \tilde{W}_2 - i \epsilon_{\mu\nu\rho\sigma} \frac{p_A^\rho q^\sigma}{M_A^2} \tilde{W}_3 \\ &+ \frac{q_\mu q_\nu}{M_A^2} \tilde{W}_4 + \frac{p_{A\mu} q_\nu + p_{A\nu} q_\mu}{M_A^2} \tilde{W}_5 + \frac{p_{A\mu} q_\nu - p_{A\nu} q_\mu}{M_A^2} \tilde{W}_6 . \end{aligned} \quad (2.9)$$

In Eq. (2.8), the normalization factor  $1/(4\pi)$  is conventional and the sum and integral ( $\oint$ ) run over all discrete and continuous configurations of  $X$ , implying that  $\tilde{W}_{\mu\nu}^A(p_A, q)$  is inclusive with respect to  $X$  (see also App. A.2). We note that, although the targets considered in this work are unpolarized nuclei, we refer to quantities such as that given in Eq. (2.8) as a hadronic tensors, in keeping with convention. For a polarized target, the decomposition into structure functions takes on a more complicated structure, see e.g. [29, 74, 83–86]. In Sec. 3.2 and App. A.5, we review the connection between the  $\tilde{W}_i$  and the internal structure of  $A$ .

With further strong but reasonable assumptions, the number of structure functions appearing in Eq. (2.9) can be reduced in real-life calculations [87–89]. For instance:  $\tilde{W}_6$  is only nonzero if QCD violates time-reversal (or charge-parity) symmetry. (Whether  $\tilde{W}_6$  is actually zero is an alternative formulation of the ‘‘strong CP problem’’ of QCD.) The coefficients for  $\tilde{W}_4$  and  $\tilde{W}_5$  contain factors of  $q_\mu$  and  $q_\nu$ . This implies that the contractions with the leptonic tensor  $L^{\mu\nu} \cdot q_\mu$  and  $L^{\mu\nu} \cdot q_\nu$  are proportional to the masses of  $\ell_1$  and  $\ell_2$ , and therefore vanish when lepton masses are negligible.  $\tilde{W}_3$  is only nonzero if parity symmetry is violated; it therefore only appears for  $W$  and  $Z$  boson exchanges. In summary, if one considers only electromagnetic interactions, standard QCD, and ignores lepton masses, then  $\tilde{W}_{\mu\nu}^A(p_A, q)$  can be described entirely by  $\tilde{W}_1$  and  $\tilde{W}_2$ .

Modern notation calls for using the structure functions  $\tilde{F}_i$  rather than  $\tilde{W}_i$ . The mapping between the two sets of dimensionless structure functions is given by

$$\begin{aligned} &\{\tilde{F}_1, \tilde{F}_2, \tilde{F}_3, \tilde{F}_4, \tilde{F}_{5,6}\} \\ &= \left\{ \tilde{W}_1, \frac{Q^2}{2x_A M_A^2} \tilde{W}_2, \frac{Q^2}{x_A M_A^2} \tilde{W}_3, \frac{Q^2}{2M_A^2} \tilde{W}_4, \frac{Q^2}{2x_A M_A^2} \tilde{W}_{5,6} \right\} . \end{aligned} \quad (2.10)$$

The purpose of using  $\tilde{F}_i$  is to factor out known dependence on  $Q^2$  and make more manifest the phenomenon of scaling, i.e., that  $\tilde{F}_i$  depend only on  $x_A$ , a dimensionless quantity, up to small logarithmic QCD corrections.

<sup>5</sup>Since  $\tilde{W}_{\mu\nu}^A(p_A, q)$  is a tensor made from the product of Dirac fermion spinors, it is a bilinear, and subsequently has six independent components. For further details, see App. A.3. Separately, we will observe in Sec. 6 that using the helicity representation similar considerations (Lorentz invariance, angular momentum conservation) also yields six independent structure functions.

In the discussion that follows, we focus on  $\tilde{F}_1, \tilde{F}_2$ , and  $\tilde{F}_3$ . However, we include a detailed discussion of  $\tilde{F}_4$  and  $\tilde{F}_5$  in Appendix A. The structure functions  $\tilde{F}_4$  and  $\tilde{F}_5$  enter into differential cross sections, but are suppressed by a factor  $\mathcal{O}(\frac{m_\ell^2}{M_A E_\ell})$ , where  $m_\ell^2$  is the lepton mass squared,  $M_A$  is the mass of the hadronic target, and  $E_\ell$  is the energy of one of the external leptons [67]. This suppression is a consequence of contracting the symmetric leptonic tensor  $L^{\mu\nu}$  with  $q_\mu$  (or  $q_\nu$ ), which subsequently vanishes due to the conservation of weak currents by massless leptons. Notably, finite lepton-mass effects could be measured in  $\nu_\tau$ -DIS, such as at the SHIP, FASER, or SND@LHC detectors at CERN [31, 90–92]. As for  $\tilde{F}_6$ , which signifies charge-parity violation, the coefficient vanishes when contracted with Eq. (2.7). Hence, it does not contribute to the cross section.

### Considerations for spin-1 and greater

Contrary to a nucleon target with spin-1/2, nuclei can have spin-1 or greater. The case of a spin-1 nuclear targets in NC DIS with charged leptons has been discussed since the 80s [93]. At leading twist, i.e., twist  $\tau = 2$ , the additional effects of scattering on a polarized spin-1 target reside in a single new structure function  $\tilde{b}_1(x)$ . This structure function effectively measures the extent to which a target nucleus deviates from a trivial bound state of protons and neutrons. For the deuteron, it is expected that  $\tilde{b}_1 \approx 0$ , but for other nuclei one could have  $\tilde{b}_1 \sim \mathcal{O}(\tilde{F}_1)$ .

More generally, using gauge invariance and P- and T-invariance for the spin-1 case, the hadronic tensor can be expressed in terms of eight independent structure functions,  $\{\tilde{F}_1, \tilde{F}_2, \tilde{b}_{1,2,3,4}, \tilde{g}_1, \tilde{g}_2\}$ . Similar results are found for the hadronic tensor of a (space-like) virtual photon target [94]. The functions  $\tilde{F}_1$ ,  $\tilde{F}_2$ ,  $\tilde{g}_1$ , and  $\tilde{g}_2$  are analogous to the scaling structure functions of a spin-1/2 target.  $\tilde{F}_1$  and  $\tilde{F}_2$  can be measured in the DIS of unpolarized leptons off an unpolarized target whereas measurements of  $\tilde{g}_1$  and  $\tilde{g}_2$  require polarized lepton beams and a polarized target. The four structure functions  $\tilde{b}_{1,2,3,4}$  are new in the spin-1 case.  $\tilde{b}_{1,2}$  are quantities that appear at leading twist, while  $\tilde{b}_{3,4}$  appear at higher twist.  $\tilde{b}_{1,2}$  are connected via  $\tilde{b}_2 = 2x\tilde{b}_1$  in a manner analogous to the Callan-Gross relation, and will receive corrections beyond lowest order in QCD. The structure functions  $\tilde{b}_{1,2,3,4}$  can be measured using an unpolarized lepton beam but require a polarized spin-1 target. The TMCs for a (spin-1) deuterium target have been calculated [95] as well as those for a virtual photon target [96].

In this work we are studying unpolarized DIS of charged and neutral leptons off an unpolarized nucleus with any spin greater or equal to 1/2. For such circumstances, the hadronic tensor has the same decomposition into structure functions as for a spin-1/2 target. For this reason we focus only on the  $\tilde{F}_i$  structure functions in the remainder of this text; the treatment of additional structure functions, such as  $\tilde{b}_i$ , can be dealt with in a similar manner, but we shall not address them explicitly.

## 3. Nuclear structure functions in the OPE

In this section, we discuss nuclear structure functions and their TMCs in the context of the OPE. We start in Sec. 3.1 with a precise stipulation of the criteria for light-cone dominance involving nuclear targets, whose masses can readily exceed  $\mathcal{O}(50 - 100)$  GeV. In Sec. 3.2, we sketch the construction of nuclear structure functions and their TMCs in the OPE; a fuller derivation is given in App. A. We then present in Sec. 3.3 the main formula for nuclear TMCs in terms of nuclear quantities  $x_A$  and  $M_A$ .

### 3.1. Light-cone dominance of nuclear DIS

A crucial step in deriving structure functions for nucleons and nuclei involves employing the OPE to expand the product of currents that comprise the hadronic tensor of Eq. (2.8). This expansion, however, requires that one is in the limit of light-cone dominance, i.e.,  $z^2 \sim 0$ , where  $z$  is the Fourier conjugate of the DIS momentum  $q$ . While this is well-established in the case of a nucleon target,<sup>6</sup> demonstrating light-cone dominance for nuclear

<sup>6</sup>A demonstration of the light cone dominance of DIS can be found, for example, in the textbook by Muta [60, 61], see (2nd edition) pages 228-229 and 262.

targets requires care due to the relative sizes of  $Q^2 = -q^2 > 0$  and  $M_A^2$ .

In many constructions of PDFs and related quantities in DIS, light cone-dominance is described as corresponding to the momentum configuration

$$Q^2 \sim |p_N \cdot q| \gg M_N^2, \quad (3.1)$$

where  $p_N = p_A/A$  and  $M_N = M_A/A$  are respectively the four-momentum and mass of a single nucleon, *c.f.*, Table 4.1. Under this condition, naively replacing  $p_N$  and  $M_N$  by the nuclear momentum  $p_A$  and nuclear mass  $M_A$  would imply (incorrectly) that light-cone dominance is only satisfied when

$$Q^2 \sim |p_A \cdot q| \gg M_A^2. \quad [\text{Incorrect}] \quad (3.2)$$

This incorrect condition suggests increasingly large  $Q^2$  are needed for increasing  $A$ , and downplays the validity of both perturbative QCD and the parton model. For example: Eq. (3.2) implies that  $Q \gg 50$  GeV, which is more than half the  $Z$  boson's mass, would be needed to describe DIS data for  $^{56}\text{Fe}$ , or that  $Q \gg 180$  GeV, which is beyond the top quark's mass, would be needed for  $^{197}\text{Au}$ . Fortunately, this is not the case as Eq. (3.1) is the correct condition.

To resolve this, we apply the arguments of Refs. [60, 61] for light-cone dominance in DIS with a nucleon to the case of an arbitrary *nucleus*. Our goal is to identify the dominant contribution to the Fourier integral in Eq. (2.8) in the deeply inelastic limit:

$$Q^2 \rightarrow \infty, \quad \nu_A \rightarrow \infty, \quad \text{such that} \quad \frac{Q^2}{\nu_A} = 2M_A x_A \quad \text{is fixed.} \quad (3.3)$$

Note that in terms of averaged nuclear quantities, one has  $Q^2/\nu_A = Q^2/\nu_N = 2M_A x_A = 2M_N x_N$ . That is to say, a bigger nuclear mass  $M_A$  is compensated by a smaller Bjorken variable  $x_A$  such that the fixed quantity  $Q^2/\nu$  is independent of the atomic number.

Following Refs. [60, 61], we examine  $\tilde{W}_{\mu\nu}^A(p_A, q)$  in Eq. (2.8), and identify the integration regions that give rise to the dominant contributions. In the DIS limit of Eq. (3.3), as  $|q \cdot z| \rightarrow \infty$  the exponential of the Fourier integral oscillates without bound and thus makes a vanishing contribution to the integral. Therefore, we need only to consider the region with finite  $|q \cdot z|$  in the deeply inelastic regime.

In the target's rest frame,  $\nu_A = q_0$ . Defining the quantity  $\varkappa = \vec{q} \cdot \vec{z}/|\vec{q}|$ , we have

$$q \cdot z = q_0 z_0 - \vec{q} \cdot \vec{z} = \nu_A \left( z_0 - \frac{|\vec{q}|}{\nu_A} \varkappa \right) = \nu_A \left( z_0 - \sqrt{1 + Q^2/\nu_A^2} \varkappa \right), \quad (3.4)$$

since  $|\vec{q}|^2 = \nu_A^2 + Q^2$ . We note again that this equation is independent of  $A$ .

In the DIS limit,  $Q^2/\nu_A^2 = (2M_A x_A)/\nu_A$  is small and we can expand the square root:

$$q \cdot z = \nu_A(z_0 - \varkappa) - M_A x_A \varkappa + \mathcal{O}\left(\frac{M_A^2 \varkappa}{\nu_A}\right). \quad (3.5)$$

Here, the target mass  $M_A$  appears but only in combination with  $x_A$  and always satisfies  $M_A x_A = M_N x_N$ . In order to keep  $|q \cdot z|$  finite in the deeply inelastic limit, each term on the right hand side of Eq. (3.5) must separately be finite. (Being separately infinite requires the scaling  $(z_0 - \varkappa) \sim (\varkappa/\nu_A) \rightarrow \infty$ , which cannot be consistently satisfied.) Since  $M_A x_A$  is fixed,  $\varkappa$  itself must be finite. Therefore, for some constants  $c > 0$  and  $d > 0$ , one has

$$|z_0 - \varkappa| < c/\nu_A \quad \text{and} \quad |\varkappa| < d/(x_A M_A). \quad (3.6)$$

The first inequality implies that  $|z_0| < |\varkappa| + c/\nu_A$ . After squaring and using  $\varkappa^2 = \vec{z}^2 - z_1^2 < \vec{z}^2$ , where  $z_1$  is the

component of  $z$  orthogonal to  $\vec{q}$ , we obtain the inequality chain

$$z_0^2 < (|\not{z} + c/\nu_A)^2 = \not{z}^2 + \frac{2c|\not{z}|}{\nu_A} + \mathcal{O}\left(\frac{1}{\nu_A^2}\right) < \bar{z}^2 + \frac{2cd}{(x_A M_A \nu_A)} + \mathcal{O}\left(\frac{1}{\nu_A^2}\right). \quad (3.7)$$

To obtain the rightmost bound, we used the second inequality in Eq. (3.6). Using the rightmost equality in Eq. (3.3), we obtain the final result:

$$z^2 = z_0^2 - \bar{z}^2 < \frac{2cd}{(x_A M_A \nu_A)} + \mathcal{O}\left(\frac{1}{\nu_A^2}\right) = \frac{4cd}{Q^2} + \mathcal{O}\left(\frac{1}{\nu_A^2}\right). \quad (3.8)$$

We therefore find that the dominant region remains  $0 \leq z^2 \leq (2cd/Q^2)$ , and is independent of the target. This assumes, of course, that no extra  $A$  dependence is hidden in the constants  $c$  and  $d$ . Such an assumption, however, is safe upon inspecting the above derivation. For example: suppose there were separate (minimal)  $c_A$  and  $d_A$  for each  $A$  that satisfied the inequality of Eq. (3.6). Since there are finite many  $A$ , we can simply take the largest  $c_A$  and  $d_A$ , and then define  $c = \max\{c_A\}$  and  $d = \max\{d_A\}$ . This implies that there is a large enough  $c$  and  $d$  such that Eq. (3.6) holds independent of  $A$ .

In light of Eq. (3.8), the requirement of Eq. (3.2) is obviously too harsh. Instead, we advocate that Eq. (3.1) should be understood as requiring  $Q^2 \gtrsim$  a few  $\text{GeV}^2$ , independent of the hadronic target, in order to justify applying perturbative QCD and the parton model. Then, given a non-perturbative (NP) scale  $\Lambda_{\text{NP}} \lesssim 1 \text{ GeV}$ , which parameterizes the onset of hadronization, light-cone dominance in DIS for a nucleus  $A$  occurs when

$$Q^2 \sim |p_A \cdot q| \gg \Lambda_{\text{NP}}^2. \quad (3.9)$$

Under this criterion, Eq. (3.1) is automatically satisfied since nucleon masses scale as  $M_N \sim \Lambda_{\text{NP}}$ . At smaller  $Q^2$ , but still satisfying  $Q^2 \gtrsim \Lambda_{\text{NP}}^2$ , perturbative techniques and the parton model can still be employed as evident by the phenomenon of ‘‘precocious scaling’’ [58, 59, 66]. This denotes the onset of Bjorken scaling at moderate energies despite  $\alpha_s(\mu_r = Q) \lesssim \mathcal{O}(1)$  being sizable, and follows from the fact that light quark masses  $m_q$  are comparable to the scale of the QCD Landau pole,  $\Lambda_{\text{QCD}} \sim \mathcal{O}(0.1) \text{ GeV}$ .

Such a separation of scales implies the inequality

$$Q^2 \gtrsim \Lambda_{\text{NP}}^2 \gg \Lambda_{\text{QCD}}^2 \sim m_q^2, \quad (3.10)$$

where we take  $m_q$  to be the light-quark constituent mass at soft quark momenta. This demonstrates that, up to corrections of order  $\mathcal{O}(\Lambda_{\text{QCD}}^2/Q^2)$ , light quarks can be approximated as free and massless partons, even for low  $Q^2$ . However, when such  $Q^2$  is probing a nuclear target  $A$  at large  $x_A$ , it is paramount to stress that  $x_A^2 M_A^2/Q^2$  is not guaranteed to be small or below unity. In this case, TMCs are important.

### 3.2. Structure functions in the OPE

In this section, we briefly outline the key elements of the OPE required to obtain expressions for structure functions with TMCs at leading twist  $\tau$ . Formally, TMCs are  $\mathcal{O}(x_A M_A^2/Q^2)$  corrections to structure functions that are first generated by the *same* operators that define the structure functions themselves at leading power. For this reason they are sometimes called ‘‘kinematical’’ power corrections [62, 63]. Such power corrections can be isolated from ‘‘dynamical’’ power corrections, by setting powers of  $(M_A^2/Q^2)$  in the OPE to zero. We generally follow the early literature of Refs. [58, 59, 66, 78, 88, 97], which shed light on the underlying dynamics of hadrons, but note that TMCs can also be derived using diagrammatic methods and finite parton  $k_T$  [62, 63]. While we only outline the derivation here, a fuller derivation of nuclear structure functions and their TMCs at leading power in the OPE is provided in App. A.

Constructing TMCs for structure functions in the OPE provides a systematic organization of short and long distance physics that does not manifestly rely on the perturbativity of QCD. (This means that it is possible to obtain results that are all orders in  $\alpha_s$ .) Inspired by the program of Refs. [58, 59], the construction of structure

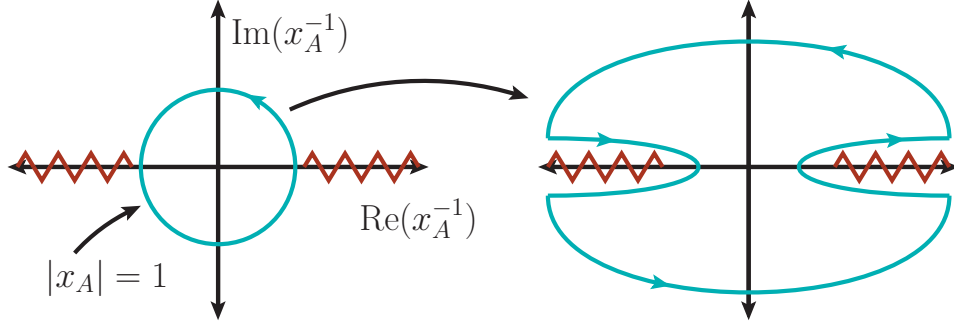


Figure 3.1: (Left) A contour (circle) along the radius of convergence of the time-ordered matrix element  $\tilde{T}_{\mu\nu}^A(p_A, q)$  in the complex  $(1/x_A)$  plane for  $\gamma^*A \rightarrow \gamma^*A$  scattering. Branch cuts (sawtooth lines) are along the real axis at  $x_A^{-1} < -1$  and  $x_A^{-1} > 1$ . (Right) A deformation of the contour along the branch cuts with vanishing arcs.

functions follows by first recognizing that the inclusive hadronic tensor describing  $\gamma^*A \rightarrow X$  scattering in the deeply inelastic limit,<sup>7</sup>

$$\tilde{W}_{\mu\nu}^A(p_A, q) = \frac{1}{4\pi} \int d^4z e^{iq \cdot z} \langle A | J_{XA\mu}^\dagger(z) J_{XA\nu}(0) | A \rangle, \quad (3.11)$$

which is equivalent to the expression in Eq. (2.8) of Sec. 2.2 [for details, see below Eq. (A.25)], and the time-ordered amplitude for virtual Compton scattering process  $\gamma^*A \rightarrow \gamma^*A$  in the short-distance limit

$$\tilde{T}_{\mu\nu}^A(p_A, q) \equiv \int d^4z e^{iq \cdot z} \langle A | \mathcal{T} J_{A\mu}^\dagger(z) J_{A\nu}(0) | A \rangle, \quad (3.12)$$

$$\begin{aligned} &= -g_{\mu\nu} \Delta \tilde{T}_1^A + \frac{p_{A\mu} p_{A\nu}}{M_A^2} \Delta \tilde{T}_2^A - i \epsilon_{\mu\nu\alpha\beta} \frac{p_A^\alpha q^\beta}{M_A^2} \Delta \tilde{T}_3^A \\ &+ \frac{q_\mu q_\nu}{M_A^2} \Delta \tilde{T}_4^A + \frac{(p_{A\mu} q_\nu \pm p_{A\nu} q_\mu)}{M_A^2} \Delta \tilde{T}_{5,6}^A, \end{aligned} \quad (3.13)$$

are related by the following dispersion relationship [49, 88]

$$\tilde{T}_{\mu\nu}^A(p_A, q) \Big|_{(1/x_A)-i\epsilon}^{(1/x_A)+i\epsilon} = 4\pi \tilde{W}_{\mu\nu}^A(p_A, q), \quad \text{for } x_A > 0, \quad (3.14a)$$

$$\tilde{T}_{\mu\nu}^A(p_A, q) \Big|_{(1/x_A)+i\epsilon}^{(1/x_A)-i\epsilon} = 4\pi [\tilde{W}_{\mu\nu}^A(p_A, -q)]^\dagger, \quad \text{for } x_A < 0. \quad (3.14b)$$

In Eq. (3.13),  $\tilde{T}_{\mu\nu}^A(p_A, q)$  is decomposed into coefficients of Lorentz structures in the same manner as  $\tilde{W}_{\mu\nu}^A(p_A, q)$  in Eq. (2.9). As  $\tilde{T}_{\mu\nu}^A(p_A, q)$  is time ordered, the first (second) relation in Eq. (3.14) is for DIS with (anti)particles. We assume here and below that the hadronic currents  $J_A^\mu$  and  $J_A^\nu$  are always renormalized objects in QCD.

The distinction between the short-distance limit and the DIS limit is important. In the DIS limit,  $(Q^2/M_A^2) \rightarrow \infty$  while  $x_A = (Q^2/2p_A \cdot q)$  is fixed. In the short-distance limit,  $(Q^2/M_A^2) \rightarrow \infty$  while  $x_A/Q$  is fixed, meaning that  $x_A$  grows with  $(Q/M_A)$ ; equivalently, the quantity  $(1/x_A)$  is small with increasing  $(Q/M_A)$  in the short-distance limit. Formally,  $\tilde{T}_{\mu\nu}^A(p_A, q)$  and  $\tilde{W}_{\mu\nu}^A(p_A, q)$  are defined in two different limits but can be related through analytic continuation. When analytically continued to complex values of  $x_A$ ,  $\tilde{T}_{\mu\nu}^A$  has desirable analytic properties for  $|(1/x_A)| < 1$  (the short-distance limit), whereas  $\tilde{W}_{\mu\nu}^A$  is meaningful for  $|(1/x_A)| > 1$  (the DIS limit). Hence the discontinuities (branch cuts) of  $\tilde{T}_{\mu\nu}^A$  correspond to the kinematics of DIS. Therefore, one can take  $\tilde{T}_{\mu\nu}^A(p_A, q)$ ,

<sup>7</sup>The subscripts  $XA$  on the vector currents  $J_\mu, J_\nu$  are simply labels to denote the hadronic current that takes  $A$  to  $X$ . The current is independent of states  $A, X$  but depends on whether the current is electromagnetic or weak.



decompose it into a contour integral over  $x_A^{-1}$  using Cauchy's integral formula, and deform the contour around the discontinuities at  $x_A^{-1} < 1$  and  $x_A^{-1} > 1$  as shown in Fig. 3.1. (The sawtooth lines along  $|x_A^{-1}| > 1$  are the branch cuts of  $\tilde{T}_{\mu\nu}^A$ .) Taking the difference of  $T_{\mu\nu}^A$  when evaluated just below and above the branch cut, i.e., at the points  $x_A^{-1} \pm i\varepsilon$  for  $x_A^{-1} > 1$ , gives  $\tilde{W}_{\mu\nu}^A(p_A, q)$ . (For a fuller derivation, see above Eq. (A.45) in App. A.3.)

An important consequence of Eq. (3.14) is establishing a link between individual  $\Delta\tilde{T}_i^A$  in Eq. (3.13) and the Mellin moments of the structure functions  $\tilde{F}_i^A$  defined in Eq. (2.10). Following the steps below Eq. (A.49) in App. A.3, one can write for the case<sup>8</sup> of  $\tilde{F}_2$  [88]

$$\left(\frac{Q^2}{2x_A M_A^2}\right) \Delta\tilde{T}_2^A(x_A, Q^2) = -4i \sum_{N=0}^{\infty} \tilde{F}_2^{AN}(Q^2) x_A^{-N}. \quad (3.15a)$$

Here,  $\tilde{F}_i^{AN}(Q^2)$  is the  $N^{\text{th}}$  Mellin moment of the structure function  $\tilde{F}_i^A(x_A, Q^2)$ . The normalizations of the Mellin transformation and its inverse are set by the definitions

$$F^N = \int_0^1 dz z^{N-1} F(z) \quad \text{with} \quad F(z) = \frac{1}{2\pi i} \int_{c-i\infty}^{c+i\infty} dN z^{-N} F^N, \quad (3.16)$$

where  $c$  has to be to the right of any poles of  $F^N$  in the complex  $N$ -plane. As a brief comment, the Mellin transform is an integral over the positive reals, while the inverse transform is an integral over the complex plane. We therefore assume that structure functions can be analytically continued. (In practice, Mellin and inverse-Mellin transforms are implemented in the many computer codes that perform the DGLAP evolution equations in Mellin space, see e.g. Ref. [98].)

The next step in deriving TMCs in the OPE formalism is to take the operator-product expansion of  $\tilde{T}_{\mu\nu}^A$  itself in the short-distance limit. After considerable reorganization (see App. A.3), one obtains expressions (see App. A.4) for  $\Delta\tilde{T}_i^A(x_A, Q^2)$  at leading power in the OPE. More specifically, one constructs a power series with respect to powers of  $x_A^{-1}$ , and therefore obtains expressions for  $\tilde{F}_i^{AN}(Q^2)$ , at leading power / leading twist.

In more detail: the OPE makes use of basic symmetries, e.g., Lorentz invariance and unitarity, to expand hadronic matrix elements into a complete set of local operators  $\mathcal{O}$  [99]. For forward Compton scattering, the OPE of  $\tilde{T}_{\mu\nu}^A$  is given by [49]:

$$\begin{aligned} \lim_{z \rightarrow 0} T_{\mu\nu}^A(p_A, q) &\stackrel{\text{OPE}}{=} -2i \sum_{\ell, n} c_{\mu\nu\mu_1 \dots \mu_n}^{\tau=2, \ell}(q) \langle A | \mathcal{O}_{\ell, \tau=2}^{\mu_1 \dots \mu_n} | A \rangle + \text{power corrections at } \mathcal{O}(\tau > 2) \quad (3.17) \\ &= -2i \sum_{k=k_{\min}}^{\infty} \left[ -2g^{\mu\nu} q_{\mu_1} q_{\mu_2} C_1^{2k} + g_{\mu_1}^{\mu} g_{\mu_2}^{\nu} Q^2 C_2^{2k} - i\epsilon^{\mu\nu\alpha\beta} g_{\alpha\mu_1} q_{\beta} q_{\mu_2} C_3^{2k} \right. \\ &\quad \left. + 4\frac{q^{\mu} q^{\nu}}{Q^2} q_{\mu_1} q_{\mu_2} C_4^{2k} + 2(g_{\mu_1}^{\mu} q^{\nu} q_{\mu_2} \pm g_{\mu_1}^{\nu} q^{\mu} q_{\mu_2}) C_{5,6}^{2k} \right] \cdot \begin{cases} 1; & k=1 \\ \prod_{m=3}^{2k} q_{\mu_m}; & k>1 \end{cases} \\ &\quad \times \frac{2^{2k}}{Q^{4k}} A_{\tau=2}^{2k} \tilde{\Pi}^{\mu_1 \dots \mu_{2k}} + \mathcal{O}(\tau > 2). \quad (3.18) \end{aligned}$$

In Eq. (3.18), the summation over  $n$  is set to  $n = 2k$ . The starting point for the summation over  $k$  depends on the particular Wilson coefficient; specifically,  $k_{\min} = 2$  for  $C_2^{2k}$ , while  $k_{\min} = 1$  for all other  $C_t^{2k}$ 's. In Eq. (3.17), the  $\mathcal{O}_{\ell, \tau}^{\mu_1 \dots \mu_n}$  are composite local operators, consisting of quark fields, QCD covariant derivatives, and/or gluon field strengths. Operators with  $n$  un-contracted Lorentz indices carry a spin of  $n$ . Operators and their coefficients are organized according to their twist  $\tau = d - n$ , where  $d$  is the dimensionality of  $\mathcal{O}_{\ell, \tau}^{\mu_1 \dots \mu_n}$  in the standard sense of dimension power counting in an effective field theory. In this study, we focus exclusively on the OPE at leading twist, i.e.,  $\tau = 2$ . We neglect power corrections at  $\tau > 2$  but attempt to keep track of their presence. The index  $\ell$  catalogs all operators  $\mathcal{O}$  at a fixed spin and twist. All numerical prefactors are sequestered into effective Wilson

<sup>8</sup>See App. A.3 for the treatment of all six  $\tilde{F}_i^A$ .

coefficients  $c_{\mu\nu\mu_1\dots\mu_n}^{\tau,\iota}(q)$ , which are only functions of the external momentum  $q$ .

The Wilson coefficients<sup>9</sup>  $C_\iota^{2k}$ , which are the same for all possible nuclei, can be identified and matched to quantities calculated in perturbative QCD. The quantity  $A_{\tau=2}^{2k}$  is the scalar-valued coefficient of the expectation value  $\langle A | \mathcal{O}_{\iota,\tau=2}^{\mu_1\dots\mu_{2k}} | A \rangle = A_{\tau=2}^{2k} \times \tilde{\Pi}^{\mu_1\dots\mu_{2k}}$ .  $A_{\tau=2}^{2k}$  is sometimes labeled as the ‘‘reduced matrix element’’ of  $\langle A | \mathcal{O}_{\iota,\tau=2}^{\mu_1\dots\mu_{2k}} | A \rangle$ . Importantly, the Lorentz structure of this expectation value ( $\tilde{\Pi}^{\mu_1\dots\mu_{2k}}$ ) can only be a function of  $p_A$  as the  $q$  dependence is sequestered elsewhere. Consequentially,  $\tilde{\Pi}^{\mu_1\dots\mu_{2k}}$  can be organized according to permutations and powers of momenta  $p_A^{\mu_m}$  and metrics  $g^{\mu_m\mu_n}$ , and scales as [58, 59]

$$\tilde{\Pi}^{\mu_1\dots\mu_{2k}} = \sum_{j=0}^k (-1)^j \frac{(2k-j)!}{2^j (2k)!} \underbrace{\{g\dots g\}}_{j \text{ } g^{\mu_n\mu_m\prime_s}} \underbrace{\{p_A\dots p_A\}}_{(2k-2j) \text{ } p_A^{\mu_n\prime_s}} (p_A^2)^j + \text{power corrections} \quad (3.19)$$

$$\sim \underbrace{\{p_A\dots p_A\}}_{2k \text{ } p_A^{\mu_m}} + \underbrace{\{p_A\dots p_A\}}_{(2k-2) \text{ } p_A^{\mu_m}} \underbrace{\{g\dots g\}}_{1 \text{ } g^{\mu_m\mu_n}} (p_A^2)^1 + \underbrace{\{p_A\dots p_A\}}_{(2k-4) \text{ } p_A^{\mu_m}} \underbrace{\{g\dots g\}}_{2 \text{ } g^{\mu_m\mu_n}} (p_A^2)^2 + \dots \quad (3.20)$$

Focusing on Eq. (3.20), one sees that the momentum factor  $\tilde{\Pi}^{\mu_1\dots\mu_{2k}}$  scales as a tower of momentum and mass terms. For a fixed index  $k$ , the series ranges from the product of  $2k$  instances of the nucleus’ momentum  $p_A^{\mu_m}$  and no instance of the nucleus’ mass  $p_A^2 = M_A^2$  (as shown in the leftmost term), to no instances of  $p_A^{\mu_m}$  but one instance of  $(p_A^2)^k = (M_A^2)^k$ . The brackets  $\{\dots\}$  represent the collection of all possible permutations of Lorentz indices. The dimension of each term is  $[\text{mass}]^{2k}$ . Again, we neglect higher-order power corrections.

Whether one retains  $(M_A^2)^j$  terms or neglects them outright is the distinction between obtaining structure functions with TMCs or obtaining structure functions without TMCs (which we shall later label as ‘‘No-TMC’’). For example: after contracting all Lorentz indices in Eq. (3.18), one can neglect all factors of  $(M_A^2/Q^2)$ . This is equivalent to truncating the summation in Eq. (3.19) at  $j=0$ . Doing so and comparing the result to Eq. (3.15) recovers (see App. A.5 for details):

$$\tilde{F}_i^{AN} = \int_0^1 dy y^{N-1} \tilde{F}_i^A(y, Q^2) = C_i^N(Q^2) A_{\tau=2}^N + \text{power corrections}, \quad \text{for } i = 1, 3, 4, 5, \quad (3.21a)$$

$$\tilde{F}_2^{A(N-1)} = \int_0^1 dy y^{N-2} \tilde{F}_2^A(y, Q^2) = C_2^N(Q^2) A_{\tau=2}^N + \text{power corrections}. \quad (3.21b)$$

Non-trivially, Eq. (3.21) states that one can identify the product of the Wilson coefficient and reduced hadronic matrix element,  $(C_\iota^{2k} A_{\tau=2}^{2k})$ , as integer Mellin moments of structure functions, up to power corrections. (We note that footnote 9 is still applicable.)

If one does not truncate the momentum factor  $\tilde{\Pi}^{\mu_1\dots\mu_{2k}}$  in Eq. (3.19) at  $j=0$  and instead retains the sums over all  $j$ , and hence retains the sum over powers of  $p_A^2 = M_A^2$ , then one obtains expressions that are analogous to Eq. (3.21). For example: one can identify the Mellin transformation of the structure function  $F_2$  with a nonzero target mass as the product  $(C_{\iota=2}^{2k} A_{\tau=2}^{2k})$  with a coefficient proportional to  $(M_A^2/Q^2)^j$ :

$$\int_0^1 dx_A x_A^{N-2} \tilde{F}_2^{A,\text{TMC}}(x_A, Q^2) = \sum_{j=0}^{\infty} \left( \frac{M_A^2}{Q^2} \right)^j \frac{(N+j)!}{j! (N-2)!} \frac{C_2^{N+2j} A_{\tau=2}^{N+2j}}{(N+2j)(N+2j-1)}. \quad (3.22)$$

Similar expressions can be found in App. A.5 for the other structure functions. Intuitively, the right hand side of Eq. (3.22) states that structure functions with TMCs can be thought simply as the product (in moment space) of a structure function for a massless target, i.e., the  $(C_\iota A_{\tau=2})$  factor, and a kinematical factor, i.e., everything else. For this reason, the TMCs under discussion are sometimes called ‘‘purely kinematical’’ [62, 63, 100]. It is not obvious but, with the use of generating functions, the inverse-Mellin transform of Eq. (3.22) has a closed

<sup>9</sup>In principle, the Wilson coefficients  $C_\iota^{2k}$  also carry a species index  $f$ , which runs over the gluon and quark flavors. In this case,  $C_\iota^{2k}$  should be replaced by  $\sum_{f=u,g,\bar{d},\dots} C_{if}^{2k}$ , but this dependence is implicit here for simplicity.

form [58, 59, 95]. That is to say, one can obtain concise expressions for structure functions with TMCs in terms of structure functions for a massless target in  $x$ -space. These results are summarized in the following section for  $F_1^A, F_2^A$ , and  $F_3^A$ , and in App. A.5 for all  $F_i$ .

### 3.3. Master formula for structure functions with TMCs in $\ell A$ DIS

Following the procedure outlined in Sec. 3.2, we obtain a set of master formulae for twist-2 target mass corrections to structure functions for nuclei that are similar to those in Eq. (23) in Ref. [73] for nucleons. Using the notation of Refs. [67, 73], the general formula for target mass-corrected structure functions  $F_j^{A,\text{TMC}}$  for  $j = 1, \dots, 6$  reads:

$$\tilde{F}_j^{A,\text{TMC}}(x_A, Q^2) = \sum_{i=1}^6 A_j^i \tilde{F}_i^{A,(0)}(\xi_A, Q^2) + B_j^i \tilde{h}_i^A(\xi_A, Q^2) + C_j \tilde{g}_2^A(\xi_A, Q^2). \quad (3.23)$$

On the left-hand side, the  $F_j^{A,\text{TMC}}$  take as arguments the Bjorken scaling variable  $x_A$  and scale  $Q$ ; on the right-hand side, individual terms are given in terms of structure functions for massless nuclei  $\tilde{F}_i^{A,(0)}$ , which take as arguments the Nachtmann variable  $\xi_A$  and scale  $Q$ . The coefficients  $A_j^i, B_j^i, C_j$  are derived in App. A, and are the same that are given in Tables I, II, III in Ref. [67] for  $j = 1, \dots, 5$ . To our knowledge, TMCs for  $\tilde{F}_6^A$  have not been previously published.

Suppressing the  $Q^2$  dependence for brevity, one finds at twist  $\tau = 2$  the following:

$$\tilde{F}_1^{A,\text{TMC}}(x_A) = \left( \frac{x_A}{\xi_A r_A} \right) \tilde{F}_1^{A,(0)}(\xi_A) + \left( \frac{M_A^2 x_A^2}{Q^2 r_A^2} \right) \tilde{h}_2^A(\xi_A) + \left( \frac{2M_A^4 x_A^3}{Q^4 r_A^3} \right) \tilde{g}_2^A(\xi_A), \quad (3.24a)$$

$$\tilde{F}_2^{A,\text{TMC}}(x_A) = \left( \frac{x_A^2}{\xi_A^2 r_A^3} \right) \tilde{F}_2^{A,(0)}(\xi_A) + \left( \frac{6M_A^2 x_A^3}{Q^2 r_A^4} \right) \tilde{h}_2^A(\xi_A) + \left( \frac{12M_A^4 x_A^4}{Q^4 r_A^5} \right) \tilde{g}_2^A(\xi_A), \quad (3.24b)$$

$$\tilde{F}_3^{A,\text{TMC}}(x_A) = \left( \frac{x_A}{\xi_A r_A^2} \right) \tilde{F}_3^{A,(0)}(\xi_A) + \left( \frac{2M_A^2 x_A^2}{Q^2 r_A^3} \right) \tilde{h}_3^A(\xi_A), \quad (3.24c)$$

$$\begin{aligned} \tilde{F}_4^{A,\text{TMC}}(x_A) &= \left( \frac{x_A}{\xi_A r_A} \right) \tilde{F}_4^{A,(0)}(\xi_A) - \left( \frac{2M_A^2 x_A^2}{Q^2 r_A^2} \right) \tilde{F}_5^{A,(0)}(\xi_A) + \left( \frac{M_A^4 x_A^3}{Q^4 r_A^3} \right) \tilde{F}_2^{A,(0)}(\xi_A) \\ &+ \left( \frac{M_A^2 x_A^2}{Q^2 r_A^3} \right) \tilde{h}_5^A(\xi_A) - \left( \frac{2M_A^4 x_A^4}{Q^4 r_A^4} \right) (2 - \xi_A^2 M_A^2 / Q^2) \tilde{h}_2^A(\xi_A) \\ &+ \left( \frac{2M_A^4 x_A^3}{Q^4 r_A^5} \right) (1 - 2x_A^2 M_A^2 / Q^2) \tilde{g}_2^A(\xi_A), \end{aligned} \quad (3.24d)$$

$$\begin{aligned} \tilde{F}_5^{A,\text{TMC}}(x_A) &= \left( \frac{x_A}{\xi_A r_A^2} \right) \tilde{F}_5^{A,(0)}(\xi_A) - \left( \frac{M_A^2 x_A^2}{Q^2 r_A^3 \xi_A} \right) \tilde{F}_2^{A,(0)}(\xi_A) \\ &+ \left( \frac{M_A^2 x_A^2}{Q^2 r_A^3} \right) \tilde{h}_5^A(\xi_A) - \left( \frac{2M_A^2 x_A^2}{Q^2 r_A^4} \right) (1 - x_A \xi_A M_A^2 / Q^2) \tilde{h}_2^A(\xi_A) \\ &+ \left( \frac{6M_A^4 x_A^3}{Q^4 r_A^5} \right) \tilde{g}_2^A(\xi_A), \end{aligned} \quad (3.24e)$$

$$\tilde{F}_6^{A,\text{TMC}}(x_A) = \left( \frac{x_A}{\xi_A r_A^2} \right) \tilde{F}_6^{A,(0)}(\xi_A) + \left( \frac{2M_A^2 x_A^2}{Q^2 r_A^3} \right) \tilde{h}_6^A(\xi_A). \quad (3.24f)$$

We remind the reader that the tilde notation ( $\sim$ ) on the  $\tilde{F}_i$  structure functions indicates these are for **nuclei**; we will consider **nucleon** structure functions  $F_i$  in the following section. Here, the functions  $\tilde{h}_i^A(\xi_A, Q^2)$  and  $\tilde{g}_2^A(\xi_A, Q^2)$  are given by the integrals

$$\tilde{h}_2^A(\xi_A, Q^2) = \int_{\xi_A}^1 du_A \frac{\tilde{F}_2^{A,(0)}(u_A, Q^2)}{u_A^2}, \quad (3.25a)$$

$$\tilde{h}_3^A(\xi_A, Q^2) = \int_{\xi_A}^1 du_A \frac{\tilde{F}_3^{A,(0)}(u_A, Q^2)}{u_A}, \quad (3.25d)$$

$$\tilde{h}_5^A(\xi_A, Q^2) = \int_{\xi_A}^1 du_A \frac{2\tilde{F}_5^{A,(0)}(u_A, Q^2)}{u_A}, \quad (3.25b)$$

$$\tilde{h}_6^A(\xi_A, Q^2) = \int_{\xi_A}^1 du_A \frac{\tilde{F}_6^{A,(0)}(u_A, Q^2)}{u_A}. \quad (3.25e)$$

$$\tilde{g}_2^A(\xi_A, Q^2) = \int_{\xi_A}^1 du_A \tilde{h}_2^A(u_A, Q^2), \quad (3.25c)$$

The equation Eq. (3.23) does not assume or imply any Callan-Gross relation [101] between  $F_1$  and  $F_2$ . This relationship is typically presented as the equality  $2xF_1 = F_2$  and is a prediction of the (massless) quark-parton model at leading order in the asymptotic limit, where  $Q^2 \rightarrow \infty$ . At this same order and without any mass contributions (either hadronic or partonic), the longitudinal structure function is given by  $F_L = F_2 - 2xF_1$ . Thus, Callan-Gross is a statement regarding  $F_L$ . This relation is modified if we include masses (either hadronic masses or partonic masses), e.g., via helicity inversion, or if we include contributions beyond leading order in QCD. Furthermore, were there elementary constituents in hadrons with spin zero, i.e., scalar quarks or scalar gluons, then these would contribute to the longitudinal structure function  $F_L$  at leading order. Thus, the Callan-Gross relation also implies that there are no elementary scalar (spin zero) constituents of a hadron.

Using the above, one can also compute the longitudinal structure function with TMCs and obtain:

$$\begin{aligned} \tilde{F}_L^{A,\text{TMC}}(x_A) &= r_A^2 \tilde{F}_2^{A,\text{TMC}}(x_A) - 2x_A \tilde{F}_1^{A,\text{TMC}}(x_A) \\ &= \frac{x_A^2}{\xi_A^2 r_A} [\tilde{F}_2^{A,(0)}(\xi_A) - 2\xi_A \tilde{F}_1^{A,(0)}(\xi_A)] + \frac{4M_A^2 x_A^3}{Q^2 r_A^2} \tilde{h}_2^A(\xi_A) + \frac{8M_A^4 x_A^4}{Q^4 r_A^3} \tilde{g}_2^A(\xi_A) \\ &= \frac{x_A^2}{\xi_A^2 r_A} \tilde{F}_L^{A,(0)}(\xi_A) + \frac{4M_A^2 x_A^3}{Q^2 r_A^2} \tilde{h}_2^A(\xi_A) + \frac{8M_A^4 x_A^4}{Q^4 r_A^3} \tilde{g}_2^A(\xi_A). \end{aligned} \quad (3.26)$$

This general result is non-zero and thus violates the Callan-Gross relation, as it should. The leading term  $\tilde{F}_L^{A,(0)}$  will be non-zero for finite quark masses, and the sub-leading terms  $\tilde{h}_2^A, \tilde{g}_2^A$  contribute for finite hadron mass  $M_A$ . Note that effects from heavy quark masses are separate from the  $M_A$ -modifications of the Nachtmann variable  $\xi_A$ , and are taken into account in the  $\tilde{F}_i^{A,(0)}$  as outlined in Sec. 4 and Ref. [73]; we address this in Sec. 4.3.

## Remarks

Note that the formula for TMCs in Eq. (3.23) was derived without invoking *perturbative* QCD. In principle, one can start from matrix elements that describe collinear parton splitting at some fixed order in perturbative QCD, construct structure functions, compare to  $\tilde{T}_{\mu\nu}^A$  in Eq. (3.18), and obtain expressions for  $C_\ell^{2k}$  at some power in the strong coupling constant  $\alpha_s$ . However, by constructing structure functions in the OPE the Wilson coefficients  $C_\ell^{2k}$  in Eq. (3.18) are exact quantities, i.e., they are defined at all orders in  $\alpha_s$ . (Expanding  $C_\ell^{2k}$  in powers of  $\alpha_s$  would then yield the perturbative QCD result.) Ultimately, this implies that all the  $\alpha_s$  dependence of  $\tilde{F}_i^{A,\text{TMC}}$  is contained in  $\tilde{F}_i^{A,(0)}$ . This also means that the coefficients  $A_j^i, B_j^i$  and  $C_j$ , and the variable  $\xi_A$  are the same irrespective of the order (LO, NLO, NNLO, ...) at which the structure functions  $\tilde{F}_i^{A,(0)}$  are considered.

In the above expressions for  $F_i^{\text{TMC}}$ , we emphasize that it is  $(x_A, Q^2)$  and not  $(\xi_A, Q^2)$  that is the correct point in phase space to evaluate structure functions. While on the surface it may appear strange to have the left-hand side of Eq. (3.23) to be a function of  $x_A$  while the right-hand side be a function of  $\xi_A$ , this difference arises naturally in the calculation. In particular, final-state kinematics in  $\ell A$  DIS are constrained by momentum conservation, with  $\delta^4(q + P_A - P_X) \sim \delta(x_A - \xi_A)$ . Thus, we can write schematically

$$F_i^{\text{TMC}}(x_A, Q^2) \sim F_i^{(0)}(x_A, Q^2) \delta(x_A - \xi_A) \sim F_i^{(0)}(\xi_A, Q^2). \quad (3.27)$$

Note that it would be incorrect to write  $F_i^{\text{TMC}}(\xi_A, Q^2) \sim F_i^{(0)}(\xi_A, Q^2)$ , as the Mellin and inverse-Mellin transformations in Sec. 3.2 are defined with respect to  $x_A$ , not  $\xi_A$ .

Another feature of Eq. (3.23) is that  $h_2$  and  $g_2$  appear in the formulae for both  $F_1^{\text{TMC}}$  and  $F_2^{\text{TMC}}$ , and is an example of the phenomenon of structure function mixing. This follows directly from the forms of  $\tilde{T}_{\mu\nu}^A$  and the momentum factor  $\tilde{\Pi}$  in Eq. (3.18), in the massive target limit. For example: the terms proportional to  $C_1^{2k}$  and to  $C_2^{2k}$  both contribute to  $\Delta\tilde{T}^{A,1}$ , which multiplies the Lorentz structure  $-g_{\mu\nu}$  in Eq. (3.18). As shown in Eq. (3.20),  $\tilde{\Pi}$  in the massive-target limit is proportional to terms that (a) consist exclusively of  $p_A^{\mu n}$  factors as well as to terms that (b) include factors of momentum  $p_A^{\mu n}$ , metric  $g^{\mu m \mu n}$ , and mass  $M_A$ . Among the many possible contractions in Eq. (3.18) are the “(a)” terms contracting with the  $C_1^{2k}$  term and the “(b)” terms contracting with the  $C_2^{2k}$  term. Both sets of contractions generate a term proportional to  $-g_{\mu\nu}$ . However, the “(b)” set of contractions only enters  $\Delta\tilde{T}^{A,1}$  as a TMC, i.e., it vanishes in the  $(M_A^2/Q^2) \rightarrow 0$  limit. Arguably, one can think of  $C_1^{2k}$  feeding into  $F_1^{\text{TMC}}$  as a helicity-conserving contribution, which survives in the massless limit, whereas the contribution from  $C_2^{2k}$  is a helicity-inverting contribution, which vanishes in the massless limit.

## 4. Rescaling

In this section we introduce a rescaling between the nuclear and averaged nucleon kinematics. Many of the key relations are summarized in Table 4.1. We typically identify the nuclear variables with an “A” subscript ( $x_A, \xi_A, r_A$ ), and those of the nucleon with an “N” subscript ( $x_N, \xi_N, r_N$ ). Similarly, the original nuclear structure functions are identified with a tilde ( $\tilde{W}, \tilde{F}$ ), while those re-scaled to the kinematics of an averaged nucleon are without ( $W, F$ ).

### 4.1. Nuclear and nucleon kinematics

From Eqs. (3.24) and (3.26), we see, perhaps with some minor algebraic manipulation, that  $M_A^{2j}$  terms are always accompanied by  $x_A^{2j}$  factors in  $x$ -space. Furthermore, since structure functions  $\tilde{F}_2^{A,(0)}(x_A)$  have their main support at<sup>10</sup>  $x_A = x_N/A \sim 1/A$ , we have effectively

$$\frac{M_A^{2j} x_A^{2j}}{Q^{2j}} = \frac{(M_N^{2j} A^{2j}) x_A^{2j}}{Q^{2j}} = \frac{M_N^{2j} x_N^{2j}}{Q^{2j}} \sim \frac{M_N^{2j}}{Q^{2j}}, \quad (4.1)$$

where  $M_N = M_A/A$  is defined as the (average) nucleon mass such that the terms with  $j > 0$  in Eq. (3.20) are suppressed for  $Q^2 > M_N^2$  independent of the nuclear target. Subsequently, we introduce the *average nucleon momentum*  $p_N := p_A/A$  inside the nucleus and define a nucleon scaling variable

$$x_N = \frac{Q^2}{2p_N \cdot q} = A x_A, \quad \text{where } x_N \in [0, A], \quad (4.2)$$

in contrast to the original Bjorken variable

$$x_A = \frac{Q^2}{2p_A \cdot q} = x_N/A, \quad \text{where } x_A \in [0, 1]. \quad (4.3)$$

Note that the original  $x_A$  variable can be constructed directly from the external momenta of the particles whereas the “averaged quantities”  $x_N$  (and  $p_N$ ) are not directly observable for nuclear targets with  $A > 1$ .

---

<sup>10</sup>Note that we have introduced the nucleon scaling variable  $x_N = Ax_A$ ; this will be discussed in detail throughout this section. Although  $x_N$  can in principle extend to  $x_N = A$ , the dominant range of the kinematics is  $0 \leq x_N \lesssim 1$ . Discussion on the  $x_N > 1$  region are given in Sec. 5.5.

### Summary table of key relations

Nucleus A	Nucleon N
$M_A = A M_N$	$M_N = M_A/A$
$p_A = A p_N$	$p_N = p_A/A$
$x_A = \frac{Q^2}{2p_A \cdot q} \equiv x_N/A$ $x_A \in [0, 1]$	$x_N = \frac{Q^2}{2p_N \cdot q} \equiv A x_A$ $x_N \in [0, A]$
$W_A^2 = (p_A + q)^2$	$W_N^2 = (p_N + q)^2$
$\nu_A = \frac{(q \cdot p_A)}{M_A} = \frac{Q^2}{2M_A x_A} \equiv \nu_N$	$\nu_N = \frac{(q \cdot p_N)}{M_N} = \frac{Q^2}{2M_N x_N} \equiv \nu_A$
$y_A = \frac{\nu_A}{E} \equiv y_N$	$y_N = \frac{\nu_N}{E} \equiv y_A$
<b>Nachtmann variable &amp; hadronic mass</b>	
$r_A = \sqrt{1 + \frac{4x_A^2 M_A^2}{Q^2}} \equiv r_N$	$r_N = \sqrt{1 + \frac{4x_N^2 M_N^2}{Q^2}} \equiv r_A$
$\xi_A = R_M x_A \equiv \xi_N/A$ $\xi_A \in [0, 1]$	$\xi_N = R_M x_N \equiv A \xi_A$ $\xi_N \in [0, A]$
<p>Since <math>r_A = r_N</math></p> <p>We define <math>r \equiv r_A = r_N</math>, such that <math>R_M = \frac{2}{1+r}</math></p>	
<p>Also, <math>\xi_A/x_A = \xi_N/x_N = R_M = \frac{2}{1+r}</math></p>	
<p>We also define <math>\varepsilon = (xM/Q)</math>.</p>	

Table 4.1: We summarize the key relations for a nucleus ( $A$ ) and nucleon ( $N$ ). We also find it convenient to define  $\varepsilon = (xM/Q)$ ; we omit the subscripts on  $\varepsilon$  for brevity as  $(x_A M_A/Q) = (x_N M_N/Q)$ . We caution that  $W_A$  and  $W_N$  are **not** simply related, *c.f.*, Sec. 5.4. Note, the target mass modifies the scaling variable via  $\xi_A = R_M x_A$ . Additionally, we introduce the shorthand notation  $r = r_A = r_N$ .



Using  $M_A = AM_N$ , we find for the Nachtmann scaling variable

$$\xi_A = \frac{2x_A}{1 + \sqrt{1 + 4x_A^2 M_A^2 / Q^2}} = \frac{1}{A} \xi_N, \quad \text{with} \quad \xi_N = \frac{2x_N}{1 + \sqrt{1 + 4x_N^2 M_N^2 / Q^2}}. \quad (4.4)$$

Conversely, the quantity  $R_M$ , which relates the Bjorken scaling  $x_A$  variable to the Nachtmann scaling variable  $\xi_A$  via  $\xi_A = R_M x_A$ , is the same for both the nucleus and (averaged) nucleon case:

$$R_M = \frac{2}{1 + r_A} = \frac{2}{1 + r_N}. \quad (4.5)$$

This is because the factor  $r_A$ , which is kinematical in origin (see Sec. 2.1) and appears throughout the master formulae of Eq. (3.23), is also the same for nuclei and the average nucleon:

$$r_A = \sqrt{1 + 4x_A^2 M_A^2 / Q^2} = \sqrt{1 + 4x_N^2 M_N^2 / Q^2} = r_N. \quad (4.6)$$

Hence, we have  $\xi_A = R_M x_A$  and  $\xi_N = R_M x_N$ , where  $R_M$  takes the same value in both equations.

## 4.2. Rescaled structure functions

Turning to the structure functions, we define a rescaled hadronic tensor via the relation

$$A W_{\mu\nu}^A(p_N, q) := \tilde{W}_{\mu\nu}^A(p_A, q), \quad (4.7)$$

expressed in terms of rescaled structure functions:

$$F_2^A(x_N, Q^2) := \tilde{F}_2^A(x_A, Q^2), \quad x_N F_{1,3-6}^A(x_N, Q^2) := x_A \tilde{F}_{1,3-6}^A(x_A, Q^2). \quad (4.8)$$

The general relations in Eq. (4.8) hold for both with and without TMCs and for any value of twist. As we show below, they are consistent with the master formula for the target-mass-corrected structure functions in Eq. (3.23). Hence, the pattern of the rescaled equations is consistent between the nucleus and nucleon.

Indeed, one easily finds from Eq. (3.25):

$$\tilde{h}_2^A(\xi_A) = \int_{\xi_A}^1 du_A \frac{\tilde{F}_2^{A(0)}(u_A)}{u_A^2} = A \int_{\xi_N}^A du_N \frac{F_2^{A(0)}(u_N)}{u_N^2} =: A h_2^A(\xi_N), \quad (4.9)$$

$$\tilde{h}_3^A(\xi_A) = \int_{\xi_A}^1 du_A \frac{\tilde{F}_3^{A(0)}(u_A)}{u_A} = A \int_{\xi_N}^A du_N \frac{F_3^{A(0)}(u_N)}{u_N} =: A h_3^A(\xi_N), \quad (4.10)$$

$$\tilde{h}_5^A(\xi_A) = \int_{\xi_A}^1 du_A \frac{2\tilde{F}_5^{A(0)}(u_A)}{u_A} = A \int_{\xi_N}^A du_N \frac{2F_5^{A(0)}(u_N)}{u_N} =: A h_5^A(\xi_N), \quad (4.11)$$

$$\tilde{h}_6^A(\xi_A) = \int_{\xi_A}^1 du_A \frac{\tilde{F}_6^{A(0)}(u_A)}{u_A} = A \int_{\xi_N}^A du_N \frac{F_6^{A(0)}(u_N)}{u_N} =: A h_6^A(\xi_N), \quad (4.12)$$

$$\tilde{g}_2^A(\xi_A) = \int_{\xi_A}^1 du_A \tilde{h}_2^A(u_A) = \frac{1}{A} \int_{\xi_N}^A du_N A h_2^A(u_N) =: g_2^A(\xi_N). \quad (4.13)$$

With these expressions, and using  $x_N = Ax_A$ ,  $\xi_N = A\xi_A$ ,  $r_A = r_N$ ,  $M_A = AM_N$ , we obtain the TMC formula for

the rescaled nuclear structure functions:

$$F_1^{A,\text{TMC}}(x_N, Q^2) = \left( \frac{x_N}{\xi_N r_N} \right) F_1^{A,(0)}(\xi_N, Q^2) + \left( \frac{M_N^2 x_N^2}{Q^2 r_N^2} \right) h_2^A(\xi_N, Q^2) + \left( \frac{2M_N^4 x_N^3}{Q^4 r_N^3} \right) g_2^A(\xi_N, Q^2), \quad (4.14a)$$

$$F_2^{A,\text{TMC}}(x_N, Q^2) = \left( \frac{x_N^2}{\xi_N^2 r_N^3} \right) F_2^{A,(0)}(\xi_N, Q^2) + \left( \frac{6M_N^2 x_N^3}{Q^2 r_N^4} \right) h_2^A(\xi_N, Q^2) + \left( \frac{12M_N^4 x_N^4}{Q^4 r_N^5} \right) g_2^A(\xi_N, Q^2), \quad (4.14b)$$

$$F_3^{A,\text{TMC}}(x_N, Q^2) = \left( \frac{x_N}{\xi_N r_N^2} \right) F_3^{A,(0)}(\xi_N, Q^2) + \left( \frac{2M_N^2 x_N^2}{Q^2 r_N^3} \right) h_3^A(\xi_N, Q^2), \quad (4.14c)$$

$$\begin{aligned} F_4^{A,\text{TMC}}(x_N, Q^2) &= \left( \frac{x_N}{\xi_N r_N} \right) F_4^{A,(0)}(\xi_N, Q^2) - \left( \frac{2M_N^2 x_N^2}{Q^2 r_N^2} \right) F_5^{A,(0)}(\xi_N, Q^2) + \left( \frac{M_N^4 x_N^3}{Q^4 r_N^3} \right) F_2^{A,(0)}(\xi_N, Q^2) \\ &+ \left( \frac{M_N^2 x_N^2}{Q^2 r_N^3} \right) h_5^A(\xi_N, Q^2) - \left( \frac{2M_N^4 x_N^4}{Q^4 r_N^4} \right) (2 - \xi_N^2 M_N^2 / Q^2) h_2^A(\xi_N, Q^2) \\ &+ \left( \frac{2M_N^4 x_N^3}{Q^4 r_N^5} \right) (1 - 2x_N^2 M_N^2 / Q^2) g_2^A(\xi_N, Q^2), \end{aligned} \quad (4.14d)$$

$$\begin{aligned} F_5^{A,\text{TMC}}(x_N, Q^2) &= \left( \frac{x_N}{\xi_N r_N^2} \right) F_5^{A,(0)}(\xi_N, Q^2) - \left( \frac{M_N^2 x_N^2}{Q^2 r_N^3 \xi_N} \right) F_2^{A,(0)}(\xi_N, Q^2) \\ &+ \left( \frac{M_N^2 x_N^2}{Q^2 r_N^3} \right) h_5^A(\xi_N, Q^2) - \left( \frac{2M_N^2 x_N^2}{Q^2 r_N^4} \right) (1 - x_N \xi_N M_N^2 / Q^2) h_2^A(\xi_N, Q^2) \\ &+ \left( \frac{6M_N^4 x_N^3}{Q^4 r_N^5} \right) g_2^A(\xi_N, Q^2), \end{aligned} \quad (4.14e)$$

$$F_6^{A,\text{TMC}}(x_N, Q^2) = \left( \frac{x_N}{\xi_N r_N^2} \right) F_6^{A,(0)}(\xi_N, Q^2) + \left( \frac{2M_N^2 x_N^2}{Q^2 r_N^3} \right) h_6^A(\xi_N, Q^2). \quad (4.14f)$$

The above rescaled equations for the **nucleon** structure functions  $F_i$  (without the “ $\sim$ ” notation) take the same form as the master equations for the **nuclear** structure functions  $\tilde{F}_i$  in Eq. (3.23) but are entirely expressed in terms of averaged nucleon variables. This is one of the main results of this rescaling demonstration.

### 4.3. Impact of quark masses

We stress that all of the above derivations have made no mention of the parton model. This can be understood from the fact that the quark and gluon sub-structure of nuclei enters only implicitly in intermediate steps of the derivation of the master and rescaled formulae since the hadronic currents appearing in the hadronic tensor are composed of quark and gluon fields and we have relied on the validity of the OPE for the products of these currents. Thus, due to the nature of the factorization, all details related to quark masses is contained entirely inside the  $F_i^{A,(0)}$  structure functions, and the forms of the rescaled formulae in Eq. (4.14) are unchanged.

The treatment of the quark masses was reviewed in detail in Ref. [73], but it is instructive to briefly mention how the quark masses effect the rescaling of the kinematic variables as summarized in Table 4.2. Just as the hadron mass modifies the scaling variable via the relation  $\xi = R_M x$  due to momentum conservation, the quark masses further modify the scaling variable via the relation [70, 71, 102]

$$\bar{\xi} = R_{ij} \xi = R_{ij} R_M x. \quad (4.15)$$

In our notation,  $\xi_A$  contains modifications due to the hadron mass  $M_A$ , while  $\bar{\xi}_A$  (with the overline) contains modifications due to **both** the hadron mass  $M_A$  and the parton masses  $m_i, m_j$ . The  $R_M$  factor, which is given in Eq. (2.4), depends on the hadron (nucleus) mass, and the  $R_{ij}$  factor depends on the incoming and outgoing quark

Partonic masses in scaling variables	
$\bar{\xi}_A = R_{ij}\xi_A = R_{ij}R_M x_A$	Nucleus
$\bar{\xi}_N = R_{ij}\xi_N = R_{ij}R_M x_N$	Nucleon
$\xi_{A,N}$ :	TMC corrections (no overbar)
$\bar{\xi}_{A,N}$ :	TMC + parton mass corrections
For $q_i + V \rightarrow q_j$	
$R_{ij} = \frac{1}{2Q^2} [Q^2 - m_i^2 + m_j^2 + \Delta(Q^2, m_i^2, m_j^2)]$	
$\Delta(a, b, c) = \sqrt{a^2 + b^2 + c^2 - 2(ab + bc + ca)}$	
For $g + V \rightarrow q_j + q_k$	
$R_{jk} = 1 + \frac{(m_j + m_k)^2}{Q^2}$	

Table 4.2: Summary of partonic mass relations in scaling variables. The target mass modifies the Nachtmann scaling variable via  $\xi_A = R_M x_A$ , where  $R_M$  is defined in Table 4.1. This is further modified by the parton masses  $\bar{\xi}_A = R_{ij}\xi_A = R_{ij}R_M x_A$ ; hence these multiplicative corrections factorize between the hadron and parton masses [73]. In the limit the initial-state parton mass  $m_i \rightarrow 0$ , we obtain the “slow rescaling” result:  $R_{ij} = (1 + m_j^2/Q^2)$ . Thus,  $\xi_A$  contains modifications due to the hadron mass  $M_A$ , while  $\bar{\xi}_A$  (with the overbar) contains modifications due to **both** the hadron mass  $M_A$  and the parton masses  $\{m_i, m_j\}$ .

masses  $\{m_i, m_j\}$ , respectively (*c.f.*, Table 4.2). Note that the hadronic and partonic correction factors factorize and are subsequently applied multiplicatively. Intuitively, this factorization signifies that hadronic kinematics can be considered separately from partonic kinematics, up to momentum conservation. Additionally, in the limit where the mass of the initial-state quark vanishes  $m_i = 0$ , we have the familiar “slow rescaling” limit  $R_{ij} \approx (1 + m_j^2/Q^2)$ . For further details, see Refs. [70, 71, 73, 102].

## 5. Parton model

We now turn to a discussion of structure functions in the context of the parton model originally proposed by Feynman in 1969 [103] and applied to electron-proton DIS by Bjorken and Paschos [104]. In the years following these works, partons were identified with quarks and gluons, and the heuristic parton model including QCD effects was rigorously derived from first principles of QCD in the context of factorization theorems [50–57]. In this section we summarize the main elements of the conventional “massless” QCD-improved parton model, also known as Zero Mass Variable Flavor Number Scheme (ZM-VFNS), where quark-mass effects in the hard scattering cross sections and target-mass effects are neglected. There is an extensive body of literature on computations with heavy partons; Collins, for example, extended the factorization proof [51] to the case of heavy partons in Ref. [54], and implementations can be found in Refs. [71, 105–108]. A discussion of the parton model including such mass effects will be given in Sec. 6.

In the QCD-improved parton model the nuclear structure functions ( $\tilde{\mathcal{F}}_k^A$ ) are given as convolutions of target-

independent, short-distance, Wilson coefficients ( $C_{k,i}$ ) with universal nuclear parton distribution functions ( $\tilde{f}_i^A$ ):

$$\tilde{\mathcal{F}}_k^A(x_A, Q^2) = \int_{x_A}^1 \frac{dy_A}{y_A} \tilde{f}_i^A(y_A, Q^2) C_{k,i}(x_A/y_A) + \dots \quad (5.1)$$

where the ellipses represent higher twist contributions  $\tilde{\mathcal{F}}_k^{A,\tau \geq 4}(x_A, Q^2)$ , and a sum over  $i = q, g$  species is understood. As in the previous section, we use the tilde notation to identify the nuclear PDFs  $\tilde{f}_i^A(x_A, Q^2)$ , and the rescaled PDFs are without the tilde  $f_i^A(x_N, Q^2)$ . Here, we use the shorthand

$$\tilde{\mathcal{F}}_k^A(x_A) = [\tilde{F}_1(x_A), \tilde{F}_2(x_A)/x_A, \tilde{F}_3(x_A)] \quad \text{for} \quad k = 1, 2, 3. \quad (5.2)$$

The nuclear PDFs ( $\tilde{f}_i^A$ ) are defined as Fourier transforms of matrix elements of local, twist-2 operators, which we denote<sup>11</sup> as  $\mathcal{O}_i(z)$  and which are defined initially in coordinate space. These operators are composed of quark and gluon fields, and are acted upon by the hadronic, i.e., nuclear, state  $A(p_A)$ :

$$\tilde{f}_i^A(x_A, Q^2) \sim \langle A(p_A) | \mathcal{O}_i | A(p_A) \rangle, \quad (5.3)$$

where  $x_A \in [0, 1]$  and the factorization and renormalization scales have been identified with the exchange boson virtuality  $\mu_F = \mu_R = Q$ .

In this paper we focus on unpolarized DIS. However, the application to polarized DIS are relatively straightforward. For a spin- $j$  target there are  $2(2j+1)$  independent helicity-dependent quark distributions  $\tilde{q}_+^m(x)$  and  $\tilde{q}_-^m(x)$  with  $-j \leq m \leq j$ . Here  $\tilde{q}_+^m(x)$  [ $\tilde{q}_-^m(x)$ ] describes the number density for finding a quark with momentum fraction  $x$  and spin  $m$  parallel [anti-parallel] to the the  $z$ -axis of a hadron moving with infinite momentum along the  $z$ -axis. Due to parity invariance of the strong interaction, we have a relation between the up (parallel) and down (anti-parallel) spin ( $\tilde{q}_+^m = \tilde{q}_-^{-m}$ ) such that there remain only  $2j+1$  independent distributions. However, this symmetry is broken once weak interaction effects are taken into account. For a spin- $j$  target, the unpolarized quark densities are related to the helicity-dependent distributions as follows:

$$\tilde{q}_i^A(x_A, Q^2) := \frac{1}{2j+1} \sum_{m=-j}^j (\tilde{q}_+^m + \tilde{q}_-^m). \quad (5.4)$$

For a spin-1/2 target (and using  $\tilde{q}_+^{1/2} = \tilde{q}_-^{-1/2}$ ), this reduces to the well-known expression:

$$\tilde{q}_i^A(x_A, Q^2) := \tilde{q}_+^{1/2} + \tilde{q}_-^{1/2}. \quad (5.5)$$

Similar definitions can be written down for the unpolarized gluon distribution.

## 5.1. Nuclear DGLAP evolution

The unpolarized nuclear PDFs (for any target spin) satisfy the usual Dokshitzer-Gribov-Lipatov-Altarelli-Parisi (DGLAP) evolution equations [109–111]:

$$\frac{d\tilde{f}_i^A(x_A, Q^2)}{d \ln Q^2} = \frac{\alpha_s(Q^2)}{2\pi} \int_{x_A}^1 \frac{dy_A}{y_A} P_{ij}(y_A) \tilde{f}_j^A(x_A/y_A, Q^2) \quad (5.6)$$

$$= \frac{\alpha_s(Q^2)}{2\pi} \int_{x_A}^1 \frac{dy_A}{y_A} P_{ij}(x_A/y_A) \tilde{f}_j^A(y_A, Q^2) \quad . \quad (5.7)$$

---

<sup>11</sup>The notation for field operators, which typically carry indices throughout this work, should not be confused with the ‘‘Big  $O$ ’’ notation  $\mathcal{O}(x)$ , which we also use in this work (without indices) to denote an uncertainty or expansion to order  $x$ .

Furthermore, the following sum rules due to charge, baryon number, and momentum conservation are satisfied:

$$\int_0^1 dx_A \tilde{u}_v^A(x_A, Q^2) = 2Z + N, \quad (5.8a)$$

$$\int_0^1 dx_A \tilde{d}_v^A(x_A, Q^2) = Z + 2N, \quad (5.8b)$$

$$\int_0^1 dx_A x_A \sum_i \tilde{f}_i^A(x_A, Q^2) = 1, \quad (5.8c)$$

where  $Z$  is the electric charge of the nucleus with baryon number  $A = Z + N$ .

## 5.2. Relation to the OPE

A Mellin transformation can turn a convolution integral  $(A \otimes B)(x) = \int_x^1 dy/y A(y)B(x/y)$  into an ordinary product of Mellin moments:

$$\int_0^1 dx x^{n-1} (A \otimes B)(x) \equiv (A \otimes B)_n = A_n \cdot B_n, \quad (5.9)$$

where

$$A_n \equiv \int_0^1 dx x^{n-1} A(x) \quad \text{and} \quad B_n \equiv \int_0^1 dx x^{n-1} B(x). \quad (5.10)$$

Applying this to structure functions of the QCD-improved parton model in Eq. (5.1), we obtain:

$$\int_0^1 dx_A x_A^{n-1} \tilde{\mathcal{F}}_k^A(x_A, Q^2) = \sum_n \tilde{f}_i^{A,n}(Q^2) C_{k,i}^n. \quad (5.11)$$

where on the RHS the Mellin transformation has yielded a simple sum of Mellin moments. (Note that we indicate the Mellin moment by the “ $n$ ” superscript, as the tilde-notation has already been used for the pre-scaled PDFs, which we discuss in the following section, and  $N$  already denotes averaged nucleon quantities.)

The relation between the structure functions in the parton model and the OPE can now be easily seen by comparing the Mellin-moment of Eq. (5.11) with the  $j=0$  term in Eq. (3.22):

$$\tilde{\mathcal{F}}_k^{(0),n} = C_{k,i}^n \tilde{A}_i^n = C_{k,i}^n \tilde{f}_i^{A,n}(Q^2), \quad \text{for } k = 1, 2, 3, \quad (5.12)$$

where a sum over  $i = q, g$  is understood. From this equation we see that the matrix elements  $\tilde{A}_i^n$  of Eq. (3.22) are simply the Mellin moments of the parton distribution functions:

$$\tilde{A}_i^n(Q^2) = \tilde{f}_i^{A,n}(Q^2) \equiv \int_0^1 dx_A x_A^{n-1} \tilde{f}_i(x_A, Q^2). \quad (5.13)$$

Similarly, the Wilson coefficients  $C_{k,i}^n$  of Eq. (5.12) are directly identified with those of Eq. (3.22) in the OPE.

## 5.3. Rescaling

The parton distributions  $\tilde{f}_i^A(x_A)$  are number densities defined on the interval  $x_A \in [0, 1]$  such that  $\tilde{f}_i^A(x_A) dx_A$  can be interpreted as the number of partons “ $i$ ” carrying a fraction of the parent hadron momentum in the interval  $[x_A, x_A + dx_A]$ . We define rescaled parton densities  $f_i^A(x_N, Q^2)$  in the variable  $x_N \in [0, A]$  with  $x_N = Ax_A$  by imposing that the number of partons remains unchanged in the corresponding momentum intervals:

$$f_i^A(x_N, Q^2) dx_N := \tilde{f}_i^A(x_A, Q^2) dx_A. \quad (5.14)$$

This equation may appear a bit odd as  $x_N \in [0, A]$  on the LHS, while  $x_A \in [0, 1]$  on the RHS; we will provide additional clarification in the following discussion. Additionally, it should be noted that the rescaled nuclear

PDF  $f_i^A(x_N, Q^2)$  are the ones usually used in the literature as  $f_i^A(x_N, Q^2)$  can be meaningfully compared across different nuclei, in contrast to  $\tilde{f}_i^A(x_A, Q^2)$ .

It can be easily checked that the rescaling defined here at the level of PDFs is consistent with the rescaling introduced above at the hadronic level. Correspondingly, the rescaled objects satisfy analogous DGLAP evolution equations:

$$\frac{df_i^A(x_N, Q^2)}{d \ln Q^2} = \frac{\alpha_s(Q^2)}{2\pi} \int_{x_N}^A \frac{dy_N}{y_N} P_{ij} \left( \frac{x_N}{y_N} \right) f_j^A(y_N, Q^2). \quad (5.15)$$

Furthermore, the sum rules take the following form after the rescaling:

$$\int_0^A dx_N \quad u_v^A(x_N, Q^2) = 2Z + N, \quad (5.16a)$$

$$\int_0^A dx_N \quad d_v^A(x_N, Q^2) = Z + 2N, \quad (5.16b)$$

$$\int_0^A dx_N \quad x_N \sum_i f_i^A(x_N, Q^2) = A, \quad (5.16c)$$

which match those in Eq. (5.8). However, note the above integrals extend to  $A$  since  $x_N \in [0, A]$ .

While the rescaled nuclear PDFs are formally defined on the interval  $x_N \in [0, A]$ , it is important to identify how the bulk of the PDFs are distributed. For a proton with three valence quarks, we generally expect the valence PDFs to be peaked in the region of  $x_A = x_N \sim 1/3$ . In a similar manner, for nuclei of mass  $A$ , which carries  $A$  nucleons, we generally expect the valence PDFs to be peaked in the region of  $x_A \sim 1/(3A)$ , or equivalently  $x_N \sim 1/3$ , which is independent of  $A$  and thus facilitates a meaningful comparison between different nuclei. Therefore, even though  $x_N$  can in principle span the range  $[0, A]$ , we expect the dominant support of the PDFs to be in the region  $x_A \leq 1/A$ , or  $x_N \leq 1$ . For  $x_N$  to exceed unity, one *parton* alone would essentially need to acquire more momentum than an average *nucleon*; this is highly unlikely. Thus, it is common to assume the probability for  $x_N > 1$  to be small, and global analyses of nPDFs typically implement the condition that  $f_i^A(x_N) = 0$  for  $x_N > 1$ . This induces only a very small error [19], and we discuss the possibility of  $x_N > 1$  further in Sec. 5.5.

Setting  $f_i^A(x_N, Q_0^2) = 0$  for  $x_N \geq 1$  at the initial scale  $Q_0$  yields an important computational benefit since the DGLAP evolution framework consistently leads to  $f_i^A(x_N, Q^2) = 0$  for  $x_N \geq 1$  at all larger scales  $Q$ . Consequently, the advantage of setting  $f_i^A(x_N \geq 1, Q^2) = 0$  is that the same evolution equations can be used for all nuclei, including nucleons:

$$\frac{df_i^A(x_N, Q^2)}{d \ln Q^2} = \begin{cases} \frac{\alpha_s(Q^2)}{2\pi} \int_{x_N}^1 \frac{dy_N}{y_N} P_{ij} \left( \frac{x_N}{y_N} \right) f_j^A(y_N, Q^2) & : 0 < x_N \leq 1, \\ 0 & : 1 < x_N \leq A. \end{cases} \quad (5.17)$$

With the above framework for nuclear PDFs, we can perform DGLAP evolution on the interval  $x \in [0, 1]$  in a manner similar to proton evolution. However, the sum rules of Eq. (5.16a), (5.16b), and (5.16c) differ from the proton case. Thus, it is common (but not necessary) to further decompose the nuclear PDF  $f_i^A$  as

$$f_i^A(x, Q) = \frac{Z}{A} f_i^{p/A}(x, Q) + \frac{A-Z}{A} f_i^{n/A}(x, Q), \quad (5.18)$$

where  $f_i^{p/A}$  and  $f_i^{n/A}$  represent effective ‘‘bound proton and neutron’’ PDFs for finding a parton ‘‘ $i$ ’’ inside a nucleon. The ‘‘bound proton’’ PDF  $f_i^{p/A}$  satisfies identical sum rules as the (free) proton PDF, so this quantity can be computed using standard DGLAP programs. The ‘‘bound neutron’’ PDF is commonly obtained from



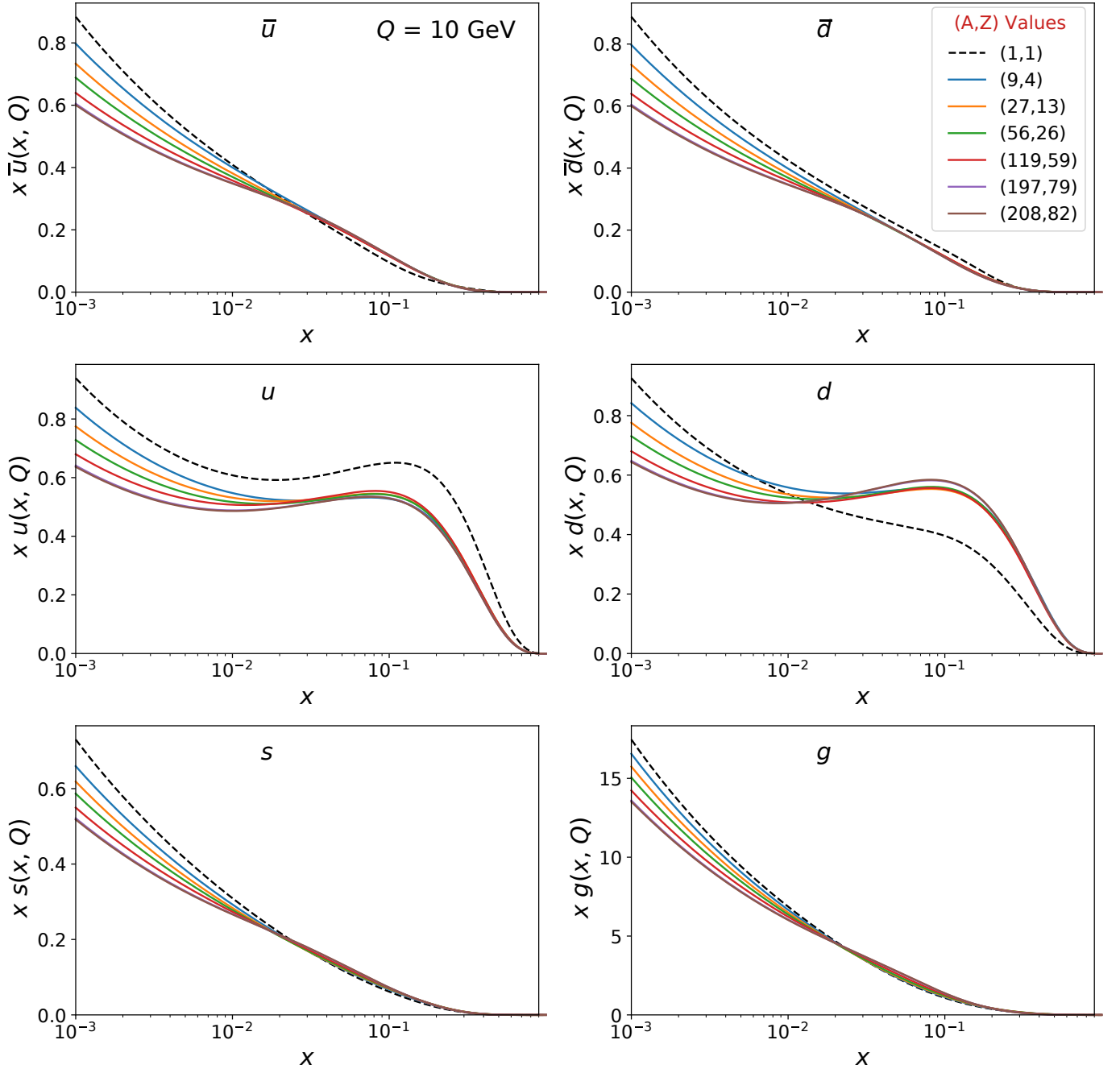


Figure 5.1: We display the nCTEQ15 nPDFs [17] as a function of  $x$  at  $Q = 10$  GeV for selected nuclear  $(A, Z)$  values as indicated in the legend. These are the scaled nPDFs of Eq. (5.18), and this feature is most evident when comparing the  $xu(x, Q)$  and  $xd(x, Q)$  of the proton ( $A = 1$ ).

the “bound proton” one by assuming isospin symmetry.<sup>12</sup>

For comparison of nPDFs across different nuclei, it is typically the scaled nPDF  $f_i^{(A,Z)}(x, Q)$  of Eq. (5.18) which can be meaningfully compared, as we illustrate in Fig. 5.1. This quantity is defined on  $x \in [0, 1]$  and normalized so that the integrated momentum is unity. Conversely, although the effective “bound proton and

<sup>12</sup>While isospin symmetry is typically used to relate  $f_i^{n/A}$  to  $f_i^{p/A}$ , in principle one could add isospin violating contributions. The recent Marathon data [112] suggests there may be isospin violations in the very large  $x$  region [113].

neutron" PDFs of Eq. (5.18) are convenient for computing the DGLAP evolution, these are *not* physically measurable objects. Caution is required when comparing them.

In particular, if we try to invert the relations of Eq. (5.18) for the up and down quarks, we find:

$$u^{p/A} = \frac{Z}{2Z-A} u^A - \frac{A-Z}{2Z-A} d^A \quad \text{and} \quad d^{p/A} = \frac{Z}{2Z-A} d^A - \frac{A-Z}{2Z-A} u^A \quad . \quad (5.19)$$

This relation has the expected limits that for a proton: with  $A = p$  and  $A = Z = 1$  we find  $\{u^{p/A}=u^{A=p}; d^{p/A}=d^{A=p}\}$ . Also, for a neutron with  $A = n$  and  $\{A, Z\} = \{1, 0\}$  we find  $\{d^{p/A}=u^{A=n}; u^{p/A}=d^{A=n}\}$ . However, for an isoscalar target ( $A = 2Z$ ), Eq. (5.19) is singular because in this limit it is impossible to differentiate the  $u^A$  and  $d^A$  distributions and the decomposition into  $u^{p/A}$  and  $d^{p/A}$  becomes arbitrary. Since the majority of the nuclear data is taken on nuclear targets which lie along the nuclear stability line in the  $\{A, Z\}$  plane where  $A \sim 2Z$  (except for very heavy nuclei), our ability to separately determine the nuclear  $u^A$  and  $d^A$  distributions is limited.

#### 5.4. Kinematic $W$ cut

Determinations of PDFs are performed by global analyses using a wide array of data sets that can be described by the parton model within the factorization framework. It is therefore important to exclude data in the kinematic region that are not reliably predicted within this model.

In lepton-nucleon scattering, there are different types of scattering scenarios depending on the value of the hadronic invariant mass,  $W^2 = (p+q)^2$ , and the virtuality of the exchanged boson  $Q$  [114]. We can divide these cases into four categories:

1. elastic scattering ( $W = M_N$ ),
2. shallowly inelastic scattering (SIS) ( $W \leq 2$  GeV),
3. soft DIS ( $W > 2$  GeV,  $Q < 1$  GeV), and
4. DIS ( $W > 2$  GeV and  $Q \geq 1$  GeV).

Among these scenarios, DIS and soft DIS (dominated by non-resonant pion production) are the most reliably described by the parton model. Therefore, a  $W$  cut is traditionally imposed on DIS data to extract PDFs.

While imposing a  $W$  cut is straightforward for the case of lepton-proton scattering, it is more subtle for lepton-nucleus scattering when we compute in terms of the rescaled variables. For  $\ell_1 + A \rightarrow \ell_2 + X$  scattering, we have:

$$W_A^2 = (p_A + q)^2 = M_A^2 + Q^2 \frac{1-x_A}{x_A} = A^2 M_N^2 + Q^2 \frac{1-x_N/A}{x_N/A} \quad . \quad (5.20)$$

The average  $W_A$  per nucleon,  $W_{\text{aver}} = W_A/A$ , is then given by

$$W_{\text{aver}}^2 = \left(\frac{W_A}{A}\right)^2 = M_N^2 + Q^2 \frac{A-x_N}{A^2 x_N} \quad . \quad (5.21)$$

Additionally, we observe that  $W_{\text{aver}}^2$  and  $W_N^2$  are not the same:

$$W_N^2 = (p_N + q)^2 = M_N^2 + Q^2 \frac{1-x_N}{x_N} \quad . \quad (5.22)$$

For  $x_N \in [0, A]$ , we find  $W_{\text{aver}}^2$  is always positive while  $W_N^2$  can be negative for  $x_N > 1$ . On the other hand,  $W_N$  is independent of  $A$  and can be used to compare nuclei as long as  $x_N$  is restricted to values below unity.

If we impose a lower bound on  $W_A$ , this translates to the well-known upper bound on  $x_A$  of

$$0 \leq x_A \leq \left[1 + \frac{W_A^2 - M_A^2}{Q^2}\right]^{-1} \leq 1 \quad . \quad (5.23)$$

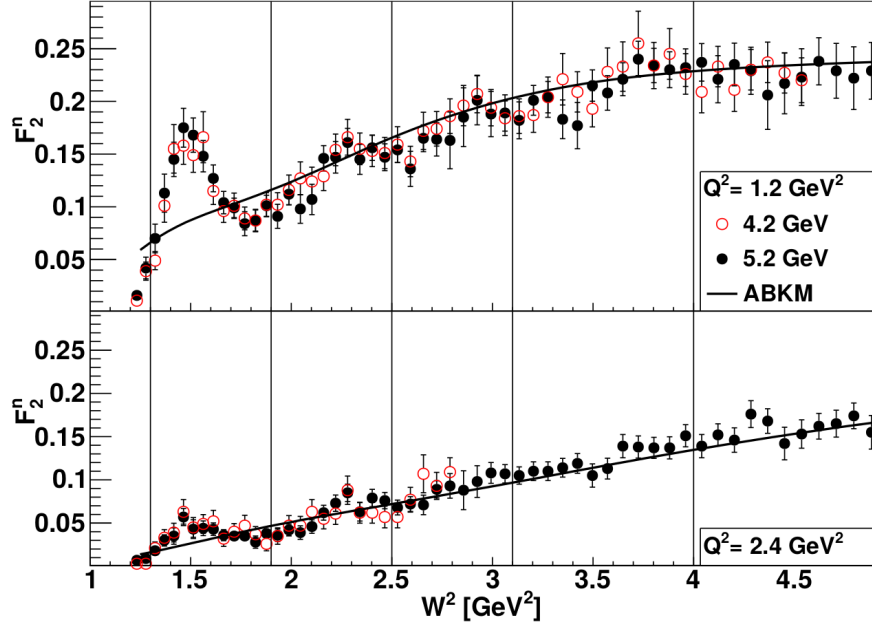


Figure 5.2: We display the neutron structure function  $F_2^n$  as measured by the BONuS data [115] at selected  $Q^2$  values. The open (filled) circles represent data for a beam energy of  $E = 4.223$  (5.262) GeV. This is compared with ABKM PDF predictions [108] including higher twist effects and target mass corrections. We observe the resonance structure at low  $W^2$  values. Figure taken from Ref. [115].

In terms of the rescaled variable  $x_N = Ax_A \in [0, A]$  this translates to

$$0 \leq x_N \leq A \left[ 1 + \frac{W_A^2 - M_A^2}{Q^2} \right]^{-1} \leq A. \quad (5.24)$$

Consequently, when we impose a  $W$  kinematic cut for the nuclear case ( $A > 1$ ), we need to be cognizant of these issues. One could try to limit the resonance region with a mass cut ( $m_{\text{cut}}$ ) by setting  $W_N^2 = M_N^2 + m_{\text{cut}}^2/A^2$ . For  $A > 1$ , the resulting high- $x$  cut turns out to be more relaxed than the usual  $W$  cut. Thus, using the traditional  $W$  cut here is much safer and hence, despite its pathological nature at  $x > 1$ , this cut can still be used. While cutting on  $W_A$  or  $(W_A/A)$  is more natural, the value of  $W_N$ , which is  $A$  dependent, needs further investigations.

## Structure function data for nucleons and nuclei

In Fig. 5.2 we display  $F_2^n$  as measured by the BONuS experiment and compared with the ABKM global fit [108]. BONuS studied electron-deuteron scattering with two electron energies ( $E = 4.2$  and 5.2 GeV) and used a novel spectator tagging technique to extract the free neutron cross section. The resonance structure is evident in the upper panel with  $Q^2 = 1.2 \text{ GeV}^2$  where we observe the first ( $\Delta$ ) resonance in the region of  $W^2 \sim 1.5 \text{ GeV}^2$ . As we go to larger  $Q^2$  values, the effect of the resonances are reduced as seen in the lower panel ( $Q^2 = 2.4 \text{ GeV}^2$ ).

Changing our focus from a nucleon to a nucleus, in Fig. 5.3 we display the  $F_2^A$  structure functions for carbon and iron at selected  $Q^2$  values as measured in Ref. [116]. The region of the first resonance is highlighted by the shaded vertical bands. We immediately note that the characteristic resonance structure is more difficult to observe for the nuclear case as compared to the nucleon (neutron) case above. Furthermore, this is complicated by the (comparably) limited data in the low  $W^2$  region.

We start by considering the bottom panels of Fig. 5.3, which plot  $F_2^A$  as a function of  $W_N^2$ . Here, we have highlighted the resonance region  $m_\Delta^2 \sim W_N^2$ . Due to the limited data in the low  $W^2$  region, it is difficult to identify the resonances; however, at larger  $Q^2$  values it is clear that any resonance structure again appears to

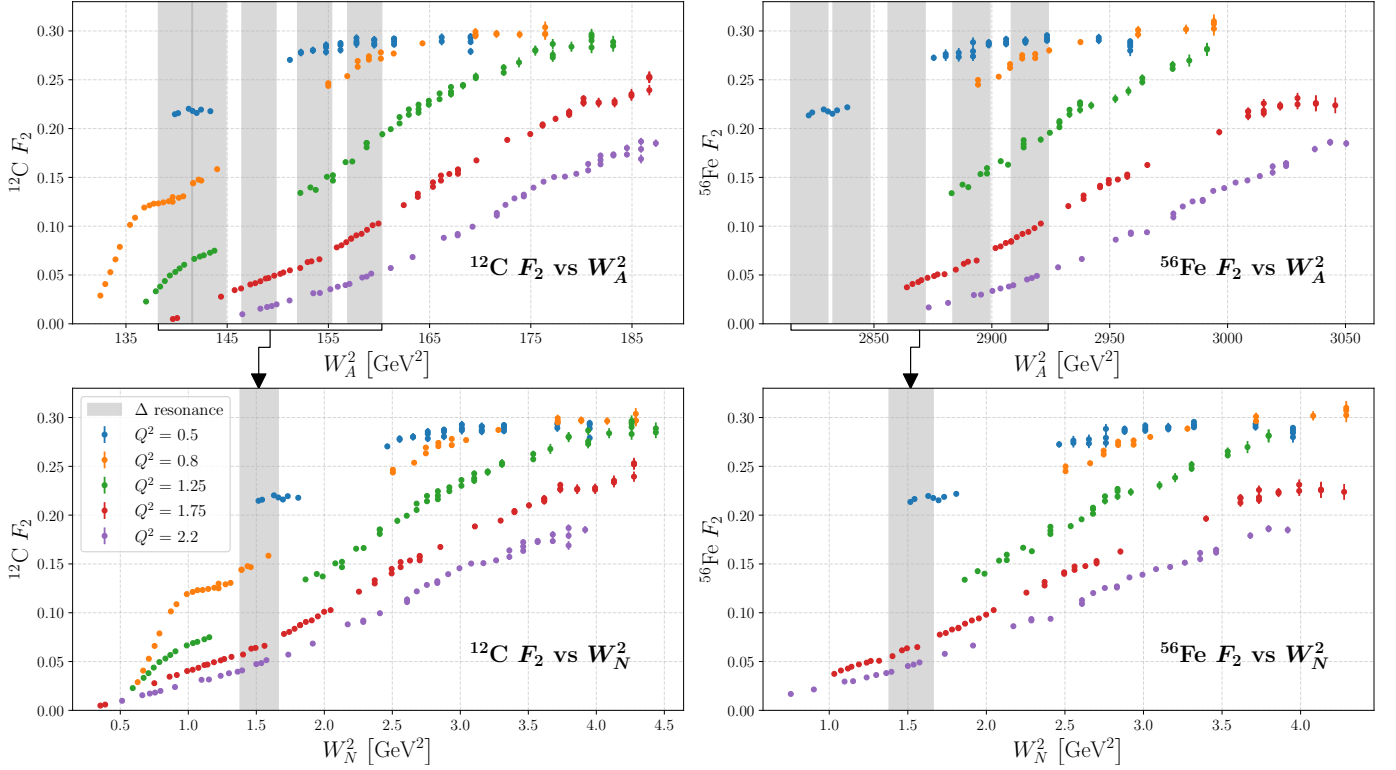


Figure 5.3: We plot  $F_2^A$  for carbon and iron for selected  $Q^2$  values (in  $\text{GeV}^2$ ) as a function of both  $W_A^2$  (upper panels) and  $W_N^2$  (lower panels). The first ( $\Delta$ ) resonance region is highlighted with the vertical shaded bands. For  $W_N^2$ , this region is  $\sim M_\Delta^2$ . For  $W_A^2$ , there is a more pronounced  $Q^2$  dependence so that the resonance region for the lowest  $Q^2$  is at the lowest  $W_A^2$ , and the one for the highest  $Q^2$  is at the highest  $W_A^2$  values. The data are taken from Ref. [116].

be reduced. We now draw attention to the upper panels of Fig. 5.3, which are plotted versus  $W_A^2$ . The  $W_A^2$ -axes of the neutron, carbon and iron all differ as they are now proportional to  $A$ . Additionally, there is a relative shift of the curves due to the different  $Q^2$  dependence as compared with  $W_N^2$ . Specifically, we have converted using:  $W_A^2 = AW_N^2 + A(A-1)M_N^2 + (A-1)Q^2$ . This conversion also shifts the resonance region in a manner dependent on  $Q^2$ ; in the upper panels, the resonance region for the lowest  $Q^2$  is at the lowest  $W_A^2$ , and the one for the highest  $Q^2$  is at the the highest  $W_A^2$  values.

We now summarize our main observations in the following.

- The resonance structure is most evident at lower  $Q^2$  values. As  $Q^2$  increases, the resonance peaks are reduced as the phase space for the DIS continuum is growing and becomes dominant.
- As we move to heavier nuclei, the resonance structure is also comparably reduced.
- The  $W_N^2$  variable has the advantage that this identifies a uniform kinematic region largely independent of  $Q^2$  or  $A$ . This simplifies the task of placing cuts on the resonance region.
- The  $W_A^2$  variable has the disadvantage that the kinematic region is dependent on  $A$  and  $Q^2$ , and this complicates the task of placing cuts on the resonance region.

## 5.5. nPDFs for $x_N \geq 1$

The rescaled PDFs allow us to compare distributions from different nuclei in a meaningful manner as illustrated in Fig. 5.1. Operationally, all current global nuclear PDF analyses work on the interval  $x_N \in [0, 1]$  even though

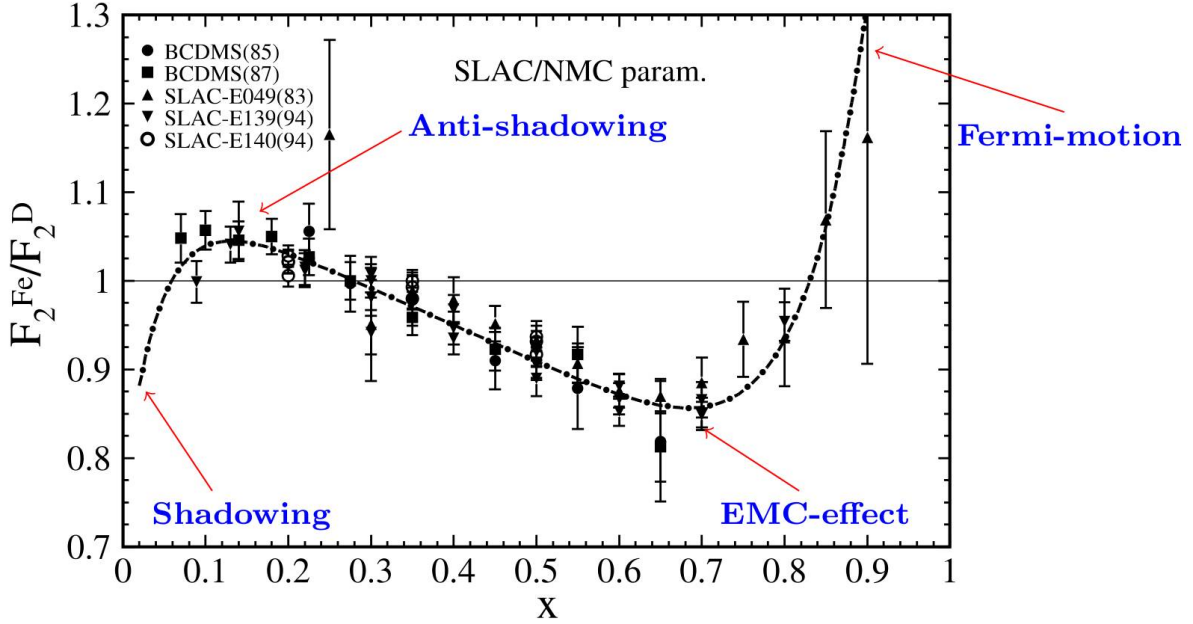


Figure 5.4: We display a characteristic nuclear correction ratio  $F_2^{Fe}/F_2^D$  for iron over deuterium. We observe the shadowing region ( $x \lesssim 0.1$ ), the anti-shadowing region ( $x \sim 0.2$ ), the EMC region ( $x \sim 0.5$ ), and the Fermi region ( $x \gtrsim 0.8$ ). The figure is taken from Ref. [76] which contains the details and references for the data sets.

the technically allowed range is  $x_N \in [0, A]$ . While details of the  $x_N > 1$  region are beyond the scope of this study, we briefly mention experimental measurements that provide insights into this extreme kinematic region.

### The Fermi region

The effects of nuclear binding can modify the partonic momentum, and thus dramatically impact the resulting structure functions [117]. Fig. 5.4 shows the characteristic form of the nuclear correction factor  $F_2^{Fe}/F_2^D$  with<sup>13</sup> shadowing at small  $x_N$  ( $x_N < 0.1$ ), anti-shadowing just beyond the shadowing region ( $x_N \sim 0.1$ ), the EMC region for intermediate  $x$ , and the Fermi region for large  $x$ . The nuclear binding effects are especially evident at larger momentum fractions (large  $x$ ) in the Fermi region where the PDFs are steeply falling. There are a variety of theoretical approaches to describe this region, as well as experimental measurements of these nuclear binding effects. We provide only a brief overview below and refer to the reference for additional details.

### Challenges of the Fermi region

The limitations of constraining the PDFs in the  $x_N \sim 1$  region are evident when examining the nuclear ratio  $F_2^A/F_2^p$  in the large  $x_N$  region. As  $x$  increases, the  $\mathcal{R} = F_2^A/F_2^p$  ratio transitions from  $\mathcal{R} \lesssim 1$  in the EMC region, to  $\mathcal{R} \gtrsim 1$  as  $x_N \rightarrow 1$  in the Fermi region. We find that  $F_2^p(x)$  with  $A = 1$  for the proton must vanish at  $x_N = 1$ , whereas  $F_2^A(x)$  can be finite since  $x_N \in [0, A]$ . This means that the denominator of  $\mathcal{R}$  is vanishing while the numerator is finite. Hence,  $\mathcal{R}$  will rapidly increase at  $x \sim 1$ , and is consistent with experimental measurements. More generally, we expect  $F_2^{A_1} > F_2^{A_2}$  for  $A_1 > A_2$ , and this is the case for  $F_2^{12C}/F_2^D$  as shown in Fig. 5.5.

<sup>13</sup>The nomenclature is historical: The term “shadowing” refers to the front of a large- $A$  nucleus casting a metaphoric shadow over its back since a leptonic probe is likelier to scatter off the front (and not “see” the back) when partons have larger wavelengths (smaller  $x_N$ ). This leads to a suppression of the  $F_2^A/F_2^D$  ratio at  $x_N \lesssim 0.1$ ; for further details of this geometric picture, see Ref. [74, 117]. The term “anti-shadowing” refers to the experimental observation that the ratio is enhanced at  $x_N \sim 0.1$ . The term “EMC effect” refers to the suppression of the  $F_2^A/F_2^D$  ratio at moderate  $x_N$  discovered by the EMC collaboration [118]. The term “Fermi region” refers to the high- $x_N$  region when Fermi motion becomes relevant enabling  $x_N \geq 1.0$  for bound nucleons

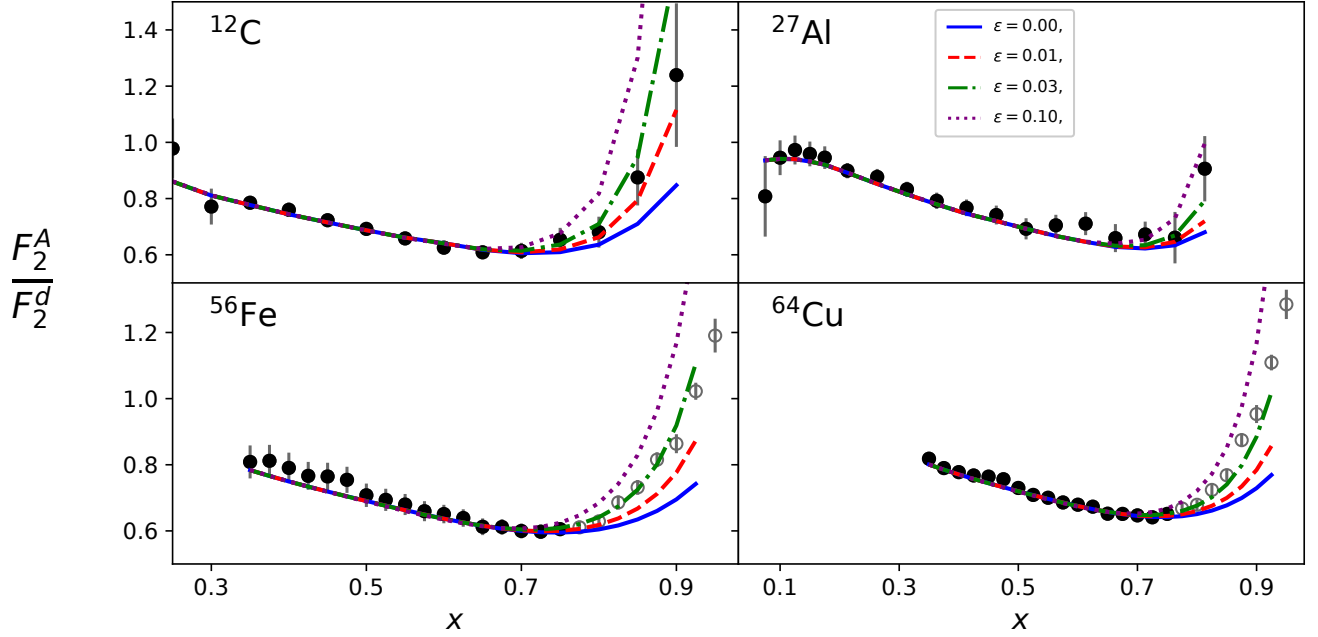


Figure 5.5: We display the ratio  $F_2^A/F_2^d$  for selected nuclei data sets in the large  $x$  region. The different curves show the impact of the  $\varepsilon$  parameter for the rescaling  $x'_N \rightarrow [x_N - \varepsilon x_N^\kappa \log_{10} A]$  with  $\kappa = 10$ , *c.f.*, Ref. [19] for details. The data with solid circles satisfy the cuts  $Q > 1.3$  GeV and  $W > 1.7$  GeV; the open circles do not satisfy the cuts and are not included in the fit. This figure is taken from Ref. [19].

### Theoretical implementations

On the theoretical side, there are a number of approaches that have been proposed to model nPDFs in the  $x_N > 1$  region, and we point to a selection of references [11, 37, 119–127]. There is also a LO solution of DGLAP equation for quarks taking into account the full support (including  $x_N > 1$  region) which is detailed in Ref. [128].

One technique to describe the  $x_N > 1$  region is to use a convolution of the nucleon PDFs  $f(x, Q)$  defined on the interval  $x \in [0, 1]$  with a smearing kernel  $S_A$  which will shift the PDFs out to larger  $x$  values:

$$f_A(x, Q) = \int_x^A \frac{dy}{y} S_A(y, Q) f(x/y, Q) \quad . \quad (5.25)$$

Here, the smearing kernel  $S_A$  is typically a Gaussian with an  $A$ -dependent width; larger nuclei have a larger smearing width, and hence a larger proportion of the  $f_A$  distribution will populate the  $x > 1$  region. The behavior of the PDF convolution can also be approximated using an  $A$ -dependent rescaling:  $x'_N \rightarrow [x_N - \varepsilon x_N^\kappa \log_{10} A]$ , *c.f.*, Ref. [19]. This mimics the PDF convolution method described above, but the rescaling avoids the convolution integral, so it is computationally fast to evaluate.

In Fig. 5.5 we display  $F_2^A/F_2^d$  for selected nuclei and data sets, and indicate various levels of rescaling (controlled by the  $\varepsilon$  parameter). The data points are described in Ref. [19], and the solid curve (blue) with  $\varepsilon=0$  is the default theory with no  $x$ -rescaling. The solid points are within the kinematic cuts of the global fit ( $Q > 1.3$  GeV,  $W_N > 1.7$  GeV), and the hollow points are outside these cuts. As we increase the  $\varepsilon$  parameter, we see this increases the ratio in the large  $x$  region, and can improve the comparison of the data and theory.

Judging from this sample of data, it appears that a detailed modeling of the Fermi region can improve the description of the data in this extreme kinematic region (low  $W_N$ , low  $Q$ , large  $x_N$ ). These corrections could be a combination of TMCs,  $x_N > 1$  effects, higher twist, or other non-perturbative corrections. Thus, a complete analysis must include and balance all these contributions.



## Experimental investigations

There are a number of studies that have explored the structure functions in the Fermi region at very large  $x_N$ , and we mention a few examples below.

For example: Refs. [129, 130] examined SLAC DIS data from a variety of nuclear targets and found that in the larger  $x_N$  region ( $x_N \gtrsim 0.5$ ) the Fermi motion effects are similar to those in the deuteron, and increase for heavier nuclei. Measurements in this region are particularly challenging, and are subject to a variety of uncertainties as outlined in the Appendix of Ref. [129].

For the CC neutrino DIS process, CCFR [131] measured  $\sim 2000$  events in the region  $x_N > 0.75$ , and used this to study  $F_2$  at very large  $x_N$ . They fit the high  $x_N$  behavior to a decaying exponential  $\propto \exp(-sx_N)$  normalized at  $x_N = 0.65$ , and find a slope of  $s = 8.3 \pm 0.7$ . They note this compares favorably with E133 at SLAC [132], which observed  $s \sim [7, 8]$ .

Hall C at Jefferson Lab measured the NC structure function  $F_2$  on a variety of nuclei ranging from  ${}^2\text{H}$  and  ${}^3\text{He}$  up to  ${}^{197}\text{Au}$  in the large  $x_N$  region [133, 134] out to  $x_N \sim 1.4$ . This work extends an earlier study of Ref. [135], and related measurements performed at SLAC [136]. Taking account of the kinematic pre-factors and the  $\{h_2, g_2\}$  contributions, they extract  $F_2^{(0)}(\xi_N, Q^2)$ , where  $\xi_N$  is the Nachtmann variable, and fit this to a decaying exponential of the form  $\exp(-s\xi_N)$  in the region  $\xi_N \geq 0.75$ . The large  $\xi_N$  fits finds the slope is in the general range  $s \sim 15 \pm 2$ . The slope has a mild increase with increasing  $Q^2$ , and a mild decrease with increasing nuclear  $A$ . These results also compare favorably with the BCDMS muon scattering data [137] which finds  $s = 16.5 \pm 0.6$  for  $x_N \sim [0.75, 1.05]$ .

## Parton momentum in the Fermi region

Based on the above large  $x_N$  measurements, we can ask the question: How much parton momentum is in the region  $x_N > 1$ ?

The experimental measurements discussed above parameterize  $F_2$  at large  $x_N$  as  $\exp[-sx_N]$ , where  $s$  can range from about  $\sim 8.3$  to  $\sim 14$ . With  $s=8.3$ , the fraction of  $F_2$  in the range  $x_N \in [1, \infty]$  is less than  $\sim 6\%$  than that in the range  $x_N \in [0.65, 1]$ . Given that the average momentum fraction in the interval  $x_N \in [0.65, 1]$  is  $\lesssim 2\%$  of the total nucleon momentum, this gives a rough estimate of the potential momentum fraction beyond  $x_N > 1$  of  $6\% \times 2\% \lesssim 0.1\%$  of the total momentum fraction. For  $s \sim 14$ , the decrease at large  $x_N$  is even steeper. Here, the  $F_2$  ratio of  $x_N \in [0.65, 1]$  compared to  $x_N \in [1, \infty]$  drops to  $\lesssim 0.1\%$ , and the potential momentum fraction beyond  $x_N > 1$  estimate becomes  $1\% \times 2\% \lesssim 0.02\%$  of the total. In both of the above cases, the integrated parton momentum is very small in the  $x_N > 1$  region, but the impact on the  $F_2^{A1}/F_2^{A2}$  ratio still yields the characteristic increase in the  $x_N \sim 1$  Fermi region.

## 5.6. Threshold problem and higher twist contributions

On the basis of the correspondence between the limits  $x_N \rightarrow 1$  and  $W_N^2 \rightarrow M_A^2$ , the very high- $x_N$  behavior of DIS structure functions at fixed  $Q^2$  is sensitive to the presence of power-suppressed corrections beyond leading twist (twist-4 for unpolarized processes). It has been conjectured that the problematic threshold behavior in target-mass corrected structure functions in the free nucleon case are at least partly due to the absence of higher-twist contributions. As an approximate test of the inclusion of twist-4 contributions, Ref. [138] proposed a  $1/Q^2$  expansion of the OPE mass-corrected structure functions, which indeed suppresses the problematic threshold behavior. These calculations were done for  $F_2$ , and later, for other tensor structure functions in Ref. [139]. While this was done for the free nucleon, a similar exercise might be carried out for nuclear structure functions as another TMC prescription.

In particular, Kulagin and Petti [138] showed that by expanding the target mass corrected structure functions to leading order in  $1/Q^2$ , the resulting functions have the correct  $x_N \rightarrow 1$  limits. While avoiding the threshold problem, this prescription, however, raises the question of whether the  $1/Q^2$  approximation is sufficiently accurate for structure functions near  $x_N \approx 1$  at moderate  $Q^2$ .

To test the convergence of the  $1/Q^2$  expansion at large  $x$ , Ref. [139] further expands the OPE result(s) to include  $\mathcal{O}(1/Q^4)$  corrections. In fact, one can demonstrate that for a structure function that behaves at large  $x$  as  $(1-x)^n$ , the target mass corrected result will vanish in the  $x_N \rightarrow 1$  limit up to order  $1/Q^{2n-2}$  in the expansion. For  $n \approx 3$ , as is typical for nucleon structure functions, the threshold problem will therefore appear only at order  $1/Q^6$ .

## 6. The parton model with quark and hadron masses

We now turn to a discussion of the parton model, including the effects of quark and hadron mass. Such mass effects can be rigorously included in the QCD-improved parton model, as shown in a general factorization proof with quark masses by Collins [55]. This work extended the factorization proof to the case of massive partons and demonstrated that all contributions proportional to the parton mass can be fully factorized. The underlying scheme is also known in the literature as the Aivazis-Collins-Olness-Tung (ACOT) scheme [70, 71, 140], which is an example of what is called a General Mass Variable Flavor Number Scheme (GM-VFNS) in the modern literature [71, 105–108, 141]. In the following subsections we summarize DIS structure functions in the ACOT scheme, including quark and hadron (nuclear) mass effects, and compare and contrast these expressions to the structure functions in the OPE. As discussed in the introduction (Sec. 1), we consider the theoretical status of both approaches, the OPE and the collinear-factorization-based QCD-improved parton model, on equal footing.

In the naïve, massless parton model, we have a hadron  $A$  of momentum  $p_A$  that emits a collinear parton of momentum  $k = x_A p_A$ . If we try and extend this simple picture to the case of massive partons, the presence of the parton's mass  $m_i$  violates collinear kinematics and we encounter ambiguities proportional to the parton mass. We work in the ACOT formalism [70, 71, 140] to compute the structure functions in the helicity basis. This has the advantage that the polarization vectors are boost invariant between the hadron and parton frame, and provides advantages for incorporating both the hadron and parton masses, as we illustrate below. We observed in Sec. 4 that hadron masses modify the scaling variable via the relation  $\xi_A = R_M x_A$ , where the  $\xi_A$  is the Nachtmann variable. Within the context of the OPE and the parton model, the effect of the quark masses factorizes from the hadronic modifications. The rescaling variable is modified by an additional factor  $R_{ij}$ , which is a function of the quark masses  $\{m_i, m_j\}$  and is defined in Table 4.2. Thus, we have  $\bar{\xi}_A = R_{ij} R_M x_A$ . Recall the Nachtmann variable  $\xi_A$  includes the TMCs due to  $M_A$ , and the variable  $\bar{\xi}_A$  (with the overline) includes both the TMCs and the parton mass corrections.

In the following, we also review the structure functions in the light-front formalism, and compare with the TMC expressions obtained from the OPE. There has been extensive discussion in the literature about computations with massive partons [71, 105–108]. The present discussion is focused on the detailed organization of the massive parton contributions in the formalism outlined by Collins [55]. Thus, we include all terms of order  $\mathcal{O}(m_i/Q)^2$ , and the non-factorizable terms are suppressed by powers of  $(\Lambda_{\text{NP}}/Q)^2$ .

### 6.1. Helicity formulation of the parton model

When we generalize the massless QCD parton model to the massive case, there are potential ambiguities proportional to the parton mass  $m_i$ , which may enter if one is not careful about organizing the perturbative expansion. This organization is more easily dealt with in the helicity basis<sup>14</sup> as we outline in this section; however, helicity and more common tensor formulation lead to identical results.

The original ACOT formalism for massive DIS was derived in the helicity basis, and this provides some advantages in working with both hadron and parton masses. For example: in the helicity formalism, we can define polarization vectors (Sec. 6.2) in a boost-invariant manner so that they are the same for both the hadron and parton reference frames (Sec. 6.3). This has the advantage that there are no mixing of terms between the partonic and hadronic structure functions<sup>15</sup> in the helicity basis that could otherwise originate from

<sup>14</sup>For clarity, this is the same technology used to compute helicity amplitudes and can be found in popular textbooks [142, 143].

<sup>15</sup>The partonic structure functions describe the theoretically calculable interaction of the partons with a vector boson.

making a boost (helicity eigenstates, e.g., polarization vectors and spinors, are not boost-invariant quantities). Additionally, by working with light-front momenta,  $\{p^\pm, k^\pm\}$ , we can take advantage of the fact that  $p^+ \gg p^-$  and  $k^+ \gg k^-$ , and define our scaling variable  $\xi$  as  $k^+ = \xi p^+$ , which is valid for both massless and massive partons. In this Section, we will initially use  $\xi$  (un-subscripted) as a generic scaling variable, and we will connect this to  $\xi_A$  and  $\tilde{\xi}_A$  in Sec. 6.4.

For the present discussion we focus on the target mass corrections that enter the hadronic structure functions. We show that the helicity formalism matches the leading terms of the OPE master formula. We compare these result both analytically in Sec. 6.4 and numerically in Sec. 6.5 (and Sec. 7).

## 6.2. Helicity decomposition

In analogy to what was done in Sec. 2, one can also decompose the hadronic tensor  $\tilde{W}_{\mu\nu}^A$  to obtain the six structure functions  $\tilde{F}_{mn}^A$  in a basis of helicity polarizations by projecting out the Lorentz tensors [70, 71, 144]. Conventionally, this basis is defined using the polarization vectors  $\varepsilon_\mu(q, \lambda)$  of the intermediate exchange boson  $V$ , with momentum  $q$  and helicity  $\lambda$ . Explicitly, the decomposition for nucleus  $A$  is given by

$$\tilde{W}_{\mu\nu}^A(p_A, q) = \sum_{m,n} \varepsilon_\mu^*(q, m) \tilde{F}_{mn}^A(p_A, q) \varepsilon_\nu(q, n), \quad (6.1)$$

where polarization vectors according to the ACOT convention are

$$\varepsilon_\mu(q, m = \pm) = \frac{1}{\sqrt{2}} (0, \mp 1, -i, 0), \quad \varepsilon_\mu(q, m = 0) = \frac{(-q^2)p_\mu + (p \cdot q)q_\mu}{\sqrt{(-q^2)[(p \cdot q)^2 - q^2 p^2]}}, \quad \varepsilon_\mu(q, m = s) = \frac{q_\mu}{\sqrt{Q^2}}. \quad (6.2)$$

(Note the  $\mp$  Condon-Shortley convention for the transverse polarizations.) Here, the transverse polarization vectors are defined in a collinear frame where  $q_z > 0$ . The longitudinal polarization vector is defined with respect to a reference vector  $p$  (usually taken to be  $p_A$ ). The scalar polarization vector  $\varepsilon_\mu(q, m = s)$ , which is sometimes called the ‘‘auxiliary polarization vector’’ [142, 145], ensures the completeness relationship for off-shell and  $t$ -channel exchanges of the photon:

$$-g_{\mu\nu} = \varepsilon_\mu(q, +)\varepsilon_\nu^*(q, +) + \varepsilon_\mu(q, -)\varepsilon_\nu^*(q, -) - \varepsilon_\mu(q, 0)\varepsilon_\nu^*(q, 0) + \varepsilon_\mu^\gamma(q, s)\varepsilon_\nu^{\gamma*}(q, s). \quad (6.3)$$

The indices  $m, n$  in Eq. (6.1) span the helicities plus (+), minus (-), longitudinal (0), and scalar ( $s$ ). Angular momentum conservation reduces these to six combination  $\{++, --, 00, ss, 0s, s0\}$ , just as we have six hadronic structure functions in the tensor basis  $F_i$  with  $\{i = 1..6\}$ . Additionally, the three combinations  $\{F_{ss}, F_{s0}, F_{0s}\}$  are suppressed by the lepton mass in a manner analogous to  $\{F_4, F_5, F_6\}$ , so typically these are ignored. We indicate the remaining combinations,  $\{F_{++}, F_{00}, F_{--}\}$ , by the short-hand notation  $F_\lambda$  with  $\lambda = \{+, 0, -\}$ .

Using the orthogonality and normalization conditions of the polarization vectors, the decomposition of Eq. (6.1) can be inverted, leading to the expression

$$\tilde{F}_{mn}^A(p_A, q) = \varepsilon^\mu(q, m) \tilde{W}_{\mu\nu}^A(p_A, q) \varepsilon^{\nu*}(q, n), \quad (6.4)$$

which can be used to construct all six structure functions in the helicity basis. Explicit calculation gives

$$\tilde{F}_{mn}^A(x_A) = \sum_{i=1}^6 R_i^{A(m,n)}(x_A, Q^2) \times \tilde{F}_i^A(x_A), \quad (6.5)$$

where the coefficient functions  $R_i^{A(m,n)}(x_A, Q^2)$  are given in Table 6.1. In the DIS limit, the  $R_i^{A(m,n)}$  coefficients simplify since  $\sqrt{1 + Q^2/(q^0)^2} = \sqrt{1 + (2x_A M_A)/q^0} \rightarrow 1$  in the high energy limit. Alternative helicity bases can lead to relative sign differences in Table 6.1, particularly for the scalar polarizations. For example: in the HELAS basis [146], Eq. (6.4) is augmented by factors of  $1/(\varepsilon \cdot \varepsilon^*)$  to account for the normalization differences. Moreover, defining Eq. (6.4) using  $\tilde{W}_i$ , as done in the original ACOT works [70, 71] can also lead to normalization

Tensor $\leftrightarrow$ Helicity	$\tilde{F}_1^A$	$\tilde{F}_2^A$	$\tilde{F}_3^A$	$\tilde{F}_4^A$	$\tilde{F}_5^A$	$\tilde{F}_6^A$
$\tilde{F}_+^A \equiv \tilde{F}_{++}^A$	1		$-r$			
$\tilde{F}_-^A \equiv \tilde{F}_{--}^A$	1		$+r$			
$\tilde{F}_0^A \equiv \tilde{F}_{00}^A$	-1	$\frac{r^2}{2x_A}$				
$\tilde{F}_S^A \equiv \tilde{F}_{SS}^A$	1	$\frac{1}{2x_A}$		$2 \frac{Q^2}{M_A^2}$	$\frac{-1}{x_A} \frac{Q^2}{M_A^2}$	
$\tilde{F}_{0S}^A + \tilde{F}_{0S}^A$		$\frac{r}{x_A}$			$\frac{-r}{x_A} \frac{Q^2}{M_A^2}$	
$\tilde{F}_{0S}^A - \tilde{F}_{0S}^A$						$\frac{-r}{x_A} \frac{Q^2}{M_A^2}$

Table 6.1: The transformation between the tensor and helicity basis. The dotted lines highlight the scalar-based modes which are suppressed by the lepton mass. This table demonstrates there is a one-to-one relation between the helicity and tensor structure functions. This table matches the ACOT convention of Table III in Ref. [70] with appropriate conversions: (i) we replace  $r \rightarrow \rho$ ; (ii) Ref. [70] includes an additional factor of  $1/2$  in the definitions of  $\{W_3, W_5, W_6\}$ , so this table includes a relative factor of 2 in the columns for  $\{\tilde{F}_3^A, \tilde{F}_5^A, \tilde{F}_6^A\}$ . Additionally, note there is a relative factor of  $2x$  between the helicity  $F_0$  and longitudinal  $F_L$  structure function definitions  $F_L = 2xF_0$  as noted in Eq. (6.13).

differences.

We obtain the hadron-level cross section by contracting the hadronic and leptonic tensors:

$$\begin{aligned}
d\sigma &\sim L^{\mu\nu}(q, k) W_{\mu\nu}(p, q) \\
&\equiv L^{m'n'}(q, k) d_{m'}^m(\psi)^{-1} d_{n'}^n(\psi) F_{mn}(p, q) ,
\end{aligned} \tag{6.6}$$

where we show the corresponding relations in both the tensor and helicity basis. Here the Wigner rotation matrix  $d_{n'}^m(\psi)$  is the  $SO(2, 1)$  analog of the familiar  $3 \times 3$  “rotation” matrix (since the exchanged particle is spin-1 with 3 polarization states), and  $\psi$  is the boost angle that transforms between the hadronic Breit (“brick wall”) frame, where  $p \parallel q$ , and the leptonic frame where  $k \parallel k'$ , with

$$\cosh \psi = \frac{2p \cdot (k + k')}{\Delta[-Q^2, p^2, p_x^2]} = \frac{\xi^2 M^2 - Q^2 + 2\xi(s - M^2)}{\xi^2 M^2 + Q^2} \xrightarrow{M \rightarrow 0} \frac{2 - y}{y} . \tag{6.7}$$

Here,  $\Delta^2[a, b, c] = a^2 + b^2 + c^2 - 2(ab + bc + ca)$ , and  $p_x$  is the the 4-momentum of the outgoing proton remnant ( $X$ ), *c.f.*, Ref. [71]. An elegant feature of Eq. (6.6) is that the leptonic ( $L^{mn}$ ) and hadronic ( $F_{mn}$ ) helicity structure functions are simple and all the kinematic complications due to the target mass are contained in the  $d(\psi)$  rotation matrices. This simplicity is a consequence of the underlying group-theoretic approach to the factorized structure.<sup>16</sup>

<sup>16</sup>While the helicity formalism elegantly exhibits the underlying symmetries of the interaction, as we go to higher-order the computation of the Wigner rotations for multiple intermediate particles can become more complex [71].

	(OPE) TMC	ACOT-TMC	$\frac{\text{ACOT-TMC}}{\text{(OPE) TMC}}$
$F_1$	$\frac{x}{\xi r}$	1	$\frac{\xi r}{x} \sim 1 + \varepsilon^2$
$F_2$	$\frac{x^2}{\xi^2 r^3}$	$\frac{x}{\xi r^2}$	$\frac{\xi r}{x} \sim 1 + \varepsilon^2$
$F_3$	$\frac{x}{\xi r^2}$	$\frac{1}{r}$	$\frac{\xi r}{x} \sim 1 + \varepsilon^2$

Table 6.2: Tabulation of prefactors from the formulae for the TMC (obtained using the OPE) of Eq. (3.24) and ACOT-TMC light-front derivations of Eq. (6.14), where  $\varepsilon = (x_A M_A / Q) = (x_N M_N / Q)$ , and  $r = r_A = r_N = \sqrt{1 + 4\varepsilon^2}$ . While the  $F_i$ 's are generally evaluated at  $x_N$ , using Table 4.1 we have  $x_N / \xi_N = x_A / \xi_A$  and these ratios are equivalent. The TMC and ACOT-TMC prefactors differ by a uniform factor  $\xi r / x$  and match to  $\mathcal{O}(\varepsilon^2)$ , and this is plotted in Fig. 6.1. The source of this factor is discussed in the text.

### 6.3. Boost-invariant polarizations

If we work in light-front coordinates  $\{x^+, \vec{x}, x^-\}$  with  $x^\pm = (x^0 \pm x^3) / \sqrt{2}$  and  $\vec{x} = \{x^1, x^2\}$ , then

$$p_A^\mu = \left\{ p_A^+, \vec{0}, \frac{M_A^2}{2p_A^+} \right\} \quad \text{and} \quad q^\mu = \left\{ -\xi p_A^+, \vec{0}, \frac{Q^2}{2\xi p_A^+} \right\}, \quad (6.8)$$

such that  $p_A^2 = M_A^2$  and  $q^2 = -Q^2$ . Additionally,  $2(p_A \cdot q) = Q^2 / x_A = Q^2 / \xi - \xi M_A^2$ . We now choose to define the parton momentum for a massive state as

$$k^\mu = \left\{ \xi p_A^+, \vec{0}, \frac{m^2}{2\xi p_A^+} \right\}, \quad (6.9)$$

such that  $k^2 = m^2$  and  $k^+ = \xi p_A^+$ , with parton mass  $m$ . This scaling relation holds for both massless and massive partons.

We require two reference vectors to define the polarizations. For the hadron polarizations  $\epsilon_n^\nu(p, q)$  we choose the vectors  $\{p, q\}$ , while for the parton polarizations  $\epsilon_n^\nu(k, q)$  we choose the vectors  $\{k, q\}$ . For both the hadron and parton polarizations, the scalar polarization is given by  $\epsilon_0^\mu = q^\mu / Q$ , and the transverse polarizations are defined as usual to be  $\epsilon^\pm = (0, \mp 1, -i, 0) / \sqrt{2}$ . The longitudinal polarizations are constructed from the reference vectors using a completeness relation [70]. The polarization vectors only depend on the reference vectors  $p^\mu$  and  $k^\mu$  to the extent that they define the  $t - z$  plane in conjunction with  $q^\mu$ ; see Ref. [70] for details.

Thus, the polarization vectors are invariant between the hadron and parton reference frame. Additionally, there is a direct relation between the hadronic helicity structure functions  $F_\lambda$  and the partonic helicity structure functions  $\omega_\lambda$ :

$$F_\lambda = \delta^{\lambda\lambda'} f \otimes \omega_{\lambda'} \quad . \quad (6.10)$$

Here,  $f$  is the PDF,  $\otimes$  represents a convolution,  $\delta^{\lambda\lambda'}$  is the usual Kronecker  $\delta$ -function, and  $\lambda$  sums over the six helicity configurations. Specifically, we note there is no mixing as indicated by the  $\delta^{\lambda\lambda'}$  function. This is in contrast to the structure functions in the tensor basis:

$$F_i = c^{ij} f \otimes \omega_j \quad (6.11)$$

where the mixing coefficients  $c^{ij}$  contain off-diagonal elements, with indices  $i, j$  summing over the six tensor structure functions [70].

## 6.4. Relationship between TMCs on the light-front and in the OPE

Finally, coming back to the hadronic level, we can relate the hadronic helicity structure functions  $F_\lambda$  to the tensor structure functions  $F_i$  using Eq. (6.5) and obtain:<sup>17</sup>

$$F_1 = \frac{1}{2} \{F_+ + F_-\} , \quad F_2 = \frac{x}{r^2} \{F_+ + F_- + 2F_0\} , \quad F_3 = \frac{1}{2r} \{-F_+ + F_-\} , \quad (6.12)$$

where  $r = r_A = r_N = \sqrt{1 + 4\varepsilon^2}$  and  $\varepsilon = (xM/Q)$ . The  $F_0$  helicity structure function is related to the longitudinal structure  $F_L$  of Eq. (3.26) via

$$F_L = 2x F_0 = r^2 F_2 - 2x F_1 . \quad (6.13)$$

Note there is a relative factor of  $2x$  connecting the helicity  $F_0$  and the longitudinal  $F_L$  structure functions.

Translating the above relations into the formulae for the TMCs in the light-front approach yields:

$$F_1^{\text{ACOT-TMC}}(x) = F_1^{(0)}(\xi) , \quad (6.14a)$$

$$F_2^{\text{ACOT-TMC}}(x) = \frac{x}{\xi r^2} F_2^{(0)}(\xi) , \quad (6.14b)$$

$$F_3^{\text{ACOT-TMC}}(x) = \frac{1}{r} F_3^{(0)}(\xi) , \quad (6.14c)$$

and  $F_L^{\text{ACOT-TMC}}(x)$  can be constructed using Eq. (3.26). The proof of collinear factorization for heavy quarks is detailed in Ref. [55].

The correspondence between the ACOT-TMC and (OPE) TMC expressions are summarized in Table 6.2. In the right-most column, we display the relative conversion factor  $(\xi r/x)$ , which is the same for all three  $F_i^{\text{ACOT-TMC}}(x)$  results. Further manipulation of the helicity structure functions in Eq. (6.5) reveals that  $F_{4,5,6}$  also follow this pattern. For  $F_i$ , we see that the TMC and ACOT-TMC approach align to  $\mathcal{O}(\varepsilon^2)$ , where  $\varepsilon = (xM/Q)$  vanishes outside the dominant TMC region of large  $x$  and small  $Q$ . Note, these comparisons are for the leading term  $F_i^{\text{Leading-TMC}}$  only (see below and Sec. 7), as the higher order terms in  $(xM/Q)^2$  with the  $h_i$  and  $g_i$  functions are not included in the ACOT expressions.

In the above Eq. 6.14, we have used generic (un-subscripted) variables  $\{x, \xi\}$ , and this equation is valid for both **nuclear** variables  $\{x_A, \xi_A\}$ , and **nucleon** variables  $\{x_N, \xi_N\}$ , (recall,  $r_A = r_N$ ). On the LHS of Eq. 6.14 we have the Bjorken scaling variable  $x$  and on the RHS this is modified by the presence of the target mass to be the Nachtmann variable  $\xi$ . Note that the nuclear structure function  $F_i^{(0)}$  was derived without knowing any details of the partonic structure; this is the essence of the factorization between the partonic ( $R_{ij}$ ) and hadronic ( $R_M$ ) corrections. Therefore, the correct scaling variable in Eq. 6.14 is  $\xi$ , and not  $\bar{\xi} = R_{ij} \xi$ .

Separately, when we compute  $F_i^{(0)}$  in the parton model, we will have individual partonic contributions  $f(\bar{\xi}, m_i, m_j)$  that will depend on the parton masses  $\{m_i, m_j\}$ . We can incorporate the parton masses by using the full rescaling variable  $\bar{\xi} = R_{ij} \xi = R_{ij} R_M x$  (with overline). This scaling of course cannot be done at the hadron level as the scaling for the light quarks  $\{u, d, s\}$  will be different from the heavy quarks  $\{c, b, t\}$ .

## 6.5. Relation of the parton model to the OPE

The parton model ACOT-TMC results differ from the TMC results obtained with OPE in two respects: i) there is an overall factor of  $(\xi r/x)$ , and ii) the OPE result contains additional  $(xM/Q)^2$  and  $(xM/Q)^4$  terms. We will discuss the origin of these differences below.

<sup>17</sup>Note that while the  $F_i$  structure functions of Eq. (4.14) are evaluated at  $x_N$ , the relations of this section hold at the nucleus and averaged nucleon level; hence, we omit here the super/subscripts on  $F_i$  and  $x_N$ .



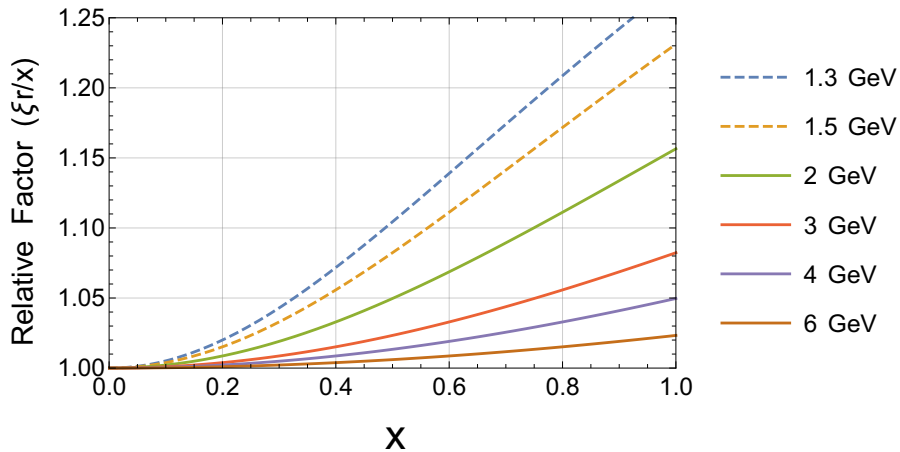


Figure 6.1: We display the relative factor  $(\xi r/x)$  between the ACOT and leading OPE terms as tabulated in Table 6.2 for  $Q = \{1.3, 1.5, 2, 3, 4, 6\}$  GeV as a function of  $x$  with  $M = M_{proton}$ . The lower two  $Q$  values  $\{1.3, 1.5\}$  are dashed to indicate these values are below typical kinematic cuts ( $Q_{cut} \sim 2$  GeV) for global PDF fits. Recall  $(\xi_{AA} r_A/x_A) = (\xi_{NN} r_N/x_N)$ .

**Correspondence of the leading factor  $(\xi r/x)$ :** The TMC (OPE) results of Eq. (4.14) contain an overall factor of  $(\xi r/x)$  as compared with the ACOT-TMC results of Eq. (6.14). The source of this factor comes from fully including the hadron mass in the calculation as outlined in A.5 which computes both the massless and massive results. The relative factor is most obvious in the case of  $F_1$ , where the ACOT-TMC result is simply given by  $F_1^{(0)}(\xi)$ .

In contrast, the massive OPE results of Eq. (A.148) include the additional  $(\xi r/x)$  factor which arises from the delta function of Eq. (A.124) using the identities of Eq. (A.125). This delta function enforces the relationship between the Bjorken and Nachtmann variables, and is a manifestation of momentum conservation. The same factor is present in all the OPE results for  $F_i$  as computed in A.5, and is summarized in Table 6.2 for  $F_{1,2,3}$ . Additionally, this factor is also present in Ref. [62]; *c.f.*, Eq. (1.24) where, matching notation,  $(1 + \mu\xi^2) = (r\xi/x)$  with  $\mu = (M/Q)^2$ .

In Fig. 6.1 we show the size of this relative factor as a function of  $x$  for selected  $Q$  values. For small  $x$  and large  $Q$  this factor is close to unity, but grows for large  $x$  and small  $Q$  values where the TMCs are typically substantial.

**Correspondence of the  $(M/Q)$  powers:** The OPE master equation, Eq. (3.24), includes higher powers of  $(xM^2/Q^2)$ , i.e., the  $\tilde{h}_i^A$  and  $\tilde{g}_2^A$  terms, which are formally twist-2 (leading twist). The source of these is the intrinsic transverse momentum of partons ( $k_T$ ) and manifests through the conservation of momentum [62, 63]. For such configurations, partonic cross sections are evaluated with (initial) parton momenta being on-shell but not collinear with the parent hadron. Details are provided in Refs. [62, 63], which include the transverse momentum in the description of the partons, [*c.f.*,  $f(x, k_T^2)$  in Eq. (1.22) of Ref. [62]]. As the transverse momentum is of order  $M$ ,  $k_T$ -dependent contributions generate the  $(M^2/Q^2)$  and  $(M^4/Q^4)$  terms of Eq. (3.24). Thus, if the transverse momentum is accounted for in the parton model, one matches the OPE result [62, 63].

**Recap:** We have derived the structure function results for the parton model using the ACOT formalism in a helicity basis as summarized in Eq. (6.14). We can obtain a complete correspondence between the parton model and OPE structure function results if i) we fully account for the hadron mass in the delta function (*c.f.*, Eq. (A.124)), which ensures the relationship between the Bjorken and Nachtmann variables, and ii) we account for the transverse momentum of the parton (*c.f.*, Ref. [62]).

## 7. Numerical results

Having discussed various theoretical and phenomenological aspects of TMCs for nuclei from an analytic perspective, we now turn our focus to the quantitative aspect of TMCs. In this section, we explore the numerical impact of TMCs on first the proton structure functions (Sec. 7.1), and then the nuclear structure functions (Sec. 7.2). We will examine both the leading-TMC and sub-leading-TMC contributions, and explore the variation across the nuclear  $A$  range. These observations will allow us to design a simple parameterization of the TMCs which are computationally efficient (Sec. 7.3). Finally, we will compute the impact of the TMCs for DIS reduced cross sections with sample kinematics from HERA, JLab, EIC, and LBNF (Sec. 7.4).

In order to build intuition for numerical results throughout this section, it is useful to recall several relations between structure functions and quark and antiquark PDFs, but which hold only at LO in the absence of CKM mixing and masses. In particular, for neutrino and antineutrino DIS on an arbitrary nuclear target ( $A$ ), where  $A$  may also be just a proton, the charged current structure functions ( $F_i^{W^\pm}$ ) and PDFs are related by:

$$F_1^{\nu A} = (d + s + \bar{u} + \bar{c}), \quad F_1^{\bar{\nu} A} = (u + c + \bar{d} + \bar{s}), \quad (7.1a)$$

$$F_2^{\nu A} = 2x(d + s + \bar{u} + \bar{c}), \quad F_2^{\bar{\nu} A} = 2x(u + c + \bar{d} + \bar{s}), \quad (7.1b)$$

$$F_3^{\nu A} = +2(d + s - \bar{u} - \bar{c}), \quad F_3^{\bar{\nu} A} = -2(u + c - \bar{d} - \bar{s}), \quad (7.1c)$$

in the limit of four quarks. Here  $\{u, d, \dots\}$  are the PDFs of a full nucleus  $A$ . Likewise, when the exchange of  $Z$  bosons can be neglected in charged lepton DIS, the neutral current structure functions ( $F_i^\gamma$ ) are related to PDFs at LO by

$$F_2^{l^\pm A} = x \frac{1}{9} [4(u + \bar{u}) + (d + \bar{d}) + 4(c + \bar{c}) + (s + \bar{s})]. \quad (7.2)$$

While the LO relations shown above are intuitively useful, our calculations are performed at full NLO in QCD including the quark mass contributions; specifically, we use the S-ACOT( $\chi$ ) scheme [147].

Since we will compare separate components of the TMC contributions, to reduce ambiguity we introduce the nomenclature which we will use throughout our presentation. Schematically, the OPE TMC terms are related as follows:

$$\underbrace{F_2^{A, \text{TMC}}(x_N, Q^2)}_{\text{TMC}} = \underbrace{\left( \frac{x_N^2}{\xi_N^2 r_N^3} F_2^{A, (0)}(\xi_N, Q^2) \right)}_{\text{Leading-TMC}} + \underbrace{\left( \frac{6M_N^2 x_N^3}{Q^2 r_N^4} \right) h_2^A(\xi_N, Q^2)}_{\text{h-term}} + \underbrace{\left( \frac{12M_N^4 x_N^4}{Q^4 r_N^5} \right) g_2^A(\xi_N, Q^2)}_{\text{g-term}} \quad (7.3)$$

We provide additional details below.

**TMC:** We identify the full set of contributions to the structure function, given by the rescaled OPE equation of Eq. (4.14), as the ‘‘TMC’’ result; this label is without additional qualifiers.

**No-TMC:** As we take the  $(xM^2/Q^2) \rightarrow 0$  limit, the pre-factors of  $F_i^{A, (0)}$  become unity, and the higher-order  $(xM/Q)^2$  and  $(xM/Q)^4$  terms containing the  $\{h_i, g_i\}$  functions vanish. Additionally, we have  $\xi \rightarrow x$  so that the expressions in Eq. (4.14) reduces to  $F_i^{A, (0)}(x_N, Q^2)$  alone. We refer to this as the ‘‘No-TMC’’ result.<sup>18</sup>

**Leading-TMC:** The ‘‘Leading-TMC’’ structure functions are obtained from Eq. (4.14) by only keeping the first term on the RHS which is proportional to  $(xM/Q)^0$ . Specifically, we are neglecting the terms proportional to  $(xM/Q)^2$  and  $(xM/Q)^4$  which contain the  $\{h_i, g_i\}$  functions.

<sup>18</sup>Note, we always retain the full quark mass dependence in all calculations as this is factorized from the hadron-level kinematics. *C.f.*, Ref. [73] for details. For this reason, we **do not** refer to the **No-TMC** term as a ‘‘massless’’ result.

**ACOT-TMC:** We obtain the “ACOT-TMC” structure functions from the ACOT TMC equation of Eq. (6.14). This result is similar to the “Leading-TMC,” but the pre-factors differ by  $(\xi r/x)$  as detailed in Table 6.2. Importantly, the “ACOT-TMC” result does not include the higher-order  $(xM/Q)^2$  and  $(xM/Q)^4$  terms containing the  $\{h_i, g_i\}$  functions.

**h-terms & g-terms:** The “h” and “g” terms are those terms in the full (OPE) TMC result that are proportional to the  $h_i$  and  $g_i$  functions. We observe that the “h” contributions are proportional to  $(M_N^2/Q^2)$ , while the “g” contributions are proportional to  $(M_N^4/Q^4)$ .

## 7.1. Proton structure functions with TMCs

In comparison to structure functions for massless protons, structure functions with TMCs for nuclei contain two additional layers of complexity. The first, of course, is the larger nucleon content; the second are the TMCs themselves. Therefore, in order to establish a baseline intuition of TMCs for nuclear structure functions, we consider briefly TMCs for proton structure functions. For more comprehensive studies of TMCs for protons, see Ref. [73] and references therein.

We will show results for a range of  $Q$  values. For a typical global analysis, the PDF evolution uses an initial scale  $Q_0$  in the range of 1.3 to 1.5 GeV, and a typical kinematic cut is  $Q \gtrsim 2$  GeV. For example, in Fig. 7.1 we display  $Q = 1.5$  GeV, which is near the initial evolution scale but below the typical kinematic cut. We also display  $Q = 10$  GeV, which is above the kinematic  $Q$  cut (the  $W$  cut is more complex).

We begin with Fig. 7.1, where in the upper panel we plot the absolute structure functions  $F_i$  for charged current ( $W^-$ ) and neutral current ( $\gamma, Z$ ) exchange showing full “TMC” (solid), “Leading-TMC” (dash), “No-TMC” (dash-dot), and “ACOT-TMC” (dotted), at  $Q = 1.5$  GeV and 10 GeV as a function of the Bjorken scaling variable  $x$ . In the lower panel we show the ratio of the full “TMC” to the “No-TMC” results.

**$F_i$  structure functions:** (Fig. 7.1 Upper Panels) We focus first on the upper panels of Fig. 7.1 which shows the proton structure functions vs.  $x$ . All the structure functions are steeply decreasing for large  $x$ . This reflects the underlying PDF structure of Eqs. (7.1) and (7.2): PDFs, and hence structure functions, must decrease at large  $x$  due to momentum conservation.

For both  $Q = 1.5$  GeV and  $Q = 10$  GeV, we observe that the full “TMC,” “Leading-TMC” and “ACOT-TMC” results roughly coincide. The good agreement between the full “TMC” and “Leading-TMC” allows us to infer that the sub-leading contributions containing the  $\{h_i, g_i\}$  terms are small; this is to be expected as they are suppressed by powers of  $(M/Q)^2$  and  $(M/Q)^4$ . We will further examine the impact of these sub-leading terms in Sec. 7.2. The approximate agreement of the “Leading-TMC” and the “ACOT-TMC” reflects the impact of the relative factor of  $(\xi r/x)$  discussed in Sec. 6.4.

In contrast, at  $Q = 1.5$  GeV, the “No-TMC” results are dramatically different from the other three curves. The “No-TMC” expression is most similar to the “Leading-TMC” as illustrated below for the case of  $F_1$ :

$$F_1^{\text{TMC-leading}}(x_N) = \frac{x_N}{\xi_N r_N} F_1^{(0)}(\xi_N) , \quad (7.4a)$$

$$F_1^{\text{No-TMC}}(x_N) = F_1^{(0)}(x_N) , \quad (7.4b)$$

where  $r_N = \sqrt{1 + 4\varepsilon^2}$ . There are two differences between these expressions: i) for “No-TMC” the pre-factor is set to unity, and ii) the argument of  $F_i^{(0)}$  is set to  $x$  instead of  $\xi$ . Given that  $\xi = 2x/(1+r) \simeq x(1 - x^2 M^2/Q^2)$ , the expression for  $F_1^{\text{No-TMC}}$  is neglecting the  $(M/Q)$  mass effects.

We can separately explore the impact of these two components and determine which is dominant. For  $F_1$  the relative factor  $x/(\xi r)$  is precisely the inverse of what is displayed in Fig. 6.1. Thus, we observe that for  $Q = 1.5$  GeV and  $x = 0.9$ , this factor yields a shift of  $\sim 20\%$ . Comparing with Fig. 7.2, we see this is clearly not sufficient to explain the observed large difference between the “No-TMC” and “Leading-TMC” results. While  $F_2$  and  $F_3$  have slightly different prefactors, we obtain the same conclusion that these prefactors do not generate the sizable differences observed between the “No-TMC” and the other results.

Symbol	A	Z	$J^P$	Symbol	A	Z	$J^P$	Symbol	A	Z	$J^P$
H	1	1	$\frac{1}{2}^+$	N	14	7	$1^+$	Ag <sub>iso</sub>	108	54	-
D	2	1	$1^+$	Ne	20	10	$0^+$	Sn <sub>iso</sub>	119	59.5	-
$^3\text{He}$	3	2	$\frac{1}{2}^+$	Al	27	13	$\frac{5}{2}^+$	Xe	131	54	$\frac{3}{2}^+$
He	4	2	$0^+$	Ar	40	18	$0^+$	W	184	74	$0^+$
Li	6	3	$1^+$	Ca	40	20	$0^+$	Au	197	79	$\frac{3}{2}^+$
Li	7	3	$\frac{3}{2}^-$	Fe	56	26	$0^+$	Au <sub>iso</sub>	197	98.5	-
Be	9	4	$\frac{3}{2}^-$	Cu <sub>iso</sub>	64	32	-	Pb <sub>iso</sub>	207	103.5	-
C	12	6	$0^+$	Kr <sub>iso</sub>	84	42	-	Pb	208	82	$0^+$

Table 7.1: List of nuclear PDFs considered in this work. We use the nCTEQ15 nPDF set [17]. The nuclei indicated with “iso” subscript are isoscalar corrected; thus, the  $Z$  value can be half-integer. We will also show results with a neutron PDF computed using isospin symmetry.

Thus, the dominant variation of  $F_i^{\text{No-TMC}}$  and  $F_i^{\text{TMC-Leading}}$  must be due to the different arguments:  $x$  vs.  $\xi$ . This correspondence of  $x$  and  $\xi$  is displayed in Fig. 2.1 where we observe that  $x \sim \xi$  for small  $x$  and large  $Q$ , but for large  $x$  and small  $Q$  we find  $\xi < x$ . Because the PDFs are steeply falling at large  $x$  (where  $x$  and  $\xi$  have the largest deviation), it is the difference of  $\xi$  vs.  $x$  in the arguments on the RHS of Eq. (7.4) that is driving the variation observed in Fig. 7.2. While we have detailed the comparison of  $F_1$  in Fig. 7.1, the same rationale applies to the other structure functions displayed.

In contrast to the sizable differences between the “No-TMC” result and the other three curves for the lower  $Q$  value (1.5 GeV), the “No-TMC” result is roughly comparable to the others for  $Q = 10$  GeV. In total, these comparisons affirm that TMCs are negligible for small- $x$  or for intermediate to large  $Q$ .

**$F_i$  structure function ratios:** (Fig. 7.1 Lower Panels) To highlight the importance of including the TMCs, we now examine the lower panels of Fig. 7.1 which display the ratio of  $F_i^{\text{TMC}}$  to  $F_i^{\text{No-TMC}}$ . The ratio plots accentuate subtle features that are not evident on the log-scale plots of the upper panels.

If we first focus on the  $Q = 1.5$  GeV results, we observe the deviation between  $F_i^{\text{TMC}}$  and  $F_i^{\text{No-TMC}}$  differs markedly for the separate  $F_{1,2,3}$  structure functions. These differences arise from: i) the different prefactors, see e.g. Eq. (4.14), ii) the different argument of  $F_i^{(0)}$  (as noted previously), and also iii) the sub-leading  $\{h_i, g_i\}$  contributions. It is the combination of these components that cause the variation among the Fig. 7.1 sub-figures. For example, we see the  $F_1$  curves deviate at smaller  $x$  values as compared with the  $F_2$  and  $F_3$  results. Additionally, the  $F_2$  and  $F_3$  ratios dip below unity for intermediate  $x$  values ( $x \sim 0.3 - 0.5$ ) while the  $F_1$  ratio is above unity.

## 7.2. Nuclear structure functions with TMCs

Having examined the proton structure functions in Fig. 7.1, we now consider the corresponding nuclear structure functions of Fig. 7.2. The list of nuclear isotopes that we consider are summarized in Tab. 7.1.

### Full TMCs for nuclei

In Fig. 7.2 we plot the ratio of the full “TMC” structure functions  $F_i^{\text{TMC}}$  to the “No-TMC” structure functions  $F_i^{\text{No-TMC}}$  for charged current ( $W^-$ ) and neutral current ( $\gamma, Z$ ) exchange for the nuclei of Table 7.1. This ratio highlights the impact of the TMCs.

We observe the general behavior of the nuclear ratios displayed in Fig. 7.2 are very similar to the corresponding proton results in the lower panels of Fig. 7.1. Because the nuclear and proton results are so similar,

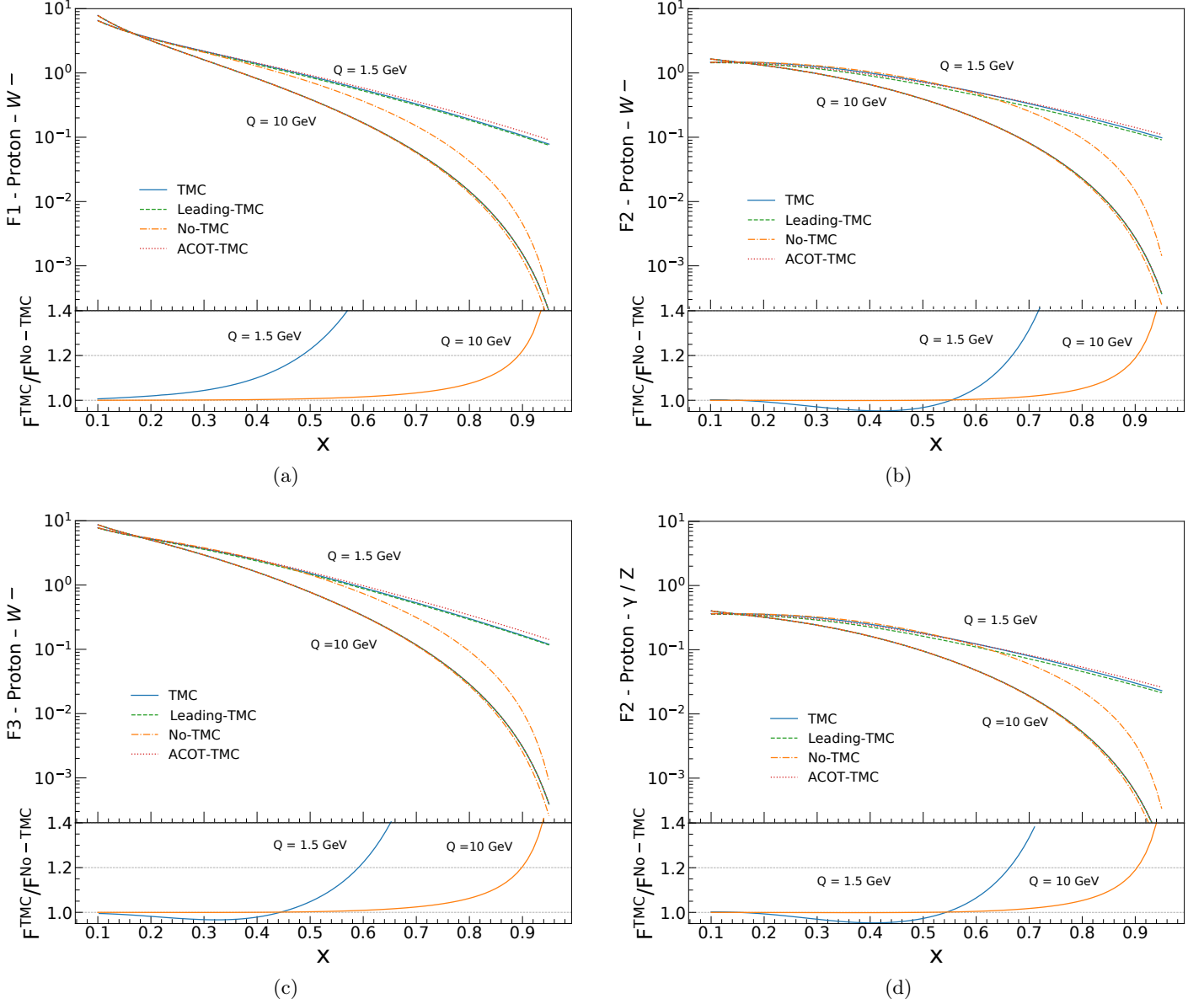


Figure 7.1: **Upper panels:** Proton structure functions for charged current  $W^-$  (a)  $F_1$ , (b)  $F_2$ , and (c)  $F_3$  and (d) neutral current  $\gamma/Z$   $F_2$  as a function of momentum fraction  $x_N$ . We display results for the full “TMC” (solid blue), “Leading-TMC” (dashed green), “No-TMC” (dot-dash orange), and “ACOT-TMC” (dotted red) at  $Q = 1.5$  GeV (upper lines) and 10 GeV (lower lines). **Lower panels:** Ratio of  $F_i$  with full “TMC” to “No-TMC” at  $Q = 1.5$  GeV and 10 GeV.

we only plot a single  $Q$  value (1.5 GeV) in Fig. 7.2 as other  $Q$  values (e.g.,  $Q = 10$  GeV) will be similar to the proton results. We will study the detailed  $Q$  dependence in the following.

The results of Fig. 7.2 clearly demonstrate that the TMCs for the nuclei are effectively independent of  $A$ . We attribute this curious finding to the re-scaling property ( $x_A M_A = x_N M_N$ ) as shown in Sec. 4. This re-scaling allows us to identically rewrite the TMCs for structure functions in Eq. (3.23), which are functions of nuclear-level quantities  $x_A$  and  $M_A$ , in terms of nucleon-level quantities  $x_N$  and  $M_N$ . As a result, the variable nucleon content of nuclei, which is the defining characteristic of nuclei, is averaged out, resulting in near universal behavior.

To illustrate the emergence of this universality, let us Taylor-expand the nuclear structure function ratio

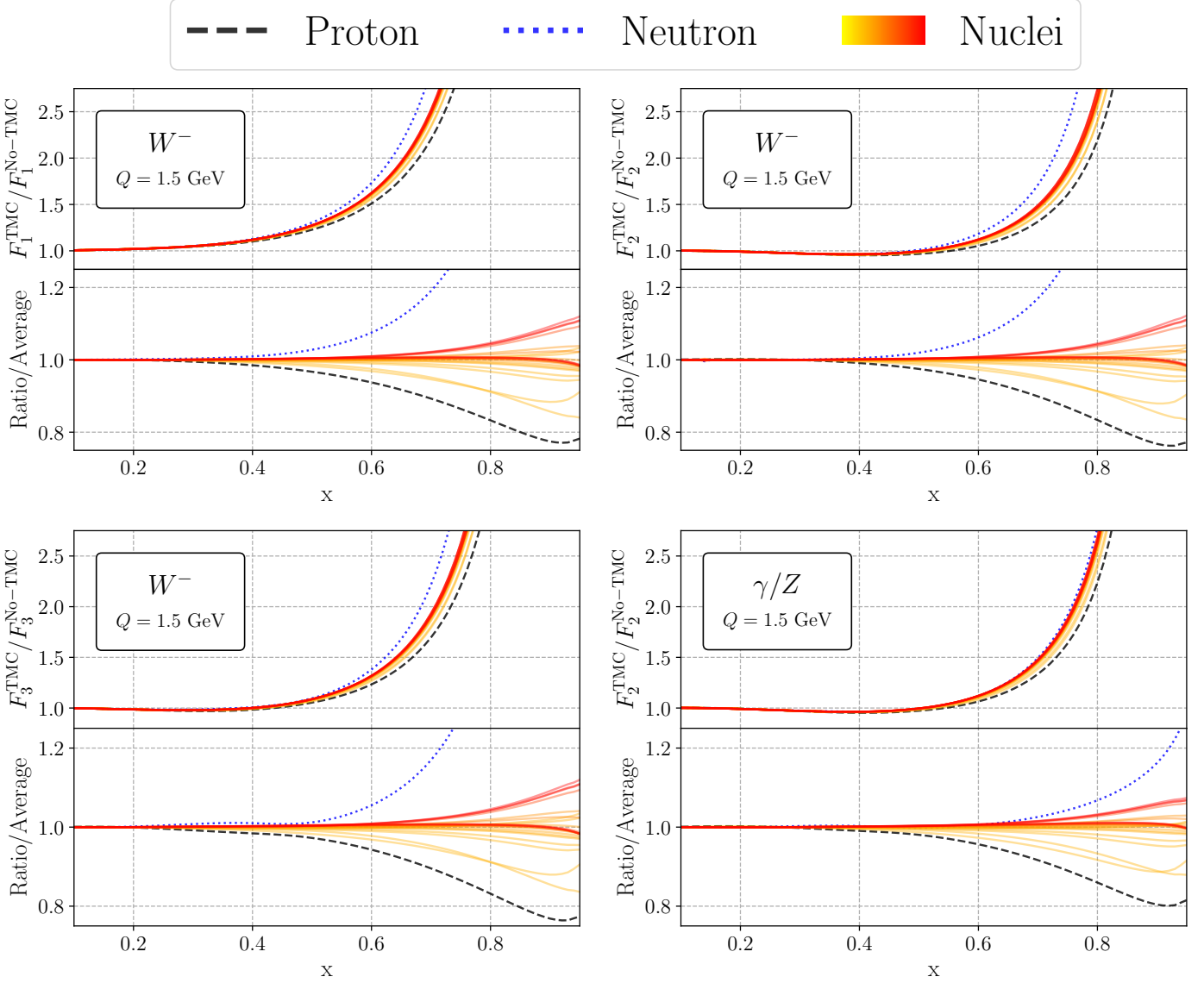


Figure 7.2: Ratio of nuclear structure functions  $F_i$  for the full “TMC” over “No-TMC” vs.  $x_N$  at  $Q = 1.5$  GeV. We display ratios for charged current  $W^-$  (a)  $F_1$ , (b)  $F_2$ , and (c)  $F_3$  and (d) neutral current  $\gamma/Z$   $F_2$  for the nuclei listed in Table 7.1. The proton is indicated with the black dashed line, and the neutron with the blue dotted line. The narrow band of colored lines shows the various nuclear results.

$F_1^{\text{TMC-Leading}}/F_1^{\text{No-TMC}}$  to show this is independent of the nuclear  $A$  value up to corrections  $\varepsilon^2 = (xM/Q)^2$ . We use the expressions of Eq. (7.4) and computing the derivative as  $F_i^{(0)}(\xi_N) \approx F_i(x_N) + \delta x_N [dF_i(y)/dy]_{y=x_N}$ , where  $\delta x_N = (\xi_N - x_N) \approx (x^3 M_p^2 / Q^2) \ll 1$ , If we apply this approximation to the  $F_1$  ratio, for example, we then obtain:

$$\frac{F_1^{\text{TMC-Leading}}(x_N)}{F_1^{\text{No-TMC}}(x_N)} \sim (1 - \varepsilon^2) \frac{F_1^{(0)}(\xi_N)}{F_1^{(0)}(x_N)} \sim (1 - \varepsilon^2) \frac{F_1^{(0)}(x_N) + \mathcal{O}(\varepsilon^2)}{F_1^{(0)}(x_N)} \sim (1 - \varepsilon^2) + \mathcal{O}(\varepsilon^4) . \quad (7.5)$$

where we have defined  $\varepsilon = (xM/Q)$ . Remarkably, we find that the ratio  $F_1^{\text{TMC-Leading}}(x_N)/F_1^{\text{No-TMC}}(x_N)$  is independent of  $A$  up to  $\varepsilon^2$ . Recall the full TMC ratio  $F_1^{\text{TMC}}(x_N)/F_1^{\text{No-TMC}}(x_N)$  differs only by the additional  $\{h_i, g_i\}$  terms which are suppressed by powers of  $(M/Q)^2$ . This implies that nuclear TMCs themselves, when



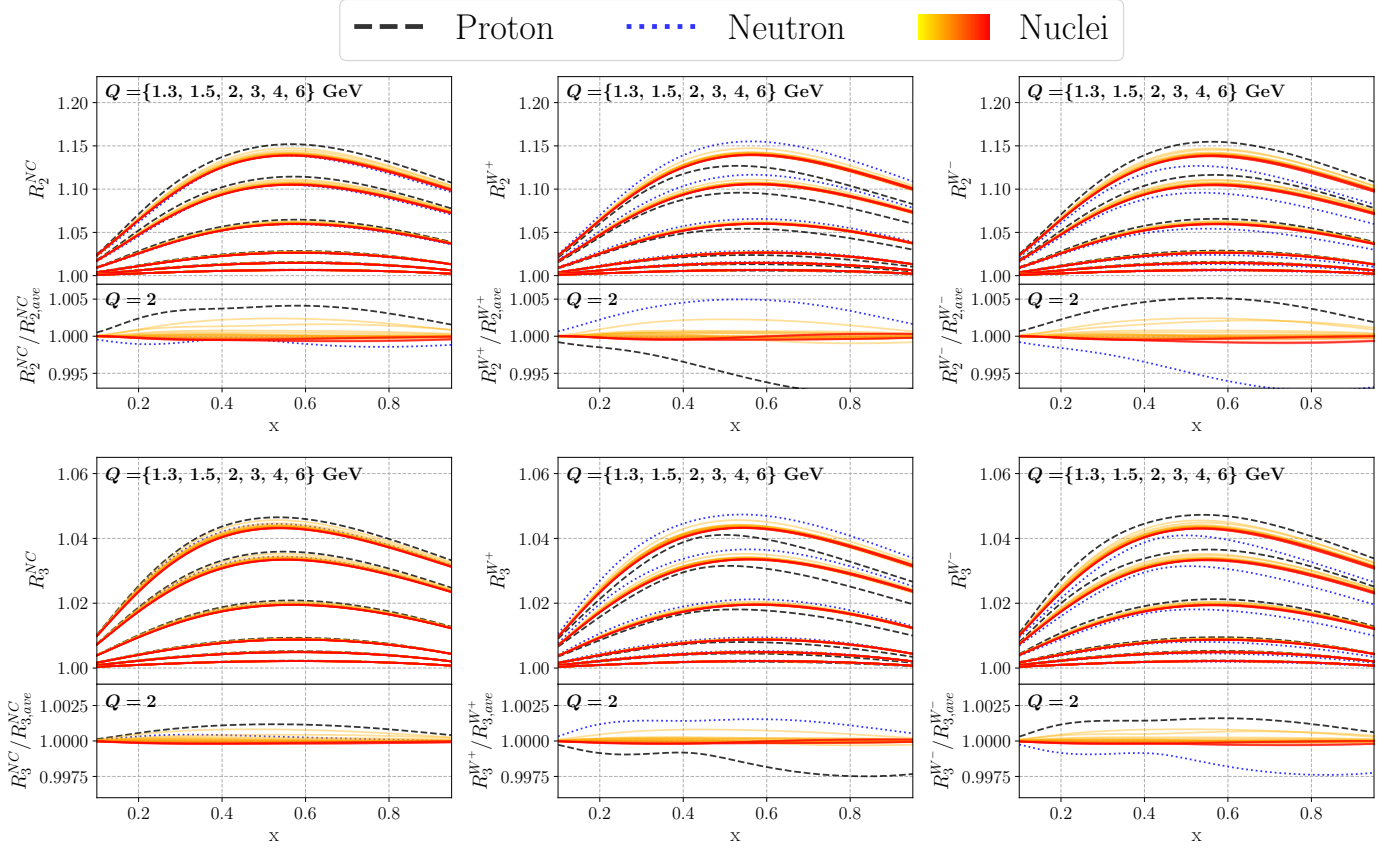


Figure 7.3: **Upper panels:** We display the nuclear structure function ratios of  $F_i^{\text{TMC}}/F_i^{\text{TMC-Leading}}$  for selected CC and NC processes for  $Q = \{1.3, 1.5, 2, 3, 4, 6\}$  GeV (from top to bottom) vs.  $x_N$ . **Lower panels:** We display the variation of this ratio compared to the average variation as computed in Eq. (7.7) for  $Q = 2$  GeV. In the top row we show  $F_2$  results for (a) NC  $\gamma/Z$  exchange, (b) CC  $W^+$  exchange, and (c) CC  $W^-$  exchange, and the bottom row shows  $F_3$  results for the same processes. In all panels, the proton is indicated with the black dashed line, and the neutron with the blue dotted line. The narrow band of colored lines shows the various nuclear results.

defined in terms of averaged quantities, are essentially universal.

We now explore this approximate universal property of the TMCs, and determine how we can exploit this property to simplify certain nuclear TMC calculations.

### Comparison of full vs. leading-TMCs for nuclei

In Fig. 7.1 we observed that the “Leading-TMC” yielded a reasonable approximation to the full “TMC” result, even at low  $Q$  and large  $x$  values. Computationally, the “Leading-TMC” result is much simpler to compute as the full “TMC” result include contributions from the  $\{h_i, g_i\}$  terms, each of which includes an integral. Additionally, if we can take advantage of the approximate  $A$  independence observed in the previous section, this may allow us to greatly simplify the calculation of TMCs for the many different nuclei present in a typical nPDF fit.

**Magnitude of ratios: (Fig. 7.3 upper panels)** We start by comparing the ratio of the “Leading-TMC” to the full “TMC” result as shown in the upper panels of Fig. 7.3. The results are shown for selected CC and NC processes with representative values  $Q = \{1.3, 1.5, 2, 3, 4, 6\}$  GeV.

We display results for all the nuclei of Table 7.1 In these plots, the individual nuclear  $A$  values are not labeled, but the ratios coalesce into clearly defined bands for each  $Q$  value. This coalescence holds for all

permutations of structure functions and boson exchanges. The different nuclei are shown as colored solid lines in the figure. We also include results for the proton (dashed black) and neutron (dotted blue).

Focusing first on the bands of the top panels, we see that for  $F_2^A$  the differences between the full TMCs and Leading-TMCs are as large as  $\mathcal{O}(10\% - 15\%)$  at  $x \sim 0.5$  for  $Q = 1.3$  GeV, and  $\mathcal{O}(4\% - 5\%)$  for  $F_3^A$ . For larger  $Q$  values we expect these differences to be reduced as they are proportional to powers of  $(M/Q)^2$ . At  $Q = 2$  GeV, which is a typical  $Q_{cut}$  value for many global PDF analyses, the ratio for  $F_2^A$  is  $\lesssim 5\%$ , and the ratio of  $F_3^A$  is  $\lesssim 2\%$ . For  $Q \gtrsim 3 - 4$  GeV, we find that these differences reduces to the sub-percent level, and effectively vanish at  $Q = 6$  GeV.

**Nuclear  $A$  dependence of ratios:** Having discussed the magnitude of the  $F_i^{\text{TMC}}/F_i^{\text{TMC-Leading}}$  ratios, we now examine the  $A$  dependence of these ratios. A distinctive feature of Fig. 7.3 is the coalescence of the results into individual bands, and this suggests that the nuclear  $A$  dependence of this ratio is minimal. [The proton and neutron ratios (shown as dashed and dotted black lines, respectively), do not necessarily lie within the bands, and we will discuss these separately.] This apparent universality of the full TMC/Leading-TMC ratios can be traced back to: i) the fact that this ratio has only mild dependence on the underlying PDF, and ii) the fact that for nuclei, in the large  $x$  region it is the average  $u + d$  (isoscalar) PDF that dominates this result.

One approach to understand these features is to consider the analytically computed upper bound for these ratios. If we assume the structure functions are monotonically decreasing (an entirely reasonable assumption in the large  $x$  region), it is possible to obtain the following constraints on these ratios [73]:

$$\frac{F_2^{\text{TMC}}}{F_2^{\text{TMC-leading}}}(x, Q^2) \leq 1 + \left(\frac{M}{Q}\right)^2 \frac{6x\xi}{r}(1 - \xi) + \left(\frac{M}{Q}\right)^4 \frac{12x^2\xi^2}{r^2}(-\ln \xi - 1 + \xi) \quad (7.6a)$$

$$\frac{F_3^{\text{TMC}}}{F_3^{\text{TMC-leading}}}(x, Q^2) \leq 1 - \left(\frac{M}{Q}\right)^2 \frac{2x\xi}{r} \ln \xi \quad . \quad (7.6b)$$

Note, these bounds have absolutely no dependence on the PDF. Here, we also explicitly see the powers of  $(M/Q)^2$  which drive the ratios to unity for large  $Q$ .

In Fig. 7.4, we plot these bounds as a function of  $x$  for selected  $Q$  values. Comparing the magnitudes of the bounds with the values of Fig. 7.3, we see the bounds are quite conservative. Note that these bounds are valid for any nPDFs in the large  $x$  region (where  $F_i^A$  is decreasing monotonically), and that is the relevant region of interest for the TMC effects. Consequently, the independence of the bound on the PDF helps us understand the comparable nuclear  $A$  independence of the  $F_i^{\text{TMC}}/F_i^{\text{TMC-Leading}}$  ratios observed in Fig. 7.3.

**Nuclear  $A$  variation of ratios:** The observation that these ratios are relatively insensitive to the nuclear  $A$  value suggests a “short cut” which can be used to efficiently implement TMCs into numerical calculations.

More specifically, computing the full TMCs for each nucleus  $A$  requires a calculation of the  $h_i^A(\xi_N, Q^2)$  and  $g_i^A(\xi_N, Q^2)$  terms in Eq. (4.14). Each term requires a separate integration over a nuclear structure function. Clearly, such steps would require significant CPU time if they were included inside the fitting loop of a global PDF analysis. If it is true that the size of TMCs to nuclear structure functions are relatively insensitive to the nuclear  $A$  value, as our works suggests, then TMCs can be estimated through the application of a “universal” correction factor,  $R_i^V(x, Q^2)$ . Such a factor can be constructed by taking an average TMC summed over the various  $n_A$  nuclei:

$$R_i^V(x_N, Q^2) = \frac{1}{n_A} \sum_k^{n_A} \frac{F_i^{A_k, \text{TMC}}(x_N, Q^2)}{F_i^{A_k, \text{TMC-Leading}}(x_N, Q^2)} = \frac{1}{n_A} \sum_k^{n_A} R_i^{k, V} \quad (7.7)$$

where “ $V$ ” labels the type of the exchanged gauge boson ( $\gamma, Z, W^\pm$ ), and the sum over  $k$  excludes the proton and neutron.

The utility of the “universal” correction factor  $R_i^V(x, Q^2)$  is that we can compute this once at the beginning of a fit, and then apply this correction factor inside the fitting loop without the need for recomputing additional integrals over  $h_i$  and  $g_i$  functions.

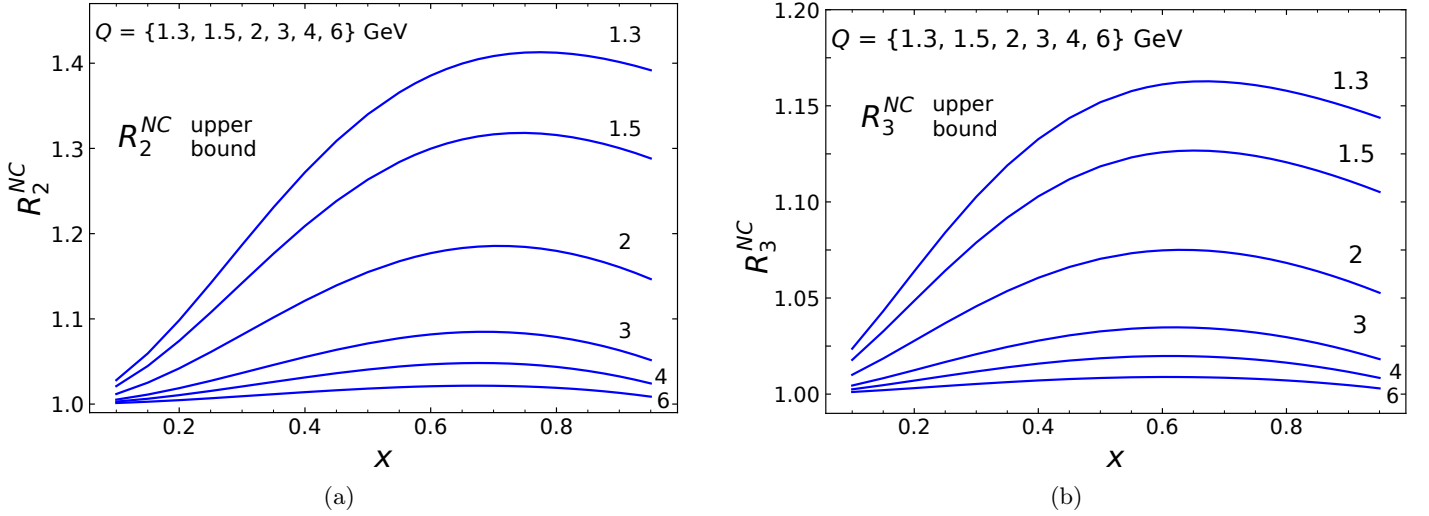


Figure 7.4: We show the upper bounds of  $R_i^{NC} = F_i^{\text{TMC}}/F_i^{\text{TMC-Leading}}$  for a)  $F_2$  and b)  $F_3$  with selected  $Q = \{1.3, 1.5, 2, 3, 4, 6\}$  GeV, (from top to bottom) *vs.*  $x_N$  as computed with Eqs. (7.6a) and (7.6b).

To determine the potential precision of such an approximation, we show in the lower panels of Fig. 7.3 a ratio of ratios constructed by taking  $(F_i^{\text{TMC}}/F_i^{\text{TMC-Leading}})$  over  $R_i^V$  for  $Q = 2$  GeV, which is a typical  $Q_{\text{cut}}$  value for global fits. It is remarkable how narrow the band of nuclear PDFs lie in comparison to the universal  $R_i^V$  function. For  $F_2$  we see the nuclear bands lie within 0.2% of the universal curve, while for  $F_3$  the bands lie within 0.1%. For larger  $Q$  values, the precision is further increased. This is clearly sufficient accuracy for any TMC calculation given the typical nPDF uncertainty in the large  $x$  region.

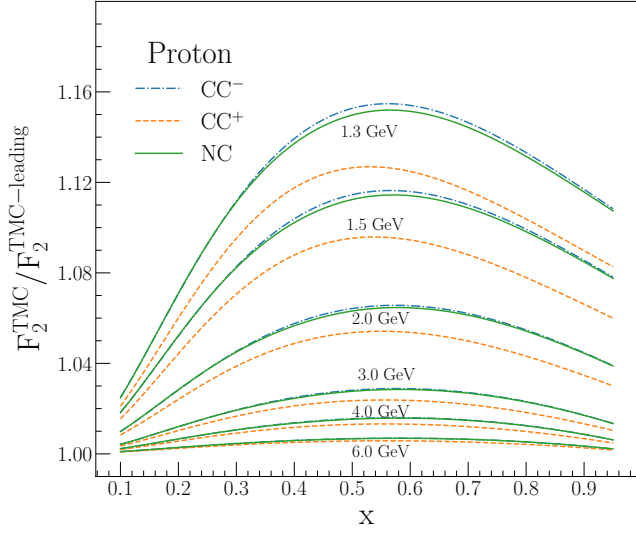
**Variation of proton & neutron ratios:** In Fig. 7.3 we observed that all the nuclear PDFs were uniformly within a narrow band. In contrast, the proton and neutron results displayed a wider variation lying outside these nuclear bands. We will explain the source of this variation, and understand why the universal correction factor  $R_i^V(x, Q^2)$  previously introduced, still works well in the case of nuclei.

Specifically, in Fig. 7.3 we see that the proton ratios lie above the nuclear band for the NC and CC  $W^-$  plots, and below for the CC  $W^+$  plots; furthermore, the behavior of the neutron ratios is exactly the opposite of the proton. We can understand these features by identifying the dominant contribution for each process. As  $x \rightarrow 1$ , we neglect the gluon and sea quarks to obtain:  $F_2(\gamma/Z) \sim \frac{x}{9}[4u(x) + d(x)]$  and  $F_2(W^-) \sim 2xu(x)$ , while  $F_2(W^+) \sim 2xd(x)$ . Recall that for a proton PDF, the  $d/u$  ratio in the large  $x$  region can typically be as small as  $\sim 0.1$ ; that is, the up quark is an order of magnitude larger than the down quark.

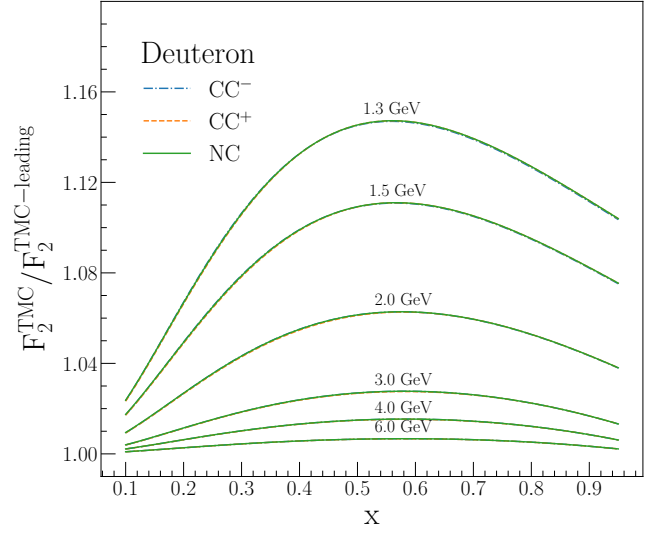
We now understand the pattern of Fig. 7.3. The structure function for the NC and CC  $W^-$  processes are driven by the up quark, while the CC  $W^+$  is driven by the down quark. Thus, the proton results are above the others for NC and CC  $W^-$  but below for CC  $W^+$  in plots of Fig. 7.3. Since we obtain the neutron PDFs by isospin symmetry ( $u \leftrightarrow d$ ), so we also understand why the neutron results are the opposite of the proton.

This exercise also demonstrates why the results for the nuclear PDFs lie together in a uniform band. Most of the nuclei are closer to the isoscalar state ( $A \sim 2Z$ ) than either the proton ( $Z = A$ ) or neutron state ( $Z = 0$ ). For an isoscalar nuclei we have  $u = d$ , and it is effectively the average of the up and down PDFs  $(u + d)/2$  which provides the dominant contributions to Fig. 7.3. Consequently, we find that the nuclear band is effectively an average of the proton and neutron result, and thus lies between the two in Figs. 7.3. The one slight variation of this pattern is the parity-violating  $F_3$  NC structure function; this effect must come from the  $Z$  boson contribution because the parity-conserving photon contribution vanishes.

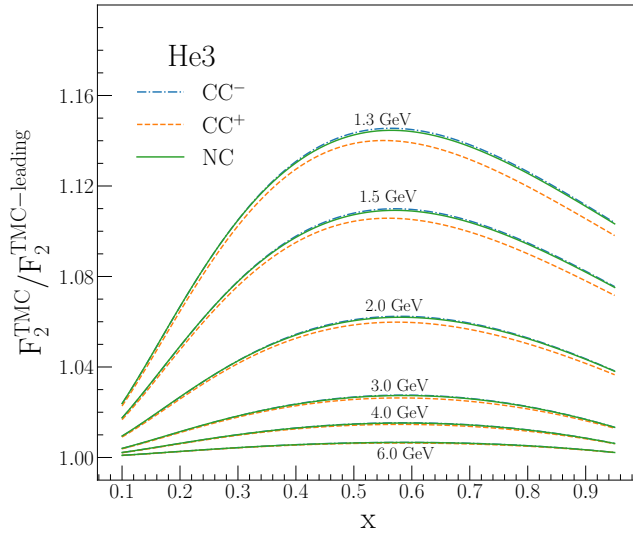
**Approximate nuclear  $A$  independence:** We illustrate this further in Fig. 7.5 which shows the ratios for the NC and CC processes for the a) proton, b) deuteron, and c)  $^3\text{He}$ . We choose these examples because the deuteron



(a)



(b)



(c)

Figure 7.5: The nuclear structure function ratio  $F_2^{\text{TMC}}/F_2^{\text{TMC-Leading}}$  as function of  $x_N$  for  $Q = \{1.3, 1.5, 2, 3, 4, 6\}$  GeV for (a) the proton, (b) deuteron, and (c)  ${}^3\text{He}$ . For each nucleus, we overlay the result for NC exchange (solid green), CC  $W^+$  exchange (dotted orange), and CC  $W^-$  exchange (dot-dashed blue). Note that for the deuteron in Fig. (b), the curves for the three CC/NC processes coincide.

is an isoscalar, and  ${}^3\text{He}$  is one of the most “non-isoscalar” nuclei (with the exception of hydrogen/proton).

The pattern in Fig. 7.5 is reminiscent of Fig. 7.3. In Fig. 7.5(a) for the proton, we see the ( $u$ -quark dominated) NC and CC  $W^-$  processes lie above the ( $d$ -quark dominated) CC  $W^+$  process. In Fig. 7.5(b) for the isoscalar deuteron, we see all the curves coincide since  $u = d$  for this nuclei. Finally, in Fig. 7.5(c) for the  ${}^3\text{He}$ , we see the NC and CC  $W^-$  processes lie slightly above the CC  $W^+$  process, but the difference is not as dramatic as for the proton case. Note in these cases, the  $u : d$  ratio is 2 : 1 in the proton, 1 : 1 in the deuteron, 5 : 4 in  ${}^3\text{He}$ . For any heavier nuclei, the  $u : d$  ratio will be comparatively closer to unity, and the results of the individual NC and CC processes will tend to coincide.

The outcome of these findings is that given the typical uncertainty of nuclear PDFs in the large  $x$  region, applying an average,  $A$ -independent set of TMCs yields precision which is sufficient for a wide variety of real-world calculations. We shall exploit this observation in Sec. 7.3 and derive an approximate parameterization for these TMCs which can be applied to the general nuclear case.

Setting aside the proton and neutron cases, at  $Q = 2$  GeV we find the deviation of individual nuclei from the average to be less than  $\sim 0.2\%$  for  $F_2$ , and less than  $\sim 0.1\%$  for  $F_3$ . And of course, these differences decrease for larger  $Q$ .

### Sub-leading TMCs for nuclei

As a final study, we want to demonstrate the individual size of the sub-leading  $h_2^A$  and  $g_2^A$  components of the full TMCs in Eq. (4.14). In Fig. 7.6 we present the results for NC ( $\gamma/Z$ ) and CC ( $W^\pm$ ) processes, and we display a pair of ratios  $F_2^{\text{TMC+h2}}/F_2^{\text{TMC-Leading}}$  and  $F_2^{\text{TMC}}/F_2^{\text{TMC-Leading}}$ , for each  $Q$  value.

Recall that  $F_2^{\text{TMC-Leading}}$  neglects the sub-leading  $h_2^A$  and  $g_2^A$  contributions, where  $h_2^A$  is suppressed by  $(M/Q)^2$ , and  $g_2^A$  is suppressed by  $(M/Q)^4$ . The  $F_2^{\text{TMC+h2}}$  expression includes the  $h_2^A$  contribution, but neglects  $g_2^A$ . Finally, the full  $F_2^{\text{TMC}}$  expression includes both  $h_2^A$  and  $g_2^A$ ; this could equivalently be called  $F_2^{\text{TMC+h2+g2}}$ .

Since the  $g_2^A$  term is suppressed by  $(M/Q)^4$ , we expect this will only contribute for very large  $x$  at low  $Q^2$  values. Therefore, we expect  $F_2^{\text{TMC+h2}}$  and  $F_2^{\text{TMC}}$  to coincide throughout most of the parameter space. This expectation is validated in Fig. 7.6 where we do see that  $F_2^{\text{TMC+h2}}$  and  $F_2^{\text{TMC}}$  differ only for the lowest few  $Q$  values in the large  $x$  region. For example, at  $Q = 2$  GeV the differences are barely discernible in the figure, and the effect is even smaller as  $Q$  increases.

Thus,  $h_2^A$  provides the dominant contribution throughout the kinematic range, but  $g_2^A$  does contribute for low  $Q$  values. The pattern for the other structure functions  $F_{1,3}^A$  is similar.

### 7.3. Parameterizing $F_i^{\text{TMC}}/F_i^{\text{Leading-TMC}}$

In Sec. 7.2 we demonstrated that the full TMC/Leading-TMC ratios were effectively insensitive to the nuclear  $A$  value. In this section, we provide a parameterization for these ratios which allows us to efficiently compute the full TMCs given the Leading-TMC structure functions.

Starting from Eq. (4.14), we divide  $F_i^{\text{TMC}}(x)$  by the leading term  $F_i^{\text{Leading-TMC}}(x)$ :

$$\frac{F_1^{\text{TMC}}(x)}{F_1^{\text{Leading-TMC}}(x)} = 1 + \frac{M^2}{Q^2} \frac{x\xi}{r} \frac{h_2(\xi)}{F_1^{(0)}(\xi)} + \frac{M^4}{Q^4} \frac{2x^2\xi}{r^2} \frac{g_2(\xi)}{F_1^{(0)}(\xi)}, \quad (7.8a)$$

$$\frac{F_2^{\text{TMC}}(x)}{F_2^{\text{Leading-TMC}}(x)} = 1 + \frac{M^2}{Q^2} \frac{6x\xi^2}{r} \frac{h_2(\xi)}{F_2^{(0)}(\xi)} + \frac{M^4}{Q^4} \frac{12x^2\xi^2}{r^2} \frac{g_2(\xi)}{F_2^{(0)}(\xi)}, \quad (7.8b)$$

$$\frac{F_3^{\text{TMC}}(x)}{F_3^{\text{Leading-TMC}}(x)} = 1 + \frac{M^2}{Q^2} \frac{2\xi x}{r} \frac{h_3(\xi)}{F_3^{(0)}(\xi)}. \quad (7.8c)$$

The goal of this section is to parameterize these ratios.

As explained in detail in B, if we assume the structure functions vanish at  $x = 1$  and expand them in a Taylor series, we can obtain simple expressions for the ratios in terms of the parameter function  $\gamma_i(Q)$ , which

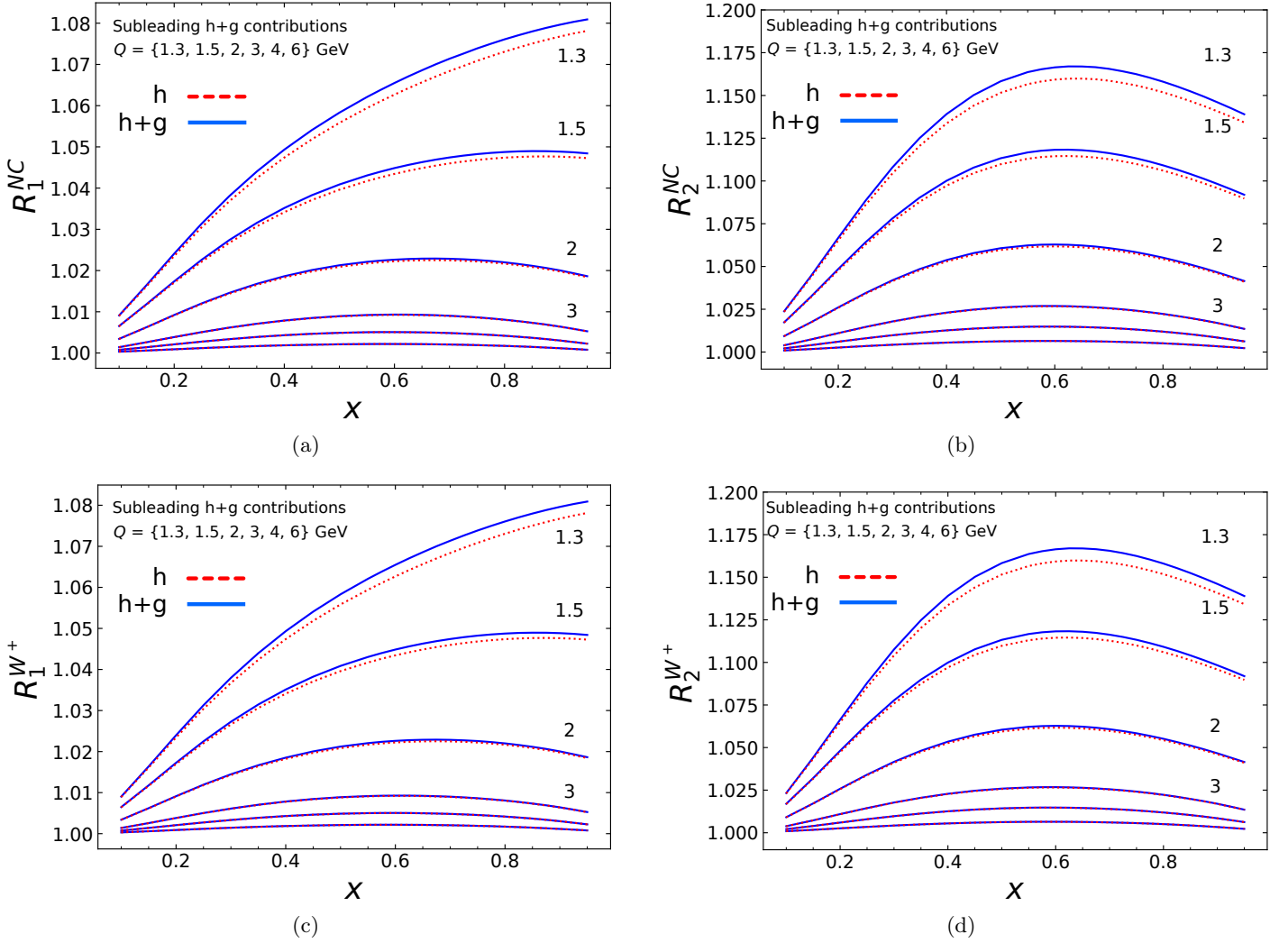


Figure 7.6: To highlight the effect of the sub-leading terms  $\{h_i, g_i\}$ , we display the ratios  $R_i^{Z, W^\pm}$ . Specifically, the “h” curve (dashed red) is the result for  $[F_i^{\text{TMC-Leading}} + F_i^{\text{h-term}}]$ , and the “h+g” curve (solid blue) is  $[F_i^{\text{TMC-Leading}} + F_i^{\text{h-term}} + F_i^{\text{g-term}}]$ , both compared to  $[F_i^{\text{TMC-Leading}}]$ . The notation is detailed in Eq. (7.3). We display selected  $Q = \{1.3, 1.5, 2, 3, 4, 6\}$  GeV (from top to bottom) as a function of  $x_N$  using the nCTEQ15 PDF for  $^{12}\text{C}$ . We observe for  $Q \geq 2$  GeV (a typical kinematic cut), the “h+g” contributions are less than  $\sim 2\%$ .

characterizes the first derivative of the structure function. This allows us to obtain the approximate expressions for the ratios  $h_i/F_j^{(0)}$  and  $g_2/F_j^{(0)}$ :

$$\frac{h_2(\xi)}{F_2^{(0)}(\xi)} = \frac{1-\xi}{\xi} + \gamma_2(Q) \frac{1-\xi}{\xi^2} \sum_{j=1}^{j_{\max}} \frac{(-1)^j}{j!(j+1)} {}_2F_1\left(2, j+1, j+2, 1-\frac{1}{\xi}\right), \quad (7.9a)$$

$$\frac{h_3(\xi)}{F_3^{(0)}(\xi)} = -\ln(\xi) + \gamma_3(Q) \frac{1-\xi}{\xi} \sum_{j=1}^{j_{\max}} \frac{(-1)^j}{j!(j+1)} {}_2F_1\left(1, j+1, j+2, 1-\frac{1}{\xi}\right), \quad (7.9b)$$

$$\frac{h_2(\xi)}{F_1^{(0)}(\xi)} = 2\xi r^2 \left[ \frac{1-\xi}{\xi} + \gamma_1(Q) \frac{1-\xi}{\xi^2} \sum_{j=1}^{j_{\max}} \frac{(-1)^j}{j!(j+1)} {}_2F_1\left(2, j+1, j+2, 1-\frac{1}{\xi}\right) \right], \quad (7.9c)$$



	$F_1^{TMC}/F_1^{leading}$		$F_2^{TMC}/F_2^{leading}$		$F_3^{TMC}/F_3^{leading}$	
nPDFs	$\lambda_1$	$\delta_1$	$\lambda_2$	$\delta_2$	$\lambda_3$	$\delta_3$
nCTEQ15	2.275	-0.014	2.144	0.100	2.183	0.029
EPPS16	2.226	-0.026	2.086	0.095	2.142	0.022
nNNPDF2.0	2.226	-0.025	2.086	0.103	2.197	0.023
TUJU19	2.290	-0.0170	2.167	0.099	2.200	0.031

Table 7.2: We approximate the  $\{h_i(\xi), g_i(\xi)\}$  contributions to  $F_i^{TMC}$  using  $F_i^{TMC\text{-Leading}}$  together with a 2-parameter function  $\gamma_a(Q)$ . Here,  $\gamma_a(Q)$  implicitly depends on the parameters  $\{\lambda_a, \delta_a\}$  which are fitted for each structure function  $\{F_{1,2,3}\}$  and for selected PDFs displayed in the table. The TMC corrections are accurate to within  $\sim 0.3\%$  for  $Q > 1.3$  GeV. The  $\{\lambda_i, \delta_i\}$  parameters are independent of the exchanged boson ( $\gamma, Z, W^\pm$ ), and are relatively insensitive to the specific underlying nPDF. Once the  $\{\lambda_i, \delta_i\}$  parameters are determined for a particular nPDF, the full TMC corrections can be efficiently computed (without convolution integrations) to high precision as illustrated in Fig. 7.7.

$$\frac{g_2(\xi)}{F_2^{(0)}(\xi)} = -\ln(\xi) - (1 - \xi) + \gamma_2(Q) \frac{(1 - \xi)^2}{\xi^2} \sum_{j=1}^{j_{\max}} \frac{(-1)^j}{j!(j+2)} {}_2F_1\left(2, j+2, j+3, 1 - \frac{1}{\xi}\right), \quad (7.9d)$$

$$\frac{g_1(\xi)}{F_1^{(0)}(\xi)} = 2\xi r^2 \left[ -\ln(\xi) - (1 - \xi) + \gamma_1(Q) \frac{(1 - \xi)^2}{\xi^2} \sum_{j=1}^{j_{\max}} \frac{(-1)^j}{j!(j+2)} {}_2F_1\left(2, j+2, j+3, 1 - \frac{1}{\xi}\right) \right], \quad (7.9e)$$

where  ${}_2F_1(a, b, c, z)$  is a hypergeometric function. Although the summation over the index  $j$  can, in principle, go to infinity, we truncate the series at  $j = j_{\max}$ . The  $1/(j!)$  prefactor of the hypergeometric function helps ensure the series converges quickly, and we find  $j_{\max} = 4$  yields results that are  $\lesssim 1\%$  accuracy.

The function  $\gamma_a(Q)$  is given by

$$\gamma_a(Q) = \lambda_a \ln(Q)^{\delta_a} \quad . \quad (7.10)$$

The values of  $\{\lambda_a, \delta_a\}$  are obtained by fitting the parameterization to the exact results for each  $F_i^{TMC}$  structure function. Note that the values of  $\{\lambda_a, \delta_a\}$  are independent of the type of the exchanged bosons; they have only a mild dependence on the specific structure function  $F_i^A$  as displayed in Table 7.2.

Additionally, while we have computed these results assuming an NLO DGLAP evolution, these results should be similar for an NNLO evolution. This is because: i) we are working at relatively low  $Q$  values where the effects of the DGLAP evolution from  $Q_0$  to  $Q$  will be minimal, and ii) since this quantity is a ratio of structure functions, the modification of the ratio is expected to be less than the impact on the individual structure functions.

We have also computed the results for a variety of different PDF sets to ensure this parameterization is largely insensitive to the specific PDF. This also is displayed in Table 7.2, where we observe a mild variation of the parameters between PDF sets.

In Figure 7.7, we show the comparison between our parameterization with the exact results obtained using nCTEQ15 nPDFs. We can see that our parameterization works very well to reproduce the exact results. The parameterization has the advantage that it can be computed efficiently whereas the full  $F_i^{TMC}$  results require additional convolution integrations for the  $\{h_i(\xi), g_i(\xi)\}$  functions. For values of  $Q \geq 2$  GeV, which is a typical cut for the global nPDF fits, we see the parameterization describes the full TMC results to better than 0.2%.

**Summary:** In the previous sections we established several results which will facilitate efficient calculation of TMCs for nuclear structure functions. We briefly summarize the key observations below.

- TMCs can yield large corrections in the double limit of large  $x$  and small  $Q$ .

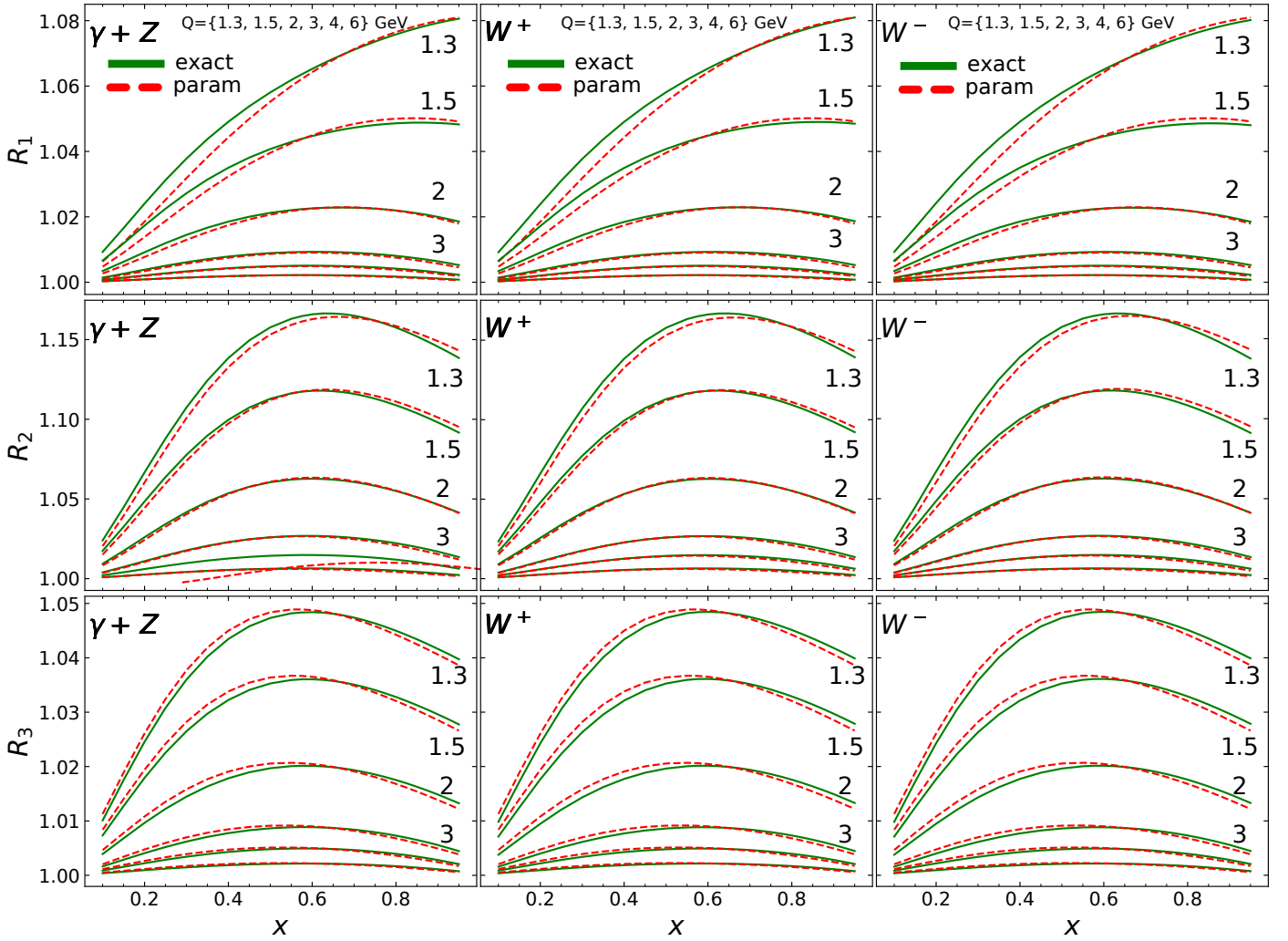


Figure 7.7: We present the nuclear structure function ratio  $R_i = F_i^{\text{TMC}}/F_i^{\text{TMC-Leading}}$  averaged over the nuclei of Table 7.1 as defined in Eq. (7.7). The ratios are shown as a function of  $x_N$  for  $Q = \{1.3, 1.5, 2, 3, 4, 6\}$  GeV (from top to bottom) using the nCTEQ15 nPDFs. We compare the exact results (green solid) of Eq. (4.14) to the approximate parameterizations (red dashed) based on Eq. (7.9) with parameters given in Table 7.2. For  $Q > 2$  GeV, we observe the parameterization can match the exact results to better than 0.2%.

- The “Leading-TMC” result provides an excellent approximation to the full “TMC” result as the  $h_{2,3}$  contributions are suppressed by additional  $(M/Q)^2$ , and the  $g_2$  contributions by additional  $(M/Q)^4$  powers.
- The nuclear dependence of the “TMC” result is approximately independent of  $A$ . This observation suggests we can determine an  $A$ -independent “universal” correction factor which can be used to quickly calculate the nuclear structure function TMCs for any nuclei. As illustrated in the bottom panels of Fig. 7.3, this “universal” approximation holds to  $\lesssim 0.1\%$  for  $Q \geq 2$  GeV.
- As demonstrated in Fig. 7.7, we can parameterize this “universal” correction factor with Eq. (7.9) into a 2-parameter form that can be easily incorporated in a efficient nuclear PDF fitting program. This parameterization matches the exact results to better than 0.2% for  $Q \geq 2$  GeV.

Given the “Leading-TMC” result, the above allows us to efficiently approximate the full “TMC” result for any nuclear structure function by applying “universal” correction factor. This avoids the computation of the numerical integrals contained in the  $\{h_2, h_3, g_2\}$  functions.

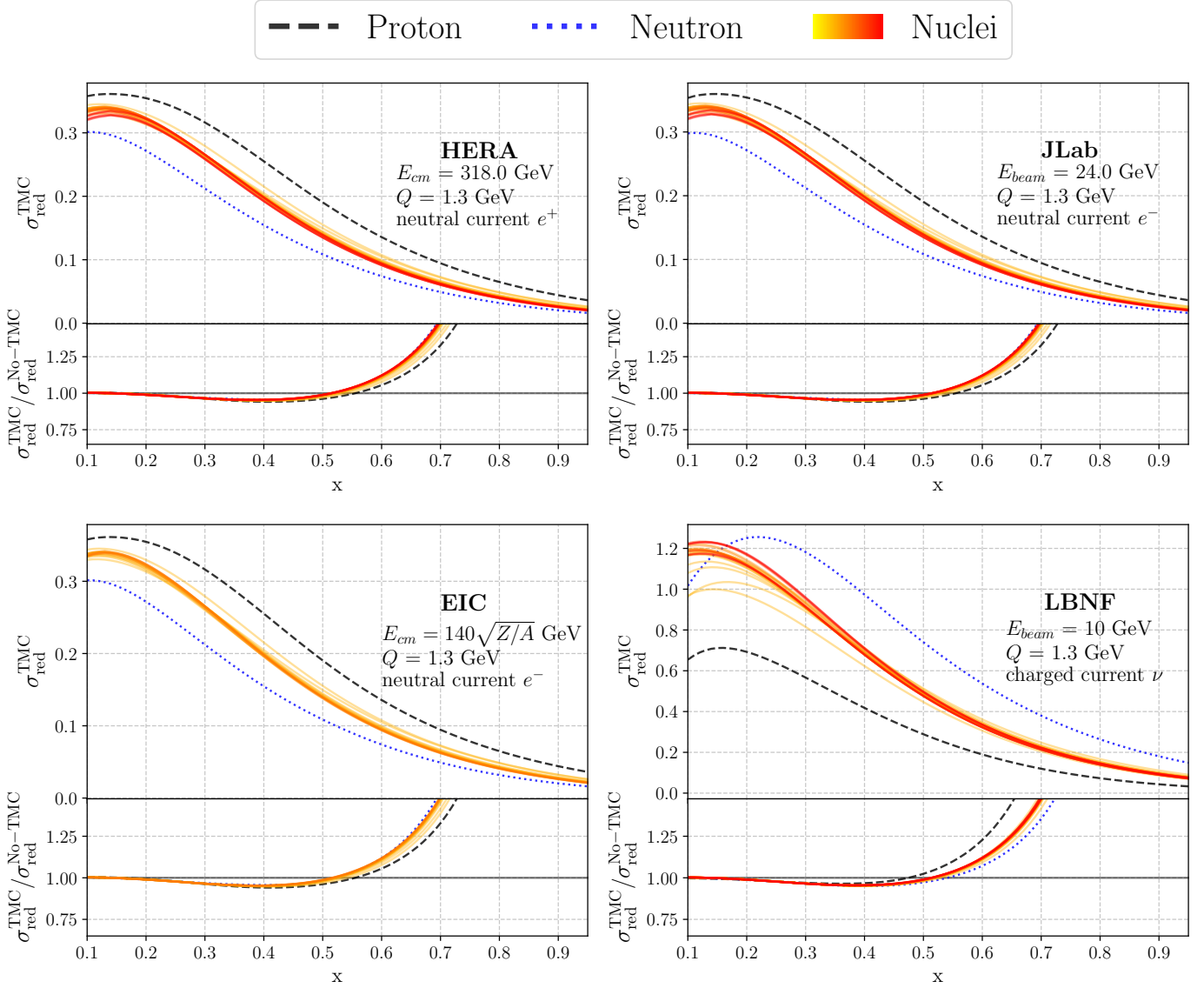


Figure 7.8: We present reduced cross sections for the following scenarios: (a) HERA inspired  $e^+p$  neutral current scattering with  $E_{cm} = 318$  GeV for  $Q = 1.3$  GeV; (b) JLab inspired  $e^-A$  charged current scattering with  $E_{beam} = 24$  GeV for  $Q = 1.3$  GeV; (c) EIC inspired  $e^-A$  neutral current scattering with  $E_{cm} = 140\sqrt{Z/A}$  GeV for  $Q = 1.3$  GeV; (d) LBNF inspired  $\nu A$  charged current scattering with  $E_{beam} = 10$  GeV for  $Q = 1.3$  GeV. **Upper panels:** The upper panels display the full “TMC” results. **Lower panels:** The lower panels display the ratio of the full “TMC” to “No-TMC”. The proton is indicated with the black dashed line, and the neutron with the blue dotted line. The narrow band of colored lines shows the various nuclear results.

#### 7.4. Reduced cross sections with TMCs for nuclei

When extracting structure functions from DIS data or comparing theoretical expectations for DIS to data, one often works with the “reduced cross section”  $\sigma_{\text{Red}}$ . These quantities are derived from double differential cross sections scaled by kinematic factors, and provide a direct connection between DIS kinematics and structure functions.

The general cross section for neutral and charged current DIS can be expressed as:[86]

$$\frac{d^2\sigma^i}{dx dy} = x(s - M^2) \frac{d^2\sigma^i}{dx dQ^2} = \frac{4\pi\alpha^2}{xyQ^2} \eta^i \left\{ \left( 1 - y - \frac{x^2 y^2 M^2}{Q^2} \right) F_2^i + (y^2 x) F_1^i \mp \left( y - \frac{y^2}{2} \right) x F_3^i \right\}, \quad (7.11)$$

where i=NC, CC corresponds to neutral-current or charged-current processes. Additionally,  $\eta^{NC} = 1$  and  $\eta^{CC} = 4\eta_W$ , with  $\eta_W = \frac{1}{2}[\frac{G_F M_W^2}{4\pi\alpha} \frac{Q^2}{Q^2 + M_W^2}]^2$ . In the last term of Eq. (7.11), the “-” sign is taken for an incoming anti-lepton  $\{e^+, \bar{\nu}\}$  and the “+” sign for an incoming lepton  $\{e^-, \nu\}$ .

**Neutral current cross section:** We find it convenient to define the reduced cross section by dividing out the leading factors.

$$\frac{d^2\sigma^{NC}}{dx dy} = x(s - M^2) \frac{d^2\sigma^{NC}}{dx dQ^2} = \frac{4\pi\alpha^2}{xyQ^2} \left[ \frac{Y_+}{2} \sigma_{\text{Red.}}^{NC} \right], \quad (7.12)$$

$$\sigma_{\text{Red.}}^{NC} = \left( 1 + \frac{2y^2\varepsilon^2}{Y_+} \right) F_2^{\text{NC}} \mp \frac{Y_-}{Y_+} x F_3^{\text{NC}} - \frac{y^2}{Y_+} F_L^{\text{NC}}, \quad (7.13)$$

with  $F_L = r^2 F_2 - 2x F_1$ ,  $r = \sqrt{1 + 4\varepsilon^2}$ ,  $\varepsilon = (xM/Q)$  and  $Y_{\pm} = 1 \pm (1 - y)^2$ ; the  $r^2$  term in  $F_L$  is essential to obtain the correct sign for the  $\varepsilon^2$  term of Eq. (7.13). Note that at LO ( $F_L \sim 0$ ) for parity-conserving photon exchange ( $F_3 = 0$ ), so that we have  $\sigma_{\text{Red.}}^{NC}$  simply reduces to  $F_2^{\text{NC}}$ .

**Charged current cross section:** For the charged current process, we have:

$$\frac{d^2\sigma^{\text{CC}}}{dx dy} = x(s - M^2) \frac{d^2\sigma^{\text{CC}}}{dx dQ^2} = \frac{G_F^2}{2\pi x} \frac{Q^2}{y} \left( \frac{M_W^2}{Q^2 + M_W^2} \right)^2 \left[ \sigma_{\text{Red.}}^{\text{CC}} \right], \quad (7.14)$$

$$\sigma_{\text{Red.}}^{\text{CC}} = \frac{Y_+}{2} \left( 1 + \frac{2y^2\varepsilon^2}{Y_+} \right) F_2^{\text{CC}} \mp \frac{Y_-}{2} x F_3^{\text{CC}} - \frac{y^2}{2} F_L^{\text{CC}} \quad (7.15)$$

Here we have followed the HERA convention[148] where the CC differs from NC by a factor of  $Y_+/2$ .

For both the NC and CC cases, the factor of  $2y^2\varepsilon^2/Y_+$  with  $\varepsilon = (xM/Q)$  multiplying  $F_2$  arises directly from the DIS kinematics; however, this is often neglected as it is small for typical HERA kinematics.

## TMCs for nuclear reduced cross sections

As described in the preceding subsections, TMCs can have a large numerical impact on nuclear structure functions in the low  $Q^2$  and large  $x$  double limit. To illustrate the TMC impact, in Fig. 7.8 we present results for experimental scenarios including HERA, JLab, EIC, and LBNF. The upper panels of Fig. 7.8 display the reduced cross sections, and the lower panels show the ratio of the full “TMC” to the “No-TMC” result. As before, all the nuclear isotopes of Table 7.1 are within the colored band, and the proton and neutron are displayed separately.

In Fig. 7.8-(a) we show the HERA-inspired  $e^+p$  neutral current  $\sigma_{\text{Red.}}^{NC}$  at  $\sqrt{s} = 318$  GeV at  $Q = 1.3$  GeV for the full “TMC” results. Although HERA ran proton beams, we also show the nuclear results which may be useful for a future LHeC/FCCeh facility. The TMCs yield a slight suppression at intermediate  $x$  values ( $\sim 0.4$ ), and an enhancement at larger  $x$  values ( $\gtrsim 0.6$ ) which can be significant. The behavior of  $\sigma_{\text{Red.}}^{NC}$  strongly resembles that of  $F_2$  in Fig. 7.1; this is expected as given our choices of  $Q$  and  $E_{\text{CM}}$  we find  $y \ll 1$  and  $Y_- \sim 0$ , so we see from Eq. (7.13) that the  $F_2$  contribution dominates. For the higher  $Q$  values (not shown) TMCs are reduced as for  $F_2$  in Fig. 7.1, and are generally negligible except in the very large  $x$  region.

In Fig. 7.8-(b) we show a JLab-inspired  $e^-A$  neutral-current  $\sigma_{\text{Red.}}^{NC}$  with  $E_{\text{Beam}} = 24$  GeV at  $Q = 1.3$  GeV. The character of the curves for  $E_{\text{Beam}} = 12$  GeV (not shown) is quite similar to the displayed results. The results here are qualitatively similar to the  $F_2$  result of Fig. 7.1 and the HERA case above with a reduction for intermediate  $x$  ( $\sim 0.4$ ), and an enhancement at larger  $x$ .

In Fig. 7.8-(c) we show an EIC-inspired  $e^- A$  neutral-current  $\sigma_{Red}^{NC}$  with  $E_{cm} = 140\sqrt{Z/A}$  GeV at  $Q = 1.3$  GeV. As with the above HERA and JLab cases, these results largely follow the  $F_2$  structure function.

In Fig. 7.8-(d) we show an LBNF-inspired  $\nu - A$  charged-current scattering with  $E_{beam} = 10$  GeV at  $Q = 1.3$  GeV. In the low  $x$  region, we see the various nuclear curves separate due to the differing nuclear mass values.

From this exercise, one can see that for large  $\sqrt{s}$ , we generally have small  $y$ , and  $\sigma_{Red}$  closely follows  $F_2$ . For smaller  $\sqrt{s}$ , we have larger  $y$ , and the  $F_3$  and  $F_L$  structure functions can now contribute.

## 8. Conclusions

The structure of the proton has been extensively investigated, and recent work has extended the precision to next-to-next-to-leading-order (NNLO) and beyond. With the upcoming Electron Ion Collider (EIC) and other experiments discussed in the introduction, we have the opportunity to build upon the proton analyses and also determine the nuclear structure with extreme precision.

To exploit the current and future nuclear measurements, and to obtain the desired accuracy of theory calculations, it is essential to include TMCs in the analyses of structure functions. However, extending the TMCs from the proton to nuclei requires a rigorous theoretical foundation. This foundation is provided by the OPE. Additionally, as we have shown, the equivalence of the OPE with the parton model (with appropriate  $M_A$  and  $k_T$  contributions) provides a familiar framework to implement TMC in analyses. Some of the tools from the proton analyses can be applied directly to the nuclear case, while other elements (such as the nuclear DGLAP equations with  $x_N \in [0, A]$  and  $W_A \neq W_N$ ) must be adapted. Ultimately, the answer to the question, *Why nucleon-like expressions could possibly be valid for nuclear targets?*, is simply that the consequences of asymptotic freedom, e.g., light-cone dominance and the validity of perturbative methods, begin to emerge when momentum transfers  $Q$  surpass the non-perturbative scale  $\Lambda_{NP} \lesssim 1$  GeV (see Sec. 3.1). While this is (accidentally) comparable to the scale of free nucleons, masses of target hadrons in DIS (albeit nucleons or nuclei) are a sub-leading ingredient and contribute as powers of  $\mathcal{O}(x_A^2 M_A^2/Q^2)$ . The goal of this presentation is to explicitly delineate the proper ingredients and adaptations required for a precision nuclear analysis.

The present investigation provides both pedagogical material and a practical reference for computing and investigating TMCs for nuclear processes. We briefly outline the key components and results in the following:

- **OPE Formalism:** We extend the OPE formalism to the case of interacting nuclei and explicitly provide the correspondence between TMC expressions for a nucleon and a nucleus, given in Eq. (3.24). To derive these relations (see Sec. 3.2 and Appendix A), we use only fundamental symmetry principles of the nuclei, and make no assumptions about the parton or other models. This is the essence of the factorization between the hadron and parton level processes.
- **TMC Power Expansion:** We investigate analytically and numerically the magnitude of TMCs and show it is the quantity  $(x_A M_A/Q) = (x_N M_N/Q)$  that enters the TMC formula for **nuclei** (Eq. (3.23)) and **nucleons** (Eq. (4.14)). This result is important for heavy nuclear  $A$  targets such as lead. While  $M_A$  can be large ( $\sim A M_N$ ), it is always combined with  $x_A \lesssim 1/A$  (since an individual parton momentum fraction will typically be less than  $1/A$  of the total **nuclear** momentum). Thus, the OPE expansion for TMCs is effectively in powers of  $(M_N/Q)$  and not  $(M_A/Q)$ , so it is equally accurate for both protons and nuclei.
- **Nuclear TMCs:** In Sec. 3.3, we extend the proton results of Ref. [73] and derive a set of master equations (Eq. (3.24)) for nuclear structure functions with TMCs that are the same for all  $A$ , including the proton, neutron, and nuclear cases. This allows us to easily apply the tools of the OPE to nuclei as well as protons.
- **Nucleon TMCs:** In Sec. 4.2, we rescale our **nuclear** structure functions of Eq. (3.24) to construct **nucleon** structure functions in Eq. (4.14). These rescaled structure functions are the ones commonly studied and presented in comparisons between different nuclear data. This facilitates extraction of the “nuclear correction factors” by taking ratios of rescaled structure functions, as illustrated in Fig. 5.4.

Additionally, this allows for investigations of collective nuclear effects (*e.g.*, shadowing, anti-shadowing, EMC, Fermi, etc.).

- **The Parton Model:** In Sec. 5.1, we extend the rescaled results to the parton model and obtain the corresponding set of DGLAP equations and associated sum rules, including isospin symmetry. We also identify the complication of separately extracting  $u(x)$  and  $d(x)$  nPDFs. This correspondence allows us (with the reasonable assumption  $x_N \leq 1$ ) to re-use our proton DGLAP evolution code for the case of nucleons.
- **Nuclear Kinematics:** We establish the relations between the kinematic variables including the **nuclear** scaling variables  $\{x_A, \xi_A\}$  and the **nucleon** scaling variables  $\{x_N, \xi_N\}$ . Furthermore, we indicate in Sec. 5.4 some subtle complications we encounter such as defining an appropriate  $W^2$  cut for the nucleon case. Specifically, as demonstrated in Fig. 5.3, the dependence of  $W_A^2$  on  $A$  and  $Q^2$ , complicate the task of placing cuts on the resonance region.
- **The OPE and the Parton Model:** We obtain a complete correspondence between the parton model and OPE structure function results, and demonstrate these are equivalent **if** we include i) target mass effects and ii)  $k_T$  transverse momentum contributions in the parton model. Additionally, in Sec. 6 we show the utility of the ACOT helicity approach with light-cone kinematics, and demonstrate the correspondence to the traditional tensor basis as shown in Table 6.1.
- **Numerical Comparisons:** In Sec. 7, we provide a variety of numerical comparisons to demonstrate the size of the TMCs in various kinematic regions. These comparisons are shown for both structure functions, and the reduced cross section for some realistic machine kinematics. We found that for typical kinematic cuts used in global analyses  $\{Q \gtrsim 2 \text{ GeV}, W \gtrsim 1.7 \text{ GeV}, x \lesssim 0.7\}$ , the  $F_i^{\text{TMC-Leading}}$  was within  $\sim 5\%$  or better of the full  $F_i^{\text{TMC}}$  result, and improves quickly to  $\sim 1\%$  or better for  $Q \gtrsim 6 \text{ GeV}$ .
- **TMC Computation:** We also present numerically the dependence of the TMCs on the nuclear  $A$  value and the exchanged vector boson  $\{\gamma, Z, W^\pm\}$ . We find the relative magnitude of the TMCs is weakly dependent on the exchanged boson, and **very** weakly dependent on the nuclear  $A$ . This latter observation allows us to derive an approximate (and computationally expedient) parameterization for the nuclear TMCs suitable for including inside a global fit function (see Sec. 7.3). For  $Q > 2 \text{ GeV}$ , the parameterized result matches the exact results to better than 0.2%, which is well below the typical nPDF precision.

In the near future, there will be ambitious new facilities and experiments that will investigate lepton-nucleus and neutrino-nucleus interactions in extreme kinematic regions with high precision. Just as Ref. [73] provided the details for the proton case, this report offers foundational and reference material that can facilitate incisive investigations of nuclear phenomena.

We can use the tools from the precision proton analyses as an archetype, and extend them into the nuclear dimension. Furthermore, the nuclear interactions open up a whole new class of phenomena (saturation, shadowing) and new states of matter (quark-gluon plasma, Color Glass Condensates) to explore. Discovering and analyzing these phenomena will require precision on both the experimental and theoretical fronts; a rigorous foundation for theoretical calculations of structure functions with TMCs is an essential step toward this goal.



## Acknowledgments

The authors would like to thank Eric Christy, John, C. Collins, Stefan Krezer, Pavel Nadolsky, Voica Radescu, and Mary Hall Reno for many useful comments and discussions.

A.K. and R.R. acknowledge the support of under Grant No. 2019/34/E /ST2/00186. R.R. also acknowledges the support of the Polska Akademia Nauk (grant agreement PAN.BFD.S.BDN. 613. 022. 2021 - PASIFIC 1, POPSICLE). This work has received funding from the European Union's Horizon 2020 research and innovation program under the Skłodowska-Curie grant agreement No. 847639, and from the Polish Ministry of Education and Science. The work at WWU Münster was funded by the DFG through the Research Training Group 2149 "Strong and Weak Interactions - from Hadrons to Dark Matter" and the SFB 1225 "Isoquant," project-id 273811115. M.K. thanks the School of Physics at the University of New South Wales in Sydney, Australia for its hospitality and financial support through the Gordon Godfrey visitors program. The work of A.A. was supported by the U.S. Department of Energy under Grant No. DE-SC0008791. The work of T.J.H. was supported by the U.S. Department of Energy under contract DE-AC02-06CH11357. The research of P. D. was funded as a part of the Center of Excellence in Quark Matter of the Academy of Finland (project 346326). The work of C.K. was supported by the U.S. Department of Energy contract DE-AC05-06OR23177, under which Jefferson Science Associates LLC manages and operates Jefferson Lab. J.G.M. has been supported by Fermi Research Alliance, LLC under Contract No. DE-AC02-07CH11359 with the U.S. Department of Energy, Office of Science, Office of High Energy Physics. The work of F.O. was supported by the U.S. Department of Energy under Grant No. DE-SC0010129, and by the Office of Science, Office of Nuclear Physics, within the framework of the Saturated Glue (SURGE) Topical Theory Collaboration. The work of I.S. was supported by the French CNRS via the IN2P3 project GLUE@NLO.

## A. Nuclear structure functions with TMCs in the OPE

In this appendix, we build structure functions for massive, unpolarized nuclear targets following a modified prescription of Ref. [58, 59]. The purpose of this is two fold. First is to establish that the TMC formulae used for free nucleons are applicable to nuclei, which is a key conclusion of this work. Second is to provide an explicit derivation of the TMC master formulae, which are summarized in Eqs. (3.23) and (A.165), with details beyond what is generally available in the literature. It is well-documented that constructing TMCs to structure functions is a tedious endeavor, with many intermediate steps omitted from the literature. Some notable exceptions exist [58, 59, 67, 73, 95, 149]. For example: Refs. [58, 59] give a largely complete treatment of  $F_2$  but implicitly employ derivative, integral, and summation identities. Some of these intermediate steps are more completely documented in Refs. [95, 149], but other steps may not be fully justified under their assumptions [88]. Similarly, while the structure functions  $W_4$  and  $W_5$  (or equivalently  $F_4$  and  $F_5$ ) are documented in Refs. [67, 73], neither works out the many permutations of contractions with the momentum factor  $\Pi^{\mu_1 \dots \mu_{2k}}$  from Eq. (3.19). Keeping track of these permutations requires care, as demonstrated for  $F_1$  and  $F_2$  in Ref. [149]. Notably, Ref. [73] documents some differences and similarities between the above treatments. The treatment in this Appendix builds on the different steps employed throughout Refs. [58–61, 67, 88, 95, 149].

We first build a formula for the inclusive DIS cross section in App. A.1 based on the notation defined in section 2.1. In App. A.2, we derive the matrix element, squared matrix element, and inclusive hadronic tensor in DIS. In App. A.3, the OPE is applied to the inclusive hadronic tensor, with the leading-power result organized according to Wilson coefficients. In App. A.4, OPE terms are reorganized by Lorentz structures, resulting in structure-function mixing. Structure functions for massless and massive nuclear targets are then constructed and summarized in App. A.5.

### A.1. Preliminaries and the inclusive DIS cross section formula

To build nuclear structure functions with TMCs in the OPE formalism, we consider the DIS process as defined in Eq. (2.1) of section 2.1 and depicted in Fig. 1.2. Given this configuration, the total cross section for a generic  $2 \rightarrow (n+1)$  scattering process is given by the formula

$$\sigma(\ell_1 + A \rightarrow \ell_2 + X_n) = \int dPS_{n+1} \frac{d\sigma}{dPS_{n+1}}, \quad \text{with} \quad \frac{d\sigma}{dPS_{n+1}} = \frac{1}{\mathcal{F}} \frac{1}{\mathcal{S}_{\ell_1} \mathcal{S}_A} \sum_{\{\lambda\}} \sum_{\text{dof}} |\mathcal{M}|^2, \quad (\text{A.1a})$$

$$\text{and } \mathcal{F} = 4\sqrt{(p_A \cdot k_1)^2 - p_A^2 k_1^2} \stackrel{k_1^2 = m_1^2 \rightarrow 0}{\approx 1} 2(s - M_A^2). \quad (\text{A.1b})$$

Here,  $\mathcal{F}$  is the Moller flux factor and reduces to  $\mathcal{F} \approx 2(s - M_A^2)$  when the mass  $k_1^2 = m_1^2$  vanishes.  $d\sigma/dPS_{n+1}$  is the totally differential, nucleus-level cross section.  $\mathcal{S}_{\ell_1}$  and  $\mathcal{S}_A$  are the spin multiplicities for  $\ell_1$  and  $A$  in unpolarized scattering. The double summations in the differential cross section run over external helicities  $\{\lambda\}$  and other discrete quantum numbers/degrees of freedom (dof). We introduce the subscript  $n$  on  $X_n$  to make explicitly that it is an  $n$ -body state. In addition,  $\mathcal{M}$  is the scattering amplitude for the  $2 \rightarrow (n+1)$  process. The associated  $(n+1)$ -body phase space measure is given by

$$dPS_{n+1}(k_1 + p_A; k_2, p_X) = (2\pi)^4 \delta^4 \left( k_1 + p_A - k_2 - \sum_{i=1}^n p_{X_i} \right) \frac{d^3 k_2}{(2\pi)^3 2k_2^0} \times \prod_{i=1}^n \frac{d^3 p_{X_i}}{(2\pi)^3 2p_{X_i}^0} \quad (\text{A.2})$$

$$= dPS_n(q + p_A; p_X) \times \frac{d^3 k_2}{(2\pi)^3 2k_2^0} \quad (\text{A.3})$$

$$= \int d^4 z e^{i(q+p_A-p_X) \cdot z} \prod_{i=1}^n \frac{d^3 p_{X_i}}{(2\pi)^3 2p_{X_i}^0} \times \frac{d^3 k_2}{(2\pi)^3 2k_2^0}, \quad (\text{A.4})$$

where  $k_2^0$  and  $p_{X_i}^0$  are the energy components of the  $k_2$  and  $p_{X_i}$  4-vectors, respectively.

In the above lines, we employed momentum conservation and  $\delta$ -function identities to rewrite the measure

in ways that will be used below. Specifically in the third line, we used

$$(2\pi)^4 \delta^4(q-p) = \int d^4z e^{i(q-p)\cdot z}, \quad (\text{A.5})$$

where  $q, p$  and  $z$  are 4-vectors. The point of these identities is to identify the phase space integral over the hadronic matrix element also as the Fourier transformation over composite operators. The modeling of  $X_n$ 's phase space is not precisely correct in many presentations of structure functions in DIS. Often,  $p_X$  is treated as a one-body configuration despite being an  $n$ -body configuration. While this mis-modeling is ultimately a technicality, it does impact the formal definition of  $W_{\mu\nu}$ ; see, for instance, Ref. [150]. We reiterate that  $X_n$  here (or  $X$  in the main text) is an  $n$ -body state.

Using the above phase space decomposition, we can write an expression for the DIS cross section that (1) is differential with respect to the kinematics of  $\{\ell_2, k_2\}$ , and (2) is explicitly inclusive over *all* hadronic activity. This expression is given by

$$k_2^0 \times \frac{d\sigma}{d^3k_2} = \frac{1}{(16\pi^2)} \frac{1}{\pi} \frac{1}{\mathcal{F}} \frac{1}{\mathcal{S}_{\ell_1} \mathcal{S}_A} \sum_{n=1}^{\infty} \int d^4z e^{i(q+p_A-p_X)\cdot z} \prod_{i=1}^n \frac{d^3p_{X_i}}{(2\pi)^3 2p_{X_i}^0} \sum_{\{\lambda\}} \sum_{\text{dof}} |\mathcal{M}|^2. \quad (\text{A.6})$$

Here,  $\mathcal{S}_{\ell_1} = 2$  for an unpolarized  $\ell_1$ , and  $\mathcal{S}_A = 2$  for an unpolarized, spin-1/2 nuclei  $A$ . Additionally,  $\mathcal{S}_{\ell_1} = 1$  when  $\ell_1$  is an incoming neutrino or antineutrino because neutrino beams are effectively 100% polarized. More broadly, for unpolarized nuclear targets with spin  $s_A > 1/2$ , the spin-averaging factor  $\mathcal{S}_A$  generalizes to  $\mathcal{S}_A = (2s_A + 1) > 2$ .

In Eq. (A.6), we inserted a sum over the multiplicity  $n$  of  $X_n$ . Conceptually, this is equivalent to the relationship

$$\ell_1 + A \rightarrow \ell_2 + \text{any hadronic activity} = \sum_{n=1}^{\infty} [\ell_1 + A \rightarrow \ell_2 + X_n]. \quad (\text{A.7})$$

For example, when  $n = 2$  this sums over the configurations  $pp, pn, p\pi, pK, \pi\pi, \dots$ , which are all included in the inclusive sum.

## A.2. The DIS matrix element and inclusive hadronic tensor

The hadronic tensor  $W_{\mu\nu}^A$  of Eq. (2.8) is built from the (squared) matrix element  $\mathcal{M}$ . For  $\ell_1 A \rightarrow \ell_2 X$  scattering via an arbitrary electroweak boson  $V(q)$ , we parameterize this by

$$-i\mathcal{M} = \langle X \ell_2 | J_{\ell_2 \ell_1}^\mu(0) \cdot \Delta_{\mu\sigma}^V(q) \cdot J_{XA}^\sigma(0) | A \ell_1 \rangle \quad (\text{A.8})$$

$$= \langle \ell_2 | J_{\ell_2 \ell_1}^\mu(0) | \ell_1 \rangle \cdot \Delta_{\mu\sigma}^V(q) \cdot \langle X | J_{XA}^\sigma(0) | A \rangle, \quad (\text{A.9})$$

where the leptonic part of the matrix element  $L^\mu$  and current  $J_{\ell_2 \ell_1}^\mu$  in terms of 4-component helicity spinors, a generic coupling normalization  $\tilde{g}$ , and chiral couplings  $g_V, g_A$ , are

$$L^\mu \equiv \langle \ell_2 | J_{\ell_2 \ell_1}^\mu(0) | \ell_1 \rangle = -i\tilde{g} \bar{u}(k_2, \lambda_2) [g_V^\ell \gamma^\mu + g_A^\ell \gamma^\mu \gamma^5] u(k_1, \lambda_1). \quad (\text{A.10})$$

We assume arbitrary vector and axial-vector couplings between the  $(\ell_2 \ell_1)$  system and  $V$  in order to accommodate the possibility of  $V$  being a photon or weak boson. The conversion between the different possibilities is given in Tab. A.1. Similarly, we write the hadronic part of the matrix element in terms of an arbitrary hadronic current  $J_{XA}^\sigma(0)$ :

$$H^{A\sigma} \equiv \langle X | J_{XA}^\sigma(0) | A \rangle \equiv \bar{u}_X(p_X, \lambda_X) [\dots]^\sigma u(p_A, \lambda_A). \quad (\text{A.11})$$

We assume here and below that  $J_{XA}^\sigma$  is always a renormalized object in QCD.

In Eq. (A.9),  $\Delta_{\mu\sigma}^V(q)$  is the propagator of  $V$  which is typically of the form  $-i(g_{\mu\sigma} - q_\mu q_\nu / M_V^2) / (q^2 - M_V^2)$ . When we assume the  $\ell_i$  are massless, the Dirac equation and  $\text{SU}(2)_L$  invariance ensure that the longitudinal

Vertex	Coupling strength	$g_R^\ell$	$g_L^\ell$	$g_V^\ell$	$g_A^\ell$
$V - \ell_1 - \ell_2$	$\tilde{g}$	$(g_V^\ell + g_A^\ell)$	$(g_V^\ell - g_A^\ell)$	$\frac{(g_R + g_L)}{2}$	$\frac{(g_R - g_L)}{2}$
$\gamma - \ell - \ell$	$eQ^\ell$	1	1	1	0
$Z - \ell - \ell$	$\frac{g_W}{\cos \theta_W}$	$-Q^\ell \sin^2 \theta_W$	$(T_3^\ell)_L - Q^\ell \sin^2 \theta_W$	$\frac{1}{2}(T_3^\ell)_L - Q^\ell \sin^2 \theta_W$	$-\frac{1}{2}(T_3^\ell)_L$
$W - \ell_1 - \ell_2$	$\frac{g_W}{\sqrt{2}}$	0	1	$\frac{1}{2}$	$-\frac{1}{2}$

Table A.1: Electroweak chiral couplings and coupling strength normalizations used for fermions  $\ell_1, \ell_2$  with weak isospin charge  $(T_3^\ell)_L = \pm 1/2$  and electric charge  $Q^\ell$ , with normalization  $Q^e = -1$ .

modes of  $\Delta_{\mu\sigma}^V$  do not contribute to the scattering process.<sup>19</sup> More specifically, the longitudinal component of  $\Delta$  scales as  $\Delta_{\mu\sigma}(q)|_{\text{long}} \propto q_\mu q_\sigma$ . Since  $\not{k}_i u(k_i) = m_i u(k_i) = 0$  and  $q_\mu = (k_1 - k_2)_\mu$ , one finds

$$L^\mu \cdot \Delta_{\mu\sigma}^V|_{\text{long}} \propto q_\mu \cdot \bar{u}(k_2, \lambda_2) [g_V^\ell \gamma^\mu + g_A^\ell \gamma^\mu \gamma^5] u(k_1, \lambda_1) \quad (\text{A.12})$$

$$= \bar{u}(k_2, \lambda_2) [g_V^\ell (\not{k}_1 - \not{k}_2) + g_A^\ell (\not{k}_1 - \not{k}_2) \gamma^5] u(k_1, \lambda_1) = 0. \quad (\text{A.13})$$

The above implies that only the transverse components of  $\Delta_{\mu\sigma}^V$  contributes to DIS for massless leptons. For  $V = \gamma, W, Z$  with mass  $M_V$  (where  $M_\gamma = 0$ ), one can then write

$$-i\mathcal{M} = L^\mu(k_2, k_1) \Delta_{\mu\sigma}^V(q) H^{A\sigma}(p_X, p_A) = L^\mu \frac{-i g_{\mu\sigma}}{q^2 - M_V^2} H^{A\sigma} = \frac{-i}{q^2 - M_V^2} L^\mu H_\mu^A. \quad (\text{A.14})$$

After squaring and summing over external helicity states, one obtains

$$\sum_{\{\lambda\}} |\mathcal{M}|^2 = \frac{1}{(q^2 - M_V^2)^2} \sum_{\{\lambda\}} L^{\mu\nu} \cdot \sum_{\{\lambda\}} H_{\mu\nu}^A. \quad (\text{A.15})$$

The leptonic tensor  $L^{\mu\nu}$  denotes the square of  $L^\mu$  and can be solved exactly using trace technology, helicity amplitudes, or other standard technology. It is given by

$$\sum_{\{\lambda\}} L^{\mu\nu} = \sum_{\{\lambda\}} (L^\dagger)^\mu L^\nu = \sum_{\{\lambda\}} \langle \ell_1 | (J_{\ell_2 \ell_1}^\dagger(0))^\mu | \ell_2 \rangle \langle \ell_2 | J_{\ell_2 \ell_1}^\nu(0) | \ell_1 \rangle \quad (\text{A.16})$$

$$= 4\tilde{g}^2 \left\{ (g_V^2 + g_A^2)(k_1^\mu k_2^\nu + k_1^\nu k_2^\mu) - [(g_V^2 + g_A^2)(k_1 \cdot k_2) - (g_V^2 - g_A^2)m_1 m_2] g^{\mu\nu} - 2i(g_V g_A) k_{1\alpha} k_{2\beta} \epsilon^{\mu\nu\alpha\beta} \right\} \quad (\text{A.17})$$

$$\stackrel{m_1, m_2 \rightarrow 0}{=} 4\tilde{g}^2 \left\{ (g_V^2 + g_A^2)(k_1^\mu k_2^\nu + k_1^\nu k_2^\mu) - (g_V^2 + g_A^2)(k_1 \cdot k_2) g^{\mu\nu} - 2i(g_V g_A) k_{1\alpha} k_{2\beta} \epsilon^{\mu\nu\alpha\beta} \right\} \quad (\text{A.18})$$

For completeness, we provide the expression for  $\sum_{\{\lambda\}} L^{\mu\nu}$  with massive leptons. If using this formula, note that Eq. (A.14) must be modified since  $\not{k}_i u(k_i) = m_i u(k_i) \neq 0$ . For the remainder of this work, we keep  $m_1, m_2 = 0$ . Note that the expression here for the leptonic tensor only sums over initial- and final-state polarizations; a symmetry factor of  $1/\mathcal{S}_{\ell_1} = 1/2$  for unpolarized initial-states has not yet been applied. Following the conventions of Table A.1, for the case of QED, where  $g_V = 1$ ,  $g_A = 0$ , and  $\tilde{g} = e$ , we recover the

<sup>19</sup>We typically neglect the mass of the leptons, except for the tau-lepton.

usual expression:

$$\sum_{\{\lambda\}} L^{\mu\nu} \Big|_{\text{QED}} = 4e^2 \left\{ k_1^\mu k_2^\nu + k_1^\nu k_2^\mu - (k_1 \cdot k_2) g^{\mu\nu} \right\}. \quad (\text{A.19})$$

For the case of  $W$  boson exchange, where  $g_V = 1/2$ ,  $g_A = -1/2$ , and  $\tilde{g} = g_W/\sqrt{2}$ , we have

$$\sum_{\{\lambda\}} L^{\mu\nu} \Big|_W = g_W^2 \left\{ k_1^\mu k_2^\nu + k_1^\nu k_2^\mu - (k_1 \cdot k_2) g^{\mu\nu} + ik_{1\alpha} k_{2\beta} \epsilon^{\mu\nu\alpha\beta} \right\}. \quad (\text{A.20})$$

The *exclusive* hadronic tensor  $H_{\mu\nu}^A$  for an  $n$ -body final state  $X$  denotes the square of  $H_\mu$ . For a fixed  $n$ , it is given by

$$\sum_{\{\lambda\}} H_{\mu\nu}^A = \sum_{\{\lambda\}} (H^{A\dagger})_\mu H_\nu^A = \sum_{\{\lambda\}} \langle A | (J_{XA}^\dagger(0))_\mu | X \rangle \langle X | J_{XA\nu}(0) | A \rangle. \quad (\text{A.21})$$

From  $H_{\mu\nu}^A$  we can build the *inclusive* hadronic tensor  $W_{\mu\nu}^A$  that sums over all final states.

### Building the inclusive hadronic tensor

In inclusive DIS, one measures the kinematics of  $\ell_2$  and remains totally inclusive regarding the hadronic system  $X$ . (Though in practice, the invariant mass of  $X$  is often measured.) The inclusiveness criterion means summing over all possible final-state multiplicities  $n$  (where  $n$  is same  $n$  in Eq. (A.2)), discrete dof, and continuous dof, i.e., momenta. Performing this summation allows us to define the *inclusive* hadronic tensor as

$$W_{\mu\nu}^A \equiv \frac{1}{4\pi} \sum_{n=1}^{\infty} \int dPS_n(q+p_A; p_X) \sum_{\text{dof}} \sum_{\{\lambda\}} H_{\mu\nu}^A \quad (\text{A.22})$$

$$= \frac{1}{4\pi} \int d^4z e^{i(q+p_A-p_X)\cdot z} \sum_{n=1}^{\infty} \int \prod_{i=1}^n \frac{d^3p_{X_i}}{(2\pi)^3 2p_{X_i}^0} \times \sum_{\text{dof}} \sum_{\{\lambda\}} \langle A | J_{XA\mu}^\dagger(0) | X \rangle \langle X | J_{XA\nu}(0) | A \rangle \quad (\text{A.23})$$

$$= \frac{1}{4\pi} \int d^4z e^{i(q+p_A-p_X)\cdot z} \oint \langle A | J_{XA\mu}^\dagger(0) | X \rangle \langle X | J_{XA\nu}(0) | A \rangle. \quad (\text{A.24})$$

In the second line, we used the phase space identities of Eq. (A.2). Following Ref. [150] (and related references), we denote the  $3^n$ -dimensional integration over momenta and triple summation by  $\oint$ . Importantly, the integration and summation constitute a summation over all possible configurations spanning the space of  $\{|X\rangle\}$ . Completeness dictates that

$$\oint |X\rangle \langle X| = \sum_{n=1}^{\infty} \int \prod_{i=1}^n \frac{d^3p_{X_i}}{(2\pi)^3 2p_{X_i}^0} \sum_{\text{dof}} \sum_{\{\lambda\}} |X\rangle \langle X| = 1. \quad (\text{A.25})$$

Before employing Eq. (A.25), we use translation invariance to build a spacetime separation between  $J_{A\mu}^\dagger$  and  $J_{A\nu}$  that is constrained by momentum conservation. Such separations in the DIS limit are restricted to be near the light cone, i.e., with  $z^2 \sim 0$  (*c.f.*, Ref. [61]). Applying translation invariance to  $J_{XA\mu}^\dagger(0)$  gives

$$\langle A | J_{XA\mu}^\dagger(0) | X \rangle = \langle A | \left[ e^{-i\hat{P}\cdot z} J_{XA\mu}(z) e^{i\hat{P}\cdot z} \right]^\dagger | X \rangle \quad (\text{A.26})$$

$$= \langle A | e^{-i\hat{P}\cdot z} J_{XA\mu}^\dagger(z) e^{i\hat{P}\cdot z} | X \rangle = e^{-i(p_A-p_X)\cdot z} \langle A | J_{XA\mu}^\dagger(z) | X \rangle, \quad (\text{A.27})$$

where  $\hat{P}^\alpha$  is the four-momentum operator that generates the eigenvalue equation  $\hat{P}^\alpha |Y(p_Y)\rangle = p_Y^\alpha |Y(p_Y)\rangle$ .

Combining the preceding expressions leads to familiar expression for  $W_{\mu\nu}^A$ :

$$W_{\mu\nu}^A = \frac{1}{4\pi} \int d^4z e^{iq \cdot z} \langle A | J_{XA\mu}^\dagger(z) J_{XA\nu}(0) | A \rangle . \quad (\text{A.28})$$

In electromagnetism, currents are Hermitian. This leads to the omission of the  $\dagger$  in many texts. In other texts, Eq. (A.28) is written using a commutator of currents [60, 61]. However, Refs. [56, 88] note that commutators are not necessary to define  $W_{\mu\nu}^A$ . And indeed, Refs. [60, 61] show that the commutator-based result reduce to Eq. (A.28) in certain limits.

We are now in position to write the differential cross section for the DIS process  $\ell_1 + A \rightarrow \ell_2 +$  anything in terms of the inclusive hadronic tensor  $W_{\mu\nu}^A$ . To do this, we take the differential cross section formula of Eq. (A.6) and insert the squared matrix element in Eq. (A.15). We then substitute the summations and integration over the exclusive hadronic tensor  $H_{\mu\nu}$  with the inclusive hadronic tensor  $W_{\mu\nu}$  to obtain the formula,

$$k_2^0 \times \frac{d\sigma}{d^3k_2} = \frac{1}{(16\pi^2)s} \frac{2}{\mathcal{S}_{\ell_1} \mathcal{S}_A} \frac{1}{(q^2 - M_V^2)^2} \left( \sum_{\{\lambda\}} L^{\mu\nu} \right) \cdot W_{\mu\nu}^A . \quad (\text{A.29})$$

This formula holds for arbitrary  $A$ , including unbound nucleons. Expressions for the leptonic tensor (summed over all external spins) are found in Eqs. (A.18)-(A.20). The factor of 2 in the numerator originates from the adopting the  $(1/4\pi)$  normalization of  $W_{\mu\nu}$ ; when  $A$  is a spin-1/2 object, it cancels the spin-averaging factor  $\mathcal{S}_A$ . The inclusive hadronic tensor is given by Eq. (A.28), but now we relate it to the time-order matrix element for virtual Compton scattering, which has a known expansion in the OPE at leading twist.

### A.3. Nuclear structure functions from the OPE I: organization

As summarized in Sec. 3.2, building structure functions in the OPE for massless and massive hadronic targets is a multi-step process. The advantage, however, is clear: the OPE, if it holds for QCD, facilitates an all-orders, operational definitions for parton densities and structure functions. Moreover, the power counting within the OPE formalism allows one to organize contributions that are not clearly captured in fixed-order perturbation theory.

To do this in the manner of Refs. [58, 59], one starts with the inclusive hadronic tensor  $W_{\mu\nu}^A$  in the DIS limit (large  $Q$ , fixed  $x_A$ ) as defined above and relates it to the time-ordered matrix element  $T_{\mu\nu}^A$  for virtual Compton scattering<sup>20</sup> in the short-distance limit (large  $Q$ , fixed  $x_A/Q$ ). The OPE of  $T_{\mu\nu}^A$  is then organized by Lorentz structures. By comparing the Lorentz structures of the expansions of  $W_{\mu\nu}^A$  and  $T_{\mu\nu}^A$ , one can identify the structure functions of  $W_{\mu\nu}^A$  in terms of the OPE. When the mass of a nucleus  $A$  is neglected, the OPE of  $T_{\mu\nu}^A$  simplifies to familiar expressions. The differences between the fully massive and simplified massless expressions are the TMCs to the structure functions of  $W_{\mu\nu}^A$ .

Following this outline, we start by taking the expression for  $W_{\mu\nu}^A(p_A, q)$  in Eq. (A.28) and decomposing it into a sum of tensor-valued coefficients multiplied by dimensionless, scalar-valued functions  $\tilde{W}_i^A$ . The  $\tilde{W}_i^A$  are the structure functions. Lorentz symmetry and hermiticity dictate that only certain combinations of  $p_A$  and  $q$

---

<sup>20</sup> $\gamma^*(q)A(p_A) \rightarrow \gamma^*A$  for electromagnetic currents,  $W^*(q)A(p_A) \rightarrow W^*A$  for charged currents, etc.



are allowed as coefficients. The most general combination allowed by symmetries for unpolarized  $A$  is

$$W_{\mu\nu}^A(p_A, q) = \frac{1}{4\pi} \int d^4z e^{iqz} \langle A | J_\mu^\dagger(z) J_\nu(0) | A \rangle \quad (\text{A.30})$$

$$\begin{aligned} &= -g_{\mu\nu} \tilde{W}_1^A + \frac{p_{A\mu} p_{A\nu}}{M_A^2} \tilde{W}_2^A - i\epsilon_{\mu\nu\rho\sigma} \frac{p_A^\rho q^\sigma}{M_A^2} \tilde{W}_3^A + \frac{q_\mu q_\nu}{M_A^2} \tilde{W}_4^A \\ &\quad + \frac{p_{A\mu} q_\nu + p_{A\nu} q_\mu}{M_A^2} \tilde{W}_5^A + \frac{p_{A\mu} q_\nu - p_{A\nu} q_\mu}{M_A^2} \tilde{W}_6^A \end{aligned} \quad (\text{A.31})$$

$$\begin{aligned} &= -g_{\mu\nu} \tilde{F}_1^A + \frac{p_{A\mu} p_{A\nu}}{Q^2} 2x_A \tilde{F}_2^A - i\epsilon_{\mu\nu\alpha\beta} \frac{p_A^\alpha q^\beta}{Q^2} x_A \tilde{F}_3^A + \frac{q_\mu q_\nu}{Q^2} 2\tilde{F}_4^A \\ &\quad + \frac{(p_{A\mu} q_\nu + p_{A\nu} q_\mu)}{Q^2} 2x_A \tilde{F}_5^A + \frac{(p_{A\mu} q_\nu - p_{A\nu} q_\mu)}{Q^2} 2x_A \tilde{F}_6^A . \end{aligned} \quad (\text{A.32})$$

The presence of six structure functions follows from the fact that (i) electromagnetic and weak currents are vector currents and (ii) the state  $X$  in the process  $\ell_1(k_1) + A(p_A) \rightarrow \ell_2(k_2) + X(p_X)$  must have *net* quantum numbers corresponding to a fermion. ( $VA$  scattering cannot, for example, convert nucleus  $A$ , which is a fermion, into a state with net scalar or vector boson quantum numbers due to Lorentz invariance / angular momentum conservation.) The first point implies that the hadronic current  $\tilde{W}_{\mu\nu}^A(p_A, q)$ , which is built by squaring the  $AV \rightarrow X$  current is a rank-2 tensor. Now, since Dirac fermions have, in general, four independent components,  $(4 \times 4)$  fermion bilinears have 16 components. These can be arranged into five different ways: a one-component scalar current, a one-component pseudoscalar current, a four-component vector current, a four-component axialvector current, and a six-component tensor current [142, 143]. Since  $\tilde{W}_{\mu\nu}^A(p_A, q)$  is made from the product of Dirac fermion spinors, it is a bilinear, and subsequently has six independent components.

Formally, the normalizations and organization of the  $\tilde{W}_i^A$  and  $\tilde{F}_i^A$  in Eqs. (A.31) and (A.32) are conventional. Following Ref. [73], the  $\tilde{W}_i^A$  are normalized such that each is dimensionless and has at most a prefactor of  $M_A^{-2}$ . The  $\tilde{F}_i^A$  are normalized to factor out known  $Q^2$  dependence and are related to  $\tilde{W}_i^A$  by

$$\tilde{F}_1^A = \tilde{W}_1^A, \quad (\text{A.33a}) \quad \tilde{F}_3^A = \left( \frac{Q^2}{x_A M_A^2} \right) \tilde{W}_3^A, \quad (\text{A.33c})$$

$$\tilde{F}_i^A = \left( \frac{Q^2}{2x_A M_A^2} \right) \tilde{W}_i^A, \quad \text{for } i = 2, 5, 6 \quad (\text{A.33b}) \quad \tilde{F}_4^A = \left( \frac{Q^2}{2M_A^2} \right) \tilde{W}_4^A. \quad (\text{A.33d})$$

The  $\tilde{F}_i^A$  normalization makes scaling with respect to  $x_A$  more manifest. Under this normalization,  $\tilde{W}_i^A$  and  $\tilde{F}_i^A$  are real for  $i = 1 - 5$ , whereas  $\tilde{W}_6^A$  and  $\tilde{F}_6^A$  are imaginary [88]. Moreover,  $\tilde{W}_6^A$  and  $\tilde{F}_6^A$  are only nonzero if charge-parity symmetry is violated in QCD. However, the coefficient of  $\tilde{W}_6^A$  and  $\tilde{F}_6^A$  will vanish when contracted with the symmetric  $L^{\mu\nu}$  tensor. Choosing  $\tilde{W}_i^A$ ,  $\tilde{F}_i^A$ , or other normalizations does not change the underlying physics. However, seemingly innocuous differences in their definitions can impact the final form of TMCs due to structure function mixing, i.e., the off-diagonal terms in  $A_j^i$  and  $B_j^i$  in Eq. (3.23).

The next step is to recognize that  $\tilde{W}_{\mu\nu}^A$  in the DIS limit can be related to the time-ordered matrix element  $T_{\mu\nu}^A$  for  $AV^* \rightarrow AV^*$  scattering in short-distance limit. This is given by [49]

$$T_{\mu\nu}^A(p_A, q) \equiv \int d^4z e^{iqz} \langle A | \mathcal{T} J_\mu^\dagger(z) J_\nu(0) | A \rangle \quad (\text{A.34})$$

$$\begin{aligned} &= \int d^4z e^{iqz} \langle A | J_\mu^\dagger(z) J_\nu(0) | A \rangle \theta(z^0 > 0) \\ &\quad + \int d^4z e^{iqz} \langle A | J_\nu(0) J_\mu^\dagger(z) | A \rangle \theta(z^0 < 0) \end{aligned} \quad (\text{A.35})$$

$$\equiv T_{z^0 > 0}(p_A, q) + T_{z^0 < 0}(p_A, q), \quad (\text{A.36})$$

where  $\theta$  is the usual Heaviside step function normalized to unity. The matrix elements under the integral can

be identified as the (inverse) Fourier transforms (FT) of  $W_{\mu\nu}^A$  over  $q$ :

$$\text{FT}[W_{\mu\nu}^A(p_A, q)](x) = \int \frac{d^4q}{(2\pi)^4} e^{-iq \cdot x} W_{\mu\nu}^A(p_A, q) = \frac{1}{4\pi} \langle A | J_\mu^\dagger(x) J_\nu(0) | A \rangle, \quad (\text{A.37a})$$

$$\text{FT}[\overline{W}_{\nu\mu}^A(p_A, q)](x) = \int \frac{d^4q}{(2\pi)^4} e^{-iq \cdot x} \overline{W}_{\nu\mu}^A(p_A, q) = \frac{1}{4\pi} \langle A | J_\nu(0) J_\mu^\dagger(x) | A \rangle. \quad (\text{A.37b})$$

Equation (A.37b) defines the ‘‘conjugate’’ hadronic tensor  $\overline{W}_{\nu\mu}^A$ . It is related to  $W_{\mu\nu}^A$  by

$$\overline{W}_{\nu\mu}^A(p_A, q) = \frac{1}{4\pi} \int d^4z e^{-i(-q) \cdot z} \langle A | J_\nu(0) J_\mu^\dagger(z) | A \rangle = [W_{\mu\nu}^A(p_A, -q)]^\dagger. \quad (\text{A.38})$$

Note that the Hermitian conjugation operator  $\dagger$  should be applied to both the structure functions and the tensor-valued coefficients of  $W_{\mu\nu}^A$ . For the case of electromagnetic currents, these are Hermitian and Eq. (A.38) reduces to  $\overline{W}_{\nu\mu}^A(p_A, q)|_{\text{EM}} = W_{\mu\nu}^A(p_A, -q)$ .

After exchanging the order of integration, the first term in Eq. (A.36) is

$$T_{z^0 > 0}(p_A, q) = 4\pi \int \frac{d^4k}{(2\pi)^4} W_{\mu\nu}^A(p_A, k) \int d^4z e^{i(q-k) \cdot z} \theta(z^0 > 0) \quad (\text{A.39})$$

$$= 4\pi \int \frac{d^4k}{(2\pi)^4} W_{\mu\nu}^A(p_A, k) (2\pi)^3 \delta(\vec{q} - \vec{k}) \left[ \pi \delta(q^0 - k^0) + \frac{i}{q^0 - k^0} \right]. \quad (\text{A.40})$$

The three-dimensional  $\delta(\vec{q} - \vec{k})$  comes from integrating over all of  $\vec{z}$ -space and the bracketed factor comes from integrating only over  $z^0 > 0$ . Following the argument of Ref. [88], momentum conservation dictates that  $(2p_A \cdot q) > Q^2$ , which implies that  $W_{\mu\nu}^A$  is zero for  $(2p_A \cdot q) < Q^2$ , or equivalently that  $W_{\mu\nu}^A$  is zero for  $x_A > 1$  and  $x_A < 0$ . Fixing  $Q^2$  and taking  $W_{\mu\nu}^A$  to be analytic on the plane  $\omega_A \equiv x_A^{-1}$  further implies branch cuts along  $|\omega_A| \geq 1$  as depicted in Fig. 3.1. Therefore, since the pole in Eq. (A.40) can be decomposed into its principal  $\mathcal{P}$  and singular parts when deformed, i.e.,

$$\frac{1}{q^0 - k^0 \mp i\varepsilon} = \mathcal{P} \pm i\pi \delta(q^0 - k^0), \quad (\text{A.41})$$

the tensor  $W_{\mu\nu}^A$  can be identified as the discontinuity of  $T_{z^0 > 0}$ . Specifically, one finds:

$$\text{disc } T_{z^0 > 0} = \lim_{\varepsilon \rightarrow 0} [T_{z^0 > 0}(q^0 + i\varepsilon) - T_{z^0 > 0}(q^0 - i\varepsilon)] \quad (\text{A.42})$$

$$= 4\pi \int \frac{d^4k}{(2\pi)^4} W_{\mu\nu}^A(p_A, k) (2\pi)^3 \delta(\vec{q} - \vec{k}) \times \{ [i\mathcal{P} - i^2\pi\delta(q^0 - k^0)] - [i\mathcal{P} + i^2\pi\delta(q^0 - k^0)] \} \quad (\text{A.43})$$

$$= 4\pi W_{\mu\nu}^A(p_A, q). \quad (\text{A.44})$$

A similar result holds for  $T_{z^0 < 0}$ . Subsequently, one can write in terms of  $\omega_A = x_A^{-1}$  the relations [49, 88]

$$T_{\mu\nu}^A(p_A, q) \Big|_{\omega_A - i\varepsilon}^{\omega_A + i\varepsilon} = 4\pi W_{\mu\nu}^A(p_A, q), \quad \text{for } \omega_A > 0, \quad (\text{A.45a})$$

$$T_{\mu\nu}^A(p_A, q) \Big|_{\omega_A + i\varepsilon}^{\omega_A - i\varepsilon} = 4\pi [W_{\mu\nu}^A(p_A, -q)]^\dagger, \quad \text{for } \omega_A < 0. \quad (\text{A.45b})$$

and with  $W_{\mu\nu}^A$  and  $W_{\nu\mu}^{A\dagger}$  vanishing for  $\omega_A < 1$  and  $\omega_A > -1$ , respectively. Intuitively, Eq. (A.45) states that  $T_{\mu\nu}^A$  and  $W_{\mu\nu}^A$ , which are defined in different kinematic limits (the short-distance and DIS limits, respectively), are nevertheless related through analytic continuation. Therefore, one can take  $T_{\mu\nu}^A(p_A, q)$ , decompose it into

a contour integral over  $x_A^{-1}$  using Cauchy's integral formula, and deform the contour around the discontinuities at  $x_A^{-1} < -1$  and  $x_A^{-1} > 1$  as shown in Fig. 3.1.

### Coefficient functions of $T_{\mu\nu}^A$ and moments of structure functions

The relationship in Eq. (A.45) can be refined by decomposing  $T_{\mu\nu}^A$  in three different ways. The first is according to Lorentz structures as was done for  $W_{\mu\nu}^A$  in Eq. (A.31):

$$T_{\mu\nu}^A = -g_{\mu\nu}\Delta\tilde{T}_1^A + \frac{p_{A\mu}p_{A\nu}}{M_A^2}\Delta\tilde{T}_2^A - i\epsilon_{\mu\nu\alpha\beta}\frac{p_A^\alpha q^\beta}{M_A^2}\Delta\tilde{T}_3^A + \frac{q_\mu q_\nu}{M_A^2}\Delta\tilde{T}_4^A + \frac{(p_{A\mu}q_\nu + p_{A\nu}q_\mu)}{M_A^2}\Delta\tilde{T}_5^A + \frac{(p_{A\mu}q_\nu - p_{A\nu}q_\mu)}{M_A^2}\Delta\tilde{T}_6^A. \quad (\text{A.46})$$

Component-by-component, the dispersion relationship of Eq. (A.45) becomes

$$\Delta\tilde{T}_i^A(p_A, q)\Big|_{\omega_A - i\varepsilon}^{\omega_A + i\varepsilon} = 4\pi \tilde{W}_i^A(p_A, q), \quad \text{for } \omega_A > 0, \quad (\text{A.47a})$$

$$\Delta\tilde{T}_i^A(p_A, q)\Big|_{\omega_A + i\varepsilon}^{\omega_A - i\varepsilon} = 4\pi (-1)^{b_i} \tilde{W}_i^A(p_A, -q), \quad \text{for } \omega_A < 0, \quad (\text{A.47b})$$

$$\text{and } b_i = 0 \text{ (1), for } i = 1, 2, 3, 4, 6 \text{ (5)}. \quad (\text{A.47c})$$

The factor of  $(-1)^{b_i}$  comes from applying the  $\dagger$  operator in Eq. (A.45b) to  $\tilde{W}_i^A$  and its prefactor in combination with propagating the argument  $-q$  into the prefactor of  $\tilde{W}_i^A$ . We also take into account whether  $\tilde{W}_i$  is real or imaginary, as discussed below Eq. (A.33); recall  $\tilde{W}_6^A$  is imaginary.

The second way of decomposing  $T_{\mu\nu}^A$  is by the OPE (done below) and gives expressions for  $\Delta\tilde{T}_i^A$ .

The third decomposition is by Taylor expansion in the short-distance limit. The distinction between this limit and the DIS limit is important: In the DIS limit,  $(Q^2/M_A^2) \rightarrow \infty$  while  $x_A = (Q^2/2p_A \cdot q)$  is fixed. In the short-distance limit,  $(Q^2/M_A^2) \rightarrow \infty$  while  $x_A/Q$  is fixed, meaning that  $x_A$  grows with  $(Q/M_A)$ . Formally, the short-distance limit corresponds to the limit  $\omega_A = 2(p_A \cdot q)/Q^2 \rightarrow 0$ . We therefore assume that we can write

$$\zeta_i^A \times \omega_A^{a_i} \times \Delta\tilde{T}_i^A(p_A, q) = \sum_{k=0}^{\infty} t_{i(k)}^A(Q^2) \omega_A^k, \quad \text{where} \quad (\text{A.48a})$$

$$a_i = 0 \text{ (1) for } i = 1, 4 \text{ (2, 3, 5, 6)}, \quad \text{and } \zeta_1^A = 1, \quad \zeta_{2,4,5,6}^A = \left(\frac{Q^2}{2M_A^2}\right), \quad \zeta_3^A = \left(\frac{Q^2}{M_A^2}\right). \quad (\text{A.48b})$$

Here,  $t_{i(k)}^A$  is the  $k^{\text{th}}$  coefficient of the expansion and is only a function of  $Q^2$ . The factors  $\zeta_i^A$  and  $\omega_A^{a_i}$ , which are fixed in the short distance limit, are the same factors relating the structure functions  $\tilde{W}_i$  and  $\tilde{F}_i$  in Eqs. (2.10) and (A.33). Following Ref. [88] and using Cauchy's integral formula

$$F(y) = \frac{1}{2\pi i} \int_{\mathcal{C}} \frac{dz}{z-y} F(z), \quad (\text{A.49})$$

where  $\mathcal{C}$  is an appropriately chosen contour, it is possible to analytically continue  $\Delta\tilde{T}_i^A$ :

$$\zeta_i^A \times \omega_A^{a_i} \times \Delta\tilde{T}_i^A(p_A, q) = \frac{\zeta_i^A}{2\pi i} \int_{\mathcal{C}} \frac{d\omega'_A}{(\omega'_A - \omega_A)} (\omega'_A)^{a_i} \Delta\tilde{T}_i^A(p_A, q') \quad (\text{A.50})$$

$$= \frac{\zeta_i^A}{2\pi i} \int_{\mathcal{C}} \frac{d\omega'_A}{\omega'_A(1 - \frac{\omega_A}{\omega'_A})} (\omega'_A)^{a_i} \Delta\tilde{T}_i^A(p_A, q') \quad (\text{A.51})$$

$$= \sum_{k=0}^{\infty} \frac{\zeta_i^A}{2\pi i} \int_{\mathcal{C}} d\omega'_A \left(\frac{\omega_A}{\omega'_A}\right)^k (\omega'_A)^{a_i-1} \Delta\tilde{T}_i^A(p_A, q'). \quad (\text{A.52})$$

The geometric series is obtained by fixing the integration variable  $\omega'_A$ , which can be large, but taking the external variable  $\omega_A \rightarrow 0$ .

Comparing Eq. (A.52) to Eq. (A.48) and using Eqs. (A.47), one obtains

$$t_{i(k)}^A(Q^2) = \frac{\zeta_i^A}{2\pi i} \int_{\mathcal{C}} d\omega'_A (\omega'_A)^{a_i-k-1} \Delta\tilde{T}_i^A(p_A, q') \quad (\text{A.53})$$

$$= \frac{4\pi\zeta_i^A}{2\pi i} \int_1^{\infty} d\omega'_A (\omega'_A)^{a_i-k-1} \tilde{W}_i^A(p_A, q')$$

$$+ \frac{4\pi\zeta_i^A}{2\pi i} \int_{-\infty}^{-1} d\omega'_A (\omega'_A)^{a_i-k-1} (-1)^{b_i} \tilde{W}_i^A(p_A, -q') \quad (\text{A.54})$$

$$= (-2i)\zeta_i^A \int_0^1 dx'_A (x'_A)^{k-1-a_i} \tilde{W}_i^A(x'_A, Q^2)$$

$$+ (-2i)\zeta_i^A \int_{-1}^0 dx'_A (x'_A)^{k-1-a_i} (-1)^{b_i} \tilde{W}_i^A(-x'_A, Q^2). \quad (\text{A.55})$$

The last line is obtained by changing to the variable  $x'_A = (\omega'_A)^{-1}$ . Changing the integration variable of the second term to  $z_A = -x'_A$ , collecting factors of  $(-1)$ , using  $(-1)^{a_i} = (-1)^{-a_i}$ , and relabeling gives

$$t_{i(k)}^A(Q^2) = (-2i) \int_0^1 dx'_A (x'_A)^{k-1}$$

$$\times \left[ \zeta_i (x'_A)^{-a_i} \tilde{W}_i^A(x'_A, Q^2) + (-1)^{k-1+a_i+b_i} \zeta_i (x'_A)^{-a_i} \tilde{W}_i^A(x'_A, Q^2) \right] \quad (\text{A.56})$$

$$= (-2i) \left[ 1 + (-1)^{k-1+a_i+b_i} \right] \int_0^1 dx'_A (x'_A)^{k-1} \tilde{F}_i^A(x'_A, Q^2). \quad (\text{A.57})$$

We now denote the  $N^{\text{th}}$  Mellin moment of the function  $M(z)$  by  $M^N$  and fix normalizations such that a Mellin transformation and its inverse (over a path  $c$ ) are:

$$M^N = \int_0^1 dz z^{N-1} M(z) \quad \text{with} \quad M(z) = \frac{1}{2\pi i} \int_{c-i\infty}^{c+i\infty} dN z^{-N} M^N. \quad (\text{A.58})$$

Under this normalization, the moments of  $\tilde{W}_i^A(x_A)$  are related to those of  $\tilde{F}_i^A(x_A)$  by

$$\tilde{F}_1^{AN} = \tilde{W}_1^{AN}, \quad (\text{A.59a}) \quad \tilde{F}_3^{AN} = \left(\frac{Q^2}{M_A^2}\right) \tilde{W}_3^{A(N-1)}, \quad (\text{A.59c})$$

$$\tilde{F}_i^{AN} = \left(\frac{Q^2}{2M_A^2}\right) \tilde{W}_i^{A(N-1)} \quad \text{for } i = 2, 5, 6, \quad (\text{A.59b}) \quad \tilde{F}_4^{AN} = \left(\frac{Q^2}{2M_A^2}\right) \tilde{W}_4^{AN}. \quad (\text{A.59d})$$

Both are related to the  $N^{\text{th}}$  coefficient function  $t_{i(k=N)}^A(Q^2)$  by

$$t_{i(N)}^A(Q^2) = -2i \left[ 1 + (-1)^{N-1+a_i+b_i} \right] \tilde{F}_i^{AN}(Q^2) \quad (\text{A.60a})$$

$$= \begin{cases} 0, & N = \text{even} \\ -4i \tilde{F}_i^{AN}(Q^2), & N = \text{odd} \end{cases}, \quad \text{for } i = 1, 4, 5, \quad (\text{A.60b})$$

$$= \begin{cases} -4i \tilde{F}_i^{AN}(Q^2), & N = \text{even} \\ 0, & N = \text{odd} \end{cases}, \quad \text{for } i = 2, 3, 6. \quad (\text{A.60c})$$

This allows us to rewrite the expansion in Eq. (A.48) as

$$\zeta_i^A \times \omega_A^{a_i} \times \Delta \tilde{T}_i^A(Q^2, \omega_A) = -4i \sum_N^{\infty} \tilde{F}_i^{AN}(Q^2) \omega_A^N, \quad (\text{A.61})$$

where it is implied that the index  $N$  runs only over odd or even integers.

We now make a few brief comments. First, in order for Eq. (A.61) to hold,  $|\omega_A| < 1$  must be satisfied, i.e., one must be in the DIS limit. Second, as  $N$  increases, the dominant contribution to  $\tilde{F}_i^{AN}$  is when the argument of  $\tilde{F}_i^A(z)$  approaches unity since (according to the definition of Eq. (A.58))  $\tilde{F}_i^{AN}$  would otherwise be suppressed by a small number. Finally, since  $\omega_A = 1$  corresponds to the elastic limit (see Eq. (2.2c)),  $Q^2$  must be made increasingly large for large- $N$  moments to be well-defined and for the invariant mass of the hadronic system to remain in the perturbative regime.

## Expanding $T_{\mu\nu}^A$ with the OPE

Using the OPE, the leading behavior of  $T_{\mu\nu}^A$  in powers of  $(1/Q^p)$  can be decomposed into a sum of operators  $\mathcal{O}^{\mu_1, \dots, \mu_k}$  and Wilson coefficients  $c_{\mu\nu\mu_1 \dots \mu_k}^{\tau, \ell}$ . This expansion is given by [49, 58, 59]

$$\lim_{z \rightarrow 0} T_{\mu\nu}^A(p_A, q) \stackrel{\text{OPE}}{=} -2i \sum_{k, \ell} c_{\mu\nu\mu_1 \dots \mu_k}^{\tau=2, \ell}(q) \langle A(p_A) | \mathcal{O}_{\ell, \tau=2}^{\mu_1 \dots \mu_k} | A(p_A) \rangle + \mathcal{O}(\tau > 2). \quad (\text{A.62})$$

At leading power, the composite operators  $\mathcal{O}_{\ell, \tau}^{\mu_1 \dots \mu_k}$  are symmetric, quark bilinears (or pairs of gluon field strengths) that sandwich uncontracted covariant derivatives. Tallying up the number of uncontracted Lorentz indices implies that  $\mathcal{O}_{\ell, \tau}^{\mu_1 \dots \mu_k}$  carries a spin of  $k$ . The operators are organized according to their twist  $\tau \equiv d - n$ , where  $d$  is the dimensionality of  $\mathcal{O}_{\ell, \tau}^{\mu_1 \dots \mu_k}$  in the standard sense of dimension power counting in an effective field theory. For a fixed spin and twist, the index  $\ell$  catalogs all the Lorentz structures that can possibly contract with  $\mathcal{O}_{\ell, \tau}^{\mu_1 \dots \mu_k}$ . Coupling and renormalization factors are sequestered into the effective Wilson coefficient  $c_{\mu\nu\mu_1 \dots \mu_k}^{\tau, \ell}(q)$ . For fixed spin  $k$ , a larger twist  $\tau$  corresponds to a larger  $(1/Q)$  suppression in the Wilson coefficient. Schematically, Eq. (A.62) stipulates that in the short-distance limit, the time-ordered matrix element  $T_{\mu\nu}^A$ , which is a function of  $p_A$  and  $q$ , can be expressed in terms of Wilson coefficients, which are only functions of  $q$ , and hadronic matrix elements, which are only functions of  $p_A$ .

The operators  $\mathcal{O}^{\mu_1, \dots, \mu_k}$  can be decomposed into symmetric (traceless) and non-symmetric parts, with  $\mathcal{O}^{\mu_1, \dots, \mu_k} \sim \hat{P}_A^{\mu_1} \dots \hat{P}_A^{\mu_k} + \text{Tr}$ . The trace term captures all contributions proportional to the spacetime metric and derivatives, which after contractions or applications of equations of motion give rise to powers of quark masses [58, 59]. Neglecting quark masses<sup>21</sup>, the matrix elements that follow from acting on  $\mathcal{O}^{\mu_1, \dots, \mu_{2k}}$  are given

<sup>21</sup>In practice, finite quark masses can be incorporated in TMCs through a rescaling of the Nachtmann scaling variable. See Appendix A.2 of Ref. [73] and references therein.

by

$$\langle A | \mathcal{O}_{\ell, \tau=2}^{\mu_1 \dots \mu_{2k}} | A \rangle = A_{\tau=2}^{2k} \times \tilde{\Pi}^{\mu_1 \dots \mu_{2k}}, \quad \text{where} \quad (\text{A.63a})$$

$$\tilde{\Pi}^{\mu_1 \dots \mu_{2k}} = \sum_{j=0}^k (-1)^j \frac{(2k-j)!}{2^j (2k)!} \eta(j, 2k-2j) \underbrace{\{g \dots g\}}_{j \text{ } g^{\mu_n \mu_m} \text{'s}} \underbrace{\{p_A \dots p_A\}}_{(2k-2j) \text{ } p_A^{\mu_n} \text{'s}} (p_A^2)^j. \quad (\text{A.63b})$$

Note the index change from  $k$  to  $2k$ . The factor  $A_{\tau=2}^{2k}$  is the scalar-valued ‘‘reduced’’ hadronic matrix element and describes long-distance hadronic dynamics. (The  $2k$  in  $A_{\tau=2}^{2k}$  is an index, not an exponent.) The index  $j$  sums over all permutations of  $p_A^{\mu_n}$  and  $g^{\mu_n \mu_m}$ , with  $\mu_n, \mu_m \in \{\mu_1, \dots, \mu_{2k}\}$ , that contract with a particular Wilson coefficient. For a given  $k$  and  $j$ , the two  $\{\dots\}$  brackets denote  $j$  spacetime metrics  $g^{\mu_n \mu_m}$  and  $(2k-2j)$  factors of momentum  $p_A^{\mu_m}$ . The permutation multiplicity  $\eta$  is

$$\eta(j \text{ metrics, } 2k-2j \text{ factors of } p_A) = \frac{1}{2^j} \frac{(2k)!}{j!(2k-2j)!}. \quad (\text{A.64})$$

The numerator of  $\eta$  is calculated from  $(2k)! = [(2k-2j) + (2j)]!$ . The denominator factor of  $2^j$  accounts for the two-fold symmetry of  $j$  symmetric metric tensors, i.e.,  $g^{\mu_n \mu_m} = g^{\mu_m \mu_n}$ . If a metric or momentum factor is pulled from either  $\{\dots\}$  bracket,  $\eta$  is updated accordingly.

In the massless target limit, i.e., when  $(M_A^2/Q^2) \rightarrow 0$ , one neglects  $j > 0$  terms since they generate powers of  $(p_A^2)^j = M_A^{2j}$ . For this reason, the  $j > 0$  terms are sometimes called ‘‘kinematical power corrections’’ [62, 63]. In the  $j = 0$  limit, Eq. (A.63) reduces to  $2k$  factors of  $p_A^{\mu_m}$ :

$$\langle A | \mathcal{O}_{\ell, \tau=2}^{\mu_1, \dots, \mu_{2k}} | A \rangle \Big|_{(M_A/Q)^2 \rightarrow 0} = A_{\tau=2}^{2k} (p_A^2) \times \tilde{\Pi}_{\mu_1 \dots \mu_{2k}} \Big|_{j=0} = A_{\tau=2}^{2k} (p_A^2) \times (p_A^{\mu_1} \dots p_A^{\mu_{2k}}). \quad (\text{A.65})$$

At leading power of  $\tau$  and for a fixed  $2k > 2$ , the  $c$  functions in Eq. (A.62) can be decomposed as

$$\begin{aligned} c_{\mu\nu\mu_1, \dots, \mu_{2k}}^{\tau=2, \ell}(q) &= \left[ -2g_{\mu\nu} q_{\mu_1} q_{\mu_2} C_1^{2k} + g_{\mu\mu_1} g_{\nu\mu_2} Q^2 C_2^{2k} - i\epsilon_{\mu\nu\alpha\beta} g_{\mu_1}^\alpha q_{\mu_2}^\beta C_3^{2k} \right. \\ &\left. + 4 \frac{q_\mu q_\nu}{Q^2} q_{\mu_1} q_{\mu_2} C_4^{2k} + 2(g_{\mu\mu_1} q_\nu q_{\mu_2} \pm g_{\nu\mu_1} q_\mu q_{\mu_2}) C_{5,6}^{2k} \right] \times \frac{2^{2k}}{(Q^2)^{2k}} \times \left( \prod_{m=3}^{2k} q_{\mu_m} \right). \end{aligned} \quad (\text{A.66})$$

Here, the  $C_{\ell=1, \dots, 6}^{2k}$  are scalar-valued coefficients that parameterize the normalization of each  $c_{\mu\nu\mu_1, \dots, \mu_{2k}}^{\tau=2, \ell}$ . The  $C_\ell$  are defined to all orders in QCD but can be identified and matched to quantities in fixed-order perturbation theory. The tensor part, i.e., the part carrying Lorentz indices, can then be organized according to Lorentz structures as in Eq. (A.46). Conventional factors of 2 in Eq. (A.66) are pulled from the  $C_\ell^{2k}$  in order to simplify later expressions.



Assembling these ingredients and contracting over all  $2k > k_{\min}$  indices, the OPE gives

$$\begin{aligned} \lim_{z \rightarrow 0} T_{\mu\nu}^A(q, p_A) \stackrel{\text{OPE}}{=} & -2i \sum_{k=k_{\min}}^{\infty} \left[ -2g_{\mu\nu} q_{\mu_1} q_{\mu_2} C_1^{2k} + g_{\mu\mu_1} g_{\nu\mu_2} Q^2 C_2^{2k} - i\epsilon_{\mu\nu\alpha\beta} g_{\mu_1}^{\alpha} q^{\beta} q_{\mu_2} C_3^{2k} \right. \\ & \left. + 4 \frac{q_{\mu} q_{\nu}}{Q^2} q_{\mu_1} q_{\mu_2} C_4^{2k} + 2(g_{\mu\mu_1} q_{\nu} q_{\mu_2} \pm g_{\nu\mu_1} q_{\mu} q_{\mu_2}) C_{5,6}^{2k} \right] \\ & \times \frac{2^{2k}}{(Q^2)^{2k}} \times \left( \prod_{m=3}^{2k} q_{\mu_m} \right) \times A_{\tau=2}^{2k}(p_A^2) \times \tilde{\Pi}^{\mu_1 \dots \mu_{2k}} + \mathcal{O}(\tau > 2) \end{aligned} \quad (\text{A.67})$$

$$\equiv \Delta\tilde{T}_{1\mu\nu}^A + \Delta\tilde{T}_{2\mu\nu}^A + \Delta\tilde{T}_{3\mu\nu}^A + \Delta\tilde{T}_{4\mu\nu}^A + \Delta\tilde{T}_{5\mu\nu}^A + \Delta\tilde{T}_{6\mu\nu}^A + \mathcal{O}(\tau > 2) \quad (\text{A.68})$$

$$\begin{aligned} = & -g_{\mu\nu} \Delta\tilde{T}_1^A + \frac{p_{A\mu} p_{A\nu}}{M_A^2} \Delta\tilde{T}_2^A - i\epsilon_{\mu\nu\alpha\beta} \frac{p_A^{\alpha} q^{\beta}}{M_A^2} \Delta\tilde{T}_3^A + \frac{q_{\mu} q_{\nu}}{M_A^2} \Delta\tilde{T}_4^A \\ & + \frac{(p_{A\mu} q_{\nu} + p_{A\nu} q_{\mu})}{M_A^2} \Delta\tilde{T}_5^A + \frac{(p_{A\mu} q_{\nu} - p_{A\nu} q_{\mu})}{M_A^2} \Delta\tilde{T}_6^A + \mathcal{O}(\tau > 2). \end{aligned} \quad (\text{A.69})$$

The starting point for the summation over  $k$  depends on the particular Wilson coefficient; specifically,  $k_{\min} = 2$  for  $C_2$  while  $k_{\min} = 1$  for the other  $C_i$  coefficients. In Eq. (A.69), the scalar-valued coefficients  $\Delta\tilde{T}_{i=1, \dots, 6}^A$ , i.e., the quantities *without* external Lorentz indices, are related to the hadronic structure functions  $W_i^A$  through the dispersion relationships of Eqs. (A.45) and (A.47), up to  $(1/Q)$  corrections. The  $\Delta\tilde{T}_i$  are given explicitly in terms of summations over  $k$  and  $j$  below in Eqs. (A.96)-(A.106).

In the intermediate step Eq. (A.68), each  $\Delta\tilde{T}_{\iota=1, \dots, 6}^A$   $\mu\nu$  denotes the collection of contractions that are respectively proportional to the coefficient  $C_{\iota}$ . We introduce this step because  $\Delta\tilde{T}_{\iota}^A$   $\mu\nu$  and  $\Delta\tilde{T}_i^A$  do not have a one-to-one correspondence when  $M_A \neq 0$ . As a consequence of the normalizations adopted for  $\tilde{W}_i^A$  in Eq. (A.31), and subsequently those for  $\Delta\tilde{T}_i^A$  in Eq. (A.46), some  $\Delta\tilde{T}_i^A$  are sourced by multiple OPE operators when  $M_A \neq 0$ . This phenomenon of  $\tilde{W}_i^A$  (or  $\Delta\tilde{T}_i^A$ ) being sourced by two or more  $C_{\iota}$  is sometimes called ‘‘structure function mixing,’’ and is discussed in App. A.4.

We now derive all six  $\Delta\tilde{T}_{\iota}^A$   $\mu\nu$  from Eq. (A.67) by contracting all  $\mu_m$  indices. After, we reorganize  $\Delta\tilde{T}_{\iota}^A$   $\mu\nu$  and group terms according to their Lorentz structure, e.g., collect all terms proportional to  $g_{\mu\nu}$  or all terms proportional to  $\epsilon_{\mu\nu\alpha\beta} p_A^{\alpha} q^{\beta}$ . We then identify the  $\Delta\tilde{T}_i^A$ , which are in terms of hadronic matrix elements  $A_{\tau=2}^{2k}$ , Wilson coefficients  $C_{\iota}^{2k}$ , and nested summations. In App. A.5, the summations are first evaluated for the case of a massless target. The results for the  $(M_A^2/Q^2) \neq 0$  case are then expressed in terms of structure functions for massless targets.

## Organization of Lorentz contractions in the OPE

Explicit evaluation of all contractions of Lorentz indices in Eq. (A.67) is an exacting task. Therefore, as a first step, we organize everything according to  $\Delta\tilde{T}_{\iota}^A$   $\mu\nu$ , and hence  $C_{\iota}$ . As a consequence, patterns in  $\Delta\tilde{T}_{\iota}^A$   $\mu\nu$  appear and simplify the work. The outcome is summarized in App. A.4.

- (i)  $\Delta\tilde{T}_{1\mu\nu}^A$ : We start with  $\Delta\tilde{T}_{1\mu\nu}^A$  for  $M_A \neq 0$  because, like  $\Delta\tilde{T}_{4\mu\nu}^A$ , the covariant tensor structure for  $\mu_{m=1} \dots \mu_{m=2k}$  consists entirely of momentum factors  $q$ . That is to say, all lowered internal indices  $\mu_m$  are carried by  $q_{\mu_m}$ . This results in the simplest possible permutations of metrics and momenta in  $\tilde{\Pi}^{\mu_1 \dots \mu_{2k}}$ . Combining terms, one gets

$$\Delta\tilde{T}_{1\mu\nu}^A = -4i \sum_{k=1}^{\infty} [-g_{\mu\nu} C_1^{2k} A_{\tau=2}^{2k}] \times \frac{2^{2k}}{(Q^2)^{2k}} \times \left( \prod_{m=1}^{2k} q_{\mu_m} \right) \times \tilde{\Pi}^{\mu_1 \dots \mu_{2k}} + \mathcal{O}(\tau > 2), \quad (\text{A.70})$$

where the production factor  $(\prod_{m=1}^{2k} q_{\mu_m})$  has (re)absorbed  $q_{\mu_1}$  and  $q_{\mu_2}$ .

The contraction of  $\prod_{m=1}^{2k} q_{\mu_m}$  and the momentum factor  $\tilde{\Pi}$  combines all possible permutations of  $2k$  instances of  $q_{\mu_m}$  with  $j$  metrics  $g^{\mu_m \mu_n}$  in  $\{g \dots g\}$  and  $(2k - 2j)$  momenta  $p_A^{\mu_m}$  in  $\{p_A \dots p_A\}$ . This results

in  $(2k-2j)$  products of  $(q \cdot p_A)$ . The remaining  $(2k-0) - (2k-2j) = 2j$  instances of  $q_{\mu_m}$  then contract with the  $2j$  indices from  $j$  metrics. As no instance of  $g^{\mu_m \mu_n}$  or  $p_A^{\mu_m}$  have been pulled from  $\tilde{\Pi}$ , its permutation factor  $\eta$  is the same as in Eq. (A.64). The outcome is

$$\left( \prod_{m=1}^{2k} q_{\mu_m} \right) \tilde{\Pi}^{\mu_1 \dots \mu_{2k}} = \sum_{j=0}^k (-1)^j \frac{(2k-j)!}{2^j (2k)!} \frac{1}{2^j} \frac{(2k)!}{j!(2k-2j)!} \times (q^2)^j (q \cdot p_A)^{(2k-2j)} (p_A^2)^j \quad (\text{A.71})$$

$$= \frac{(Q^2)^{2k}}{2^{2k}} \sum_{j=0}^k \frac{(2k-j)!}{j!(2k-2j)!} \left( \frac{M_A^2}{Q^2} \right)^j x_A^{-(2k-2j)}, \quad (\text{A.72})$$

where  $x_A = Q^2/(2p_A \cdot q)$  is the Bjorken scaling variable and  $p_A^2 = M_A^2$ . Altogether,

$$\begin{aligned} \Delta \tilde{T}_{1\mu\nu}^A &= -g_{\mu\nu} \times (-4i) \sum_{k=1}^{\infty} [C_1^{2k} A_{\tau=2}^{2k}] \sum_{j=0}^k \frac{(2k-j)!}{j!(2k-2j)!} \left( \frac{M_A^2}{Q^2} \right)^j x_A^{-(2k-2j)} \\ &+ \mathcal{O}(\tau > 2). \end{aligned} \quad (\text{A.73})$$

We stress that that the quantity to the right of  $g_{\mu\nu}$  here is not  $\Delta \tilde{T}_1^A$  in Eq. (A.69). In general, the coefficients  $\Delta \tilde{T}_i^A$  receive contributions from more than one  $\Delta \tilde{T}_{i\mu\nu}^A$ .

(ii)  $\Delta \tilde{T}_{4\mu\nu}^A$ : The next term we construct is  $\Delta \tilde{T}_{4\mu\nu}^A$  for  $M_A \neq 0$ , which has an identical tensor structure of contracted covariant indices as  $\Delta \tilde{T}_{1\mu\nu}^A$ . In other words, like  $\Delta \tilde{T}_{1\mu\nu}^A$ , all the lowered internal indices  $\mu_m$  are carried exclusively by factors of  $q_{\mu_m}$ . The result is then,

$$\begin{aligned} \Delta \tilde{T}_{4\mu\nu}^A &= \frac{q_\mu q_\nu}{Q^2} \times (-8i) \sum_{k=1}^{\infty} [C_4^{2k} A_{\tau=2}^{2k}] \sum_{j=0}^k \frac{(2k-j)!}{j!(2k-2j)!} \left( \frac{M_A^2}{Q^2} \right)^j x_A^{-(2k-2j)} \\ &+ \mathcal{O}(\tau > 2). \end{aligned} \quad (\text{A.74})$$

(iii)  $\Delta \tilde{T}_{3\mu\nu}^A$ : Moving onto  $\Delta \tilde{T}_{3\mu\nu}^A$  for  $M_A \neq 0$ , exactly one covariant index from the collection  $\mu_{m=1} \dots \mu_{m=2k}$  is carried by the metric  $g_{\mu_1}^\alpha$ . All other covariant instances of  $\mu_m$  are carried by  $(2k-1)$  instances of  $q_{\mu_m}$ . This difference among the lowered indices introduces a complication that was absent in the previous cases but nevertheless allows us to write

$$\begin{aligned} \Delta \tilde{T}_{3\mu\nu}^A &= -2i \sum_{k=1}^{\infty} [-i \epsilon_{\mu\nu\alpha\beta} q^\beta C_3^{2k} A_{\tau=2}^{2k}] \times \frac{2^{2k}}{(Q^2)^{2k}} \times g_{\mu_1}^\alpha \times \left( \prod_{m=2}^{2k} q_{\mu_m} \right) \times \tilde{\Pi}^{\mu_1 \dots \mu_{2k}} \\ &+ \mathcal{O}(\tau > 2). \end{aligned} \quad (\text{A.75})$$

In principle,  $g_{\mu_1}^\alpha$  can contract with a metric from the collection  $\{g \dots g\}$  when it contains the index  $\mu_{m=1}$ . This extracts a factor of  $q^\alpha$  out of the production factor  $(\prod_{m=2}^{2k} q_{\mu_m})$ , and hence potential permutations, through the chain  $q^\alpha = g_{\mu_1}^\alpha q_{\mu_n} g^{\mu_n \mu_1}$ . However, this generates a term proportional to  $\epsilon_{\mu\nu\alpha\beta} q^\beta q^\alpha$ , which is zero due to the antisymmetric tensor.

It is also possible for the metric  $g_{\mu_1}^\alpha$  to contract with a momentum factor from the collection  $\{p_A \dots p_A\}$ . This extracts a factor of  $p_A^\alpha = g_{\mu_1}^\alpha p_A^{\mu_1}$ , and reduces the possible number of permutations in the momentum factor  $\tilde{\Pi}$ . The contractions within  $\Delta \tilde{T}_{3\mu\nu}^A$  then involve  $(2k-1)$  instances of  $q_{\mu_m}$  contracting with  $(2k-2j-1)$  instances of  $p_A^{\mu_m}$ , to make  $(2k-2j-1)$  powers of  $(q \cdot p_A)$ . The remaining  $(2k-1) - (2k-2j-1) = 2j$  instances of  $q_{\mu_m}$  then contract with the remaining  $j$  metrics. Finally, since the number of available  $p_A^{\mu_m}$  has shifted (by one unit), the multiplicity factor in Eq. (A.64) must be updated accordingly. With the

updated  $\eta$  factor, the outcome is

$$g_{\mu_1}^\alpha \left( \prod_{m=2}^{2k} q_{\mu_m} \right) \tilde{\Pi}^{\mu_1 \dots \mu_{2k}} = p_A^\alpha \sum_{j=0}^{k-1} (-1)^j \frac{(2k-j)!}{2^j (2k)!} \frac{1}{2^j} \frac{(2k-1)!}{j! (2k-2j-1)!} \times (q^2)^j (q \cdot p_A)^{(2k-2j-1)} (p_A^2)^j \quad (\text{A.76})$$

$$= \frac{2p_A^\alpha}{Q^2} \frac{(Q^2)^{2k}}{2^{2k}} \sum_{j=0}^{k-1} \frac{(2k-j)! (2k-1)!}{(2k)! j! (2k-2j-1)!} \left( \frac{M_A^2}{Q^2} \right)^j x_A^{-(2k-2j-1)}. \quad (\text{A.77})$$

Note that the summation over  $j$  extends only to  $j = k - 1$  since there are fewer allowed permutations; this can be surmised from the denominator factor  $1/(2k - 2j - 1)!$ , which would reduce to  $1/(-1)!$  were  $j = k$ . After assembling the different terms, we obtain

$$\begin{aligned} \Delta \tilde{T}_{3\mu\nu}^A &= -i \epsilon_{\mu\nu\alpha\beta} \frac{p_A^\alpha q^\beta}{Q^2} \times (-4i) \sum_{k=1}^{\infty} [C_3^{2k} A_{\tau=2}^{2k}] \\ &\times \sum_{j=0}^{k-1} \frac{(2k-j)! (2k-1)!}{(2k)! j! (2k-2j-1)!} \left( \frac{M_A^2}{Q^2} \right)^j x_A^{-(2k-2j-1)} + \mathcal{O}(\tau > 2). \end{aligned} \quad (\text{A.78})$$

Unlike the other  $\Delta \tilde{T}_i^A$  in Eq. (A.69), we can identify the quantity to the right of the antisymmetric tensor  $\epsilon_{\mu\nu\alpha\beta}$  as  $\Delta \tilde{T}_3^A$  since there is a one-to-one correspondence.

- (iv)  $\Delta \tilde{T}_{5\mu\nu}^A$ : The steps to determine  $\Delta \tilde{T}_{5\mu\nu}^A$  (and  $\Delta \tilde{T}_{6\mu\nu}^A$ ) for  $M_A \neq 0$  closely follow those of  $\Delta \tilde{T}_{3\mu\nu}^A$  due to the presence of only one metric carrying a lowered index from the collection  $\mu_{m=1} \dots \mu_{m=2k}$ . The difference, however, is the absence of an antisymmetric tensor. The contractions of  $g_{\mu\mu_1}$  and  $g_{\nu\mu_1}$  with the collections  $\{g \dots g\}$  and  $\{p_A \dots p_A\}$  will thus generate two sets of terms each. To obtain both sets of terms, we first write

$$\begin{aligned} \Delta \tilde{T}_{5\mu\nu}^A &= -4i \sum_{k=1}^{\infty} [(g_{\mu\mu_1} q_\nu + g_{\nu\mu_1} q_\mu) C_5^{2k} A_{\tau=2}^{2k}] \times \frac{2^{2k}}{(Q^2)^{2k}} \times \left( \prod_{m=2}^{2k} q_{\mu_m} \right) \times \tilde{\Pi}^{\mu_1 \dots \mu_{2k}} \\ &+ \mathcal{O}(\tau > 2). \end{aligned} \quad (\text{A.79})$$

For the case of the metric  $g_{\alpha\mu_1}$  contracting with  $\{p_A \dots p_A\}$ , we have from Eq. (A.77)

$$\begin{aligned} g_{\alpha\mu_1} \left( \prod_{m=2}^{2k} q_{\mu_m} \right) \tilde{\Pi}^{\mu_1 \dots \mu_{2k}} \Big|_{\mu_1 \in \{p_A \dots p_A\}} &= \\ \frac{2p_{A\alpha}}{Q^2} \frac{(Q^2)^{2k}}{2^{2k}} \sum_{j=0}^{k-1} \frac{(2k-j)! (2k-1)!}{(2k)! j! (2k-2j-1)!} \left( \frac{M_A^2}{Q^2} \right)^j x_A^{-(2k-2j-1)}. \end{aligned} \quad (\text{A.80})$$

For the second case,  $g_{\alpha\mu_1}$  contracts with a metric in  $\{g \dots g\}$  and extracts a factor of  $q_\alpha = g_{\alpha\mu_1} q_{\mu_n} g^{\mu_n \mu_1}$  out of the production factor  $(\prod_{m=2}^{2k} q_{\mu_m})$ . The precise factor of  $q_{\mu_n}$  that is extracted can be any one of the  $(2k - 1)$  elements in the product factor, implying an additional multiplicity factor of this size [67]. The remaining  $(2k - 2)$  instances of  $q_{\mu_m}$  then contract with  $(2k - 2j)$  instances of  $p_A^{\mu_m}$  to make  $(2k - 2j)$  powers of  $(q \cdot p_A)$ . The remaining  $(2k - 2) - (2k - 2j) = 2j - 2$  factors of  $q_{\mu_m}$  then contract with the  $2(j - 1)$  indices of the remaining  $(j - 1)$  metrics. After updating  $\eta$  and noting that the sum now starts at  $j = 1$ ,

the outcome is

$$g_{\alpha\mu_1} \left( \prod_{m=2}^{2k} q_{\mu_m} \right) \tilde{\Pi}^{\mu_1 \dots \mu_{2k}} \Big|_{\mu_1 \in \{g \dots g\}} = q_\alpha \sum_{j=1}^k (-1)^j \frac{(2k-j)!}{2^j (2k)!} \frac{1}{2^{j-1}} \frac{(2k-2)!}{(j-1)!(2k-2j)!} \times (2k-1) \times (q^2)^{(j-1)} (q \cdot p_A)^{(2k-2j)} (p_A^2)^j \quad (\text{A.81})$$

$$= -\frac{2q_\alpha}{Q^2} \frac{(Q^2)^{2k}}{2^{2k}} \sum_{j=1}^k \frac{(2k-j)!(2k-1)!}{(2k)!(j-1)!(2k-2j)!} \left( \frac{M_A^2}{Q^2} \right)^j x_A^{-(2k-2j)}. \quad (\text{A.82})$$

Assembling all terms for both  $g_{\mu\mu_1}$  and  $g_{\nu\mu_1}$ , we obtain the expression

$$\begin{aligned} \Delta \tilde{T}_{5\mu\nu}^A &= \frac{(p_{A\mu}q_\nu + p_{A\nu}q_\mu)}{Q^2} \\ &\times (-8i) \sum_{k=1}^{\infty} [C_5^{2k} A_{\tau=2}^{2k}] \sum_{j=0}^{k-1} \frac{(2k-j)!(2k-1)!}{(2k)!j!(2k-2j-1)!} \left( \frac{M_A^2}{Q^2} \right)^j x_A^{-(2k-2j-1)} \\ &- \frac{(q_\mu q_\nu + q_\nu q_\mu)}{Q^2} \\ &\times (-8i) \sum_{k=1}^{\infty} [C_5^{2k} A_{\tau=2}^{2k}] \sum_{j=1}^k \frac{(2k-j)!(2k-1)!}{(2k)!(j-1)!(2k-2j)!} \left( \frac{M_A^2}{Q^2} \right)^j x_A^{-(2k-2j)} \\ &+ \mathcal{O}(\tau > 2). \end{aligned} \quad (\text{A.83})$$

Importantly, there are two tensor structures: The first is  $(p_{A\mu}q_\nu + p_{A\nu}q_\mu)$ , whose coefficient contributes to  $\Delta \tilde{T}_5^A$  in Eq. (A.69). The second is  $q_\mu q_\nu$ , whose coefficient contributes to  $\Delta \tilde{T}_4^A$  in Eq. (A.69). Note that the second term can equally be written as  $2(q_\mu q_\nu)$ ; we do not (yet) condense the result in order to emphasize that  $g_{\mu\mu_1}$  and  $g_{\nu\mu_1}$  each generates two terms.

- (v)  $\Delta \tilde{T}_{6\mu\nu}^A$ : The next term,  $\Delta \tilde{T}_{6\mu\nu}^A$  for  $M_A \neq 0$ , can be obtained directly from  $\Delta \tilde{T}_{5\mu\nu}^A$  by making the replacement  $q_\mu \rightarrow -q_\mu$  and  $C_5 \rightarrow C_6$ . When making this replacement, the second part of Eq. (A.83) vanishes since  $(q_\mu q_\nu + q_\nu q_\mu) \rightarrow (q_\mu q_\nu - q_\nu q_\mu) = 0$ . The final result for  $\Delta \tilde{T}_{6\mu\nu}^A$  is

$$\begin{aligned} \Delta \tilde{T}_{6\mu\nu}^A &= \frac{(p_{A\mu}q_\nu - p_{A\nu}q_\mu)}{Q^2} \times (-8i) \times \sum_{k=1}^{\infty} [C_6^{2k} A_{\tau=2}^{2k}] \\ &\times \sum_{j=0}^{k-1} \frac{(2k-j)!(2k-1)!}{(2k)!j!(2k-2j-1)!} \left( \frac{M_A^2}{Q^2} \right)^j x_A^{-(2k-2j-1)} + \mathcal{O}(\tau > 2). \end{aligned} \quad (\text{A.84})$$

- (vi)  $\Delta \tilde{T}_{2\mu\nu}^A$ : The final term  $\Delta \tilde{T}_{2\mu\nu}^A$  for  $M_A \neq 0$ , which is given by

$$\begin{aligned} \Delta \tilde{T}_{2\mu\nu}^A &= (-2i) \sum_{k=2}^{\infty} [Q^2 C_2^{2k} A_{\tau=2}^{2k}] \times \frac{2^{2k}}{(Q^2)^{2k}} \times g_{\mu\mu_1} g_{\nu\mu_2} \times \left( \prod_{m=3}^{2k} q_{\mu_m} \right) \times \tilde{\Pi}^{\mu_1 \dots \mu_{2k}} \\ &+ \mathcal{O}(\tau > 2). \end{aligned} \quad (\text{A.85})$$

is the most nuanced because the covariant tensor structure involves two metrics. That is to say, two lowered indices from the collection  $\mu_{m=1} \dots \mu_{m=2k}$  are carried by  $g_{\mu\mu_1}$  and  $g_{\nu\mu_2}$ . The contraction of these metrics with the collections  $\{g \dots g\}$  and  $\{p_A \dots p_A\}$ , in turn, generates five terms with four distinct Lorentz structures. The five possible ways are:

- (a) both  $g_{\mu\mu_1}$  and  $g_{\nu\mu_2}$  contract with momenta from  $\{p_A \dots p_A\}$  and extract  $p_{A\mu} p_{A\nu}$ ;

- (b) both  $g_{\mu\mu_1}$  and  $g_{\nu\mu_2}$  contract with *different* metrics from  $\{g \dots g\}$  and extract the quantity  $q_\mu q_\nu$  from the production factor  $(\prod_{m=3}^{2k} q_{\mu_m})$ ;
- (c) both  $g_{\mu\mu_1}$  and  $g_{\nu\mu_2}$  contract with *the same* metric from  $\{g \dots g\}$  and extract  $g_{\mu\nu}$ ;
- (d)  $g_{\mu\mu_1}$  contracts with  $\{p_A \dots p_A\}$  and  $g_{\nu\mu_2}$  with  $\{g \dots g\}$  to extract  $(p_{A\mu} q_\nu)$ ;
- (e) same as (d) but with the index exchange  $\mu \leftrightarrow \nu$  to extract the quantity  $(p_{A\nu} q_\mu)$ .

In case (a), contracting the metrics with the collection  $\{p_A \dots p_A\}$  leaves  $(2k - 2j - 2)$  instances of  $p_A^{\mu_m}$  to contract with  $(2k - 2)$  instances of  $q_{\mu_m}$ . The remaining  $(2k - 2) - (2k - 2j - 2) = 2j$  instances of  $q_{\mu_m}$  then contracts with the  $2j$  indices of the  $j$  metrics in the collection  $\{g \dots g\}$ . Updating the permutation factor, we get

$$g_{\mu\mu_1} g_{\nu\mu_2} \left( \prod_{m=3}^{2k} q_{\mu_m} \right) \tilde{\Pi}^{\mu_1 \dots \mu_{2k}} \Big|_{\mu_1, \mu_2 \in \{p_A \dots p_A\}} = p_{A\mu} p_{A\nu} \sum_{j=0}^{k-1} \frac{(2k-j)!}{2^j (2k)!} \frac{1}{2^j j! (2k-2j-2)!} \frac{(2k-2)!}{(2k-2j-2)!} \times (-1)^j (q^2)^j (q \cdot p_A)^{(2k-2j-2)} (p_A^2)^j \quad (\text{A.86})$$

$$= \frac{4p_{A\mu} p_{A\nu}}{Q^4} \frac{(Q^2)^{2k}}{2^{2k}} \sum_{j=0}^{k-1} \frac{(2k-j)!(2k-2)!}{(2k)! j! (2k-2j-2)!} \left( \frac{M_A^2}{Q^2} \right)^j x_A^{-(2k-2j-2)}. \quad (\text{A.87})$$

Note that the summation over  $j$  extends only to  $j = k - 1$  since there are fewer allowed permutations; this can be inferred from the denominator factor  $1/(2k - 2j - 2)!$ .

In case (b), contracting  $g_{\mu\mu_1}$  and  $g_{\nu\mu_2}$  with different metrics from the collection  $\{g \dots g\}$  leaves  $(2k - 4)$  instances of  $q_{\mu_m}$  to contract with  $(2k - 2j)$  instances of  $p_A^{\mu_m}$ . The precise  $q_{\mu_m}$  that are extracted from the product factor  $(\prod_{m=3}^{2k} q_{\mu_m})$  can be any two of its  $(2k - 2)$  elements, implying the additional multiplicity factor  $(2k - 2) \times (2k - 3)$ . The remaining  $(2k - 4) - (2k - 2j) = (2j - 4)$  factors of  $q_{\mu_m}$  then contract with the  $(j - 2)$  metrics remaining in  $\{g \dots g\}$ . Updating the  $\eta$  factor and noting the summation over  $j$  starts at  $j = 2$ , we get

$$g_{\mu\mu_1} g_{\nu\mu_2} \left( \prod_{m=3}^{2k} q_{\mu_m} \right) \tilde{\Pi}^{\mu_1 \dots \mu_{2k}} \Big|_{\mu_1, \mu_2 \in \{g \dots g\}} = q_\mu q_\nu \sum_{j=2}^k \frac{(2k-j)!}{2^j (2k)!} \frac{1}{2^{j-2} (j-2)! (2k-2j)!} \frac{(2k-4)!}{(2k-2j)!} \times (2k-3)(2k-2) \times (-1)^j (q^2)^{(j-2)} (q \cdot p_A)^{(2k-2j)} (p_A^2)^j \quad (\text{A.88})$$

$$= \frac{4q_\mu q_\nu}{Q^4} \frac{(Q^2)^{2k}}{2^{2k}} \sum_{j=2}^k \frac{(2k-j)!(2k-2)!}{(2k)! (j-2)! (2k-2j)!} \left( \frac{M_A^2}{Q^2} \right)^j x_A^{-(2k-2j)}. \quad (\text{A.89})$$

In case (c), contracting  $g_{\mu\mu_1}$  and  $g_{\nu\mu_2}$  with the same metric from the collection  $\{g \dots g\}$  leaves  $(2k - 2)$  instances of  $q_{\mu_m}$  to contract with all  $(2k - 2j)$  instances of  $p_A^{\mu_m}$ . The  $(2k - 2) - (2k - 2j) = (2j - 2)$  uncontracted instances of  $q_{\mu_m}$  are then matched with the  $(j - 1)$  metrics that are left in  $\{g \dots g\}$ . Updating  $\eta$  and the summation over  $j$ , which now starts from  $j = 1$ , we get

$$g_{\mu\mu_1} g_{\nu\mu_2} \left( \prod_{m=3}^{2k} q_{\mu_m} \right) \tilde{\Pi}^{\mu_1 \dots \mu_{2k}} \Big|_{g^{\mu_1 \mu_2} \in \{g \dots g\}} = g_{\mu\nu} \sum_{j=1}^k \frac{(2k-j)!}{2^j (2k)!} \times \frac{1}{2^{j-1} (j-1)! (2k-2j)!} \frac{(2k-2)!}{(2k-2j)!} (-1)^j (q^2)^{(j-1)} (q \cdot p_A)^{(2k-2j)} (p_A^2)^j \quad (\text{A.90})$$

$$= -\frac{2g_{\mu\nu}}{Q^2} \frac{(Q^2)^{2k}}{2^{2k}} \sum_{j=1}^k \frac{(2k-j)!(2k-2)!}{(2k)! (j-1)! (2k-2j)!} \left( \frac{M_A^2}{Q^2} \right)^j x_A^{-(2k-2j)}. \quad (\text{A.91})$$

In case (d),  $g_{\mu\mu_1}$  contracts with  $\{p_A \dots p_A\}$ , leaving  $(2k-2j-1)$  instances of  $p_A^{\mu_m}$ , while  $g_{\nu\mu_2}$  contracts with  $\{g \dots g\}$ , and eventually  $(\prod_{\mu=3}^{2k} q_{\mu_m})$ , leaving a total of  $(2k-3)$  instances of  $q_{\mu_m}$ . The result is  $(2k-2j-1)$  powers of  $(q \cdot p_A)$  and  $(2k-3) - (2k-2j-1) = (2j-2)$  factors of  $q_{\mu_m}$  to contract with  $(j-1)$  metrics. The  $q_{\mu_m}$  that is extracted from the product factor can be any one of its initial  $(2k-2)$  elements, implying an additional multiplicity factor of this size. Updating  $\eta$  and noting the summation over  $j$  runs from  $j=1$  to  $j=k-1$ , we obtain

$$g_{\mu\mu_1} g_{\nu\mu_2} \left( \prod_{m=3}^{2k} q_{\mu_m} \right) \tilde{\Pi}^{\mu_1 \dots \mu_{2k}} \left[ \begin{array}{l} \mu_1 \in \{p_A \dots p_A\} \\ \mu_2 \in \{g \dots g\} \end{array} \right] = p_{A\mu} q_\nu \sum_{j=1}^{k-1} \frac{(2k-j)!}{2^j (2k)!} \\ \times \frac{1}{2^{j-1}} \frac{(2k-3)!}{(j-1)!(2k-2j-1)!} \times (2k-2) (-1)^j (q^2)^{(j-1)} (q \cdot p_A)^{(2k-2j-1)} (p_A^2)^j \quad (\text{A.92})$$

$$= -\frac{4p_{A\mu} q_\nu}{Q^4} \frac{(Q^2)^{2k}}{2^{2k}} \sum_{j=1}^{k-1} \frac{(2k-j)!(2k-2)!}{(2k)!(j-1)!(2k-2j-1)!} \left( \frac{M_A^2}{Q^2} \right)^j x_A^{-(2k-2j-1)}. \quad (\text{A.93})$$

Case (e) follows from case (d) but with  $\mu \leftrightarrow \nu$  exchanged.

After assembling all five cases and regrouping, we find

$$\Delta \tilde{T}_{2\mu\nu}^A = \frac{2p_{A\mu} p_{A\nu}}{Q^2} \times (-4i) \sum_{k=1}^{\infty} [C_2^{2k} A_{\tau=2}^{2k}] \\ \times \sum_{j=0}^{k-1} \frac{(2k-j)!(2k-2)!}{(2k)!j!(2k-2j-2)!} \left( \frac{M_A^2}{Q^2} \right)^j x_A^{-(2k-2j-2)} \\ - g_{\mu\nu} \times (-4i) \sum_{k=1}^{\infty} [C_2^{2k} A_{\tau=2}^{2k}] \sum_{j=1}^k \frac{(2k-j)!(2k-2)!}{(2k)!(j-1)!(2k-2j)!} \left( \frac{M_A^2}{Q^2} \right)^j x_A^{-(2k-2j)} \\ + \frac{2q_\mu q_\nu}{Q^2} \times (-4i) \sum_{k=2}^{\infty} [C_2^{2k} A_{\tau=2}^{2k}] \sum_{j=2}^k \frac{(2k-j)!(2k-2)!}{(2k)!(j-2)!(2k-2j)!} \left( \frac{M_A^2}{Q^2} \right)^j x_A^{-(2k-2j)} \\ - \frac{2(p_{A\mu} q_\nu + p_{A\nu} q_\mu)}{Q^2} \times (-4i) \sum_{k=2}^{\infty} [C_2^{2k} A_{\tau=2}^{2k}] \\ \times \sum_{j=1}^{k-1} \frac{(2k-j)!(2k-2)!}{(2k)!(j-1)!(2k-2j-1)!} \left( \frac{M_A^2}{Q^2} \right)^j x_A^{-(2k-2j-1)} + \mathcal{O}(\tau > 2). \quad (\text{A.94})$$

The result implies that  $\Delta \tilde{T}_{2\mu\nu}^A$ , and hence the Wilson coefficient  $C_2^{2k}$ , contributes to  $\Delta T_1^A$ ,  $\Delta T_2^A$ ,  $\Delta T_4^A$ , and  $\Delta T_5^A$  in Eq. (A.69). The absence of contributions to  $\Delta T_3^A$  and  $\Delta T_6^A$ , which are asymmetric under  $\mu \leftrightarrow \nu$  exchange, can be traced to the tensor coefficient multiplying  $C_2^{2k}$  in  $c_{\mu\nu\mu_1, \dots, \mu_{2k}}^{\tau=2, \nu}$ , which is symmetric under  $\mu \leftrightarrow \nu$  exchange.



#### A.4. Nuclear structure functions from the OPE II: structure-function mixing

Using the expressions for  $\Delta\tilde{T}_l^A$ , we finally obtain the quantities  $\Delta\tilde{T}_i^A$  in Eq. (A.69). For  $\Delta\tilde{T}_1^A$  and  $M_A \neq 0$ , we collect like-terms from  $\Delta\tilde{T}_{1\mu\nu}^A$  and  $\Delta\tilde{T}_{2\mu\nu}^A$  to obtain

$$\begin{aligned} \Delta\tilde{T}_1^A &= (-4i) \sum_{k=1}^{\infty} [C_1^{2k} A_{\tau=2}^{2k}] \sum_{j=0}^k \frac{(2k-j)!(2k)!}{(2k)!j!(2k-2j)!} \left(\frac{M_A^2}{Q^2}\right)^j x_A^{-(2k-2j)} \\ &+ (-4i) \sum_{k=1}^{\infty} [C_2^{2k} A_{\tau=2}^{2k}] \sum_{j=1}^k \frac{(2k-j)!(2k-2)!}{(2k)!(j-1)!(2k-2j)!} \left(\frac{M_A^2}{Q^2}\right)^j x_A^{-(2k-2j)} + \mathcal{O}(\tau > 2) \end{aligned} \quad (\text{A.95})$$

$$\begin{aligned} &= (-4i) \sum_{l=0}^{\infty} x_A^{-(2l+1)} \sum_{j=0}^{\infty} \frac{(2l+j+1)!}{j!(2l+1)!} \left(\frac{M_A^2}{Q^2}\right)^j \\ &\quad \times \left[ \left( C_1^{2l+2j+1} A_{\tau=2}^{2l+2j+1} \right) + \frac{j \left( C_2^{2l+2j+1} A_{\tau=2}^{2l+2j+1} \right)}{(2l+2j+1)(2l+2j)} \right] + \mathcal{O}(\tau > 2). \end{aligned} \quad (\text{A.96})$$

To reach Eq. (A.96), a factor of  $1 = (2k)(2k-1)j/(2k)(2k-1)j$  is introduced into the  $C_2$  term to complete the factorials. The summation in the  $C_2$  term can then be extended to include  $j = 0$  since the contribution is zero. We also re-index the summation over  $k$  into a summation over  $2l = 2k - 2j - 1$ . After this shift it becomes manifest that the contribution from the  $C_2$  Wilson coefficient vanishes when the summation over  $j$  is truncated at  $j = 0$ . It also becomes clear that structure-function mixing is due to TMCs since neglecting terms where  $j > 0$  is equivalent to taking the  $(M_A^2/Q^2) \rightarrow 0$  limit.

The coefficient  $\Delta\tilde{T}_2^A$  is sourced entirely from  $\Delta\tilde{T}_{\mu\nu 2}^A$ , and is given by

$$\begin{aligned} \Delta\tilde{T}_2^A &= (-4i) \frac{2M_A^2}{Q^2} \sum_{k=1}^{\infty} [C_2^{2k} A_{\tau=2}^{2k}] \sum_{j=0}^{k-1} \frac{(2k-j)!(2k-2)!}{(2k)!j!(2k-2j-2)!} \left(\frac{M_A^2}{Q^2}\right)^j x_A^{-(2k-2j-2)} \\ &+ \mathcal{O}(\tau > 2) \end{aligned} \quad (\text{A.97})$$

$$\begin{aligned} &= (-4i) \frac{2M_A^2}{Q^2} \sum_{l=0}^{\infty} x_A^{-(2l-1)} \sum_{j=0}^{\infty} \frac{(2l+j+1)!}{j!(2l+1)!} \left(\frac{M_A^2}{Q^2}\right)^j (2l+1)(2l) \frac{\left( C_2^{(2l+2j+1)} A_{\tau=2}^{(2l+2j+1)} \right)}{(2l+2j+1)(2l+2j)} \\ &+ \mathcal{O}(\tau > 2). \end{aligned} \quad (\text{A.98})$$

In reaching Eq. (A.98) we again completed the factorials and set  $2l = 2k - 2j - 1$ .

Similarly,  $\Delta\tilde{T}_3^A$  for  $M_A \neq 0$  is sourced entirely from  $\Delta\tilde{T}_{\mu\nu 3}^A$ . It is given by

$$\begin{aligned} \Delta\tilde{T}_3^A &= (-4i) \frac{M_A^2}{Q^2} \sum_{k=1}^{\infty} [C_3^{2k} A_{\tau=2}^{2k}] \sum_{j=0}^{k-1} \frac{(2k-j)!(2k-1)!}{(2k)!j!(2k-2j-1)!} \left(\frac{M_A^2}{Q^2}\right)^j x_A^{-(2k-2j-1)} \\ &+ \mathcal{O}(\tau > 2) \end{aligned} \quad (\text{A.99})$$

$$\begin{aligned} &= (-4i) \frac{M_A^2}{Q^2} \sum_{l=0}^{\infty} x_A^{-(2l-1)} \sum_{j=0}^{\infty} \frac{(2l+j)!}{j!(2l)!} \left(\frac{M_A^2}{Q^2}\right)^j (2l) \frac{\left( C_3^{(2l+2j)} A_{\tau=2}^{(2l+2j)} \right)}{(2l+2j)} \\ &+ \mathcal{O}(\tau > 2), \end{aligned} \quad (\text{A.100})$$

where the index  $l = k - j$  was used after completing the factorials.

For  $\Delta\tilde{T}_4^A$  and  $M_A \neq 0$ , we collect terms from  $\Delta\tilde{T}_{\mu\nu 4}^A$ ,  $\Delta\tilde{T}_{\mu\nu 2}^A$ , and  $\Delta\tilde{T}_{\mu\nu 6}^A$ . The result is

$$\begin{aligned} \Delta\tilde{T}_4^A &= (-4i) \frac{2M_A^2}{Q^2} \sum_{k=1}^{\infty} [C_4^{2k} A_{\tau=2}^{2k}] \sum_{j=0}^k \frac{(2k-j)!(2k)!}{(2k)!j!(2k-2j)!} \left(\frac{M_A^2}{Q^2}\right)^j x_A^{-(2k-2j)} \\ &+ (-4i) \frac{2M_A^2}{Q^2} \sum_{k=2}^{\infty} [C_2^{2k} A_{\tau=2}^{2k}] \sum_{j=2}^k \frac{(2k-j)!(2k-2)!}{(2k)!(j-2)!(2k-2j)!} \left(\frac{M_A^2}{Q^2}\right)^j x_A^{-(2k-2j)} \\ &- (-4i) \frac{4M_A^2}{Q^2} \sum_{k=1}^{\infty} [C_5^{2k} A_{\tau=2}^{2k}] \sum_{j=1}^k \frac{(2k-j)!(2k-1)!}{(2k)!(j-1)!(2k-2j)!} \left(\frac{M_A^2}{Q^2}\right)^j x_A^{-(2k-2j)} \\ &+ \mathcal{O}(\tau > 2) \end{aligned} \tag{A.101}$$

$$\begin{aligned} &= (-4i) \frac{2M_A^2}{Q^2} \sum_{l=0}^{\infty} x_A^{-(2l+1)} \sum_{j=0}^{\infty} \frac{(2l+j+1)!}{j!(2l+1)!} \left(\frac{M_A^2}{Q^2}\right)^j \\ &\times \left[ \left(C_4^{(2l+2j+1)} A_{\tau=2}^{(2l+2j+1)}\right) + \frac{j(j-1) \left(C_2^{(2l+2j+1)} A_{\tau=2}^{(2l+2j+1)}\right)}{(2l+2j+1)(2l+2j)} - \frac{2j \left(C_5^{(2l+2j+1)} A_{\tau=2}^{(2l+2j+1)}\right)}{(2l+2j+1)} \right] \\ &+ \mathcal{O}(\tau > 2) . \end{aligned} \tag{A.102}$$

We complete the factorials using factors of  $1 = (2k)j/(2j)j$ , etc., and use  $2l = 2k - 2j - 1$  to re-index the summation over  $k$ . The summations over  $j$  can also be extended to  $j = 0$  since the additional terms are proportional to  $j$  or  $j(j-1)$ , i.e., are zero at  $j = 0$  and/or  $j = 1$ , and hence do not contribute.

The coefficient  $\Delta\tilde{T}_5^A$  for  $M_A \neq 0$  is generated by  $\Delta\tilde{T}_{2\mu\nu}^A$  and  $\Delta\tilde{T}_{5\mu\nu}^A$ . The result is

$$\begin{aligned} \Delta\tilde{T}_5^A &= (-4i) \frac{2M_A^2}{Q^2} \sum_{k=1}^{\infty} [C_5^{2k} A_{\tau=2}^{2k}] \sum_{j=0}^{k-1} \frac{(2k-j)!(2k-1)!}{(2k)!j!(2k-2j-1)!} \left(\frac{M_A^2}{Q^2}\right)^j x_A^{-(2k-2j-1)} \\ &- (-4i) \frac{2M_A^2}{Q^2} \sum_{k=2}^{\infty} [C_2^{2k} A_{\tau=2}^{2k}] \sum_{j=1}^{k-1} \frac{(2k-j)!(2k-2)!}{(2k)!(j-1)!(2k-2j-1)!} \left(\frac{M_A^2}{Q^2}\right)^j x_A^{-(2k-2j-1)} \\ &+ \mathcal{O}(\tau > 2) \end{aligned} \tag{A.103}$$

$$\begin{aligned} &= (-4i) \frac{2M_A^2}{Q^2} \sum_{l=0}^{\infty} x_A^{-2l} \sum_{j=0}^{\infty} \frac{(2l+j+1)!}{j!(2l+1)!} \left(\frac{M_A^2}{Q^2}\right)^j \\ &\times \left[ \frac{(2l+1) \left(C_5^{(2l+2j+1)} A_{\tau=2}^{(2l+2j+1)}\right)}{(2l+2j+1)} - \frac{j(2l+1) \left(C_2^{(2l+2j+1)} A_{\tau=2}^{(2l+2j+1)}\right)}{(2l+2j+1)(2l+2j)} \right] \\ &+ \mathcal{O}(\tau > 2) , \end{aligned} \tag{A.104}$$

where the index reassignment is  $2l = 2k - 2j - 1$ .

Finally, the coefficient  $\Delta\tilde{T}_6^A$  is generated solely by  $\Delta\tilde{T}_{6\mu\nu}^A$ . It is given by

$$\begin{aligned} \Delta\tilde{T}_6^A &= (-4i) \frac{2M_A^2}{Q^2} \sum_{k=1}^{\infty} [C_6^{2k} A_{\tau=2}^{2k}] \sum_{j=0}^{k-1} \frac{(2k-j)!(2k-1)!}{(2k)!j!(2k-2j-1)!} \left(\frac{M_A^2}{Q^2}\right)^j x_A^{-(2k-2j-1)} \\ &+ \mathcal{O}(\tau > 2) \end{aligned} \tag{A.105}$$

$$\begin{aligned} &= (-4i) \frac{2M_A^2}{Q^2} \sum_{l=0}^{\infty} x_A^{-(2l-1)} \sum_{j=0}^{\infty} \frac{(2l+j)!}{j!(2l)!} \left(\frac{M_A^2}{Q^2}\right)^j (2l) \frac{\left(C_6^{(2l+2j)} A_{\tau=2}^{(2l+2j)}\right)}{(2l+2j)} \\ &+ \mathcal{O}(\tau > 2) , \end{aligned} \tag{A.106}$$

where the index  $l = k - j$  was used after completing the factorials.

We briefly stress that the  $(M_A^2/Q^2)$  prefactor in all  $\Delta\tilde{T}_i^A$  is conventional. They exist to match the normalization of  $\tilde{T}_i^A$  in Eq. (A.69) and structure functions  $W_i^A$  in Eq. (A.31). The massless target limit should be understood as truncating the summation over  $j$  at  $j = 0$ . In addition, the re-indexing from  $k$  to  $l$  in the above expressions is not random. Different choices of relabeling can be found in the literature and depend on the precise interpretation of the quantities to the right of the  $x_A^{-N}$  factor. Our choices are motivated by the attempt to align the ratio of factorials into binomial distributions, e.g.,  $\binom{k+j}{j} = (k+j)!/j!k!$ .

## A.5. Nuclear structure fns. from the OPE III: massless and massive targets

### Massless nuclear targets

As a final preliminary step to obtaining TMCs at leading twist, we establish the connection between the effective Wilson coefficients  $C_\nu$ , the reduced matrix element  $A_{\tau=2}$ , and structure functions in the limit that  $(M_A^2/Q^2) \rightarrow 0$ ; in this limit, the TMCs will not be present, and we label this result as ‘‘No TMC’’ in Eq. (A.107). For each  $\Delta\tilde{T}_i^A$  above, truncating terms with  $j > 0$  and using the Taylor expansion of  $\Delta\tilde{T}_i^A$  from Eq. (A.61) gives the following:

$$\Delta\tilde{T}_1^A \Big|_{j=0} = -4i \sum_{l=0}^{\infty} x_A^{-(2l+1)} (C_1^{2l+1} A_{\tau=2}^{2l+1}) + \mathcal{O}(\tau > 2) = \sum_{l=0}^{\infty} \omega_A^{2l+1} \tilde{F}_1^{A(2l+1)} \Big|_{\text{No TMC}}, \quad (\text{A.107a})$$

$$\left(\frac{Q^2}{2x_A M_A^2}\right) \Delta\tilde{T}_2^A \Big|_{j=0} = -4i \sum_{l=0}^{\infty} x_A^{-2l} (C_2^{2l+1} A_{\tau=2}^{2l+1}) + \mathcal{O}(\tau > 2) = \sum_{l=0}^{\infty} \omega_A^{2l} \tilde{F}_2^{A(2l)} \Big|_{\text{No TMC}}, \quad (\text{A.107b})$$

$$\left(\frac{Q^2}{x_A M_A^2}\right) \Delta\tilde{T}_3^A \Big|_{j=0} = -4i \sum_{l=0}^{\infty} x_A^{-2l} (C_3^{2l} A_{\tau=2}^{2l}) + \mathcal{O}(\tau > 2) = \sum_{l=0}^{\infty} \omega_A^{2l} \tilde{F}_3^{A(2l)} \Big|_{\text{No TMC}}, \quad (\text{A.107c})$$

$$\left(\frac{Q^2}{2M_A^2}\right) \Delta\tilde{T}_4^A \Big|_{j=0} = -4i \sum_{l=0}^{\infty} x_A^{-(2l+1)} (C_4^{2l+1} A_{\tau=2}^{2l+1}) + \mathcal{O}(\tau > 2) = \sum_{l=0}^{\infty} \omega_A^{2l+1} \tilde{F}_4^{A(2l+1)} \Big|_{\text{No TMC}}, \quad (\text{A.107d})$$

$$\left(\frac{Q^2}{2x_A M_A^2}\right) \Delta\tilde{T}_5^A \Big|_{j=0} = -4i \sum_{l=0}^{\infty} x_A^{-(2l+1)} (C_5^{2l+1} A_{\tau=2}^{2l+1}) + \mathcal{O}(\tau > 2) = \sum_{l=0}^{\infty} \omega_A^{2l+1} \tilde{F}_5^{A(2l+1)} \Big|_{\text{No TMC}}, \quad (\text{A.107e})$$

$$\left(\frac{Q^2}{2x_A M_A^2}\right) \Delta\tilde{T}_6^A \Big|_{j=0} = -4i \sum_{l=0}^{\infty} x_A^{-2l} (C_6^{2l} A_{\tau=2}^{2l}) + \mathcal{O}(\tau > 2) = \sum_{l=0}^{\infty} \omega_A^{2l} \tilde{F}_6^{A(2l)} \Big|_{\text{No TMC}}. \quad (\text{A.107f})$$

The conclusion is that, in the massless target limit, one can identify the leading power of the product of the  $N^{\text{th}}$  Wilson coefficient  $C_i^N$  (note the index shift from  $\nu$  to  $i$ ) and hadronic matrix element  $A_{\tau=2}^N$  as a Mellin moment of structure functions themselves. This is summarized by

$$\tilde{F}_i^{AN} \Big|_{\text{No TMC}} = C_i^N A_{\tau=2}^N + \mathcal{O}(\tau > 2) \quad \text{for } i = 1, 3 - 6, \quad (\text{A.108a})$$

$$\tilde{F}_2^{A(N-1)} \Big|_{\text{No TMC}} = C_2^N A_{\tau=2}^N + \mathcal{O}(\tau > 2). \quad (\text{A.108b})$$

As a technical remark, the normalization of Eq. (A.108) fixes the normalizations of  $C_i$  in Eqs. (A.66) and (A.67).

### Massive nuclear targets

Given the relationship between the moments of  $\tilde{F}_i^A \Big|_{\text{No TMC}}$  and the product  $(C_i A_{\tau=2})$  in the massless target limit, we are now in position to bootstrap expressions for  $\tilde{F}_i^A$  with target mass corrections. The key to this

is comparing the expansion of  $\Delta\tilde{T}_i^A$  in Eq. (A.61) with the full expressions for  $\Delta\tilde{T}_i^A$  in Eqs. (A.96)-(A.106). One can identify the moments of structure functions with TMCs as everything encapsulated by the summation over  $j$ , i.e., the coefficients multiplying the  $x_A^{-2l(\pm 1)}$  factor. Using Eq. (A.108), the unknown/non-perturbative ( $C_i A_{\tau=2}$ ) can then be replaced by the measurable  $\tilde{F}_i^A|_{\text{No TMC}}$ . Expressions in  $x_A$ -space are obtained by inverse Mellin transformations. The transformations and summations over  $j$  are solvable using various identities.

$\tilde{F}_2^A$ : To build  $\tilde{F}_2^A$  for a non-zero target mass, we start from  $\Delta\tilde{T}_2^A$  in Eq. (A.98). Using Eq. (A.61) (or Eq. (A.107)), we identify everything to the right of  $x_A^{-(2l-1)}$  in Eq. (A.98) as the  $(2l)^{\text{th}}$  moment of  $\tilde{F}_2^A(x_A, Q^2)$  with TMCs. This allows us to write

$$\tilde{F}_2^{A(2l)} = \sum_{j=0}^{\infty} \frac{(2l+j+1)!}{j!(2l+1)!} \left(\frac{M_A^2}{Q^2}\right)^j (2l+1)(2l) \frac{\left(C_2^{(2l+2j+1)} A_{\tau=2}^{(2l+2j+1)}\right)}{(2l+2j+1)(2l+2j)}. \quad (\text{A.109})$$

For an arbitrary integrable function  $B(y)$  over  $y \in [0, 1]$  and  $m \geq 0$ , we have the identities

$$\frac{1}{(m+1)} \int_0^1 dy y^{m+1} B(y) = \int_0^1 dy y^m H(y), \quad (\text{A.110a})$$

$$\frac{1}{(m+2)(m+1)} \int_0^1 dy y^{(m+2)} B(y) = \int_0^1 dy y^m G(y), \quad (\text{A.110b})$$

$$\text{where} \quad H(y) = \int_y^1 dy' B(y'), \quad (\text{A.110c})$$

$$\text{and} \quad G(y) = \int_y^1 dy' \int_{y'}^1 dy'' B(y'') = \int_y^1 dy' (y' - y) B(y') \quad (\text{A.110d})$$

These identities will be used repeatedly for the different structure functions. Schematically, the identities show that each factor of “ $1/m$ ,” which originates from completing the (numerator) factorials in  $\Delta\tilde{T}_i^A$ , corresponds to an additional integral over a structure function. Using the second identity and Eq. (A.108), we have

$$\frac{C_2^{(2l+2j+1)} A_{\tau=2}^{(2l+2j+1)}}{(2l+2j+1)(2l+2j)} = \frac{1}{(2l+2j+1)(2l+2j)} \int_0^1 dy y^{2l+2j+1} \cdot y^{-2} \tilde{F}_2^A(y) \Big|_{\text{No TMCs}} \quad (\text{A.111})$$

$$= \int_0^1 dy y^{2l+2j-1} \tilde{g}_2(y), \quad \text{where} \quad (\text{A.112})$$

$$\tilde{g}_2(y) \equiv \int_y^1 dy' \int_{y'}^1 dy'' (y'')^{-2} \tilde{F}_2^A(y'') \Big|_{\text{No TMCs}}. \quad (\text{A.113})$$

This allows us to evaluate the summation over  $j$ :

$$\tilde{F}_2^{A(2l)} = \int_0^1 dy y^{2l-1} \tilde{g}_2(y) (2l+1)(2l) \sum_{j=0}^{\infty} \frac{(2l+j+1)!}{j!(2l+1)!} \left(\frac{y^2 M_A^2}{Q^2}\right)^j \quad (\text{A.114})$$

$$= \int_0^1 dy y^{-1} \tilde{g}_2(y) \frac{(2l+1)(2l) y^{2l}}{(1-y^2 M_A^2/Q^2)^{2l+2}}, \quad (\text{A.115})$$

where we used the first of the following identities, which also hold for  $z > 1$ :

$$\sum_{j=0}^{\infty} \frac{(n+j)!}{j! n!} z^j = \frac{1}{(1-z)^{(n+1)}} , \quad (\text{A.116a})$$

$$\sum_{j=1}^{\infty} j \frac{(n+j)!}{j! n!} z^j = \frac{(n+1) z}{(1-z)^{(n+2)}} , \quad (\text{A.116b})$$

$$\sum_{j=2}^{\infty} j(j-1) \frac{(n+j)!}{j! n!} z^j = \frac{(n+1)(n+2) z^2}{(1-z)^{(n+3)}} . \quad (\text{A.116c})$$

The first identity is derived by Taylor expanding the right-hand side and completing the factorial. The second follows from taking the derivative of the first identity and multiplying by  $z$ ; similarly, the third by taking two derivatives and scaling by  $z^2$ .

After relabeling  $N = 2l$ , and using the second of the following identities

$$(n+a)z^{-n} = -z^{(1+a)} \frac{d}{dz} z^{-(n+a)} , \quad (\text{A.117a})$$

$$(n+a)(n+a+1)z^{-n} = z^{(2+a)} \frac{d^2}{dz^2} z^{-(n+a)} , \quad (\text{A.117b})$$

we can take the inverse Mellin transformation of  $\tilde{F}_2^{AN}$ . We remark that these derivative identities will be used repeatedly for the different structure functions. Schematically, they show that each factor of “ $n$ ” or “ $(n+1)$ ,” which originates from completing the factorials in  $\Delta \tilde{T}_i^A$ , corresponds to a derivative over the generating functions  $G(y)$  and  $H(y)$ .

Inserting the derivative identity and taking the inverse Mellin transformation gives

$$\tilde{F}_2^A(x_A) = \frac{1}{2\pi i} \int_{c-i\infty}^{c+i\infty} dN x_A^{-N} \tilde{F}_2^{AN} \quad (\text{A.118})$$

$$= \frac{x_A^2}{2\pi i} \frac{d^2}{dx_A^2} \int_0^1 dy \frac{\tilde{g}_2(y)}{y(1-y^2 M_A^2/Q^2)^2} \int_{c-i\infty}^{c+i\infty} dN \frac{(y/x_A)^N}{(1-y^2 M_A^2/Q^2)^N} \quad (\text{A.119})$$

$$= x_A^2 \frac{d^2}{dx_A^2} \int_0^1 dy \frac{\tilde{g}_2(y)}{y(1-y^2 M_A^2/Q^2)^2} \delta \left[ \log \left( \frac{(y/x_A)}{(1-y^2 M_A^2/Q^2)} \right) \right] , \quad (\text{A.120})$$

where we employed the contour integral

$$\int_{c-i\infty}^{c+i\infty} dN z^N = (2\pi i) \delta [\log(z)] . \quad (\text{A.121})$$

To evaluate the  $\delta$  function, we use the decomposition formula

$$\delta [g(z)] = \sum_{z_k} \frac{1}{|g'(z_k)|} \delta(z - z_k), \quad \text{such that } g(z = z_k) = 0. \quad (\text{A.122})$$

This allows us to express the  $\delta$  function in  $\tilde{F}_2^A(x_A)$  in terms of the zeros of the logarithm, i.e., when  $(y/x) = (1 - y^2 M_A^2/Q^2)$ . While the logarithm vanishes for two values of  $y$ , only one is physical. The unphysical solution  $y_2$  lies outside the domain  $y \in [0, 1]$ , meaning the contribution from  $\delta(y - y_2)$  is always zero. The physical solution is the Nachtmann scaling variable [78]:

$$\xi_A = \frac{2x_A}{1+r_A} , \quad \text{where } r_A \equiv \sqrt{1 + 4x_A^2 M_A^2/Q^2} = \frac{(1 + \xi_A^2 M_A^2/Q^2)}{(1 - \xi_A^2 M_A^2/Q^2)} , \quad (\text{A.123})$$

and corresponds to the following solution for the  $\delta$  function:

$$\delta \left[ \log \left( \frac{(y/x_A)}{(1 - y^2 M_A^2/Q^2)} \right) \right] = \left[ \frac{y(1 - y^2 M_A^2/Q^2)}{(1 + y^2 M_A^2/Q^2)} \right] \delta(\xi_A - y). \quad (\text{A.124})$$

Some identities that are useful for mapping between results in the literature include

$$\frac{x_A}{r_A \xi_A} = \frac{1}{(1 + \xi_A^2 M_A^2/Q^2)} \quad \text{and} \quad \frac{x_A}{\xi_A} = \frac{1}{(1 - \xi_A^2 M_A^2/Q^2)}. \quad (\text{A.125})$$

Replacing the  $\delta$  function with Eq. (A.124) allows us to finally write

$$\tilde{F}_2^A(x_A) = x_A^2 \frac{d^2}{dx_A^2} \int_0^1 dy \frac{\tilde{g}_2(y)}{y(1 - y^2 M_A^2/Q^2)^2} \left[ \frac{y(1 - y^2 M_A^2/Q^2)}{(1 + y^2 M_A^2/Q^2)} \right] \delta(\xi - y) \quad (\text{A.126})$$

$$\boxed{\tilde{F}_2^A(x_A) = x_A^2 \frac{d^2}{dx_A^2} \left[ \frac{(1 + r_A)^2}{4r_A} \tilde{g}_2(\xi_A) \right]}. \quad (\text{A.127})$$

Allowing the derivative to act on the quantities inside the bracket recovers Eq. (3.24b). The final expression is summarized in Eq. (A.165). We omit intermediate steps, which is a tedious but straightforward exercise in (one dimensional) differentiation when  $r_A$  and  $\xi_A$  are treated as functions of  $x_A$ . After successive applications of the product rule, i.e.,  $(u \cdot v)' = u' \cdot v + u \cdot v'$ , and the chain rule, i.e.,  $(g \circ \xi \circ x)' = (g' \circ \xi) \cdot \xi'(x)$ , the  $\mathcal{O}(\tilde{g}_2)$  term in Eqs. (3.24b) and (A.165) is generated when both derivatives act on the  $(1 + r_A)^2/4r_A$  factor. Likewise, the  $\mathcal{O}(\tilde{h}_2)$  term is generated when only one derivative acts on  $\tilde{g}_2(\xi_A)$ , and the  $\mathcal{O}(\tilde{F}_2^A)$  term is generated when both derivatives act on  $\tilde{g}_2(\xi_A)$ .

Some identities that are helpful to obtain the final result include:

$$\frac{d}{dx_A} r_A = \frac{(r_A^2 - 1)}{x_A r_A}, \quad (\text{A.128a}) \quad \frac{d}{dx_A} \xi_A = \frac{2}{r_A(1 + r_A)}, \quad (\text{A.128e})$$

$$\frac{d}{dx_A} \frac{1}{r_A^n} = \frac{(-n)(r_A^2 - 1)}{x_A r_A^{n+2}}, \quad (\text{A.128b}) \quad \frac{d}{dx_A} \tilde{g}_2(\xi_A) = \left( \frac{d\xi_A}{dx_A} \right) \frac{d}{d\xi_A} \tilde{g}_2(\xi_A) \\ = - \left( \frac{d\xi_A}{dx_A} \right) \tilde{h}_2(\xi_A), \quad (\text{A.128f})$$

$$\frac{d}{dx_A} \left( \frac{(1 + r_A)^2}{4r_A} \right) = \frac{(r_A^2 - 1)^2}{4x_A r_A^2}, \quad (\text{A.128c}) \quad \frac{d}{dx_A} \tilde{h}_2(\xi_A) = \left( \frac{d\xi_A}{dx_A} \right) \frac{d}{d\xi_A} \tilde{h}_2(\xi_A) \\ r_A^2 - 1 = \frac{4x_A^2 M_A^2}{Q^2}, \quad (\text{A.128d}) \quad = - \left( \frac{d\xi_A}{dx_A} \right) \xi_A^{-2} \tilde{F}_2^A(\xi_A) \Big|_{\text{No TMCs}}. \quad (\text{A.128g})$$

$\tilde{F}_3^A$ : To build  $\tilde{F}_3^A$ , we similarly use Eq. (A.61) and identify everything to the right of  $x_A^{-(2l-1)}$  in Eq. (A.100) as the  $2l^{\text{th}}$  moment of  $\tilde{F}_3^A(x_A, Q^2)$  with TMCs. We then write

$$\tilde{F}_3^{A(2l)} = \sum_{j=0}^{\infty} \frac{(2l + j)!}{j!(2l)!} \left( \frac{M_A^2}{Q^2} \right)^j (2l) \frac{(C_3^{(2l+2j)} A_{\tau=2}^{(2l+2j)})}{(2l + 2j)}. \quad (\text{A.129})$$

Using the integral identity of Eq. (A.110a) and the relationship in Eq. (A.108) between the moment of



$F_3^A$  and the product  $(C_3 A_{\tau=2})$  when  $(M_A^2/Q^2) \rightarrow 0$ , we have

$$\frac{C_3^{(2l+2j)} A_{\tau=2}^{(2l+2j)}}{(2l+2j)} = \frac{1}{(2l+2j)} \int_0^1 dy y^{2l+2j} \cdot y^{-1} \tilde{F}_3^A(y) \Big|_{\text{No TMCs}} \quad (\text{A.130})$$

$$= \int_0^1 dy y^{2l+2j-1} \tilde{h}_3(y), \quad \text{where} \quad (\text{A.131})$$

$$\tilde{h}_3(y) \equiv \int_y^1 dy' (y')^{-1} \tilde{F}_3^A(y') \Big|_{\text{No TMCs}}. \quad (\text{A.132})$$

Using this, the summation over  $j$  is then given by

$$\tilde{F}_3^{A(2l)} = \int_0^1 dy y^{2l-1} \tilde{h}_3(y) (2l) \sum_{j=0}^{\infty} \frac{(2l+j)!}{j!(2l)!} \left( \frac{y^2 M_A^2}{Q^2} \right)^j \quad (\text{A.133})$$

$$= \int_0^1 dy y^{-1} \tilde{h}_3(y) \frac{(2l) y^{2l}}{(1-y^2 M_A^2/Q^2)^{2l+1}}. \quad (\text{A.134})$$

After relabeling  $N = 2l$ , using the first derivative identity in Eq. (A.117), the contour integral of Eq. (A.121), the  $\delta$  function decomposition of Eq. (A.124), and the identities for  $\xi_A$ , we get as the inverse Mellin transformation of  $\tilde{F}_3^A$

$$\tilde{F}_3^A(x_A) = \frac{1}{2\pi i} \int_{c-i\infty}^{c+i\infty} dN x_A^{-N} \tilde{F}_3^{AN} \quad (\text{A.135})$$

$$= \frac{-x_A}{2\pi i} \frac{d}{dx_A} \int_0^1 dy \frac{\tilde{h}_3(y)}{y(1-y^2 M_A^2/Q^2)} \int_{c-i\infty}^{c+i\infty} dN \frac{(y/x_A)^N}{(1-y^2 M_A^2/Q^2)^N} \quad (\text{A.136})$$

$$= -x_A \frac{d}{dx_A} \int_0^1 dy \frac{\tilde{h}_3(y)}{y(1-y^2 M_A^2/Q^2)} \left[ \frac{y(1-y^2 M_A^2/Q^2)}{(1+y^2 M_A^2/Q^2)} \right] \delta(\xi_A - y), \quad (\text{A.137})$$

$$\boxed{\tilde{F}_3^A(x_A) = -x_A \frac{d}{dx_A} \left[ \frac{(1+r_A)}{2r_A} \tilde{h}_3(\xi_A) \right]}. \quad (\text{A.138})$$

Allowing the derivative to act on the quantities inside the bracket recovers Eq. (3.24c). The final expression is summarized in Eq. (A.165). In addition to Eq. (A.128), helpful identities include:

$$\frac{d}{dx_A} \left( \frac{(1+r_A)}{2r_A} \right) = -\frac{(r_A^2-1)}{2x_A r_A^3} \quad \text{and} \quad \frac{d}{dx_A} \tilde{h}_3(\xi_A) = -\left( \frac{d\xi_A}{dx_A} \right) \xi_A^{-1} \tilde{F}_3^A(\xi_A) \Big|_{\text{No TMCs}}. \quad (\text{A.139})$$

$\tilde{F}_6^A$ : Building  $\tilde{F}_6^A$  with TMCs proceeds identically to  $\tilde{F}_3^A$ . We first identify everything to the right of  $x_A^{-(2l-1)}$  in Eq. (A.106) as the  $2l^{\text{th}}$  moment of  $\tilde{F}_6^A(x_A, Q^2)$ . Explicitly,

$$\tilde{F}_3^{A(2l)} = \sum_{j=0}^{\infty} \frac{(2l+j)!}{j!(2l)!} \left( \frac{M_A^2}{Q^2} \right)^j (2l) \frac{(C_6^{(2l+2j)} A_{\tau=2}^{(2l+2j)})}{(2l+2j)}. \quad (\text{A.140})$$

The procedure for this case is similar to  $\tilde{F}_3^A$ . Using the relationship in Eq. (A.108), we obtain

$$\boxed{\tilde{F}_6^A(x_A) = -x_A \frac{d}{dx_A} \left[ \frac{(1+r_A)}{2r_A} \tilde{h}_6(y) \right]}, \quad \text{where} \quad \tilde{h}_6(y) \equiv \int_y^1 dy' y'^{-1} \tilde{F}_6^A(y') \Big|_{\text{No TMCs}}. \quad (\text{A.141})$$

The final expression is summarized in Eq. (A.165) and can be obtained by using identities analogous to Eq. (A.139). To our knowledge, the TMCs to the  $\tilde{F}_6$  structure function have not been previously reported.

$\tilde{F}_1^A$ : In principle, building  $\tilde{F}_1^A$  follows the same procedure as the previous cases. However, the nuance here is that there are contributions from  $(C_1 A_{\tau=2})$  and  $(C_2 A_{\tau=2})$  when  $j > 0$ . The solution is to decompose these into the moments of  $\tilde{F}_1^A$  and  $\tilde{F}_2^A$ , respectively. Using Eqs. (A.61) and (A.107), we identify everything to the right of  $x_A^{-(2l+1)}$  in Eq. (A.96) as the  $(2l+1)^{st}$  moment of  $\tilde{F}_1^A(x_A, Q^2)$  with TMCs. Symbolically, this is given by

$$\tilde{F}_1^{A(2l+1)} = \sum_{j=0}^{\infty} \frac{(2l+j+1)!}{j!(2l+1)!} \left(\frac{M_A^2}{Q^2}\right)^j \left[ \left( C_1^{2l+2j+1} A_{\tau=2}^{2l+2j+1} \right) + \frac{j \left( C_2^{2l+2j+1} A_{\tau=2}^{2l+2j+1} \right)}{(2l+2j+1)(2l+2j)} \right] \quad (\text{A.142})$$

$$= \int_0^1 dy \sum_{j=0}^{\infty} \frac{(2l+j+1)!}{j!(2l+1)!} \left(\frac{M_A^2}{Q^2}\right)^j \left[ y^{2l+2j} \tilde{F}_1^A(y) \Big|_{\text{No TMCs}} + j y^{2l+2j-1} \tilde{g}_2(y) \right], \quad (\text{A.143})$$

where we expressed  $(C_2 A_{\tau=2})$  as an integral over  $\tilde{g}_2(y)$  according to Eq. (A.111). Using Eq. (A.116), we evaluate the summation of each term separately, giving

$$\begin{aligned} \tilde{F}_1^{A(2l+1)} &= \int_0^1 dy \frac{\tilde{F}_1^A(y) \Big|_{\text{No TMCs}}}{y(1-y^2 M_A^2/Q^2)} \left[ \frac{y^{2l+1}}{(1-y^2 M_A^2/Q^2)^{2l+1}} \right] \\ &\quad + \left(\frac{M_A^2}{Q^2}\right) \int_0^1 dy \frac{\tilde{g}_2(y)}{(1-y^2 M_A^2/Q^2)^2} \left[ \frac{(2l+2)y^{2l+1}}{(1-y^2 M_A^2/Q^2)^{2l+1}} \right]. \end{aligned} \quad (\text{A.144})$$

We now set  $N = (2l+1)$ , take the inverse Mellin transformation with respect to  $N$ , and use the first derivative identity in Eq. (A.117) to remove the  $(N+1)$ . The result is

$$\tilde{F}_1^A(x_A) = \frac{1}{2\pi i} \int_{c-i\infty}^{c+i\infty} dN x_A^{-N} \tilde{F}_1^{AN} \quad (\text{A.145})$$

$$\begin{aligned} &= \frac{1}{2\pi i} \int_0^1 dy \frac{\tilde{F}_1^A(y) \Big|_{\text{No TMCs}}}{y(1-y^2 M_A^2/Q^2)} \int_{c-i\infty}^{c+i\infty} dN \left[ \frac{(y/x_A)^N}{(1-y^2 M_A^2/Q^2)^N} \right] \\ &- \left(\frac{M_A^2 x_A^2}{2\pi i Q^2}\right) \frac{d}{dx_A} \int_0^1 dy \frac{\tilde{g}_2(y)}{(1-y^2 M_A^2/Q^2)^2} \int_{c-i\infty}^{c+i\infty} dN \left[ \frac{(y/x_A)^N x_A^{-1}}{(1-y^2 M_A^2/Q^2)^N} \right] \end{aligned} \quad (\text{A.146})$$

$$\begin{aligned} &= \left[ \frac{\tilde{F}_1^A(y) \Big|_{\text{No TMCs}}}{(1+y^2 M_A^2/Q^2)} \right]_{y=\xi_A} \\ &- \left(\frac{M_A^2 x_A^2}{Q^2}\right) \frac{d}{dx_A} \left[ \frac{\tilde{g}_2(y) x_A^{-1} y}{(1-y^2 M_A^2/Q^2)(1+y^2 M_A^2/Q^2)} \right]_{y=\xi_A}. \end{aligned} \quad (\text{A.147})$$

To reach the last line, we used the contour integral of Eq. (A.121) and the  $\delta$  function decomposition of Eq. (A.124). Using the  $\xi_A$  identities, the final expressions is

$$\boxed{\tilde{F}_1^A(x_A) = \frac{x_A}{r_A \xi_A} \tilde{F}_1^A(\xi_A) \Big|_{\text{No TMCs}} - \left(\frac{M_A^2 x_A^2}{Q^2}\right) \frac{d}{dx_A} \left[ \frac{(1+r_A)}{2r_A} \tilde{g}_2(\xi_A) \right]} \quad (\text{A.148})$$

Applying the derivative recovers Eq. (3.24a). Helpful identities are given in Eqs. (A.128) and (A.139). Note that the factor of 1/2 in the square brackets is absent in Eq. (14) of Ref. [73]. This appears to be a typo in Ref. [73] as the final result matches Eq. (3.24a). Furthermore, after employing  $\xi_A$  identities, we find agreement with Eq. (3.1) of Ref. [67]. The final expression is summarized in Eq. (A.165).

$\tilde{F}_5^A$ : Building  $\tilde{F}_5^A$  with TMCs, which involves mixing with  $\tilde{F}_2^A$ , is similar to  $\tilde{F}_1^A$ . Subsequently, we identify

everything to the right of  $x_A^{-(2l)}$  in Eq. (A.104) as the  $(2l+1)^{th}$  moment of  $\tilde{F}_5^A(x_A, Q^2)$ :

$$\begin{aligned} \tilde{F}_5^{A(2l+1)} &= \sum_{j=0}^{\infty} \frac{(2l+j+1)!}{j! (2l+1)!} \left( \frac{M_A^2}{Q^2} \right)^j \\ &\times \left[ \frac{(2l+1) \left( C_5^{(2l+2j+1)} A_{\tau=2}^{(2l+2j+1)} \right)}{(2l+2j+1)} - \frac{j(2l+1) \left( C_2^{(2l+2j+1)} A_{\tau=2}^{(2l+2j+1)} \right)}{(2l+2j+1)(2l+2j)} \right] + \mathcal{O}(\tau > 2) \end{aligned} \quad (\text{A.149})$$

$$\begin{aligned} &= \int_0^1 dy \sum_{j=0}^{\infty} \frac{(2l+j+1)!}{j! (2l+1)!} \left( \frac{M_A^2}{Q^2} \right)^j \left[ \frac{(2l+1)}{2} y^{2l+2j} \tilde{h}_5(y) - j(2l+1) y^{2l+2j-1} \tilde{g}_2(y) \right] \\ &+ \mathcal{O}(\tau > 2), \end{aligned} \quad (\text{A.150})$$

where we used Eqs. (A.108) and (A.111) to decompose both  $(C_i A_{\tau=2})$  products as integrals over  $\tilde{F}_i^A(y)|_{\text{No TMCs}}$ , and have defined via the identity Eq. (A.110a) the generating integral

$$\tilde{h}_5(y) \equiv \int_y^1 dy' (y')^{-1} 2\tilde{F}_5^A(y') \Big|_{\text{No TMCs}}. \quad (\text{A.151})$$

Note the factor of 2 in the definition of  $\tilde{h}_5$ , which follows the convention of Eq. (3.15) in Ref. [67].

Using Eq. (A.116), we evaluate the summation of each term separately. This gives

$$\begin{aligned} \tilde{F}_5^{A(2l+1)} &= \int_0^1 dy \frac{\tilde{h}_5(y)}{2y(1-y^2 M_A^2/Q^2)} \left[ \frac{(2l+1) y^{2l+1}}{(1-y^2 M_A^2/Q^2)^{(2l+1)}} \right] \\ &- \left( \frac{M_A^2}{Q^2} \right) \int_0^1 dy \frac{\tilde{g}_2(y)}{(1-y^2 M_A^2/Q^2)^2} \left[ \frac{(2l+2)(2l+1) y^{2l+1}}{(1-y^2 M_A^2/Q^2)^{(2l+1)}} \right] + \mathcal{O}(\tau > 2). \end{aligned} \quad (\text{A.152})$$

Setting  $N = (2l+1)$ , taking the inverse Mellin transform with respect to  $x_A$ , and using the derivative identities of Eq. (A.117) allows us to obtain  $\tilde{F}_5^A(x_A)$ . It is given by

$$\begin{aligned} \tilde{F}_5^A(x_A) &= \frac{1}{2\pi i} \int_{c-i\infty}^{c+i\infty} dN x_A^{-N} \tilde{F}_5^{A(N)} \\ &= \left( \frac{-x_A}{4\pi i} \right) \frac{d}{dx_A} \int_0^1 dy \frac{\tilde{h}_5(y)}{y(1-y^2 M_A^2/Q^2)} \int_{c-i\infty}^{c+i\infty} dN \left[ \frac{(y/x_A)^N}{(1-y^2 M_A^2/Q^2)^N} \right] \\ &- \left( \frac{x_A^2 M_A^2}{2\pi i Q^2} \right) \frac{d^2}{dx_A^2} \int_0^1 dy \frac{\tilde{g}_2(y)}{(1-y^2 M_A^2/Q^2)^2} \int_{c-i\infty}^{c+i\infty} dN \left[ \frac{(y/x_A)^N}{(1-y^2 M_A^2/Q^2)^N} \right] \\ &+ \mathcal{O}(\tau > 2). \end{aligned} \quad (\text{A.154})$$

Applying the contour integral of Eq. (A.121) and the identity of Eq. (A.124), we get

$$\boxed{\tilde{F}_5^A(x_A) = \left( \frac{-x_A}{2} \right) \frac{d}{dx_A} \left[ \frac{(1+r_A)}{2r_A} \tilde{h}_5(\xi_A) \right] - \left( \frac{x_A^2 M_A^2}{Q^2} \right) \frac{d^2}{dx_A^2} \left[ \frac{(1+r_A)^2}{4r_A} \xi_A \tilde{g}_2(\xi_A) \right] + \mathcal{O}(\tau > 2)}. \quad (\text{A.155})$$

After accounting for the difference between  $\tilde{W}_5^A$  and  $\tilde{F}_5^A$ , this agrees with Eq. (3.5) of Ref. [67]. The final expression is summarized in Eq. (A.165). In addition to Eqs. (A.128) and (A.139), a helpful identity is

$$\frac{d}{dx_A} \tilde{h}_5(\xi_A) = -2 \left( \frac{d\xi_A}{dx_A} \right) \xi_A^{-1} \tilde{F}_5^A(\xi_A) \Big|_{\text{No TMCs}}. \quad (\text{A.156})$$

$\tilde{F}_4^A$ : Building  $\tilde{F}_4^A$  follows the same procedure as above with the complication that the result is sourced by three contributions for  $j > 0$ . Using Eqs. (A.61) and (A.107), we identify everything to the right of of  $x_A^{-(2l+1)}$  in Eq. (A.102) as the  $(2l+1)^{st}$  moment of  $\tilde{F}_4^A(x_A, Q^2)$ . This is given by

$$\begin{aligned} \tilde{F}_4^{A(2l+1)} &= \sum_{j=0}^{\infty} \frac{(2l+j+1)!}{j!(2l+1)!} \left( \frac{M_A^2}{Q^2} \right)^j \\ &\times \left[ \left( C_4^{(2l+2j+1)} A_{\tau=2}^{(2l+2j+1)} \right) + \frac{j(j-1) \left( C_2^{(2l+2j+1)} A_{\tau=2}^{(2l+2j+1)} \right)}{(2l+2j+1)(2l+2j)} - \frac{2j \left( C_5^{(2l+2j+1)} A_{\tau=2}^{(2l+2j+1)} \right)}{(2l+2j+1)} \right] \\ &+ \mathcal{O}(\tau > 2), \end{aligned} \quad (\text{A.157})$$

$$\begin{aligned} &= \int_0^1 dy \sum_{j=0}^{\infty} \frac{(2l+j+1)!}{j!(2l+1)!} \left( \frac{M_A^2}{Q^2} \right)^j \\ &\times \left[ y^{2l+2j} \tilde{F}_4^A(y)|_{\text{No TMC}} + j(j-1)y^{2l+2j-1} \tilde{g}_2(y) - jy^{2l+2j} \tilde{h}_5(y) \right] + \mathcal{O}(\tau > 2). \end{aligned} \quad (\text{A.158})$$

Here, we again used the Eqs. (A.108), (A.111), and (A.151) to rewrite  $(C_i A_{\tau=2})$ .

Distributing the summations and using the identities listed in Eq. (A.116), we obtain

$$\begin{aligned} \tilde{F}_4^{A(2l+1)} &= \int_0^1 dy \left[ y^{2l} \tilde{F}_4^A(y)|_{\text{No TMC}} \sum_{j=0}^{\infty} \frac{(2l+j+1)!}{j!(2l+1)!} \left( \frac{M_A^2 y^2}{Q^2} \right)^j \right. \\ &\quad + y^{2l-1} \tilde{g}_2(y) \sum_{j=0}^{\infty} j(j-1) \frac{(2l+j+1)!}{j!(2l+1)!} \left( \frac{M_A^2 y^2}{Q^2} \right)^j \\ &\quad \left. - y^{2l} \tilde{h}_5(y) \sum_{j=0}^{\infty} j \frac{(2l+j+1)!}{j!(2l+1)!} \left( \frac{M_A^2 y^2}{Q^2} \right)^j \right] + \mathcal{O}(\tau > 2) \end{aligned} \quad (\text{A.159})$$

$$\begin{aligned} &= \int_0^1 dy \left[ \frac{\tilde{F}_4^A(y)|_{\text{No TMC}}}{y(1-y^2 M_A^2/Q^2)} \left[ \frac{y^{2l+1}}{(1-y^2 M_A^2/Q^2)^{2l+1}} \right] \right. \\ &\quad + \left( \frac{M_A^2}{Q^2} \right)^2 \frac{y^2 \tilde{g}_2(y)}{(1-y^2 M_A^2/Q^2)^3} \left[ \frac{(2l+2)(2l+3)y^{2l+1}}{(1-y^2 M_A^2/Q^2)^{2l+1}} \right] \\ &\quad \left. - \left( \frac{M_A^2}{Q^2} \right) \frac{y \tilde{h}_5(y)}{(1-y^2 M_A^2/Q^2)} \left[ \frac{(2l+2)y^{2l+1}}{(1-y^2 M_A^2/Q^2)^{2l+1}} \right] \right] + \mathcal{O}(\tau > 2). \end{aligned} \quad (\text{A.160})$$

Relabeling  $N = (2l+1)$  and using the derivative identities in Eq. (A.117) gives

$$\tilde{F}_4^A(x_A) = \frac{1}{2\pi i} \int_{c-i\infty}^{c+i\infty} dN x_A^{-N} \tilde{F}_4^{AN} \quad (\text{A.161})$$

$$\begin{aligned} &= \frac{1}{2\pi i} \int_0^1 dy \frac{\tilde{F}_4^A(y)|_{\text{No TMC}}}{y(1-y^2 M_A^2/Q^2)} \int_{c-i\infty}^{c+i\infty} dN \left[ \frac{(y/x_A)^N}{(1-y^2 M_A^2/Q^2)^N} \right] \\ &\quad + \left( \frac{M_A^2}{Q^2} \right)^2 \left( \frac{x_A^3}{2\pi i} \right) \frac{d^2}{dx_A^2} \int_0^1 dy \frac{y^2 x_A^{-1} \tilde{g}_2(y)}{(1-y^2 M_A^2/Q^2)^3} \int_{c-i\infty}^{c+i\infty} dN \left[ \frac{(y/x_A)^N}{(1-y^2 M_A^2/Q^2)^N} \right] \\ &\quad + (-1)^2 \left( \frac{M_A^2}{Q^2} \right) \left( \frac{x_A^2}{2\pi i} \right) \frac{d}{dx_A} \int_0^1 dy \frac{y x_A^{-1} \tilde{h}_5(y)}{(1-y^2 M_A^2/Q^2)^2} \int_{c-i\infty}^{c+i\infty} dN \left[ \frac{(y/x_A)^N}{(1-y^2 M_A^2/Q^2)^N} \right] \\ &\quad + \mathcal{O}(\tau > 2). \end{aligned} \quad (\text{A.162})$$

Finally, using contour integral of Eq. (A.121) and the  $\xi_A$  identities, we get

$$\boxed{\tilde{F}_4^A(x_A) = \frac{(1+r_A)}{2r_A} \tilde{F}_4^A(\xi_A) \Big|_{\text{No TMC}} + \left(\frac{M_A^2}{Q^2}\right)^2 x_A^3 \frac{d^2}{dx_A^2} \left[ \left(\frac{x_A^2}{r_A}\right) \tilde{g}_2(\xi_A) \right] + \left(\frac{M_A^2}{Q^2}\right) x_A^2 \frac{d}{dx_A} \left[ \left(\frac{x_A}{r_A}\right) \tilde{h}_5(\xi_A) \right] + \mathcal{O}(\tau > 2)}. \quad (\text{A.163})$$

After accounting for differences between  $\tilde{W}_4^A$  and  $\tilde{F}_4^A$ , this agrees with Eq. (3.4) of Ref. [67]. The final expression is summarized in Eq. (A.165). In addition to Eqs. (A.128), (A.139), and (A.156), a helpful identity is

$$\frac{d}{dx_A} \frac{x_A^n}{r_A} = \frac{(r_A^2 + n - 1)x_A^{n-1}}{r_A}. \quad (\text{A.164})$$

## Summary

We now give the full expressions for all six structure functions with TMCs. These are obtained by successive applications of the product and chain rules to the several expressions above. The final results are:

$$\tilde{F}_1^A(x_A) = \frac{x_A}{\xi_A r_A} \tilde{F}_1^A(\xi_A) \Big|_{\text{No TMCs}} + \left(\frac{M_A^2 x_A^2}{Q^2 r_A^2}\right) \tilde{h}_2(\xi_A) + \left(\frac{2M_A^4 x_A^3}{Q^4 r_A^3}\right) \tilde{g}_2(\xi_A) + \mathcal{O}(\tau > 2), \quad (\text{A.165a})$$

$$\tilde{F}_2^A(x_A) = \frac{x_A^2}{\xi_A^2 r_A^3} \tilde{F}_2^A(\xi_A) \Big|_{\text{No TMCs}} + \left(\frac{6M_A^2 x_A^3}{Q^2 r_A^4}\right) \tilde{h}_2(\xi_A) + \left(\frac{12M_A^4 x_A^4}{Q^4 r_A^5}\right) \tilde{g}_2(\xi_A) + \mathcal{O}(\tau > 2), \quad (\text{A.165b})$$

$$\tilde{F}_3^A(x_A) = \frac{x_A}{\xi_A r_A^2} \tilde{F}_3^A(\xi_A) \Big|_{\text{No TMCs}} + \left(\frac{2M_A^2 x_A^2}{Q^2 r_A^3}\right) \tilde{h}_3(\xi_A) + \mathcal{O}(\tau > 2), \quad (\text{A.165c})$$

$$\begin{aligned} \tilde{F}_4^A(x_A) &= \frac{x_A}{\xi_A r_A} \tilde{F}_4^A(\xi_A) \Big|_{\text{No TMCs}} - \left(\frac{2M_A^2 x_A^2}{Q^2 r_A^2}\right) \tilde{F}_5^A(\xi_A) \Big|_{\text{No TMCs}} + \left(\frac{M_A^4 x_A^3}{Q^4 r_A^3}\right) \tilde{F}_2^A(\xi_A) \Big|_{\text{No TMCs}} \\ &+ \left(\frac{M_A^2 x_A^2}{Q^2 r_A^3}\right) \tilde{h}_5^A(\xi_A) - \left(\frac{2M_A^4 x_A^4}{Q^4 r_A^4}\right) (2 - \xi_A^2 M_A^2 / Q^2) \tilde{h}_2^A(\xi_A) \\ &+ \left(\frac{2M_A^4 x_A^3}{Q^4 r_A^5}\right) (1 - 2x_A^2 M_A^2 / Q^2) \tilde{g}_2^A(\xi_A) + \mathcal{O}(\tau > 2), \end{aligned} \quad (\text{A.165d})$$

$$\begin{aligned} \tilde{F}_5^A(x_A) &= \frac{x_A}{\xi_A r_A^2} \tilde{F}_5^A(\xi_A) \Big|_{\text{No TMCs}} - \left(\frac{M_A^2 x_A^2}{Q^2 r_A^3 \xi_A}\right) \tilde{F}_2^A(\xi_A) \Big|_{\text{No TMCs}} \\ &+ \left(\frac{M_A^2 x_A^2}{Q^2 r_A^3}\right) \tilde{h}_5^A(\xi_A) - \left(\frac{2M_A^2 x_A^2}{Q^2 r_A^4}\right) (1 - x_A \xi_A M_A^2 / Q^2) \tilde{h}_2^A(\xi_A) \\ &+ \left(\frac{6M_A^4 x_A^3}{Q^4 r_A^5}\right) \tilde{g}_2^A(\xi_A) + \mathcal{O}(\tau > 2), \end{aligned} \quad (\text{A.165e})$$

$$\tilde{F}_6^A(x_A) = \frac{x_A}{\xi_A r_A^2} \tilde{F}_6^A(\xi_A) \Big|_{\text{No TMCs}} + \left(\frac{2M_A^2 x_A^2}{Q^2 r_A^3}\right) \tilde{h}_6(\xi_A) + \mathcal{O}(\tau > 2). \quad (\text{A.165f})$$

Importantly, the above expressions for *nuclear* structure functions  $\tilde{F}_1, \dots, \tilde{F}_5$  agree with those for *nucleon* structure functions  $F_1, \dots, F_5$  in Eq. (3.17) of Ref. [73]. This is a main conclusion of our work: TMCs for unpolarized protons and neutrons are the same for unpolarized nuclei.

Using Table 6.1, the TMCs to the  $\tilde{F}_+^A$ ,  $\tilde{F}_-^A$ , and  $\tilde{F}_0^A$  structure functions in the helicity basis are explicitly

$$\tilde{F}_\pm^A = \tilde{F}_1^A \mp r_A \tilde{F}_3^A \quad (\text{A.166})$$

$$\begin{aligned} &= \frac{x_A}{\xi_A r_A} [\tilde{F}_1^A(\xi_A) \mp \tilde{F}_3^A(\xi_A)]_{\text{No TMCs}} + \left( \frac{M_A^2 x_A^2}{Q^2 r_A^2} \right) [\tilde{h}_2(\xi_A) \mp 2\tilde{h}_3(\xi_A)] \\ &\quad + \left( \frac{2M_A^4 x_A^3}{Q^4 r_A^3} \right) \tilde{g}_2(\xi_A) + \mathcal{O}(\tau > 2), \end{aligned} \quad (\text{A.167})$$

$$\tilde{F}_0^A = \left( \frac{r_A^2}{2x_A} \right) \tilde{F}_2^A - \tilde{F}_1^A \quad (\text{A.168})$$

$$\begin{aligned} &= \frac{x_A}{2\xi_A^2 r_A} [\tilde{F}_2^A(\xi_A) - 2\xi \tilde{F}_1^A(\xi_A)]_{\text{No TMCs}} + \left( \frac{2M_A^2 x_A^2}{Q^2 r_A^2} \right) \tilde{h}_2(\xi_A) + \left( \frac{4M_A^4 x_A^3}{Q^4 r_A^3} \right) \tilde{g}_2(\xi_A) \\ &\quad + \mathcal{O}(\tau > 2). \end{aligned} \quad (\text{A.169})$$

As noted in Eq. (6.13), there is a relative factor of  $2x_A$  between the helicity  $\tilde{F}_0^A$  and the longitudinal  $\tilde{F}_L^A$  structure functions such that  $\tilde{F}_L^A = 2x_A \tilde{F}_0^A$ .

## B. Derivation of the Full/Leading TMC Parameterization

In this appendix, we derive our parameterizations of Eq. (7.9) by approximating the general form of the structure functions in the TMC region. First, we assume the structure functions  $F_a^{(0)}(x)$ ,  $a = 1, 2, 3$ , vanish at  $x = 1$ . This follows from our working assumption that the nPDFs vanish at  $x \geq 1$  c.f., Sec. 5.5.

Next, we use a finite difference formula to approximate derivatives of  $F_a^{j,(0)}(x = \xi)$  as

$$F_a'^{(0)}(u = \xi) \approx -\frac{\gamma_a F_a^{(0)}(\xi)}{1 - \xi} \quad (\text{B.1})$$

$$F_a^{j,(0)}(u = \xi) \approx \frac{0 - F_a^{j-1,(0)}(\xi)}{(1 - \xi)} = (-1)^j \frac{\gamma_a F_a^{(0)}(\xi)}{(1 - \xi)^j}. \quad (\text{B.2})$$

Here,  $\gamma_a$  is a universal correction factor for the first derivative which we assume to be independent of  $x$  and the underlying PDFs, and to have a mild  $Q$  dependence. We can then expand  $F_a^{(0)}(u)$  about  $u = \xi$  as

$$F_a^{(0)}(u) = \sum_{j=0}^{\infty} \frac{1}{j!} F_a^{j,(0)}(\xi) (u - \xi)^j \quad (\text{B.3})$$

$$\approx F_a^{(0)}(\xi) \left( 1 + \sum_{j=1}^{\infty} \frac{1}{j!} (-1)^j \frac{\gamma_a}{(1 - \xi)^j} (u - \xi)^j \right) \quad (\text{B.4})$$

$$\equiv F_a^{(0)}(\xi) K_a(u, \xi, \gamma_a) \quad (\text{B.5})$$

Here,

$$K_a(u, \xi, \gamma_a) = 1 + \sum_{j=1}^{\infty} \frac{1}{j!} (-1)^j \frac{\gamma_a}{(1 - \xi)^j} (u - \xi)^j. \quad (\text{B.6})$$

As  $K_a(u, \xi, \gamma)$  is independent of the PDFs, this implies that the ratios

$$\frac{h_a(\xi)}{F_a^{(0)}(\xi)} = \int_{\xi}^1 L_a(u) K_a(\xi, x, \gamma) du \quad (\text{B.7})$$

$$\frac{g_2(\xi)}{F_2^{(0)}(\xi)} = \int_{\xi}^1 \frac{u - \xi}{u^2} K_a(\xi, x, \gamma) du \quad (\text{B.8})$$



are also independent of the underlying PDFs. Here we have defined  $L_1(u) = 2/u$ ,  $L_2(u) = 1/u^2$ , and  $L_3(u) = 1/u$ .

Evaluating the explicit expression for  $K_a(u, \xi, \gamma_a)$  in the above relations, we obtain (7.9a), (7.9b), and (7.9d). To calculate  $h_2(\xi)/F_1^{(0)}(\xi)$  and  $g_2(\xi)/F_1^{(0)}(\xi)$ , which are needed to calculate the ratio  $F_1^{TMC}(x)/F_1^{Leading-TMC}$ , one can assume an approximate Callan-Gross relation. Deviations from the Callan-Gross relation can be absorbed into the fitted  $\gamma_1(Q)$ . We note that in practice, we calculate the massless structure function using Eq. (6.14), namely :

$$F_1^{(0)}(\xi) = F_1^{TMC-ACOT}(x), \quad (\text{B.9a})$$

$$F_2^{(0)}(\xi) = \frac{\xi r^2}{x} F_2^{TMC-ACOT}(x), \quad (\text{B.9b})$$

$$F_3^{(0)}(\xi) = r F_3^{TMC-ACOT}(x), \quad (\text{B.9c})$$

Assuming Callan-Gross relation at the level of the TMC-ACOT structure functions, implies

$$F_2^{(0)}(\xi) = 2\xi r^2 F_1^{(0)}(\xi) \quad (\text{B.10})$$

Using Eq. (B.10), one can easily obtain  $h_2(\xi)/F_1^{(0)}(\xi)$  and  $g_2(\xi)/F_1^{(0)}(\xi)$  from  $h_2(\xi)/F_2^{(0)}(\xi)$  and  $g_2(\xi)/F_2^{(0)}(\xi)$ , as shown in Eqs. (7.9c) and (7.9e).

If we perform a single parameter fit and take  $\gamma_a$  as a constant, we find reasonable agreement with the exact TMC result at the level of  $\lesssim 0.75\%$  for  $Q = 1.3$  GeV and  $Q = 2$  GeV. We can do even better if we perform a 2-parameter fit and replace  $\gamma_a$  with:

$$\gamma_a \rightarrow \gamma_a(Q) = \lambda_a \ln(Q)^{\delta_a} \quad (\text{B.11})$$

Thus, we give a mild  $Q$  dependence to the parameter  $\gamma_a$ . This 2-parameter fit is superior to the one parameter fit as the agreement is  $\lesssim 0.6\%$  for  $Q = 1.3$  GeV, and  $\lesssim 0.2\%$  for  $Q = 2$  GeV which is a typical kinematic cut for the global PDF fits.

- [1] R. E. Taylor, “Deep inelastic scattering: The Early years,” *Rev. Mod. Phys.* **63** (1991) 573–595.
- [2] H. W. Kendall, “Deep inelastic scattering: Experiments on the proton and the observation of scaling,” *Rev. Mod. Phys.* **63** (1991) 597–614.
- [3] J. I. Friedman, “Deep inelastic scattering: Comparisons with the quark model,” *Rev. Mod. Phys.* **63** (1991) 615–629.
- [4] R. Devenish and A. Cooper-Sarkar, *Deep inelastic scattering*. Oxford University Press, 2004.
- [5] T.-J. Hou *et al.*, “New CTEQ global analysis of quantum chromodynamics with high-precision data from the LHC,” *Phys. Rev. D* **103** no. 1, (2021) 014013, [arXiv:1912.10053 \[hep-ph\]](#).
- [6] A. Accardi, L. T. Brady, W. Melnitchouk, J. F. Owens, and N. Sato, “Constraints on large- $x$  parton distributions from new weak boson production and deep-inelastic scattering data,” *Phys. Rev. D* **93** no. 11, (2016) 114017, [arXiv:1602.03154 \[hep-ph\]](#).
- [7] S. Bailey, T. Cridge, L. A. Harland-Lang, A. D. Martin, and R. S. Thorne, “Parton distributions from LHC, HERA, Tevatron and fixed target data: MSHT20 PDFs,” *Eur. Phys. J. C* **81** no. 4, (2021) 341, [arXiv:2012.04684 \[hep-ph\]](#).
- [8] **H1, ZEUS** Collaboration, H. Abramowicz *et al.*, “Combination of measurements of inclusive deep inelastic  $e^\pm p$  scattering cross sections and QCD analysis of HERA data,” *Eur. Phys. J. C* **75** no. 12, (2015) 580, [arXiv:1506.06042 \[hep-ex\]](#).
- [9] **NNPDF** Collaboration, R. D. Ball *et al.*, “Parton distributions from high-precision collider data,” *Eur. Phys. J. C* **77** no. 10, (2017) 663, [arXiv:1706.00428 \[hep-ph\]](#).
- [10] S. Alekhin, J. Blümlein, S. Moch, and R. Placakyte, “Parton distribution functions,  $\alpha_s$ , and heavy-quark masses for LHC Run II,” *Phys. Rev. D* **96** no. 1, (2017) 014011, [arXiv:1701.05838 \[hep-ph\]](#).
- [11] M. Hirai, S. Kumano, and T. H. Nagai, “Determination of nuclear parton distribution functions and their uncertainties in next-to-leading order,” *Phys. Rev. C* **76** (2007) 065207, [arXiv:0709.3038 \[hep-ph\]](#).
- [12] D. de Florian, R. Sassot, P. Zurita, and M. Stratmann, “Global Analysis of Nuclear Parton Distributions,” *Phys. Rev. D* **85** (2012) 074028, [arXiv:1112.6324 \[hep-ph\]](#).
- [13] K. J. Eskola, H. Paukkunen, and C. A. Salgado, “EPS09: A New Generation of NLO and LO Nuclear Parton Distribution Functions,” *JHEP* **04** (2009) 065, [arXiv:0902.4154 \[hep-ph\]](#).
- [14] K. J. Eskola, P. Paakkinen, H. Paukkunen, and C. A. Salgado, “EPPS16: Nuclear parton distributions with LHC data,” *Eur. Phys. J. C* **77** no. 3, (2017) 163, [arXiv:1612.05741 \[hep-ph\]](#).
- [15] K. J. Eskola, P. Paakkinen, H. Paukkunen, and C. A. Salgado, “EPPS21: a global QCD analysis of nuclear PDFs,” *Eur. Phys. J. C* **82** no. 5, (2022) 413, [arXiv:2112.12462 \[hep-ph\]](#).
- [16] I. Schienbein, J. Y. Yu, K. Kovarik, C. Keppel, J. G. Morfin, F. Olness, and J. F. Owens, “PDF Nuclear Corrections for Charged and Neutral Current Processes,” *Phys. Rev. D* **80** (2009) 094004, [arXiv:0907.2357 \[hep-ph\]](#).
- [17] K. Kovarik *et al.*, “nCTEQ15 - Global analysis of nuclear parton distributions with uncertainties in the CTEQ framework,” *Phys. Rev. D* **93** no. 8, (2016) 085037, [arXiv:1509.00792 \[hep-ph\]](#).
- [18] A. Kusina, F. Lyonnet, D. B. Clark, E. Godat, T. Jezo, K. Kovarik, F. I. Olness, I. Schienbein, and J. Y. Yu, “Vector boson production in pPb and PbPb collisions at the LHC and its impact on nCTEQ15 PDFs,” *Eur. Phys. J. C* **77** no. 7, (2017) 488, [arXiv:1610.02925 \[nucl-th\]](#).

- [19] E. P. Segarra *et al.*, “Extending nuclear PDF analyses into the high- $x$ , low- $Q^2$  region,” *Phys. Rev. D* **103** no. 11, (2021) 114015, [arXiv:2012.11566 \[hep-ph\]](#).
- [20] A. Kusina *et al.*, “Impact of LHC vector boson production in heavy ion collisions on strange PDFs,” *Eur. Phys. J. C* **80** no. 10, (2020) 968, [arXiv:2007.09100 \[hep-ph\]](#).
- [21] P. Duwentäster, L. A. Husová, T. Ježo, M. Klasen, K. Kovařík, A. Kusina, K. F. Muzakka, F. I. Olness, I. Schienbein, and J. Y. Yu, “Impact of inclusive hadron production data on nuclear gluon PDFs,” *Phys. Rev. D* **104** (2021) 094005, [arXiv:2105.09873 \[hep-ph\]](#).
- [22] P. Duwentäster, T. Ježo, M. Klasen, K. Kovařík, A. Kusina, K. F. Muzakka, F. I. Olness, R. Ruiz, I. Schienbein, and J. Y. Yu, “Impact of heavy quark and quarkonium data on nuclear gluon PDFs,” *Phys. Rev. D* **105** no. 11, (2022) 114043, [arXiv:2204.09982 \[hep-ph\]](#).
- [23] K. F. Muzakka *et al.*, “Compatibility of neutrino DIS data and its impact on nuclear parton distribution functions,” *Phys. Rev. D* **106** no. 7, (2022) 074004, [arXiv:2204.13157 \[hep-ph\]](#).
- [24] **NNPDF** Collaboration, R. Abdul Khalek, J. J. Ethier, and J. Rojo, “Nuclear parton distributions from lepton-nucleus scattering and the impact of an electron-ion collider,” *Eur. Phys. J. C* **79** no. 6, (2019) 471, [arXiv:1904.00018 \[hep-ph\]](#).
- [25] R. Abdul Khalek, J. J. Ethier, J. Rojo, and G. van Weelden, “nNNPDF2.0: quark flavor separation in nuclei from LHC data,” *JHEP* **09** (2020) 183, [arXiv:2006.14629 \[hep-ph\]](#).
- [26] R. Abdul Khalek, R. Gauld, T. Giani, E. R. Nocera, T. R. Rabemananjara, and J. Rojo, “nNNPDF3.0: evidence for a modified partonic structure in heavy nuclei,” *Eur. Phys. J. C* **82** no. 6, (2022) 507, [arXiv:2201.12363 \[hep-ph\]](#).
- [27] M. Walt, I. Helenius, and W. Vogelsang, “Open-source QCD analysis of nuclear parton distribution functions at NLO and NNLO,” *Phys. Rev. D* **100** no. 9, (2019) 096015, [arXiv:1908.03355 \[hep-ph\]](#).
- [28] H. Khanpour, M. Soleymaninia, S. Atashbar Tehrani, H. Spiesberger, and V. Guzey, “Nuclear parton distribution functions with uncertainties in a general mass variable flavor number scheme,” *Phys. Rev. D* **104** no. 3, (2021) 034010, [arXiv:2010.00555 \[hep-ph\]](#).
- [29] A. Accardi *et al.*, “Electron Ion Collider: The Next QCD Frontier: Understanding the glue that binds us all,” *Eur. Phys. J. A* **52** no. 9, (2016) 268, [arXiv:1212.1701 \[nucl-ex\]](#).
- [30] R. Abdul Khalek *et al.*, “Science Requirements and Detector Concepts for the Electron-Ion Collider: EIC Yellow Report,” *Nucl. Phys. A* **1026** (2022) 122447, [arXiv:2103.05419 \[physics.ins-det\]](#).
- [31] J. L. Feng *et al.*, “The Forward Physics Facility at the High-Luminosity LHC,” *J. Phys. G* **50** no. 3, (2023) 030501, [arXiv:2203.05090 \[hep-ex\]](#).
- [32] J. Arrington *et al.*, “Physics with CEBAF at 12 GeV and future opportunities,” *Prog. Part. Nucl. Phys.* **127** (2022) 103985, [arXiv:2112.00060 \[nucl-ex\]](#).
- [33] **DUNE** Collaboration, R. Acciarri *et al.*, “Long-Baseline Neutrino Facility (LBNF) and Deep Underground Neutrino Experiment (DUNE): Conceptual Design Report, Volume 2: The Physics Program for DUNE at LBNF,” [arXiv:1512.06148 \[physics.ins-det\]](#).
- [34] P. A. Machado, O. Palamara, and D. W. Schmitz, “The Short-Baseline Neutrino Program at Fermilab,” *Ann. Rev. Nucl. Part. Sci.* **69** (2019) 363–387, [arXiv:1903.04608 \[hep-ex\]](#).
- [35] L. A. Ruso *et al.*, “Theoretical tools for neutrino scattering: interplay between lattice QCD, EFTs, nuclear physics, phenomenology, and neutrino event generators,” [arXiv:2203.09030 \[hep-ph\]](#).

- [36] E. D. Bloom and F. J. Gilman, “Scaling, Duality, and the Behavior of Resonances in Inelastic electron-Proton Scattering,” *Phys. Rev. Lett.* **25** (1970) 1140.
- [37] W. Melnitchouk, R. Ent, and C. Keppel, “Quark-hadron duality in electron scattering,” *Phys. Rept.* **406** (2005) 127–301, [arXiv:hep-ph/0501217](#).
- [38] C. Andreopoulos *et al.*, “The GENIE Neutrino Monte Carlo Generator,” *Nucl. Instrum. Meth. A* **614** (2010) 87–104, [arXiv:0905.2517 \[hep-ph\]](#).
- [39] J. Alwall, R. Frederix, S. Frixione, V. Hirschi, F. Maltoni, O. Mattelaer, H. S. Shao, T. Stelzer, P. Torrielli, and M. Zaro, “The automated computation of tree-level and next-to-leading order differential cross sections, and their matching to parton shower simulations,” *JHEP* **07** (2014) 079, [arXiv:1405.0301 \[hep-ph\]](#).
- [40] **Sherpa** Collaboration, E. Bothmann *et al.*, “Event Generation with Sherpa 2.2,” *SciPost Phys.* **7** no. 3, (2019) 034, [arXiv:1905.09127 \[hep-ph\]](#).
- [41] **KM3NeT** Collaboration, A. Garcia and A. Heijboer, “High-energy neutrino event simulation at NLO in Genie for KM3NeT and other observatories,” *PoS ICRC2019* (2020) 895, [arXiv:1908.10077 \[hep-ex\]](#).
- [42] A. Garcia, R. Gauld, A. Heijboer, and J. Rojo, “Complete predictions for high-energy neutrino propagation in matter,” *JCAP* **09** (2020) 025, [arXiv:2004.04756 \[hep-ph\]](#).
- [43] C. Bierlich *et al.*, “A comprehensive guide to the physics and usage of PYTHIA 8.3,” [arXiv:2203.11601 \[hep-ph\]](#).
- [44] J. Isaacson, W. I. Jay, A. Lovato, P. A. N. Machado, and N. Rocco, “Introducing a novel event generator for electron-nucleus and neutrino-nucleus scattering,” *Phys. Rev. D* **107** no. 3, (2023) 033007, [arXiv:2205.06378 \[hep-ph\]](#).
- [45] I. Helenius, M. Walt, and W. Vogelsang, “NNLO nuclear parton distribution functions with electroweak-boson production data from the LHC,” *Phys. Rev. D* **105** no. 9, (2022) 094031, [arXiv:2112.11904 \[hep-ph\]](#).
- [46] R. Abdul Khalek, R. Gauld, T. Giani, E. R. Nocera, T. R. Rabemananjara, and J. Rojo, “nNNPDF3.0: evidence for a modified partonic structure in heavy nuclei,” *Eur. Phys. J. C* **82** no. 6, (2022) 507, [arXiv:2201.12363 \[hep-ph\]](#).
- [47] K. G. Wilson, “Nonlagrangian models of current algebra,” *Phys. Rev.* **179** (1969) 1499–1512.
- [48] R. A. Brandt and G. Preparata, “Operator product expansions near the light cone,” *Nucl. Phys. B* **27** (1971) 541–567.
- [49] N. H. Christ, B. Hasslacher, and A. H. Mueller, “Light cone behavior of perturbation theory,” *Phys. Rev. D* **6** (1972) 3543.
- [50] G. T. Bodwin, “Factorization of the Drell-Yan Cross-Section in Perturbation Theory,” *Phys. Rev. D* **31** (1985) 2616. [Erratum: *Phys.Rev.D* 34, 3932 (1986)].
- [51] J. C. Collins, D. E. Soper, and G. F. Sterman, “Factorization for Short Distance Hadron - Hadron Scattering,” *Nucl. Phys. B* **261** (1985) 104–142.
- [52] J. C. Collins, D. E. Soper, and G. F. Sterman, “Soft Gluons and Factorization,” *Nucl. Phys. B* **308** (1988) 833–856.
- [53] J. C. Collins and D. E. Soper, “The Theorems of Perturbative QCD,” *Ann. Rev. Nucl. Part. Sci.* **37** (1987) 383–409.

- [54] J. C. Collins, D. E. Soper, and G. F. Sterman, “Factorization of Hard Processes in QCD,” *Adv. Ser. Direct. High Energy Phys.* **5** (1989) 1–91, [arXiv:hep-ph/0409313](#).
- [55] J. C. Collins, “Hard scattering factorization with heavy quarks: A General treatment,” *Phys. Rev. D* **58** (1998) 094002, [arXiv:hep-ph/9806259](#).
- [56] J. Collins, *Foundations of perturbative QCD*, vol. 32. Cambridge University Press, 11, 2013.
- [57] E. L. Berger and F. Coester, “Nuclear Effects in Deep Inelastic Lepton Scattering,” *Ann. Rev. Nucl. Part. Sci.* **37** (1987) 463–491.
- [58] H. Georgi and H. D. Politzer, “Freedom at Moderate Energies: Masses in Color Dynamics,” *Phys. Rev. D* **14** (1976) 1829.
- [59] H. Georgi and H. D. Politzer, “Precocious Scaling, Rescaling and xi Scaling,” *Phys. Rev. Lett.* **36** (1976) 1281. [Erratum: *Phys.Rev.Lett.* 37, 68 (1976)].
- [60] T. Muta, *Foundations of Quantum Chromodynamics: An Introduction to Perturbative Methods in Gauge Theories*, (2nd ed.), vol. 57 of *World scientific Lecture Notes in Physics*. World Scientific, Hackensack, N.J., 2nd ed., 1998.
- [61] T. Muta, *Foundations of Quantum Chromodynamics: An Introduction to Perturbative Methods in Gauge Theories*, (3rd ed.), vol. 78 of *World scientific Lecture Notes in Physics*. World Scientific, Hackensack, N.J., 3rd ed., 2010.
- [62] R. K. Ellis, W. Furmanski, and R. Petronzio, “Power Corrections to the Parton Model in QCD,” *Nucl. Phys. B* **207** (1982) 1–14.
- [63] R. K. Ellis, W. Furmanski, and R. Petronzio, “Unraveling Higher Twists,” *Nucl. Phys. B* **212** (1983) 29.
- [64] R. Barbieri, J. R. Ellis, M. K. Gaillard, and G. G. Ross, “Mass Corrections to Scaling in Deep Inelastic Processes,” *Nucl. Phys. B* **117** (1976) 50–76.
- [65] R. Barbieri, J. R. Ellis, M. K. Gaillard, and G. G. Ross, “A Quest for a Wholly Scaling Variable,” *Phys. Lett. B* **64** (1976) 171–176.
- [66] A. De Rujula, H. Georgi, and H. D. Politzer, “Demythification of Electroproduction, Local Duality and Precocious Scaling,” *Annals Phys.* **103** (1977) 315.
- [67] S. Kretzer and M. H. Reno, “Target mass corrections to electroweak structure functions and perturbative neutrino cross-sections,” *Phys. Rev. D* **69** (2004) 034002, [arXiv:hep-ph/0307023](#).
- [68] J. C. Collins and G. F. Sterman, “Soft Partons in QCD,” *Nucl. Phys. B* **185** (1981) 172–188.
- [69] A. Accardi, T. Hobbs, and W. Melnitchouk, “Hadron mass corrections in semi-inclusive deep inelastic scattering,” *JHEP* **11** (2009) 084, [arXiv:0907.2395 \[hep-ph\]](#).
- [70] M. A. G. Aivazis, F. I. Olness, and W.-K. Tung, “Leptoproduction of heavy quarks. 1. General formalism and kinematics of charged current and neutral current production processes,” *Phys. Rev. D* **50** (1994) 3085–3101, [arXiv:hep-ph/9312318](#).
- [71] M. A. G. Aivazis, J. C. Collins, F. I. Olness, and W.-K. Tung, “Leptoproduction of heavy quarks. 2. A Unified QCD formulation of charged and neutral current processes from fixed target to collider energies,” *Phys. Rev. D* **50** (1994) 3102–3118, [arXiv:hep-ph/9312319](#).
- [72] S. Kretzer and M. H. Reno, “Tau neutrino deep inelastic charged current interactions,” *Phys. Rev. D* **66** (2002) 113007, [arXiv:hep-ph/0208187](#).

- [73] I. Schienbein *et al.*, “A Review of Target Mass Corrections,” *J. Phys. G* **35** (2008) 053101, [arXiv:0709.1775 \[hep-ph\]](#).
- [74] R. L. Jaffe, “Deep Inelastic Scattering with Application to Nuclear Targets: Lectures at the 1985 Los Alamos School on Relativistic Dynamics and Quark Nuclear Physics,” in *Research Program at CEBAF (I): Report of the 1985 Summer Study Group*. 7, 1985. [arXiv:2212.05616 \[hep-ph\]](#).
- [75] J.-w. Qiu, “QCD factorization and rescattering in proton nucleus collisions,” [arXiv:hep-ph/0305161](#).
- [76] I. Schienbein, J. Y. Yu, C. Keppel, J. G. Morfin, F. Olness, and J. F. Owens, “Nuclear parton distribution functions from neutrino deep inelastic scattering,” *Phys. Rev. D* **77** (2008) 054013, [arXiv:0710.4897 \[hep-ph\]](#).
- [77] K. Kovarik, I. Schienbein, F. I. Olness, J. Y. Yu, C. Keppel, J. G. Morfin, J. F. Owens, and T. Stavreva, “Nuclear Corrections in Neutrino-Nucleus DIS and Their Compatibility with Global NPDF Analyses,” *Phys. Rev. Lett.* **106** (2011) 122301, [arXiv:1012.0286 \[hep-ph\]](#).
- [78] O. Nachtmann, “Positivity constraints for anomalous dimensions,” *Nucl. Phys. B* **63** (1973) 237–247.
- [79] P. G. Blunden, W. Melnitchouk, and J. A. Tjon, “Two photon exchange and elastic electron proton scattering,” *Phys. Rev. Lett.* **91** (2003) 142304, [arXiv:nucl-th/0306076](#).
- [80] P. G. Blunden, W. Melnitchouk, and J. A. Tjon, “Two-photon exchange in elastic electron-nucleon scattering,” *Phys. Rev. C* **72** (2005) 034612, [arXiv:nucl-th/0506039](#).
- [81] J. Arrington, W. Melnitchouk, and J. A. Tjon, “Global analysis of proton elastic form factor data with two-photon exchange corrections,” *Phys. Rev. C* **76** (2007) 035205, [arXiv:0707.1861 \[nucl-ex\]](#).
- [82] J. Arrington, P. G. Blunden, and W. Melnitchouk, “Review of two-photon exchange in electron scattering,” *Prog. Part. Nucl. Phys.* **66** (2011) 782–833, [arXiv:1105.0951 \[nucl-th\]](#).
- [83] J. Blumlein and A. Tkabladze, “Target mass corrections for polarized structure functions and new sum rules,” *Nucl. Phys. B* **553** (1999) 427–464, [arXiv:hep-ph/9812478](#).
- [84] C. A. Aidala, S. D. Bass, D. Hasch, and G. K. Mallot, “The Spin Structure of the Nucleon,” *Rev. Mod. Phys.* **85** (2013) 655–691, [arXiv:1209.2803 \[hep-ph\]](#).
- [85] A. Deshpande, R. Milner, R. Venugopalan, and W. Vogelsang, “Study of the fundamental structure of matter with an electron-ion collider,” *Ann. Rev. Nucl. Part. Sci.* **55** (2005) 165–228, [arXiv:hep-ph/0506148](#).
- [86] **Particle Data Group** Collaboration, P. A. Zyla *et al.*, “Review of Particle Physics,” *PTEP* **2020** no. 8, (2020) 083C01.
- [87] S. B. Treiman, R. Jackiw, and D. J. Gross, *Lectures on Current Algebra and Its Applications*. Princeton University Press, 1972. <http://www.jstor.org/stable/j.ctt13x1c2c>.
- [88] J. C. Collins, *Renormalization: An Introduction to Renormalization, The Renormalization Group, and the Operator Product Expansion*, vol. 26 of *Cambridge Monographs on Mathematical Physics*. Cambridge University Press, Cambridge, 1986.
- [89] G. F. Sterman, “Partons, factorization and resummation, TASI 95,” in *Theoretical Advanced Study Institute in Elementary Particle Physics (TASI 95): QCD and Beyond*, pp. 327–408. 6, 1995. [arXiv:hep-ph/9606312](#).
- [90] S. Alekhin *et al.*, “A facility to Search for Hidden Particles at the CERN SPS: the SHiP physics case,” *Rept. Prog. Phys.* **79** no. 12, (2016) 124201, [arXiv:1504.04855 \[hep-ph\]](#).



- [91] **FASEER** Collaboration, H. Abreu *et al.*, “Detecting and Studying High-Energy Collider Neutrinos with FASER at the LHC,” *Eur. Phys. J. C* **80** no. 1, (2020) 61, [arXiv:1908.02310 \[hep-ex\]](#).
- [92] **SHiP** Collaboration, C. Ahdida *et al.*, “SND@LHC,” [arXiv:2002.08722 \[physics.ins-det\]](#).
- [93] P. Hoodbhoy, R. L. Jaffe, and A. Manohar, “Novel Effects in Deep Inelastic Scattering from Spin 1 Hadrons,” *Nucl. Phys. B* **312** (1989) 571–588.
- [94] I. Schienbein, “Two photon processes and photon structure,” *Annals Phys.* **301** (2002) 128–156, [arXiv:hep-ph/0205301](#).
- [95] W. Detmold, “Target mass effects in deep-inelastic scattering on the deuteron,” *Phys. Lett. B* **632** (2006) 261–269, [arXiv:hep-ph/0509011](#).
- [96] Y. Kitadono, K. Sasaki, T. Ueda, and T. Uematsu, “Target Mass Corrections for the Virtual Photon Structure Functions to the Next-to-next-to-leading Order in QCD,” *Phys. Rev. D* **77** (2008) 054019, [arXiv:0801.0937 \[hep-ph\]](#).
- [97] R. L. Jaffe and M. Soldate, “Twist Four in Electroproduction: Canonical Operators and Coefficient Functions,” *Phys. Rev. D* **26** (1982) 49–68.
- [98] A. Vogt, “Efficient evolution of unpolarized and polarized parton distributions with QCD-PEGASUS,” *Comput. Phys. Commun.* **170** (2005) 65–92, [arXiv:hep-ph/0408244](#).
- [99] J. L. Miramontes and J. Sanchez Guillen, “UNDERSTANDING HIGHER TWIST: OPERATOR APPROACH TO POWER CORRECTIONS,” *Z. Phys. C* **41** (1988) 247.
- [100] E. Moffat, W. Melnitchouk, T. C. Rogers, and N. Sato, “What are the low- $Q$  and large- $x$  boundaries of collinear QCD factorization theorems?,” *Phys. Rev. D* **95** no. 9, (2017) 096008, [arXiv:1702.03955 \[hep-ph\]](#).
- [101] C. G. Callan, Jr. and D. J. Gross, “High-energy electroproduction and the constitution of the electric current,” *Phys. Rev. Lett.* **22** (1969) 156–159.
- [102] F. I. Olness and W.-K. Tung, “Factorization of Helicity Amplitudes and Angular Correlations for Electroweak Processes,” *Phys. Rev. D* **35** (1987) 833.
- [103] R. P. Feynman, “Very high-energy collisions of hadrons,” *Phys. Rev. Lett.* **23** (1969) 1415–1417.
- [104] J. D. Bjorken and E. A. Paschos, “Inelastic Electron Proton and gamma Proton Scattering, and the Structure of the Nucleon,” *Phys. Rev.* **185** (1969) 1975–1982.
- [105] F. I. Olness, R. J. Scalise, and W.-K. Tung, “Heavy quark hadroproduction in perturbative QCD,” *Phys. Rev. D* **59** (1999) 014506, [arXiv:hep-ph/9712494](#).
- [106] R. S. Thorne and R. G. Roberts, “A Variable number flavor scheme for charged current heavy flavor structure functions,” *Eur. Phys. J. C* **19** (2001) 339–349, [arXiv:hep-ph/0010344](#).
- [107] S. Alekhin, J. Blümlein, and S. Moch, “Heavy-flavor PDF evolution and variable-flavor number scheme uncertainties in deep-inelastic scattering,” *Phys. Rev. D* **102** no. 5, (2020) 054014, [arXiv:2006.07032 \[hep-ph\]](#).
- [108] S. Alekhin, J. Blumlein, S. Klein, and S. Moch, “The 3, 4, and 5-flavor NNLO Parton from Deep-Inelastic-Scattering Data and at Hadron Colliders,” *Phys. Rev. D* **81** (2010) 014032, [arXiv:0908.2766 \[hep-ph\]](#).



- [109] V. N. Gribov and L. N. Lipatov, “Deep inelastic e p scattering in perturbation theory,” *Sov. J. Nucl. Phys.* **15** (1972) 438–450.
- [110] G. Altarelli and G. Parisi, “Asymptotic Freedom in Parton Language,” *Nucl. Phys. B* **126** (1977) 298–318.
- [111] Y. L. Dokshitzer, “Calculation of the Structure Functions for Deep Inelastic Scattering and e+ e- Annihilation by Perturbation Theory in Quantum Chromodynamics.,” *Sov. Phys. JETP* **46** (1977) 641–653.
- [112] **Jefferson Lab Hall A Tritium** Collaboration, D. Abrams *et al.*, “Measurement of the Nucleon  $F_2^n/F_2^p$  Structure Function Ratio by the Jefferson Lab MARATHON Tritium/Helium-3 Deep Inelastic Scattering Experiment,” *Phys. Rev. Lett.* **128** no. 13, (2022) 132003, [arXiv:2104.05850 \[hep-ex\]](#).
- [113] **Jefferson Lab Angular Momentum (JAM)** Collaboration, C. Cocuzza, C. E. Keppel, H. Liu, W. Melnitchouk, A. Metz, N. Sato, and A. W. Thomas, “Isovector EMC Effect from Global QCD Analysis with MARATHON Data,” *Phys. Rev. Lett.* **127** no. 24, (2021) 242001, [arXiv:2104.06946 \[hep-ph\]](#).
- [114] M. Sajjad Athar and J. G. Morfin, “Neutrino(antineutrino)–nucleus interactions in the shallow- and deep-inelastic scattering regions,” *J. Phys. G* **48** no. 3, (2021) 034001, [arXiv:2006.08603 \[hep-ph\]](#).
- [115] I. Niculescu *et al.*, “Direct observation of quark-hadron duality in the free neutron  $F_2$  structure function,” *Phys. Rev. C* **91** no. 5, (2015) 055206, [arXiv:1501.02203 \[hep-ex\]](#).
- [116] S. A. Alsalmi, *Measurement of the Nuclear Dependence of  $F_2$  and  $R=\sigma_L/\sigma_T$  in The Nucleon Resonance Region*. PhD thesis, Kent State University, Kent State U., 2019.
- [117] B. Z. Kopeliovich, J. G. Morfin, and I. Schmidt, “Nuclear Shadowing in Electro-Weak Interactions,” *Prog. Part. Nucl. Phys.* **68** (2013) 314–372, [arXiv:1208.6541 \[hep-ph\]](#).
- [118] **European Muon** Collaboration, J. J. Aubert *et al.*, “The ratio of the nucleon structure functions  $F_2^n$  for iron and deuterium,” *Phys. Lett. B* **123** (1983) 275–278.
- [119] L. L. Frankfurt and M. I. Strikman, “Hard Nuclear Processes and Microscopic Nuclear Structure,” *Phys. Rept.* **160** (1988) 235–427.
- [120] L. L. Frankfurt, M. I. Strikman, D. B. Day, and M. Sargsian, “Evidence for short range correlations from high  $Q^2$  (e, e-prime) reactions,” *Phys. Rev. C* **48** (1993) 2451–2461.
- [121] L. L. Frankfurt and M. I. Strikman, “High-Energy Phenomena, Short Range Nuclear Structure and QCD,” *Phys. Rept.* **76** (1981) 215–347.
- [122] M. M. Sargsian *et al.*, “Hadrons in the nuclear medium,” *J. Phys. G* **29** no. 3, (2003) R1–R45, [arXiv:nucl-th/0210025](#).
- [123] J. Rozynek and M. C. Birse, “Nucleon Nucleon Correlation Effects on Deeply Inelastic Lepton Scattering in the Region  $X > 1$ ,” *Phys. Rev. C* **38** (1988) 2201–2204.
- [124] I. Niculescu, J. Arrington, R. Ent, and C. E. Keppel, “Moments of nuclear and nucleon structure functions at low  $Q^2$  and the momentum sum rule,” *Phys. Rev. C* **73** (2006) 045206, [arXiv:hep-ph/0509241](#).
- [125] L. A. Kondratyuk and M. Shmatikov, “EMC EFFECT AND MULTI - QUARK BAGS IN NUCLEI,” *Yad. Fiz.* **41** (1985) 222–235.

- [126] M. M. Sargsian, “Superfast quarks in the nuclear medium,” *Nucl. Phys. A* **782** (2007) 199–206.
- [127] A. J. Freese, M. M. Sargsian, and M. I. Strikman, “Probing superfast quarks in nuclei through dijet production at the LHC,” *Eur. Phys. J. C* **75** no. 11, (2015) 534, [arXiv:1411.6605 \[hep-ph\]](#).
- [128] A. J. Freese, W. Cosyn, and M. M. Sargsian, “QCD evolution of superfast quarks,” *Phys. Rev. D* **99** no. 11, (2019) 114019, [arXiv:1511.06044 \[hep-ph\]](#).
- [129] A. Bodek and J. L. Ritchie, “Fermi Motion Effects in Deep Inelastic Lepton Scattering from Nuclear Targets,” *Phys. Rev. D* **23** (1981) 1070.
- [130] A. Bodek and J. L. Ritchie, “Further Studies of Fermi Motion Effects in Lepton Scattering from Nuclear Targets,” *Phys. Rev. D* **24** (1981) 1400.
- [131] **CCFR** Collaboration, M. Vakili *et al.*, “Nuclear structure functions in the large  $x$  large  $Q^{*2}$  kinematic region in neutrino deep inelastic scattering,” *Phys. Rev. D* **61** (2000) 052003, [arXiv:hep-ex/9905052](#).
- [132] S. Rock, “Elastic electron - proton scattering at high  $Q^{*2}$ ,” 11, 1986.
- [133] J. Arrington *et al.*, “Inclusive Scattering from Nuclei at  $x > 1$  in the quasielastic and deeply inelastic regimes,” *JLab Proposal PR12-06-105* (2006) 1–21.  
[https://www.jlab.org/exp\\_prog/proposals/06/PR12-06-105.pdf](https://www.jlab.org/exp_prog/proposals/06/PR12-06-105.pdf).
- [134] N. Fomin *et al.*, “Scaling of the  $F_2$  structure function in nuclei and quark distributions at  $x > 1$ ,” *Phys. Rev. Lett.* **105** (2010) 212502, [arXiv:1008.2713 \[nucl-ex\]](#).
- [135] J. Arrington *et al.*, “Inclusive electron scattering from nuclei at  $x$  approximately = 1,” *Phys. Rev. C* **53** (1996) 2248–2251, [arXiv:nucl-ex/9504003](#).
- [136] B. W. Filippone *et al.*, “Nuclear structure functions at  $x > 1$ ,” *Phys. Rev. C* **45** (1992) 1582–1585.
- [137] **BCDMS** Collaboration, A. C. Benvenuti *et al.*, “Nuclear structure function in carbon near  $x = 1$ ,” *Z. Phys. C* **63** (1994) 29–36.
- [138] S. A. Kulagin and R. Petti, “Global study of nuclear structure functions,” *Nucl. Phys. A* **765** (2006) 126–187, [arXiv:hep-ph/0412425](#).
- [139] L. T. Brady, A. Accardi, T. J. Hobbs, and W. Melnitchouk, “Next-to leading order analysis of target mass corrections to structure functions and asymmetries,” *Phys. Rev. D* **84** (2011) 074008, [arXiv:1108.4734 \[hep-ph\]](#). [Erratum: *Phys.Rev.D* 85, 039902 (2012)].
- [140] M. A. G. Aivazis, F. I. Olness, and W.-K. Tung, “QCD formulation of charm production in deep inelastic scattering and the sea quark - gluon dichotomy,” *Phys. Rev. Lett.* **65** (1990) 2339–2342.
- [141] B. A. Kniehl, G. Kramer, I. Schienbein, and H. Spiesberger, “Collinear subtractions in hadroproduction of heavy quarks,” *Eur. Phys. J. C* **41** (2005) 199–212, [arXiv:hep-ph/0502194](#).
- [142] F. Halzen and A. D. Martin, *QUARKS AND LEPTONS: AN INTRODUCTORY COURSE IN MODERN PARTICLE PHYSICS*. John Wiley & Sons,, 1984.
- [143] M. E. Peskin and D. V. Schroeder, *An Introduction to quantum field theory*. Addison-Wesley, Reading, USA, 1995.
- [144] **CTEQ** Collaboration, R. Brock *et al.*, “Handbook of perturbative QCD: Version 1.0,” *Rev. Mod. Phys.* **67** (1995) 157–248.

- [145] D. Buarque Franzosi, O. Mattelaer, R. Ruiz, and S. Shil, “Automated predictions from polarized matrix elements,” *JHEP* **04** (2020) 082, [arXiv:1912.01725 \[hep-ph\]](#).
- [146] H. Murayama, I. Watanabe, and K. Hagiwara, “HELAS: HELicity amplitude subroutines for Feynman diagram evaluations,”.
- [147] M. Krämer, F. I. Olness, and D. E. Soper, “Treatment of heavy quarks in deeply inelastic scattering,” *Phys. Rev. D* **62** (2000) 096007, [arXiv:hep-ph/0003035](#).
- [148] **H1, ZEUS** Collaboration, H. Abramowicz *et al.*, “Combination of measurements of inclusive deep inelastic  $e^\pm p$  scattering cross sections and QCD analysis of HERA data,” *Eur. Phys. J. C* **75** no. 12, (2015) 580, [arXiv:1506.06042 \[hep-ex\]](#).
- [149] F. M. Steffens, M. D. Brown, W. Melnitchouk, and S. Sanches, “Parton distributions in the presence of target mass corrections,” *Phys. Rev. C* **86** (2012) 065208, [arXiv:1210.4398 \[hep-ph\]](#).
- [150] T. Becher, M. Neubert, and L. Rothen, “Factorization and  $N^3LL_p$ +NNLO predictions for the Higgs cross section with a jet veto,” *JHEP* **10** (2013) 125, [arXiv:1307.0025 \[hep-ph\]](#).